

**SYNTHESIS AND CHARACTERIZATION OF NOVEL ORGANIC
MATERIALS**

DUANGRATCHANEKORN MUENMART

**A THESIS SUBMITTED IN PARTIAL FULFILLMENT OF THE REQUIREMENTS
FOR THE DEGREE OF DOCTOR OF PHILOSOPHY
MAJOR IN CHEMISTRY
FACULTY OF SCIENCE
UBON RATCHATHANI UNIVERSITY
ACADEMIC YEAR 2014
COPYRIGHT OF UBON RATCHATHANI UNIVESITY**



UBON RATCHATHANI UNIVERSITY

THESIS APPROVAL

DOCTOR OF PHILOSOPHY

MAJOR IN CHEMISTRY FACULTY OF SCIENCE

TITLE SYNTHESIS AND CHARACTERIZATION OF NOVEL ORGANIC MATERIALS

AUTHOR MISS DUANGRATCHANEKORN MUENMART

EXAMINATION COMMITTEE

ASST. PROF. DR. BOOSAYARAT TOMAPATANAGET CHAIRPERSON

ASST. PROF. DR. TAWEESAK SUDYOADSUK MEMBER

ASSOC. PROF. DR. VINICH PROMARAK MEMBER

ASSOC. PROF. DR. SIRIPORN JUNGSUTTIWONG MEMBER

ADVISORS

T. Sudyoadsuk
..... ADVISOR
(ASST. PROF. DR. TAWEESAK SUDYOADSUK)

V. Promarak
..... CO-ADVISOR
(ASSOC. PROF. DR. VINICH PROMARAK)

Utith Inprasit
.....
(ASSOC. PROF. DR. UTITH INPRASIT)
DEAN, FACULTY OF SCIENCE

H. Juthamas
.....
(DR. JUTHAMAS HONGTHONG)
ACTING FOR VICE PRESIDENT
FOR ACADEMIC AFFAIRS

COPYRIGHT OF UBON RATCHATHANI UNIVERSITY

ACADEMIC YEAR 2014

ACKNOWLEDGEMENTS

I am really thankful to my advisors Assoc. Prof. Dr. Vinich Promarak and Asst. Prof. Dr. Taweesak Sudyoasuk for their support, understanding and patience during the entire project in the past six years. Thank you so much to the Office of the Higher Education Commission, Thailand for the research grant under the program Strategic Scholarships for Frontier Research Network for the Joint Ph.D. Thanks to Center of Excellence for Innovation in Chemistry (PERCH-CIC) for financial support.

I would also like to thank Prof. Michael L. Turner, School of Chemistry, the University of Manchester, UK, for his kindness and constant advice. My aboard stay in UK would not have succeeded without his support. Thanks to Dr. Andrew B. Foster and Dr. Mark C. McCairn for their help and suggestions while I worked in the Organic Materials Innovation Centre (OMIC) and also thanks to the OMIC members (past and current) for a nice atmosphere and the conversations during lunch break. Many thanks to the people who contributed their times and advices to my project. In particular, Dr. Tinnagon Keawin for NMR Experiment, Mr. Ruangchai Tarsang and Miss Rattanawalee Rattanawan for computational calculation, Mr. Pongsathorn Tongkasee for DSC devices. Thank you so much to all members of the Center for Organic Electronic and Alternative Energy (past and current).

Finally, I would like to thank my family who has provided me endless support. Thanks to my mother for being by my side in every situation. My brother and sister who always support me no matter what I have decided to do.


(Miss Duangratchaneekorn Muenmart)
Researcher

บทคัดย่อ

ชื่อเรื่อง : การสังเคราะห์และพิสูจน์เอกลักษณ์ของวัสดุอินทรีย์ชนิดใหม่

โดย : ดวงรัตน์กร เหมือนมาตย์

ชื่อปริญญา : ปรัชญาคุณภูมิบัณฑิต

สาขาวิชา : เคมี

ประธานกรรมการที่ปรึกษา : ผู้ช่วยศาสตราจารย์ ดร. ทวีศักดิ์ สูดยอดสุข

ศัพท์สำคัญ : สารกึ่งตัวนำอินทรีย์ โอลิโกโรโอฟิน ทรานซิสเตอร์สนามไฟฟ้าสารอินทรีย์ เซลล์แสงอาทิตย์สารอินทรีย์ อนุภาคขนาดนาโน

ในงานวิจัยนี้รายงานการสังเคราะห์และพิสูจน์เอกลักษณ์ของวัสดุอินทรีย์ชนิดใหม่ เพื่อนำไปใช้ในอุปกรณ์อิเล็กทรอนิกส์ โดยโมเลกุลของสารเป้าหมายถูกแบ่งออกตามการนำไปใช้งาน สารอนุพันธ์ของโอลิโกโรโอฟินที่มีหมู่ปิดท้ายเป็น dialkylaniline ถูกสังเคราะห์ขึ้น เพื่อนำไปใช้เป็นสารกึ่งตัวนำในอุปกรณ์สนามไฟฟ้าสารอินทรีย์ PTn และ PTnF แสดงคุณสมบัติทางแสงที่ดีที่ความยาวคลื่น 420-470 nm เป็นการดูดกลืนแสงของโอลิโกโรโอฟิน การดูดกลืนแสงที่ความยาวคลื่นแตกต่างกันนี้เป็นผลของความยาวคอนจูเกชันที่ยาวขึ้น ตามจำนวนของหมู่โรโอฟินที่เพิ่มขึ้น นอกจากนี้ยังแสดงคุณสมบัติทางเคมีไฟฟ้าที่ดีอีกด้วย โดยสังเกตได้จากการแสดงพีคออกซิเดชันที่ย้อนกลับได้ และไม่มีการเปลี่ยนแปลงคุณสมบัติหลังจากสูญเสียอิเล็กตรอน สีข้อมไวแสงสำหรับอุปกรณ์แสงอาทิตย์ชนิดสีข้อมไวแสง ได้ถูกสังเคราะห์เช่นเดียวกัน สีข้อมที่มีหมู่ให้อิเล็กตรอนเป็น dialkylaniline phenothiazine และ coumarin มีหมู่สะพานอิเล็กตรอนเป็นหมู่โรโอฟินและฟีนิลิน หมู่รับอิเล็กตรอนเป็นหมู่ cyanoacetic acid สารเป้าหมายแสดงการดูดกลืนแสงในช่วง 450-600 nm ซึ่งเหมาะสมกับการใช้งานในเซลล์แสงอาทิตย์ นอกจากนี้การศึกษาประสิทธิภาพของเซลล์แสงอาทิตย์โดยใช้สีข้อมที่สังเคราะห์ได้ ยังแสดงประสิทธิภาพที่ดี ที่มีประสิทธิภาพการเปลี่ยนพลังงานแสงอาทิตย์เป็นพลังงานไฟฟ้าที่ร้อยละ 3.55 ที่ AM 1.5 G ($J_{sc} = 7.69 \text{ mA cm}^{-2}$, $V_{oc} = 0.63 \text{ V}$, $ff = 0.73$) เมื่อใช้ PT2dye เป็นสีข้อมไวแสง เซลล์แสงอาทิตย์ที่ใช้ PhCT1Pdye เป็นสีข้อมไวแสง พบว่าอุปกรณ์แสดงประสิทธิภาพการเปลี่ยนพลังงานแสงอาทิตย์เป็นพลังงานไฟฟ้าที่ร้อยละ 4.33 ที่ AM 1.5 G ($J_{sc} = 9.58 \text{ mA cm}^{-2}$, $V_{oc} = 0.64 \text{ V}$ และ $ff = 0.70$) คอนจูเกตพอลิเมอร์ขนาดนาโน PFO, PF8T2, PF8BT และ PF8TAA ถูกสังเคราะห์โดยใช้ emulsion polymerization ภายใต้สภาวะ Suzuki coupling polymerisation ที่อุณหภูมิ 30 °C ขนาดของอนุภาคจากการศึกษาด้วยการวัดการ

กระเจิงแสงและภาพถ่ายจากกล้องจุลทรรศน์ส่องผ่านพบว่ามีความอยู่ในช่วงนาโน ขนาดของอนุภาคขึ้นอยู่กับความเข้มข้นของสารตั้งต้นในตัวทำละลาย และแสดงคุณสมบัติที่เหมาะสมสำหรับใช้เป็นสารกึ่งตัวนำ

ABSTRACT

TITLE : SYNTHESIS AND CHARACTERIZATION OF NOVEL ORGANIC MATERIALS
BY : DUANGRATCHANEKORN MUENMART
DEGREE : DOCTOR OF PHILOSOPHY
MAJOR : CHEMISTRY
CHAIR : ASST. PROF. TAWEESAK SUDYOADSUK, Ph.D

KEYWORDS : ORGANIC SEMICONDUCTOR OLIGOTHIOPHENE FIELD-EFFECT TRANSISTORS DYE-SENSITIZED SOLAR CELLS NANOPARTICLES

In this work presents the synthesis and characterization of novel organic materials for application in electronics devices. The target molecules were classified as its application. Oligothiophene derivatives bearing dialkylaniline end-capped were successfully synthesised and characterized. These compounds will be used as semiconductors in organic field-effect transistors, **PTn** and **PTnF**, respectively. All molecules show good optical property with the maximum wavelength depending on the number of thiophenes. In addition, the electrochemical property was also studied. The desired molecules show reversible oxidation stability. Dye-sensitiser for dye-sensitised solar cells based on dialkylaniline, phenothiazine and coumarin as electron-donor were synthesised. Thiophene, phenylene and cyanoacetic acid were used as π -bridge and electron-acceptor, respectively. The desired molecules exhibit the absorption at 450-600, which is suitable for using as dye-sensitiser in solar cell. The devices based on **PT2dye** show power conversion efficiency of 3.55% ($J_{sc} = 7.69 \text{ mA cm}^{-2}$, $V_{oc} = 0.63 \text{ V}$, $ff = 0.73$) at AM 1.5 G. Moreover, the DSSCs based on **PhCT1Pdye** show the power conversion efficiency of 4.33% ($J_{sc} = 9.58 \text{ mA cm}^{-2}$, $V_{oc} = 0.64 \text{ V}$, $ff = 0.70$) at AM 1.5 G. Conjugated polymer nanoparticles, **PFO**, **PF8T2**, **PF8BT** and **PF8TAA**, were carried out using emulsion polymerisation under Suzuki coupling condition at 30°C. The particle sizes were studied using dynamic light scattering (DLS) and transmission electron microscopy (TEM). The results show that the particles size is in nanometer range. The nanoparticles reveal a promising property as semiconductor for organic field-effect transistors.

CONTENTS

	PAGES
ACKNOWLEDGEMENTS	I
ABSTRACT IN THAI	II
ABSTRACT IN ENGLISH	IV
CONTENTS	V
LIST OF TABLES	VII
LIST OF FIGURES	VIII
LIST OF SCHEMES	XI
LIST OF ABBREVIATIONS	XII
CHAPTER	
1 INTRODUCTION	
1.1 Introduction	1
1.1.1 Organic materials	1
1.1.2 Organic field-effect transistors (OFETs)	1
1.1.3 Dye-sensitized solar cells (DSCs)	4
1.1.4 Conjugated polymer nanoparticles	11
1.2 Aims	13
2 SYNTHESIS AND CHARACTERIZATION OF OLIGOTHIOPHENES FOR APPLICATION IN ORGANIC FIELD-EFFECT TRANSISTORS (OFETs)	
2.1 Introduction	15
2.2 Synthesis	16
2.3 Optical properties	21
2.4 Electrochemical property	23
2.5 Thermal property	30
2.6 Computational calculation	32
2.7 Conclusion	34
3 NOVEL DYE SENSITIZERS BASED ON ANILINE-THIOPHENE FOR DYE-SENSITIZED SOLAR CELLS (DSSCs)	
3.1 Introduction	35
3.2 Synthesis	36
3.3 optical properties	38
3.4 Electrochemical property	40
3.5 Computational calculation	42

CONTENTS (CONTINUED)

	PAGES
3.6 Devices performance	43
3.7 Conclusion	44
4 NOVEL D-π-A DYE SENSITIZERS: SYNTHESIS, CHARACTERIZATION AND DEVICES PERFORMANCE	
4.1 Introduction	46
4.2 Synthesis	47
4.3 Optical properties	53
4.4 Electrochemical property	56
4.5 Thermal property	59
4.6 Computational calculation	61
4.7 Devices performance	61
4.8 Conclusion	63
5 THE CONJUGATED POLYMER NANOPARTICLES AS ORGANIC SEMICONDUCTOR	
5.1 Introduction	64
5.2 Synthesis	66
5.3 Particles size	71
5.4 Optical properties	78
5.5 Conclusion	83
6 CONCLUSION	85
7 EXPERIMENT	
7.1 General procedures and instruments	87
7.2 Synthesis of intermediates	89
7.3 Synthesis of target molecules	103
REFERENCES	117
APPENDIX	130
VITAE	138

LIST OF TABLES

TABLE		PAGES
2.1	The summary of Absorption and fluorescence data of PT2, PT3, PT4, PT5, PT6, PT1F and PT2F	23
2.2	Cyclic voltammetric results for PT2, PT3, PT4, PT5, PT6, PT1F and PT2F	29
2.3	The DSC and TGA results of PT4, PT5 and PT6	31
3.1	The summary of Absorption and fluorescence data of PT2dye, PT1Pdye and PT2Pdye	40
3.2	Cyclic voltammetric results for PT2, PT3, PT4, PT5, PT6, PT1F and PT2F	42
3.3	Computational modeling of PTdyes	42
3.4	Photovoltaic performance of DSCs based on PT2dye, PT1Pdye and PT2Pdye	44
4.1	The optical properties results of phenothiazine and coumarin base dyes	56
4.2	Cyclic voltammetry results for phenothiazine and coumarin base dyes	59
4.3	The thermal property results of PhCPdye, PhCT1Pdye and PhCT2dye	60
4.4	The frontier molecular orbital of phenothiazine base dyes and coumarin base dye	61
4.5	Photovoltaic performance of DSSCs based on phenothiazine dyes	63
5.1	Sample concentration amount of monomer, percent surfactant, solvent and Molar mass of PFO at various concentration	67
5.2	Sample concentration amount of monomer, percent surfactant, solvent and Molar mass of PF8T2 at various concentration	68
5.3	Sample concentration amount of monomer, percent surfactant, solvent and Molar mass of PF8BT at various concentration	69
5.4	Sample concentration amount of monomer, percent surfactant, solvent and Molar mass of PF8TAA at various concentration	70
5.5	Particles size of PFO in water at 25°C	73
5.6	Particles size of PF8T2 in water at 25°C	74
5.7	Particles size of PF8BT in water at 25°C	75
5.8	Particles size of PF8TAA in water at 25°C	77
5.9	Summarized optical properties of PFO in water	79
5.10	Summarized optical properties of PF8T2 in water	81
5.11	Summarized optical properties of PF8BT in water	82
5.12	Summarized optical properties of PF8TAA in water	83

LIST OF FIGURES

FIGURE	PAGES
1.1 OFETs components and operation	2
1.2 Chemical structure of single molecules for OFETs	4
1.3 Photon flux of the AM 1.5 G spectrum at 1000 W m^{-2} (ASTM G173-03), and calculated accumulated photocurrent	6
1.4 Schematic working principle of a DSC	7
1.5 Energy level and operation diagram of DSSCs	8
1.6 Chemical structures of <i>N,N</i> -dialkylaniline dyes	10
1.7 Chemical structures of coumarin derivative dyes	10
1.8 Chemical structures of phenothiazine dyes	11
1.9 A schematic representation of the micelle nucleation model	12
1.10 The preparation of nanoparticles using the miniemulsion method	13
1.11 Chemical structure of target molecules	14
2.1 The chemical structure of TAA derivatives	15
2.2 The chemical structure of thiophene-phenylene oligomers	16
2.3 Absorption spectra of PT2, PT3, PT4, PT5 and PT6	21
2.4 Absorption spectra of PT3, PT5, PT1F and PT2F	22
2.5 Fluorescence spectra of PT2, PT3, PT4, PT5 and PT6	22
2.6 Fluorescence spectra of PT3, PT5, PT1F and PT2F	23
2.7 a) the triangular potential sweep used for CV b) a quasi-reversible CV trace for a redox process	24
2.8 Cyclic voltammogram of target molecules PT2	25
2.9 Cyclic voltammogram of target molecules PT3	26
2.10 Cyclic voltammogram of target molecules PT4	26
2.11 Cyclic voltammogram of target molecules PT5	27
2.12 Cyclic voltammogram of target molecules PT6	27
2.13 Cyclic voltammogram of target molecules PT1F	28
2.14 Cyclic voltammogram of target molecules PT2F	29
2.15 The thermograms of DSC plot of PT4, PT5 and PT6	31
2.16 TGA plot of PT4, PT5 and PT6	31
2.17 Optimized structure of oligothiophenes derivatives	34

LIST OF FIGURES (CONTINUED)

FIGURE		PAGES
3.1	Chemical structure of aniline based dyes	36
3.2	The absorption spectra of PT2dye , PT1Pdye and PT2Pdye	39
3.3	Fluorescence spectra of PT2dye , PT1Pdye and PT2Pdye	39
3.4	Cyclic voltammogram of target molecules PT2dye	40
3.5	Cyclic voltammogram of target molecules PT1Pdye	41
3.6	Cyclic voltammogram of target molecules PT2Pdye	41
3.7	Spectra of monochromatic incident photon-to-current conversion efficiencies (IPCEs) for DSSCs based on PT2dye , PT1Pdye and PT2Pdye	43
3.8	<i>J-V</i> curves of DSSCs based on PT2dye , PT1Pdye and PT2Pdye	44
4.1	Chemical structure of phenothiazine based dyes	46
4.2	The absorption spectra of PhCPdye , PhCT1Pdye , PhCT2Pdye and PhCT3dye	53
4.3	The chemical structure of CT3A	54
4.4	The absorption spectra of CoT3dye and CT3A	54
4.5	The photoluminescence spectra of PhCPdye , PhCT1Pdye , PhCT2Pdye and PhCT3dye	55
4.6	The photoluminescence of coumarin base dyes	55
4.7	The cyclic voltammogram and different pulse voltammogram of PhCPdye	56
4.8	The cyclic voltammogram and different pulse voltammogram of PhCT1Pdye	57
4.9	The cyclic voltammogram and different pulse voltammogram of PhCT2Pdye	57
4.10	The cyclic voltammogram and different pulse voltammogram of PhCT3dye	58
4.11	The cyclic voltammogram and different pulse voltammogram of CoT3dye	58
4.12	The DSC plots of PhCPdye , PhCT1Pdye and PhCT2dye	60
4.13	The TGA plots of PhCPdye , PhCT1Pdye and PhCT2dye	60
4.14	Spectra of monochromatic incident photon-to-current conversion efficiencies (IPCEs) for DSSCs based on phenothiazine dyes	62
4.15	<i>J-V</i> curves of DSSCs based on phenothiazine dyes	62
5.1	Chemical structure of IPr*PdTEACl₂ and Triton X-102	66
5.2	Log molecular weight and WF/dLogM plot of PFO	67
5.3	Log molecular weight and WF/dLogM plot of PF8T2	68
5.4	Log molecular weight and WF/dLogM plot of PF8BT	69
5.5	Log molecular weight and WF/dLogM plot of PF8TAA	70
5.6	Particles size of PFO in water at 25°C	72

LIST OF FIGURES (CONTINUED)

FIGURE		PAGES
5.7	TEM images of nanoparticles present in PFO emulsion	73
5.8	Particles size of PF8T2 in water at 25°C	74
5.9	TEM images of nanoparticles present in PF8T2 emulsion	75
5.10	Particles size of PF8BT in water at 25°C	76
5.11	TEM images of nanoparticles present in PF8BT emulsion	76
5.12	Particles size of PF8TAA in water at 25°C	77
5.13	TEM images of nanoparticles present in PF8TAA emulsion	78
5.14	Absorption and Emission spectra of PFO in water	78
5.15	Area normalized absorbance of PFO at ~20 °C (LM42)	79
5.16	Absorption and Emission spectra of PF8T2 in water	80
5.17	Absorption and Emission spectra of LM45 in water	81
5.18	Absorption and Emission spectra of PF8BT in water	82
5.19	Absorption and Emission spectra of PF8TAA in water	83

LIST OF SCHEMES

FIGURE		PAGES
2.1	The synthetic route of intermediates	16
2.2	Proposed mechanism of alkylation of aniline	17
2.3	Proposed mechanism of Br ₂ generation	17
2.4	Proposed mechanism of Suzuki coupling	18
2.5	Synthetic route of PT2 , PT4 and PT6	19
2.6	The mechanism of Stille coupling reaction	19
2.7	synthetic routes of PT3 , PT5 , PT1F and PT2F	20
3.1	Synthetic routes of aldehyde intermediates	36
3.2	Synthetic routes of PTdyes	37
3.3	Knoevenagel condensation mechanism	38
4.1	Synthetic route of PhCPdye	48
4.2	Synthetic route of PhCT1Pdye	49
4.3	Synthetic route of PhCT2Pdye	50
4.4	Synthetic route of PhCT3dye	52
4.5	Synthetic route of CoT3dye	53
5.1	Synthetic route of PFO	66
5.2	Synthetic route of PF8T2	68
5.3	Synthetic route of PF8BT	69
5.4	Synthetic route of PF8TAA	70

LIST OF ABBREVIATIONS

δ	Chemical shift in ppm relative to tetramethylsilane
DCM	Dichloromethane
DMSO	<i>N,N</i> -Dimethylsulphoxide
d	Doublet
dd	Doublet of doublets
ϵ	Molar absorption
eV	Electron volt
h	Hour/hours
HOMO	Highest occupied molecular orbital
LUMO	Lowest unoccupied molecular orbital
IPCE	Incident photon to current efficiency
ITO	Indium-tin oxide
IR	Infrared
<i>J</i>	Coupling constant
M	Molar concentration
MHz	Megahertz
M^+/MH^+	Molecular ion
min	Minutes
μA	Microamperes
μm	Micrometers
mol	Moles
mmol	Milimoles
m	unresolved multiple
N	Normal concentration
NBS	<i>N</i> -Bromosuccinamide
nm	Nanometers
NMR	Nuclear magnetic resonance
Ω	Ohm
ppm	Parts per million
PCE	Power conversion efficiency
rt	Room temperature
s	Singlet
TBA	tetra- <i>n</i> -butylammonium

LIST OF ABBREVIATIONS (CONTINUED)

THF	Tetrahydrofuran
TLC	Thin-layer chromatography
TPAI	tetrapro- pylammonium iodide
t	Triplet
UV	Ultra-violet
cm ⁻¹	Wavenumber

CHAPTER 1

INTRODUCTION

1.1 Introduction

1.1.1 Organic materials

With the invention of the transistor around the middle of the last century, inorganic semiconductors such as Si or Ge began to take over the role as the dominant material in electronics from the previously dominant metals. At the same time, the replacement of vacuum tube based electronics by solid-state devices initiated a development which by the end of the 20th century has led to the omnipresence of semiconductor microelectronics in our everyday life. Now at the beginning of the 21st century we are facing a new electronics revolution that has become possible due to the development and understanding of a new class of materials, commonly known as *organic semiconductors*. The enormous progress in this field has been driven by the anticipation of novel applications, such as large area, flexible light sources and displays, low-cost printed integrated circuits or plastic solar cells from these materials.

Since the 1970s, the successful synthesis and controlled doping of conjugated polymers established the second important class of organic semiconductors, which was honored with the Nobel Prize in Chemistry in the year 2000. [1] The interest in undoped organic semiconductors revived in the 1980s due to the demonstration of an efficient photovoltaic cell incorporating an organic hetero-junction of p- and n-conducting materials [2] as well as the first successful fabrication of thin film transistors from conjugated polymers and oligomers. [3-5] The main impetus, however, came from the demonstration of high-performance electroluminescent diodes from vacuum-evaporated molecular films [6] and from conjugated polymers [7]. Owing to the large efforts of both academic and industrial research laboratories during the last 15 years, organic light-emitting devices (OLEDs) have progressed rapidly and meanwhile led to first commercial products incorporating OLED displays. Other applications of organic semiconductors, e.g., as logic circuits with organic field-effect transistors (OFETs) or organic photovoltaic cells (OPVCs) are expected to follow in the near future.

1.1.2 Organic field-effect transistors (OFETs)

Field effect transistors (FETs) are the basis for all electronic circuits and processors, and the ability to create FETs from organic materials [4, 8-14] raises exciting possibilities for low cost disposable electronics such as ID tags and smart barcodes. The molecular nature of organic semiconductors allows sub-micron structures to be created at low

cost using new soft-lithography [15] and self-assembly techniques [16] in place of expensive conventional optical lithography [9], and their emissive nature allows for optical transmission elements to be integrated directly with electronic circuits [17-20] in a way that is not possible with (non-emissive) silicon circuitry. However, although it is easy to argue for the importance of plastic FETs by drawing comparisons with silicon circuits, one must be aware that the two material systems (and the corresponding device structures) are very different, and the behaviour and performance of organic FETs do not necessarily match those of their silicon counterparts.

1.1.2.1 Principles of operation

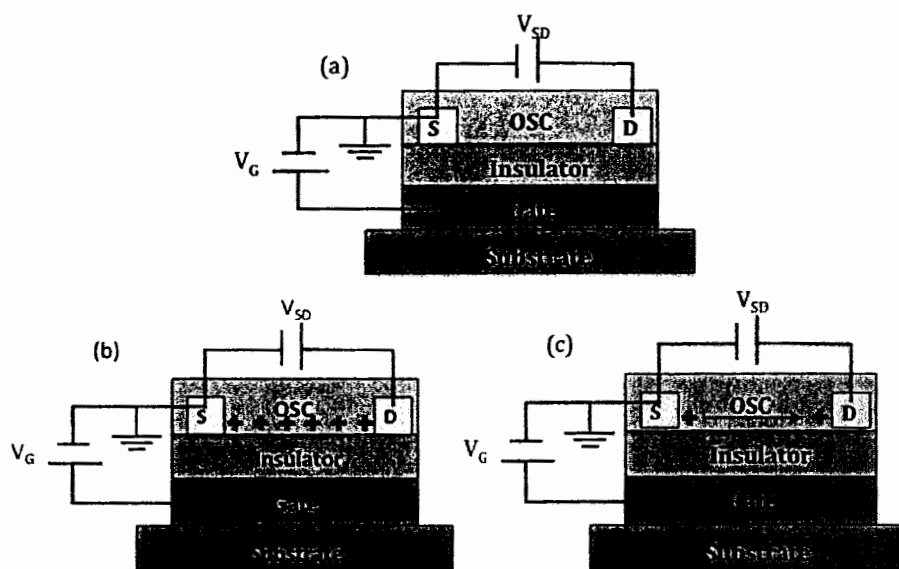


Figure 1.1 OFETs components and operation

OFET has a switching device configuration consisting of source-drain electrodes, gate electrode, active layer and gate insulator. In the case of OFET, organic semiconductors are used as an active layer. Applying a gate voltage results either accumulation or inversion of charge carriers at the organic semiconductor (OSC)/gate insulator interface.

The current flowing between the source and drain electrodes is modulated by the gate voltage, which is also used to turn the device from the off to the on state. The OFETs structure is illustrated in Figure 1.1.

There are two externally controlled biases for current manipulation, namely the potential V_{SD} applied between source and drain and the potential across the source and gate electrodes V_G (Figure 1a). The effect of the gate potential V_G is to accumulate charge carriers at the semiconductor–insulator interface, forming a channel, the so-called accumulation layer filled with charge carriers connecting the source and drain (Figure 1b). This is easily understood if one keeps in mind that a transistor is akin to a capacitor. If, in addition, a voltage V_{SD} is applied,

the accumulated charge carriers establish the current I_{SD} (Figure 1c). Therefore, I_{SD} can be modified in a transistor by variation of V_G and V_{SD} . [21, 22]

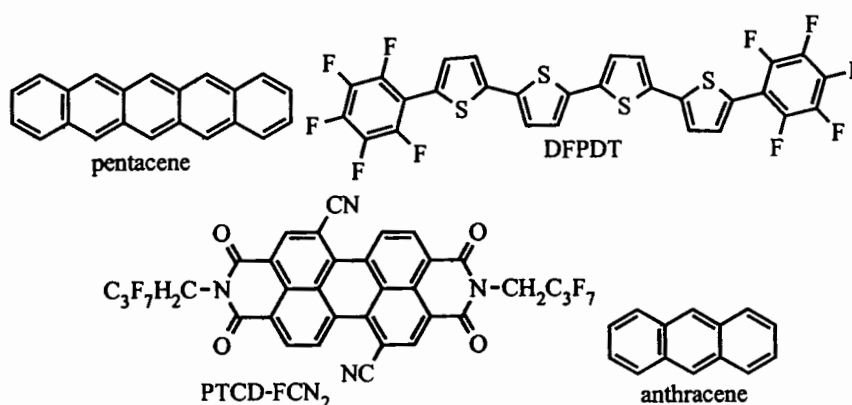
The most important parameter quantifying FET performance is the charge carrier mobility (μ). For transistors operating in saturation I_{SD} is given by

$$I_{SD} = \frac{W}{2L} \mu_{sat} C_i (V_G - V_T)^2 \quad (1)$$

where W denotes the transistor channel width (or the width of the source and drain electrodes), L the channel length (or the separation distance between the two contacts), μ_{sat} is the charge carrier mobility, C_i the capacitance per unit area of the insulator, V_G the gate voltage and V_T the threshold voltage (the gate bias V_G which needs to be applied in order for the transistor to turn on). Nowadays in large area electronic devices like flat panel displays, transistors are used that consist of amorphous silicon. Those transistors have a charge carrier mobility of typically higher than $0.1 \text{ cm}^2 \text{ V}^{-1} \text{ s}^{-1}$. That is, organic FETs are also aimed to at least reach this value in order to be appealing for their incorporation in commercial electronic products.

1.1.2.2 Materials for OFETs

A key factor that influences the charge mobility of an organic semiconductor, as well its overall performance in organic electronic devices, is the intermolecular ordering of the molecules in the solid state. It is generally believed that face-to-face contact between the molecules is preferred for organic electronics, as there is the possibility of increased $\pi \cdots \pi$ overlap between the faces of adjacent molecules, which facilitates the carrier pathway in the solid. Designing an aromatic system that will stack in a face-to-face fashion requires the overcome favourable edge-to-face interactions. One way commonly used to accomplish this is to build aromatic systems with a sufficiently large ratio of π -surface-to-circumference in order to avoid herringbone packing. In addition, adding side chains were introduced in order to increase solubility. Substituents can also be incorporated in order to force face-to-face interactions by creating steric effects that do not allow for efficient edge-to-face interactions. [23]



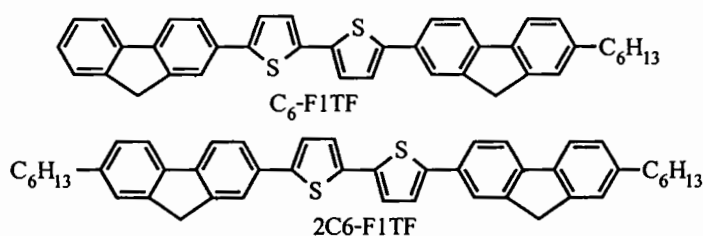


Figure 1.2 Chemical structure of single molecules for OFETs

Anthracene, the smallest member of the acene family with reported transistor characteristics, showed a mobility of $0.02 \text{ cm}^2 \text{ V}^{-1} \text{ s}^{-1}$ measured at low temperature in SC-OFETs. [24] Pentacene, one of the most studied acenes, has five linearly fused benzene rings exhibiting an even higher degree of conjugation. Charge mobilities for pentacene-based SC-OFETs are in the range of $5\text{-}40 \text{ cm}^2 \text{ V}^{-1} \text{ s}^{-1}$. [25, 26] Oligothiophenes of 5,5''-diperfluorophenyl-2,2':5',2'':5'',2'''-quaterthiophene (DFPDT) exhibited n-type charge transport behavior, with mobility as high as $0.43 \text{ cm}^2 \text{ V}^{-1} \text{ s}^{-1}$.

The most studied air-stable n-channel OSCs is perhaps perylene diimide and naphthalene diimide derivatives. With additional electron withdrawing substitution on these already electron-deficient molecules, many high mobility air-stable n-channel OSCs have been reported. [27] The addition of highly electron withdrawing groups, such as -CN and -F, on the PTCDI core lowers the LUMO levels below that of most atmospheric trapping species, which, together with a close-packed solid state resulting from fluorinated substituents at the N,N'-positions, rendered ambient stability to PTCDI-F₂ and PTCDI-CN₂. [28]

The effects of asymmetric alkylation on molecular packing and thin film morphology have also been investigated, complementary to the aforementioned symmetrical substitution. [29-31] Fluorene-bithiophene-fluorene (FITF), together with the addition of some alkyl chains did not change the molecular packing motif. Interestingly, the conjugated core of FITF in the asymmetric derivatives is in direct contact with the substrate surface, and its single alkyl chain is aligned away from that interface, making the FITF core distribution near the dielectric interface different from its symmetric counterparts. Additionally, it was found that the alkyl chain size (e.g., molecular aspect ratio) plays a significant role in 2D and 3D polycrystallite formation, which directly affects the charge mobility. [32]

1.1.3 Dye-sensitized solar cells (DSCs)

As a new type of photovoltaic technology, dye-sensitized solar cells (DSSCs) have been considered to be a credible alternative to conventional inorganic silicon-based solar cells, because of their easy fabrication, high efficiency and low cost, since the pioneering report by O'Regan and Grätzel. [33] To date, a 12.3% efficiency of DSSCs has been achieved by

employing a combination of a zinc porphyrin dye (YD2-*o*-C8) and an organic dye (Y123) in conjunction with a tris(2,2'-bipyridine)cobalt(II/III) redox couple, speeding up the large-scale practical application of DSSCs.

One of the drawbacks of organic dyes is their relatively narrow absorption spectrum, whose maxima usually remain in the shorter wavelength region. The optimal organic sensitizer for solar cell applications should possess a broadly extended absorption spectrum ranging to the near-IR regime in order to attain good overlap with the solar emission spectrum and to produce large photocurrent responses. In addition, suitable energy levels of the highest occupied molecular orbital (HOMO) and lowest unoccupied molecular orbital (LUMO) of the dye are required to match the iodide/triiodide redox potential and the conduction band edge level of the TiO₂ semiconductor electrode in order to assure efficient electron injection into the TiO₂ conduction band. For the latter process, the electron density distribution in the dye's HOMO and LUMO is also of crucial importance. One way of extending the absorption range to enhance the photocurrent response is to reduce the HOMO-LUMO energy gap of the sensitizer. For this purpose, various low bandgap sensitizers for DSSCs have been prepared by implementing, e.g., the electron-deficient benzothiadiazole (BTDA) unit into the bridging framework of D- π -A molecules. [34-38]

1.1.3.1 Solar energy

The sun emits light with a range of wavelengths from the ultraviolet and visible to the infrared. It peaks in the visible, resembling the spectrum of a blackbody at a temperature of 5760 K. It is, however, influenced by atmospheric absorption and the position of the sun. Ultraviolet light is filtered out by ozone, and water and CO₂ absorb mainly in the infrared making dips in the solar spectrum at 900, 1100, 1400, and 1900 nm (H₂O) and at 1800 and 2600 nm (CO₂). When skies are clear, the maximum radiation strikes the earth's surface when the sun is directly overhead, having the shortest path length through the atmosphere. The path length is called the *air mass* (AM) and can be approximated by $AM = 1/\cos \varphi$, where φ is the angle of elevation of the sun. The standard solar spectrum used for efficiency measurements of solar cells is AM 1.5 G (global), giving that $\varphi = 42^\circ$. This spectrum is normalized so that the integrated irradiance (the amount of radiant energy received from the sun per unit area per unit time) is 1000 W m⁻². The irradiance varies depending on the position of the sun, orientation of the Earth, and sky conditions. One also distinguishes sunlight in direct or diffuse light. The direct component can be concentrated, which increases the solar cell efficiency by increasing cell voltage outputs. Diffuse light arises by scattering of the sunlight in the atmosphere. This fraction is around 15% on average [39] but larger at higher latitudes and in regions with a significant amount of cloud cover. Materials with rough surfaces such as DSCs are relatively better suited for diffuse light

than perfectly flat surfaces and are less sensitive to movements of the sun.

The AM 1.5 G solar radiation spectrum can be found from different sources. [40] The spectrum is shown in Figure 1.3 as the irradiance of the sun as a function of wavelength.

The maximum power is obtained as the product of the photocurrent and photovoltage at the voltage where the power output of the cell is maximal. Another fundamental measurement of the performance of a solar cell is the “external quantum efficiency”, which in the DSC community is normally called the incident photon to current conversion efficiency (IPCE). The IPCE value corresponds to the photocurrent density produced in the external circuit under monochromatic illumination of the cell divided by the photon flux that strikes the cell. From such an experiment the IPCE as a function of wavelength can be calculated from

$$IPCE = \frac{J_{sc}}{e\Phi} = 1240 \frac{J_{sc}}{\lambda P_{in}} \quad (2)$$

where e is the elementary charge. IPCE values provide practical information about the monochromatic quantum efficiencies of a solar cell.

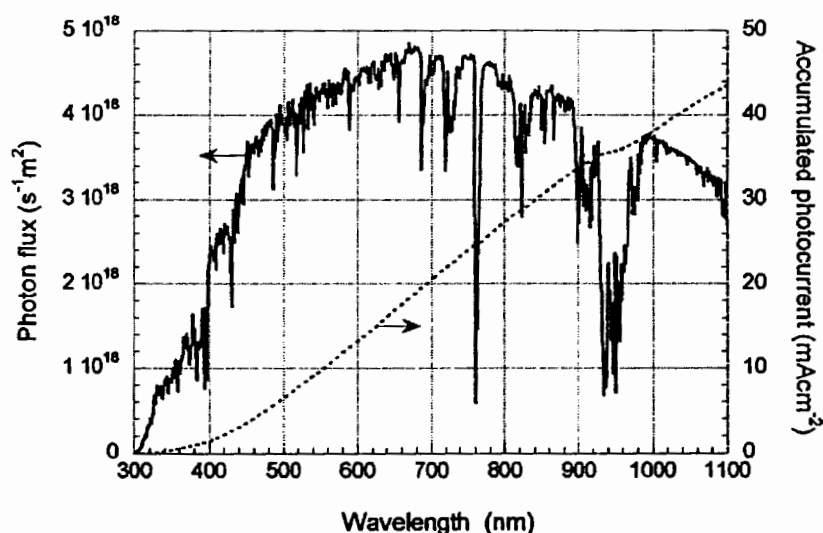


Figure 1.3 Photon flux of the AM 1.5 G spectrum at 1000 W m^{-2} (ASTM G173-03), and calculated accumulated photocurrent [41]

1.1.3.2 Principles of operation

Typically, a DSSC contains the following key components: (1) a conductive mechanical support such as fluorine-doped SnO_2 (FTO) over layer, (2) a mesoporous semiconductor metal oxide (such as nanocrystalline TiO_2) film, (3) a sensitizer (dye), (4) an electrolyte/hole transporter, and (5) a counter electrode, which is usually made of noble-metal

platinum or carbon on FTO, as schematically shown in Figure 1.4. In the DSSCs system, light is absorbed by the dye anchored on the TiO_2 surface and then electrons from the excited dye inject into the conduction band (CB) of the TiO_2 , generating an electric current, while the ground state of the dye is regenerated by the electrolyte to give efficient charge separation. The iodide is regenerated in turn by the reduction of triiodide at the counter electrode and the circuit is completed via electron migration through the external load. The voltage generated under illumination corresponds to the difference between the Fermi level of the electron in the TiO_2 and the redox potential of the electrolyte. [42] Thus, the device generates electric power from light continuously. A unique feature of DSSCs compared with other solar cell technologies is that they separate the function of light absorption from charge carrier transport, [41] allowing optimisation of the device by careful screening of the light absorber and charge transport materials.

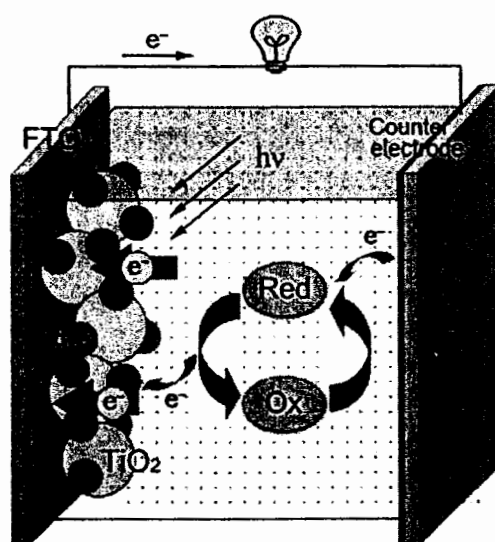


Figure 1.4 Schematic working principle of a DSC [43]

The current-voltage (I - V) characteristics of a solar cell under illumination are used to determine the power conversion efficiency, η . Because dye-sensitised solar cells have a relatively slow electrical response due to their high interfacial capacity, the voltage scan should be sufficiently slow to avoid errors in the current measurement due to capacitive (dis)-charging. Alternatively, the currents from a rapid forward and reverse voltage scan can be averaged. From the I - V curve, the short-circuit current, I_{sc} (or short circuit current density, J_{sc}), is determined at the $V = 0$ intercept, while the open-circuit potential, V_{oc} , is found at the $I = 0$ intercept. The maximum output power of the solar cell is found where the product $|I \times V|$ reaches a maximum (the maximum power point). The power conversion efficiency is given by

$$\eta = \frac{|V|_{max}}{P_{in}} = \frac{I_{sc}V_{oc}FF}{P_{in}} \quad (3)$$

where P_{in} is the power density of the incident light and FF is the fill factor. The fill factor can assume values between 0 and less than 1 and is defined by the ratio of the maximum power (P_{max}) of the solar cell per unit area divided by the V_{oc} and J_{sc} according to

$$FF = \frac{P_{max}}{I_{sc}V_{oc}} \quad (4)$$

Charge recombination at the nanocrystallite/redox electrolyte interface is expected to play a significant role in lowering the photovoltage. There are two likely recombination pathways, occurring at the interface. The injected conduction-band electrons may recombine with oxidized dye molecules or react with redox species in the electrolyte, as shown in Figure 1.5. It is known that to get an efficient charge separation, the LUMO of the dye from where the electron injection occurs has to be at sufficiently more negative potential than the conduction band edge of the TiO_2 (E_{CB}), and the HOMO has to be more positive than the redox potential of iodide/triiodide.

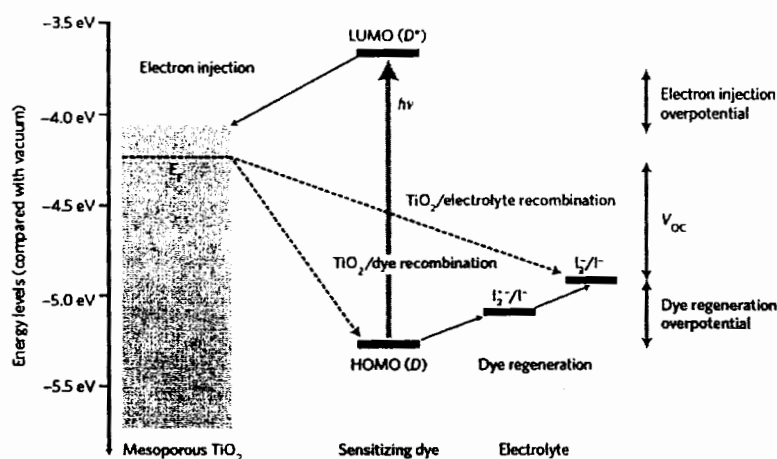


Figure 1.5 Energy level and operation diagram of DSSCs [44]

1.1.3.3 Materials for DSCs

As one of the crucial parts in dye-sensitized solar cells (DSSCs), the photosensitizer should fulfill some essential characteristics:

- 1) The absorption spectrum of the photosensitizer should cover the whole visible region and even the part of the near-infrared (NIR).
- 2) The photosensitizer should have anchoring groups ($-COOH$, $-H_2PO_3$, $-SO_3H$, etc.) to strongly bind the dye onto the semiconductor surface.
- 3) The excited state level of the photosensitizer should be higher in energy than the conduction band edge of n-type semiconductor (n-type DSSCs), so that an

efficient electron transfer process between the excited dye and conduction band (CB) of the semiconductor can take place. In contrast, for p-type DSSCs, the HOMO level of the photosensitizer should be at more positive potential than the valence band (VB) level of p-type semiconductor.

4) For dye regeneration, the oxidized state level of the photosensitiser must be more positive than the redox potential of the electrolyte.

5) Unfavourable dye aggregation on the semiconductor surface should be avoided through optimisation of the molecular structure of the dye or by addition of co-adsorbers that prevent aggregation. Dye aggregates can, however, be controlled (H- and J-aggregates) leading to an improved performance compared with a monomer dye layer.

6) The photosensitiser should be photostable, and electrochemical and thermal stability are also required.[41]

Organic dyes as an alternative to the noble Ru complexes sensitiser exhibit many advantages: (1) The molecular structures of organic dyes are diverse and can be easily designed and synthesised. (2) Concerning the cost and environment issues, organic dyes are superior to noble metal complexes. (3) The molar extinction coefficients of organic dyes are usually higher than those of Ru complexes, making them attractive for thin film and solid-state DSSCs. (4) To date, organic dyes exhibit higher efficiencies compared with that of Ru complexes in p-type DSSCs. Generally, donor- π -bridge-acceptor (D- π -A) structure is the common character of these organic dyes. With this construction it is easy to design new dye structures, extend the absorption spectra, adjust the HOMO and LUMO levels and complete the intramolecular charge separation. When a dye absorbs light, intramolecular charge transfer occurs from subunit A to D through the π -bridge. For n-type DSSCs, the excited dye injects the electron into the conduction band of the semiconductor via the electron acceptor group, A. However, in p-type DSSCs, the excited dye captures the electron from the valence band of the semiconductor to complete the interfacial charge transfer.

N,N-Dialkylaniline dyes have been investigated in many groups, the example as shown in Figure 1.6. NKX-2569 was reported with the highest power conversion efficiency (η) of 6.8% under AM 1.5 G. [45, 46] In 2004, Kitamura et al. reported *N,N*-diethylaniline dye with $\eta = 6.6\%$ under AM 1.5 G. [47] The thienothiophene was used as π -bridge in D-ST dye, which showed power conversion efficiency (η) of 6.23 % under AM 1.5 G. [48]

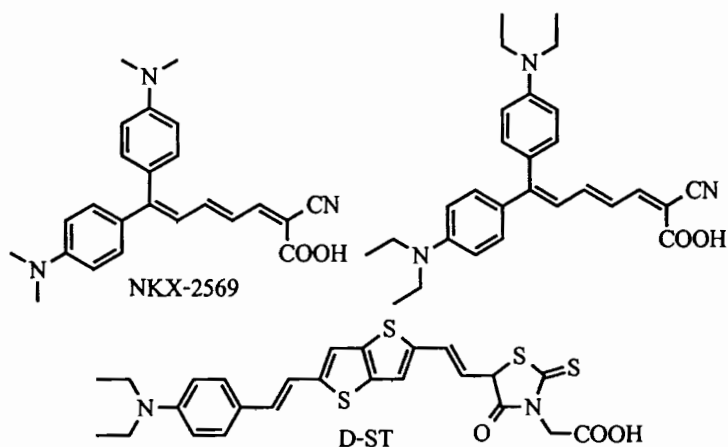


Figure 1.6 Chemical structures of *N,N*-dialkylaniline dyes

Coumarin dyes linked by vinylene or thiophene unit introduced a good device performance. Hara et al. reported coumarin dyes with different linkers.[49-53] *N,N*-diethylcoumarin (NKX-2510) with vinylene linker showed power conversion efficiency of 4.7% at AM 1.5 G. NKX-2311 was successfully synthesised and used light harvesting in dye-sensitised solar cells. The device showed quite high efficiency of 5.2% at AM 1.5 G. Thiophene was used as linker in order to improve the power conversion efficiency. NKX-2593 with vinylene-thiophene linker showed good performance at 7.2% at AM 1.5 G while NKX-2677 with bithiophene linker showed high power conversion efficiency of 7.4% at AM 1.5 G.

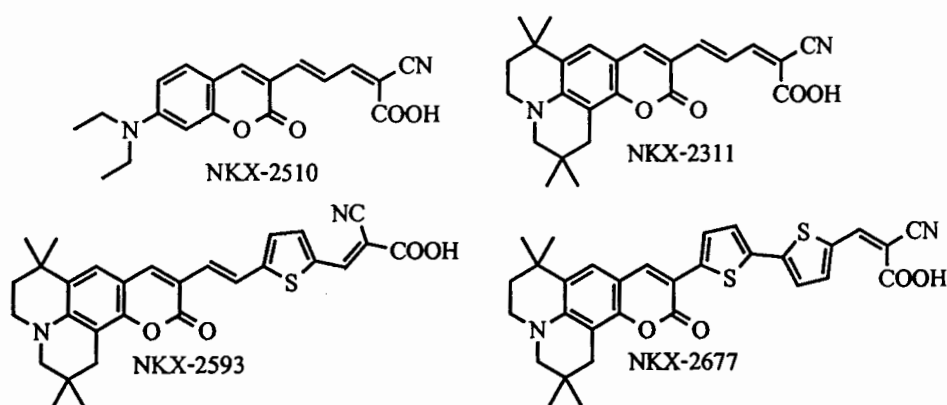


Figure 1.7 Chemical structures of coumarin derivative dyes

Phenothiazine derivative dyes as T2-1 have been successfully synthesised and used as light harvesting material in dye-sensitized solar cells. The device performance is 5.5% (with short-circuit photocurrent density (J_{sc}) = 10.9 mA cm⁻², open-circuit photovoltage (V_{oc}) = 712 mV, and fill factor (ff) = 0.71). [54] In 2010, Tain et al. continued his

work with phenothiazine by adding thiophene unit (TH208) as linker which improve the power conversion efficiency to 6.4% at AM 1.5 G. [55] A year later, Kim et al. compared the effect of the π -bridge using furan and thiophene (SH-6 and SH-7), they found that furan shows a better performance at $\eta = 6.58\%$ (SH-7 at $\eta = 6.32\%$) due to the lower resonance energy and flatter structure. [56]

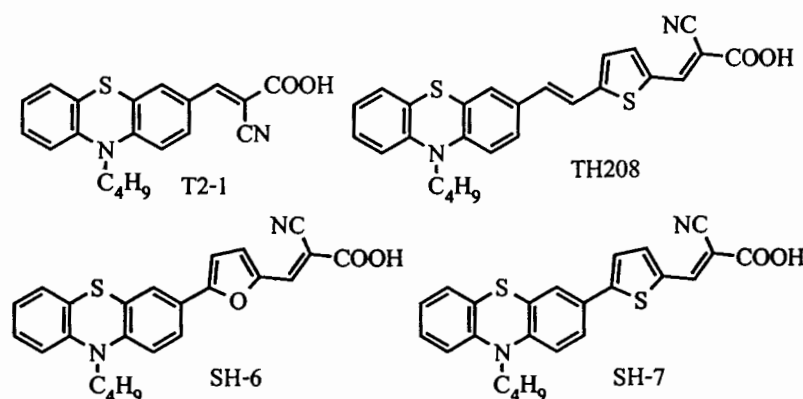


Figure 1.8 Chemical structures of phenothiazine dyes

1.1.4 Conjugated polymer nanoparticles

Highly fluorescent nanoparticles have been demonstrated in a wide range of applications such as high-throughput screening, ultrasensitive assays, live cell imaging, and intracellular dynamics. [57-60] Currently available fluorescent nanoparticles include colloidal inorganic semiconductor quantum dots, [60, 61] dye-loaded latex spheres, [62] and dye-doped silica colloids. [63] These nanoparticles possess high brightness and improved photostability as compared to conventional fluorescent dyes. [64] Conjugated polymer nanoparticles can be prepared using a variety of methods, including nano-precipitation, [65-69] miniemulsion dispersion, [70-72] mini-emulsion polymerisation, [73-75] self-assembly of polymer brushes, [76] and dendrimer-based strategies. [77]

1.1.4.1 Emulsion polymerisation

Emulsion polymerisation is a unique chemical process widely used to produce waterborne resins with various colloidal and physicochemical properties, which is mostly used for radical polymerisation. This heterogeneous free radical polymerization process involves emulsification of the relatively hydrophobic monomer in water by an oil-in-water emulsifier, followed by the initiation reaction with either a water-insoluble initiator (e.g. sodium persulfate (NaPS)) or an oil-soluble initiator (2,2'-azobisisobutyronitrile (ASBN)). [78]

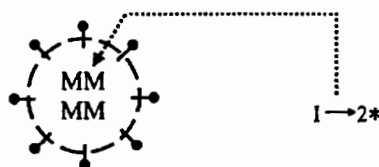
Priest [79], Roe [80], and Fitch and Tsai [81] proposed the homogeneous nucleation mechanism for the formation of particle nuclei in the continuous aqueous phase, as shown

schematically in Figure 1.9. First, waterborne initiator radicals are generated by the thermal decomposition of initiator and they can grow in size via the propagation reaction with those monomer molecules dissolved in the aqueous phase. The oligomeric radicals then become water-insoluble when a critical chain length is reached. The hydrophobic oligomeric radical may thus coil up and form a particle nucleus in the aqueous phase. This is followed by formation of stable primary particles via the limited flocculation of the relatively unstable particle nuclei and adsorption of surfactant molecules on their particle surfaces. The surfactant species required to stabilise these primary particles come from the aqueous phase and is adsorbed by the monomer droplet surfaces. The ideas above were incorporated into the following kinetic model developed by Fitch and Tsai [81]

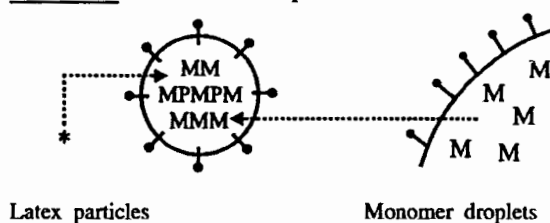
$$dN_p/dt = b\rho_i - R_c - R_f \quad (5)$$

where t is the reaction time, ρ_i the rate of generation of free radicals in the aqueous phase, b a parameter that takes into account the aggregation of oligomeric radicals, R_c the rate of capture of free radicals by the particles, and R_f the rate of flocculation of the particles.

Interval I: Nucleation of monomer-swollen micelles



Interval II: Growth of latex particles



Interval III: Consumption of residual monomer

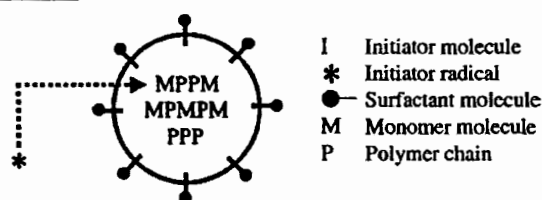


Figure 1.9 A schematic representation of the micelle nucleation model [78]

1.1.4.2 Mini-emulsion polymerisation

This is the most common method used in the synthesis of conjugated

nanoparticles. Using this method illustrated in Figure 1.10, Landfester and co-workers prepared nanoparticles from various polymers including conjugated polymers. [70, 72, 82, 83] To prepare CPNs, the polymer is dissolved in a water immiscible organic solvent and then the resulting solution is injected into an aqueous solution of an appropriate surfactant. [84] The mixture is stirred rapidly by ultrasonication to form stable mini-emulsions containing small droplets of the polymer solution. The organic solvent is evaporated to obtain a stable dispersion of polymer nanoparticles in water. The size of nanoparticles could vary from 30 nm to 500 nm depending on the concentration of the polymer solution. However, the droplets could be destabilized by Ostwald ripening as well as the flocculation caused by the coalescence of droplets. To prevent flocculation appropriate surfactants are used, while Ostwald ripening can be suppressed by the addition of a hydrophobic agent (a hydrophobe) to the dispersed phase. The hydrophobe promotes the formation of an osmotic pressure inside the droplets that counteracts the Laplace pressure (the pressure difference between the inside and the outside of a droplet) preventing diffusion from one droplet to the surrounding aqueous medium.

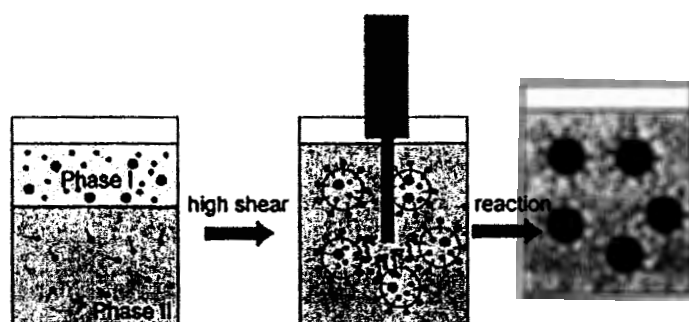


Figure 1.10 The preparation of nanoparticles using the mini-emulsion method [72]

1.2 Aims

Aims of this work are as followed;

- (1) To synthesise novel organic materials as show in Figure 1.11.
- (2) To characterize and to study the electronic, electrochemical and thermal properties of the target molecules.
- (3) To investigate their potential application as organic semiconductor.

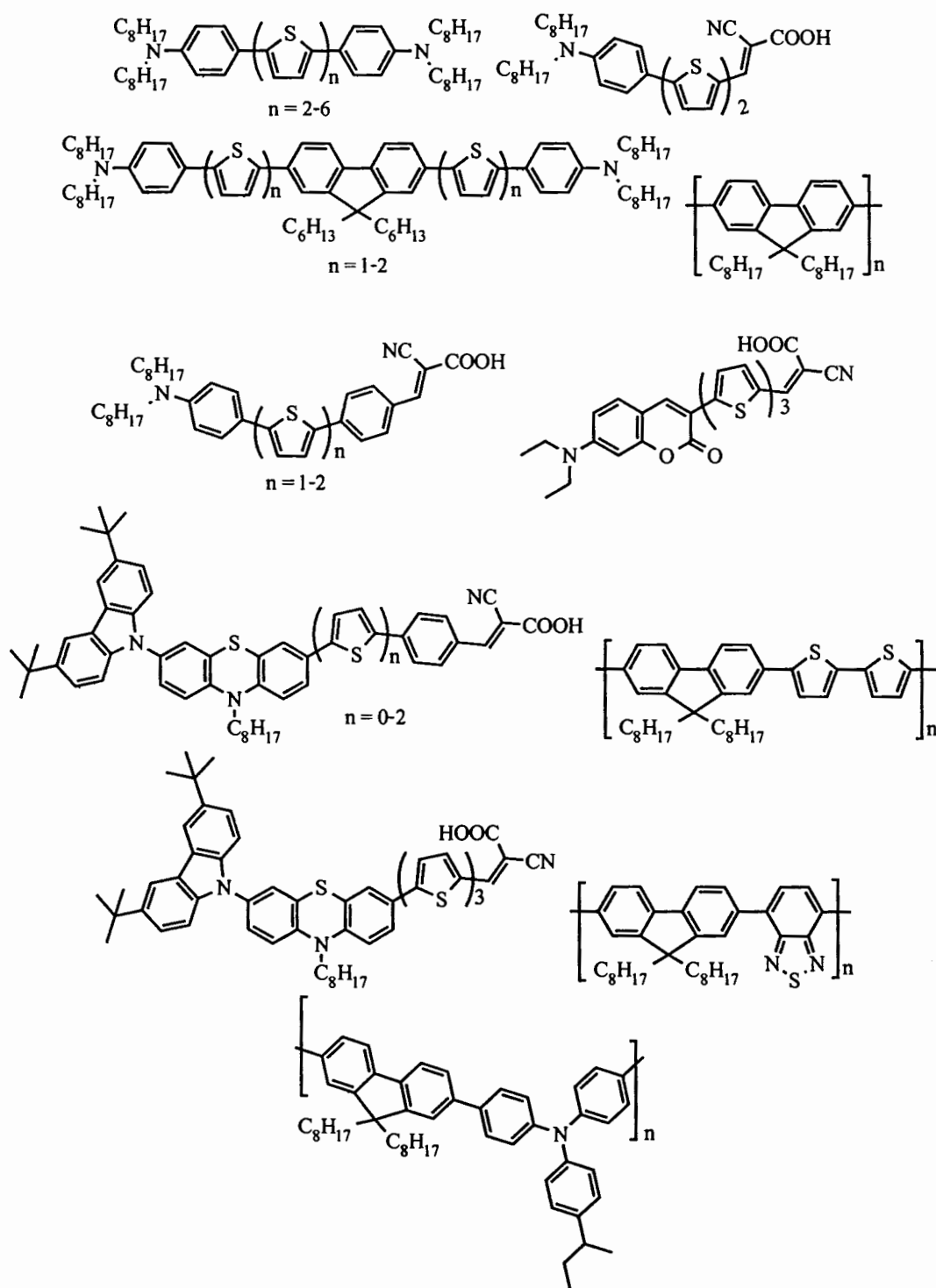


Figure 1.11 Chemical structure of target molecules



CHAPTER 2

SYNTHESIS AND CHARACTERIZATION OF OLIGOTHIOPHENES FOR APPLICATION IN ORGANIC FIELD-EFFECT TRANSISTORS (OFETs)

2.1 Introduction

The most important material properties for semiconductors that comprise the active materials in organic field-effect transistor are high mobility, low “off-conductivity”, stability and processibility. The energy level of the material should match with the energy level of the electrodes in order to provide for facile hole injection from electrode materials at accessible voltages, while the molecular shape ensures useful mobility by virtue of the intermolecular overlap and molecular orientation in a solid film. [85]

Poly- and oligothiophene-based compounds are widely used within the field of organic electronics. [86-88] They display remarkable conductivity with excellent chemo- and thermostability, and they are, in general, readily synthesised or structurally modified to meet electronic and spectroscopic requirements. Moreover, it was shown that the use of triarylamine subunits had a positive influence on both the conductivity and the tendency to form amorphous glasses. Thus, combinations of oligothiophenes with triaryl moieties are widely used in all fields of organic electronics. [89-91] Thieno[3,2-b]thieno[20,30:4,5]thieno[2,3-d]thiophene (tetrathienoacene; TTA) is a four thiophene-fused system which is widely used as semiconductor in OFETs. Liu et al. reported the OFETs using TTA with phenyl end-capped (1a-1c). The device using 1a reveal the best performance with mobilities as high as $0.14 \text{ cm}^2 \text{ V}^{-1} \text{ s}^{-1}$ and an on/off ratio up to 10^6 . This good performance related to good film morphology. [92]

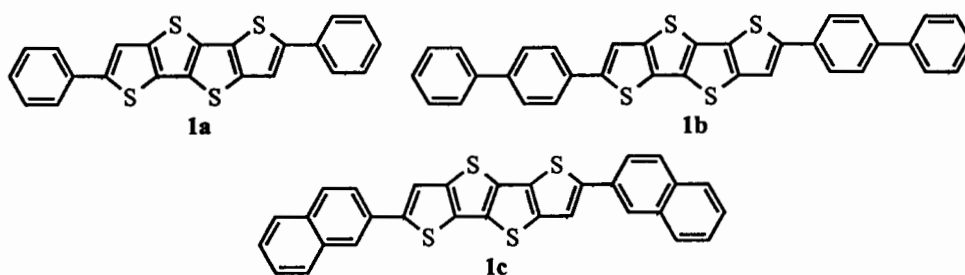


Figure 2.1 The chemical structure of TAA derivatives

The OFETs fabricated with thiophene-phenylene oligomer with high mobility was reported at charge mobility at $1.4 \times 10^{-2} \text{ cm}^2 \text{ V}^{-1} \text{ s}^{-1}$ and an on/off ratio at 2×10^3 . [93] The

incorporation of phenylene unit into the thiophene backbone results in a small lowering of the HOMO energy and it has been shown that this lowering is accompanied by reduction in the off currents, thus increasing the device on/off ratio.

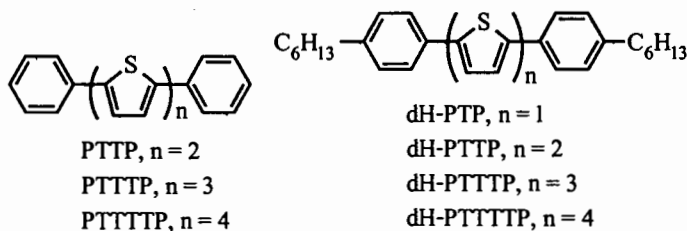
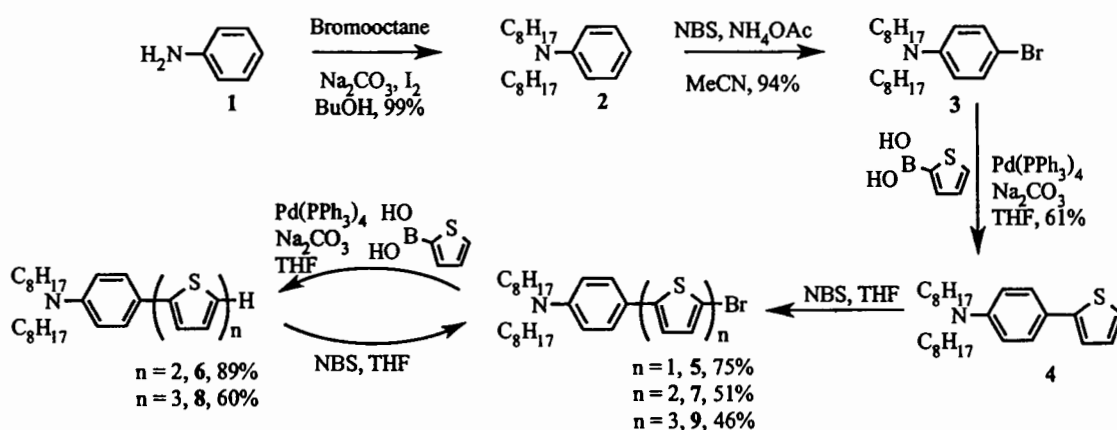


Figure 2.2 The chemical structure of thiophene-phenylene oligomers

In order to improve the processibility of OFETs, a new series of *n*-hexyl-substituted thiophene-phenylene oligomers was synthesised and used in p-channel transistors. The transistor based on dH-PTTP shows the best performance at $0.02 \text{ cm}^2 \text{ V}^{-1} \text{ s}^{-1}$ and an on/off ratio at 2×10^4 under drop-casting film process. [94]

In this work we reported the synthesis and characterization of oligothiophenes with dialkylaniline end-capped. The alkyl chains at the N-position of aniline moieties are expected to induce the crystal order in solid state and also to improve the solubility in common organic solvents. The optical, electrochemical, thermal properties and computational calculation are also evaluated.

2.2 Synthesis



Scheme 2.1 The synthetic route of intermediates

incorporation of phenylene unit into the thiophene backbone results in a small lowering of the HOMO energy and it has been shown that this lowering is accompanied by reduction in the off currents, thus increasing the device on/off ratio.

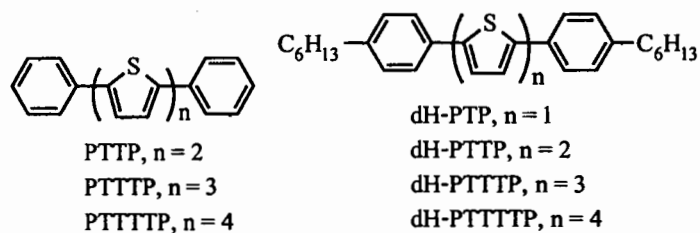
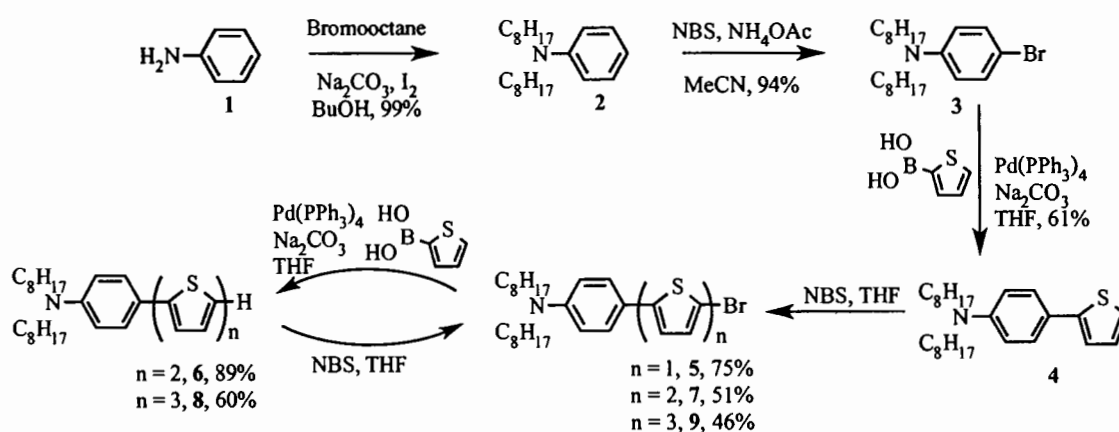


Figure 2.2 The chemical structure of thiophene-phenylene oligomers

In order to improve the processibility of OFETs, a new series of *n*-hexyl-substituted thiophene-phenylene oligomers was synthesised and used in p-channel transistors. The transistor based on dH-PTTP shows the best performance at $0.02 \text{ cm}^2 \text{ V}^{-1} \text{ s}^{-1}$ and an on/off ratio at 2×10^4 under drop-casting film process. [94]

In this work we reported the synthesis and characterization of oligothiophenes with dialkylaniline end-capped. The alkyl chains at the N-position of aniline moieties are expected to induce the crystal order in solid state and also to improve the solubility in common organic solvents. The optical, electrochemical, thermal properties and computational calculation are also evaluated.

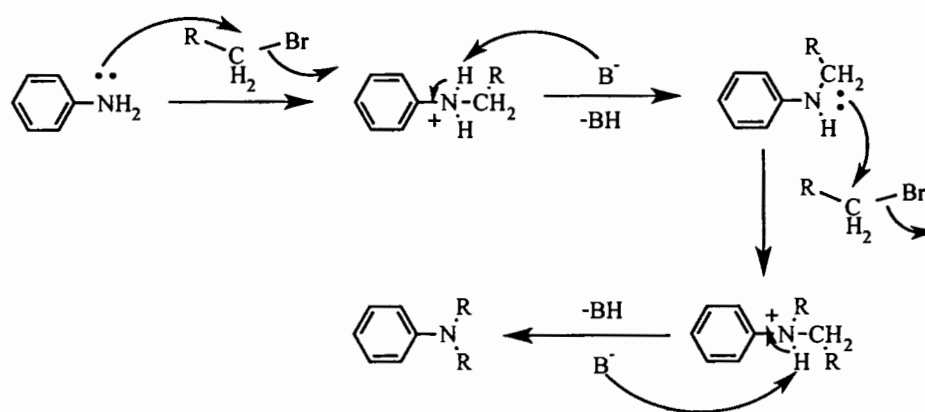
2.2 Synthesis



Scheme 2.1 The synthetic route of intermediates

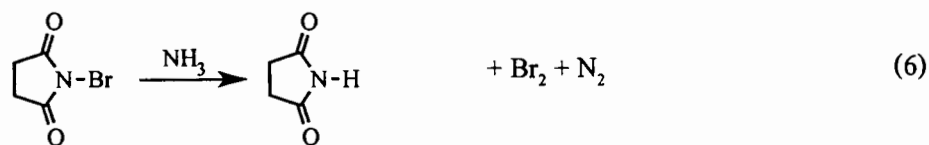
To obtain the target oligothiophenes, the synthesis part was separated into two parts. Firstly, the intermediates were synthesised as shown in Scheme 2.1. Then the desired molecules were synthesised.

N,N-dioctylaniline (**2**) was obtained by reacting aniline with bromooctane in the presence of Na_2CO_3 in BuOH [95] afforded *N,N*-dioctylaniline in quantitative yield. Under this condition, substitution of aniline was occurred under nucleophilic substitution ($\text{S}_{\text{N}}2$) as explained mechanism in Scheme 2.2. The $^1\text{H-NMR}$ of **2** showed a double peak at chemical shift of 3.33 ppm (4 protons, $J = 6.9$ Hz) assigned as the protons of the alkyl chain next to the N-atom and a double peak at chemical shift of 6.71 ppm (2 protons, $J = 88.6$ Hz) assigned as the aromatic protons of the phenyl ring.



Scheme 2.2 Proposed mechanism of alkylation of aniline

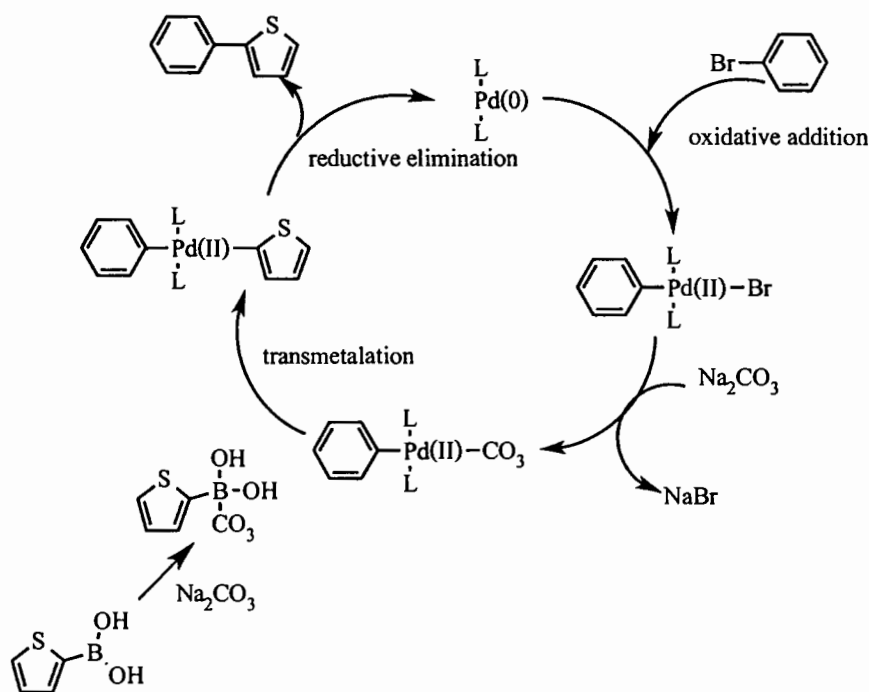
In order to obtain compound **3**, the dialkylaniline was brominated with NBS in the present of ammonium acetate as catalyst in acetonitrile to give 4-bromo-*N,N*-dioctylaniline in quantitative yield. [96] Regarding mechanism of the reaction it may be mentioned that the reaction of NBS and NH_4OAc is known to produce HOAc and HBr which can polarise the N-Br bond of NBS and facilitate the nuclear bromination of phenols and anilines. [97] A possible mechanism for generation of Br_2 and HBr is shown in Scheme 2.3.



Scheme 2.3 Proposed mechanism of Br_2 generation

In the presence of NH_4OH the reaction of aniline with NBS requires shorter time to form the product and the yield and the selectivity were higher. The chemical structure of brominated product **3**, after purification, was confirmed by $^1\text{H-NMR}$ analysis. The $^1\text{H-NMR}$ spectrum shows a doublet peak at chemical shift of 6.48 ppm (2 protons, $J = 6.7$ Hz) assigned as the proton of aniline, which is next to Br.

The bromination resultant was brought to react with 2-thiophene boronic acid under Suzuki coupling condition. Under this condition, $\text{Pd}(\text{PPh}_3)_4$ was used as catalyst, Na_2CO_3 as base and THF as solvent afforded the desired product **4** in 61%. The reaction follows a three-step mechanism cycle, oxidative addition, transmetalation and reductive elimination as described in Scheme 2.4. The chemical structure of 4-thiophenyl-*N,N*-dioctylaniline was confirmed by $^1\text{H-NMR}$ analysis. The $^1\text{H-NMR}$ spectrum of **4** shows a doublet peak at chemical shift of 7.05 ppm (1 proton, $J = 4.2\text{Hz}$) assigned as the a proton at C-5 atom of the thiophene ring and a doublet peak at chemical shift of 6.65 ppm (2 proton, $J = 8.4$ Hz) assigned as the protons of phenyl ring.

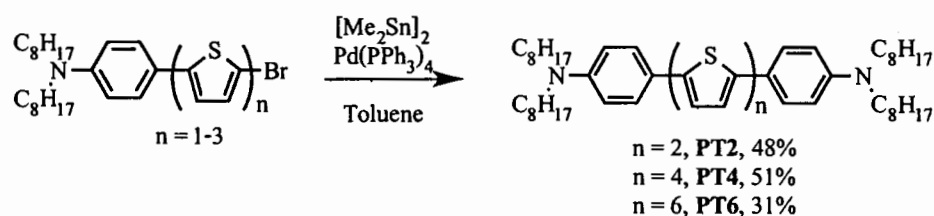


Scheme 2.4 Proposed mechanism of Suzuki coupling

5-Bromo-4-thiophenyl-*N,N*-dialkylaniline was obtained by bromination of **4** with NBS in THF. The crude product was purified using column chromatography (silica gel) afforded the brominated product **5** in 75% yield. The chemical structure of the resultant was confirmed by $^1\text{H-NMR}$ analysis. The doublet peak at chemical shift of 6.85 ppm (1 proton, $J = 3.6$ Hz), assigned as the proton of thiophene next to Br-atom, was found.

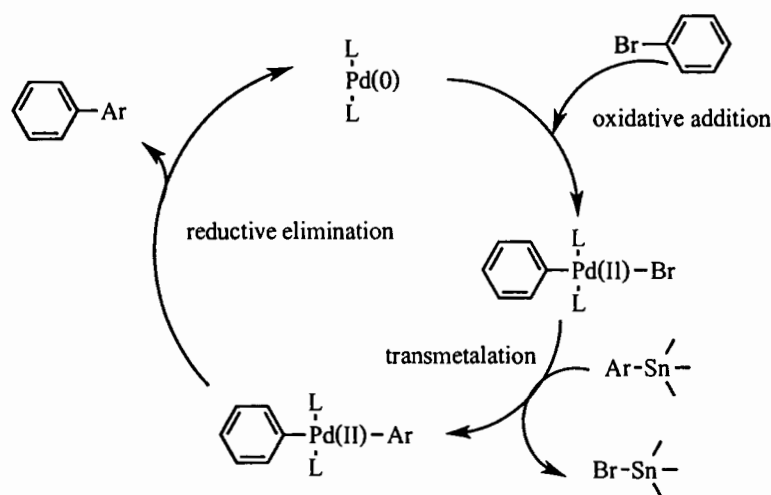
In order to get more thiophene units, the Suzuki coupling reaction and bromination were repeated. The percent yield of 4-(2,2'-bithiophen)-*N,N*-dioctylaniline and 4-(2,2':5',2''-terthiophen)-*N,N*-dioctylaniline were 89% and 60%, respectively. In the other hand, the percent yield of bromination reaction to give 4-(5'-bromo-[2,2'-bithiophen])-*N,N*-dioctylaniline and 4-(5''-bromo-[2,2':5',2''-terthiophen])-*N,N*-dioctylaniline were 51% and 46%, respectively. All of desired molecule structures were confirmed by $^1\text{H-NMR}$ analysis.

The oligothiophenes molecules were successfully synthesised using Suzuki coupling reaction. The even number of thiophene units was obtained using Stille coupling reaction as depicted in Scheme 2.5. [98] The brominated products with various thiophene moieties, **5**, **7**, and **9**, were reacted with $[\text{Me}_2\text{Sn}]_2$ in the presence of $\text{Pd}(\text{PPh}_3)_4$ as catalyst in toluene at reflux to give the target molecules **PT2**, **PT4**, and **PT6** in 48%, 51% and 31%, respectively.



Scheme 2.5 Synthetic route of **PT2**, **PT4** and **PT6**

The mechanism of Stille reaction follows three steps consisted of oxidative addition, transmetalation and reductive elimination, respectively. The recently proposed mechanism is shown in Scheme 2.6.

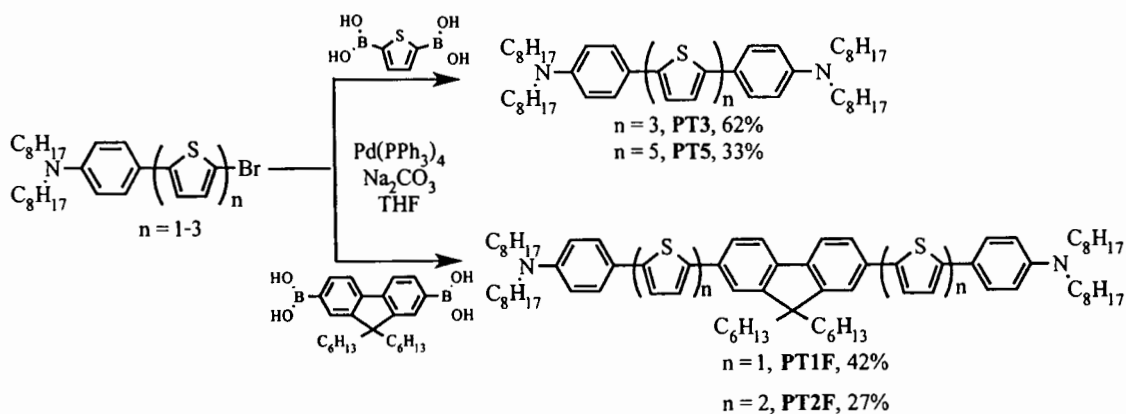


Scheme 2.6 The mechanism of Stille coupling reaction

The chemical structure of **PT2**, **PT4** and **PT6** were confirmed by $^1\text{H-NMR}$ analysis. The $^1\text{H-NMR}$ of **PT2** shows a doublet doublet peak at chemical shift of 6.61 ppm (4 protons, $J =$

6.13 Hz) assigned as the protons of phenyl rings and a doublet peak at chemical shift of 7.12 ppm (2 protons, $J = 3.5$ Hz) assigned as the protons of thiophene units. **PT4** shows a singlet peak at chemical shift of 6.65 ppm (4 protons) assigned as the protons of phenyl rings and a doublet peak at chemical shift of 7.09 ppm (8 protons, $J = 8.4$ Hz) assigned as the protons of thiophene units. **PT6** shows a doublet peak at chemical shift of 6.61 ppm (4 protons, $J = 8.4$ Hz) assigned as the protons of phenyl rings and multiplet and doublet peaks at chemical shift of 7.06-7.16 ppm (12 protons) assigned as the protons of thiophene rings. The MALDI mass spectrometry analysis shows the molecular ion peaks centered at $m/z = 961$ for **PT4**, 1124 for **PT6** corresponding to an expect M^+ mass ion of oligothiophenes derivatives. The product was soluble in chlorinated solvents and tetrahydrofuran at room temperature.

The odd number of thiophene units and the fluorene core were synthesised by Suzuki coupling reaction as depicted in Scheme 2.7. The reaction underwent between the brominated compound and boronic acid compound using $\text{Pd}(\text{PPh}_3)_4$ as catalyst, Na_2CO_3 as base in THF. The chemical structure of target molecules was confirmed by $^1\text{H-NMR}$ analysis. The $^1\text{H-NMR}$ spectrum of **PT3** shows a doublet peak at chemical shift of 6.55 ppm (4 protons, $J = 5.0$ Hz) assigned as the protons of phenyl ring and a triplet peak at chemical shift of 6.69 ppm (6 protons, $J = 5.0$ Hz) assigned as the protons of thiophene units. **PT5** shows a doublet peak at chemical shift of 6.64 (4 protons, $J = 8.7$ Hz) assigned as the protons of phenyl rings and a multiplet peak at chemical shift of 7.08 ppm (10 protons) assigned as the protons of thiophene units. **PT1F** shows a doublet peak at chemical shift of 6.61 ppm (4 protons, $J = 8.4$ Hz) assigned as the protons of phenyl rings and doublet peak at chemical shift of 7.31 (2 protons, $J = 3.6$ Hz) assigned as the protons of fluorene ring. Whilst **PT2F** shows a doublet peak at chemical shift of 6.63 ppm (4 protons, $J = 8.4$ Hz) assigned as the protons of phenyl rings and doublet peak at chemical shift of 7.45 (4 protons, $J = 8.1$ Hz) assigned as the protons of fluorene ring.



Scheme 2.7 synthetic routes of **PT3**, **PT5**, **PT1F** and **PT2F**

The MALDI mass spectrometry analysis shows the molecular ion peaks centered at $m/z = 879$ for **PT3**, 1044 for **PT5**, 1129 for **PT1F** and 1294 for **PT2F** corresponding to an expected M^+ mass ion of oligothiophenes derivatives. The products were soluble in chlorinated solvents and tetrahydrofuran at room temperature.

2.3. Optical properties

The optical properties of the oligothiophenes derivatives were investigated in dry dichloromethane solution. The absorption spectra of **PT2**, **PT3**, **PT4**, **PT5**, **PT6**, **PT1F** and **PT2F** are shown in Figure 2.3 and 2.4. The desired oligothiophenes exhibited a strong UV-visible absorption band at 421, 438, 457, 464, 433, 423 and 443 nm, respectively, which are the π - π^* transition of the thiophene moieties. [99] The red-shift occurred due to longer conjugation of the prolonged thiophene units.

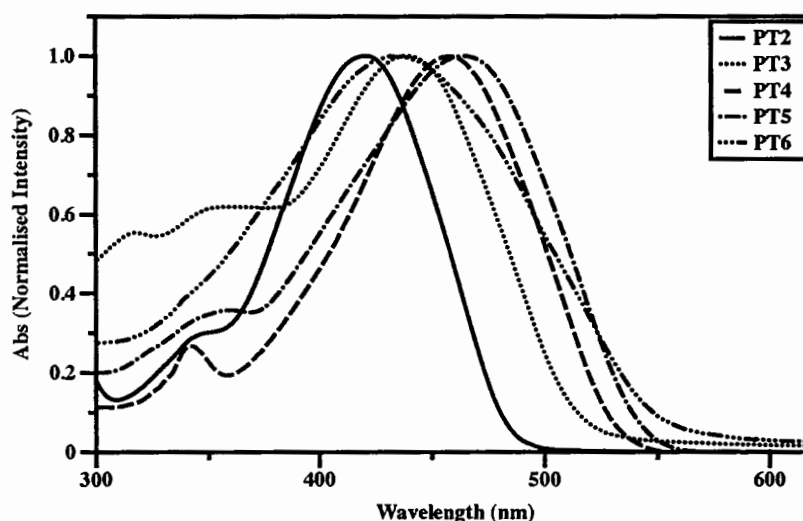


Figure 2.3 Absorption spectra of **PT2**, **PT3**, **PT4**, **PT5** and **PT6**

By comparison, **PT3** to **PT1F**, **PT3** shows an absorption peak at 438 nm while **PT1F** shows a maximum peak at 423 nm and **PT5** to **PT2F**. **PT5** exhibits an absorption peak at 464 nm while **PT2F** shows an absorption peak at 443 nm indicating that the thiophene unit can be used to extend the conjugation of molecules.

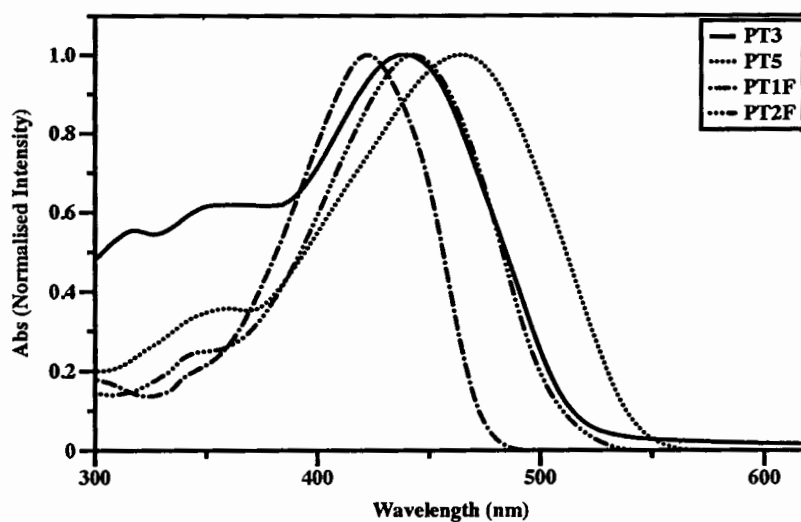


Figure 2.4 Absorption spectra of PT3, PT5, PT1F and PT2F

The photoluminescence spectra of target molecules excited at the maximum absorption wavelength are depicted in Figure 2.5 and 2.6. The desired molecules, PT2, PT3, PT4, PT5, PT6, PT1F and PT2F exhibited maxima peaks at 495, 528, 543, 549, 549, 491 and 530, respectively, which is related to their absorption wavelength.

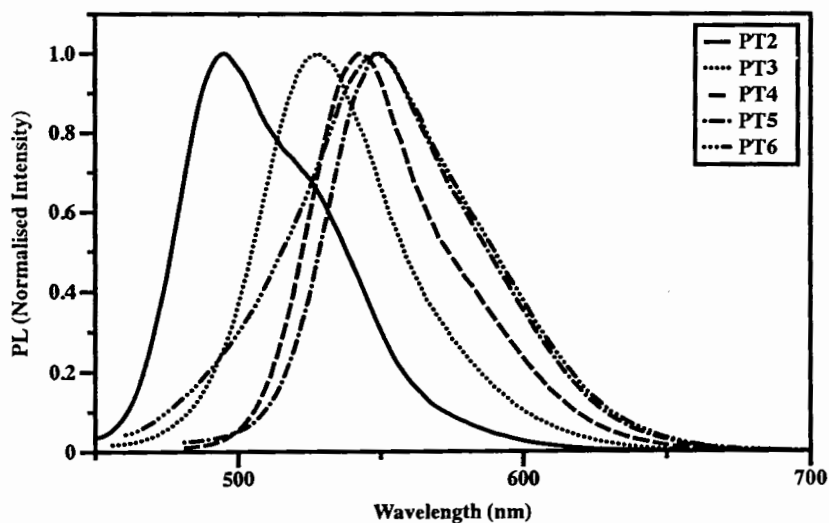


Figure 2.5 Fluorescence spectra of PT2, PT3, PT4, PT5 and PT6

According to the fluorescence spectra, PT2 shows the shortest absorption band since it is the smallest molecule with the shortest conjugation length. The energy gap of the PT series is decreasing when the number of thiophenes increases due to extended conjugation. PTF series also shows the same trend that PT2F exhibits a lower energy gap than PT1F.

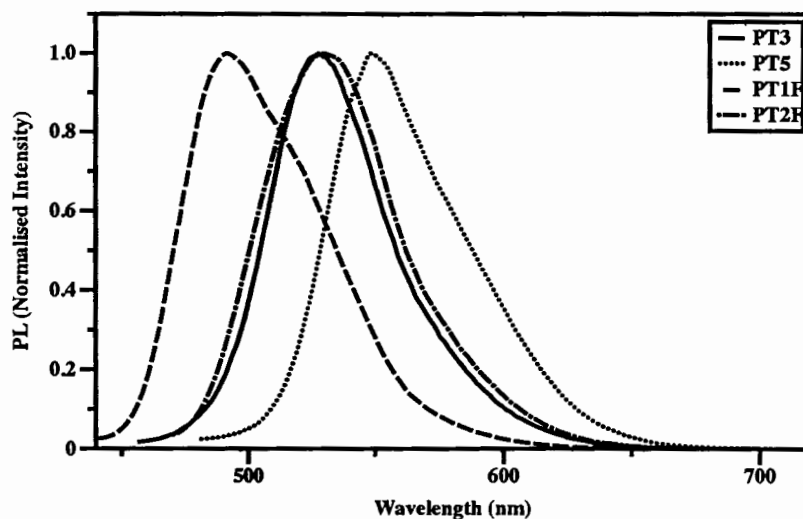


Figure 2.6 Fluorescence spectra of PT3, PT5, PT1F and PT2F

Table 2.1 The summary of Absorption and fluorescence data of PT2, PT3, PT4, PT5, PT6, PT1F and PT2F

Compound	λ_{\max} of absorbance (nm) ^a	λ_{\max} (nm) and log ϵ	λ_{\max} of emission (nm) ^b
PT2	421	421 (4.65)	495
PT3	438	438 (3.95)	528
PT4	457	457 (4.95)	543
PT5	464	464 (4.10)	549
PT6	433	433 (4.63)	549
PT1F	423	423 (4.11)	491
PT2F	443	443 (5.02)	530

^aMeasured in dilute CH_2Cl_2 solution, ^bExcited at the absorption maxima

2.3 Electrochemical property

Cyclic voltammetry (CV) is a technique measuring the current versus potential of a solution of a compound. A typical electrochemical cell consists of three electrodes; working, counter and reference electrodes, controlled by a potentiostat. The potential difference is applied between the working and counter. The third electrode is the reference electrode, through which no current flows, and from which the potentials of the other electrodes are measured. Apart from the solutions, the solute in this work contains an electrolyte to decrease the resistance.

In the CV experiment the potential is varied with time, either in a positive or negative

direction, in a linear sweep to a potential E_p , called the switching potential, and then back to the starting potential (Figure 2.7a). During the linear sweep potential, the current is measured and the presence of a peak during the sweep indicates that redox process has occurred (Figure 2.7b).

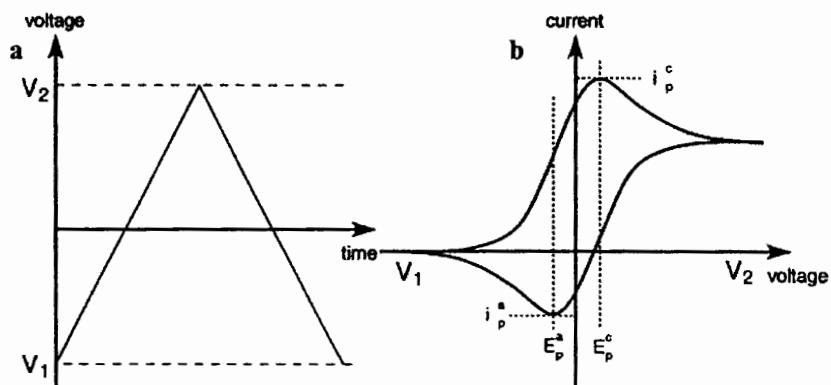


Figure 2.7 a) the triangular potential sweep used for CV b) a quasi-reversible CV trace for a redox process

A negative sweep of the potential causes reduction and positive sweep causes oxidation. If there is a reverse peak of the trace observed in the forward potential sweep, then redox process is chemically reversible. This means the reduced or oxidised species is stable or the kinetics of the electron transfer process between the electrodes and the solution are fast on the timescale of the experiment. If there is no reverse peak then the redox process is chemically irreversible. The irreversible behavior results from either a following chemical processing occurring on a time scale fast compared with the timescale of the experiment, or due to heterogeneous electron transfer which is slow compared to the timescale of the experiment. In CV, with a reversible oxidation and reduction process, the difference in potential (ΔE_p) between the cathodic and anodic peaks for a one-electron process at 25 °C is 57 mV and for a two-electron process $\Delta E_p = 28.5$ mV. When ΔE_p is significantly greater than 57 mV at 25 °C but the oxidation and reduction in chemically reversible, then the process is termed quasi-reversible behavior occurs when reduced or oxidised species is stable, but the rate of heterogeneous electron transfer between the compound and the electrode is slow in comparison to the timescale of the experiment. Increasing the scan rate of the potential sweep can cause a reversible process to become a quasi-reversible process, while an irreversible process becomes reversible in case of prolonged scan rates.

In this work all CV experiments were performed in dry dichloromethane using a platinum wire counter electrode, a Ag/AgCl/NaCl reference electrode, and glassy carbon working electrode. The electrolyte used was tetra-n-butylammonium hexafluorophosphate and this was chosen because it is soluble in organic solvents. The concentration of the electrolyte in solution was 0.1 M, and the concentrations of the oligothiophenes derivatives in solution were in the range

0.5 mM-0.1 mM. It is important to use very dry solvents and to removed oxygen from the solution by degassing with an inert gas, as O_2 is a good scavenger of radicals and so many react with the oxidized and reduced species. The internal standard used in this work was the ferrocenium/ferrocene (Fc^+/Fc) couple, and the data presented is relative to this standard.

The values of $E_{1/2}$ of a redox couple are the average values of the cathodic and anodic potentials.

The cyclic voltammogram and different pulse voltammogram of the PT2 in dichloromethane solution at scan rate 0.05V/s are shown in Figure 2.8 and are summarized in Table 2.2. PT2 reveals three reversible oxidation waves with half-wave potential ($E_{1/2}$) at 0.42, 0.52 and 1.45 V vs Ag/Ag^+ , which are assigned as the formation of alkyylaniline radical cation and thiophene radical cation, respectively. No reduction wave was observed.

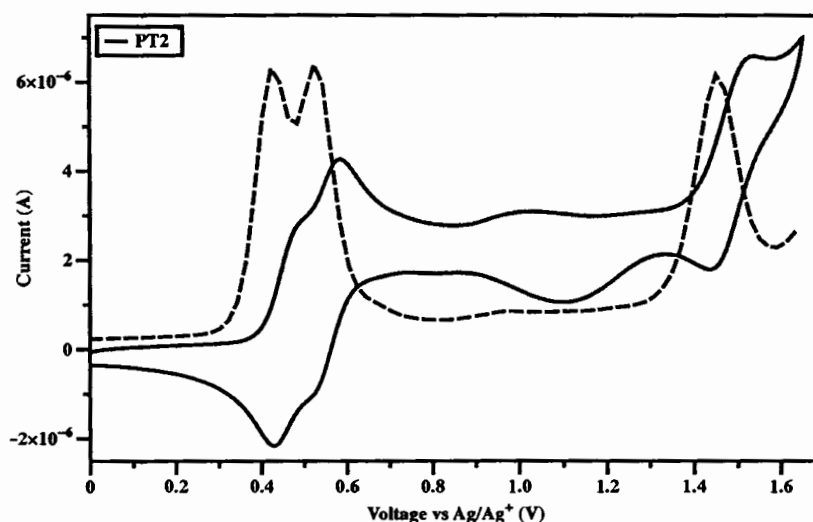


Figure 2.8 Cyclic voltammogram of target molecules PT2

The cyclic voltammograms and different pulse voltammogram of the PT3 in dichloromethane solution at scan rate 0.05V/s are shown in Figure 2.9 and are summarized in Table 2.2. PT3 shows three reversible oxidation waves with half-wave potential ($E_{1/2}$) at 0.46, 0.54 and 1.16 V vs Ag/Ag^+ , which are assigned as the formation of alkyylaniline radical cation and thiophene radical cation, respectively. No reduction wave was observed.

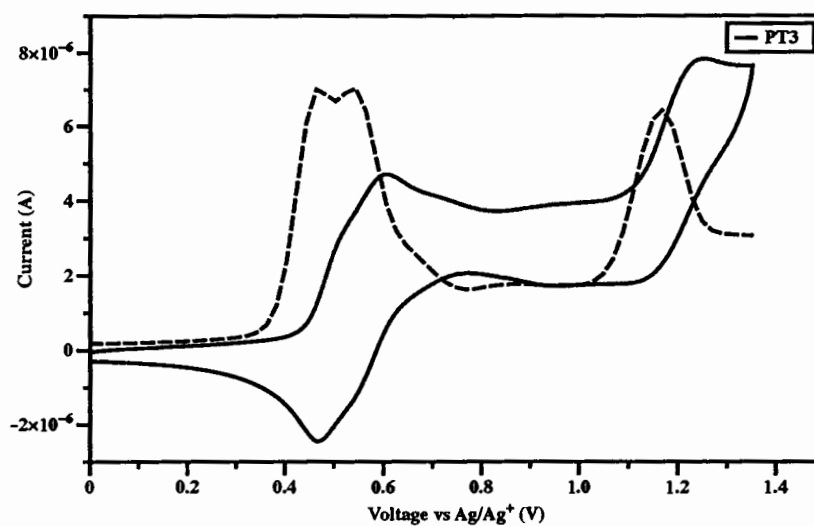


Figure 2.9 Cyclic voltammogram of target molecules PT3

The cyclic voltammograms and different pulse voltammogram of the PT4 in dichloromethane solution at scan rate 0.05V/s are shown in Figure 2.10 and are summarized in Table 2.2. PT4 shows three reversible oxidation waves with half-wave potential ($E_{1/2}$) at 0.48, 0.60 and 0.98 V vs Ag/Ag^+ , which are assigned as the formation of alkylaniline radical cation and thiophene radical cation, respectively. No reduction wave was observed.

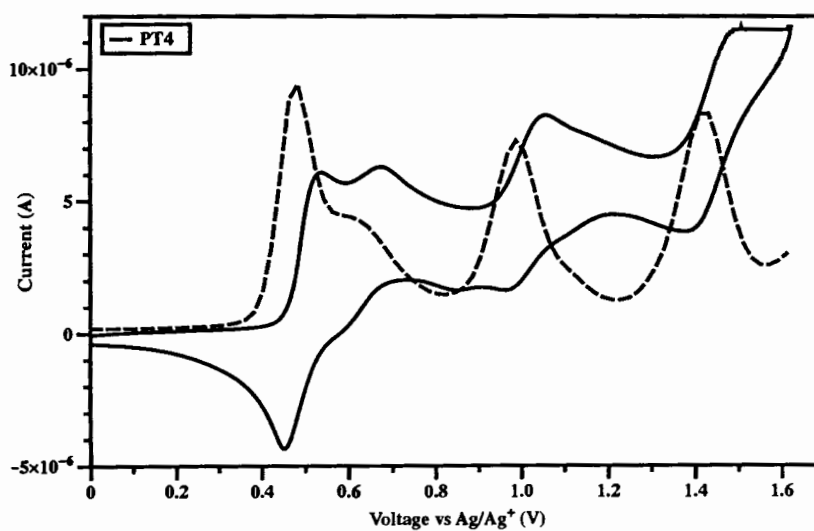


Figure 2.10 Cyclic voltammogram of target molecules PT4

The cyclic voltammograms and different pulse voltammogram of the PT5 in dichloromethane solution at scan rate 0.05V/s are shown in Figure 2.11 and are summarized in Table 2.2. PT5 shows three reversible oxidation waves with half-wave potential ($E_{1/2}$) at 0.46,

0.60 and 0.87 V vs Ag/Ag^+ , which are assigned as the formation of alkyaniline radical cation and thiophene radical cation, respectively. No reduction wave was observed.

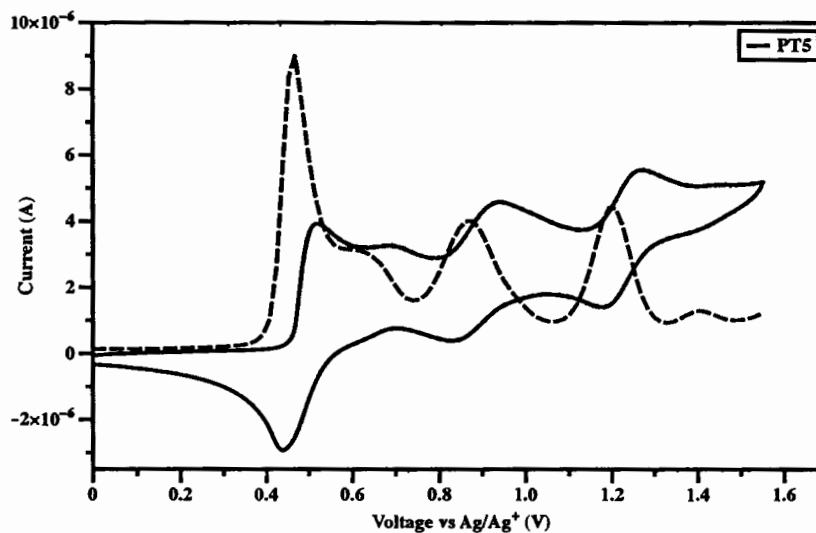


Figure 2.11 Cyclic voltammogram of target molecules PT5

The cyclic voltammograms and different pulse voltammogram of the PT6 in dichloromethane solution at scan rate 0.05V/s are shown in Figure 2.12 and are summarized in Table 2.2. The reversible oxidation waves with half-wave potential ($E_{1/2}$) at 0.54 and 1.08 V vs Ag/Ag^+ , which are assigned as the formation of alkyaniline radical cation and thiophene radical cation, respectively.

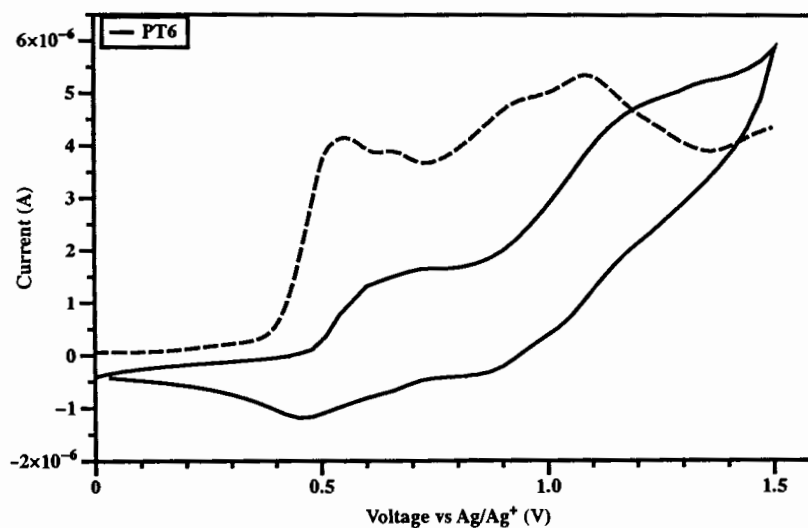


Figure 2.12 Cyclic voltammogram of target molecules PT6

The cyclic voltammograms and different pulse voltammogram of the **PT1F** in dichloromethane solution at scan rate 0.05V/s are shown in Figure 2.13 and are summarized in Table 2.2. **PT1F** shows three reversible oxidation waves with half-wave potential ($E_{1/2}$) at 0.59, 1.05 and 1.33 V vs Ag/Ag^+ , which are assigned as the formation of alkyaniline radical cation, thiophene radical cation and fluorene radical cation, respectively. No reduction wave was observed.

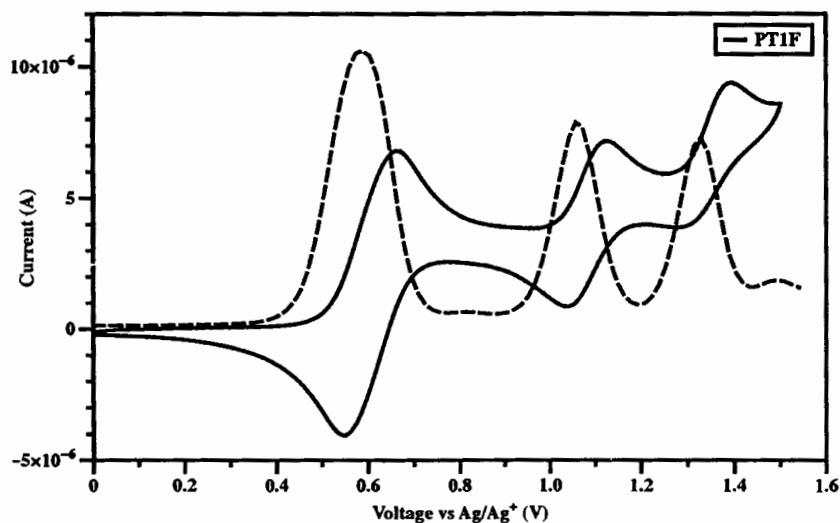


Figure 2.13 Cyclic voltammogram of target molecules **PT1F**

The cyclic voltammograms and different pulse voltammogram of the **PT2F** in dichloromethane solution at scan rate 0.05V/s are shown in Figure 2.14 and are summarized in Table 2.2. **PT2F** shows five reversible oxidation waves with half-wave potential ($E_{1/2}$) at 0.57, 0.74, 0.91, 1.01 and 1.43 V vs Ag/Ag^+ , which are assigned as the formation of alkyaniline radical cation thiophene radical cation and fluorene radical cation, respectively. No reduction wave was observed.

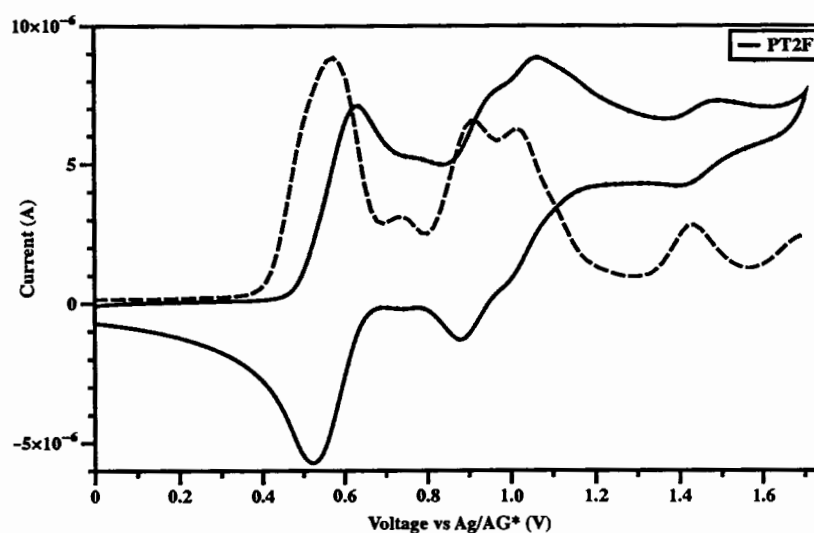


Figure 2.14 Cyclic voltammogram of target molecules PT2F

Table 2.2 Cyclic voltammetric results for PT2, PT3, PT4, PT5, PT6, PT1F and PT2F^a

Compound	E_{10} (V)	E_{20} (V)	E_{30} (V)	E_{40} (V)	E_{50} (V)	E_g^d (eV)	HOMO ^c (eV)	LUMO ^f (eV)
PT2	0.48 ^b (0.42) ^c	0.58 (0.52)	1.52 (1.45)	-	-	2.56	-4.82	-2.26
PT3	0.52 (0.46)	0.60 (0.54)	1.24 (1.16)	-	-	2.39	-4.87	-2.48
PT4	0.53 (0.48)	0.66 (0.60)	1.04 (0.98)	1.48 (1.43)	-	2.32	-4.88	-2.56
PT5	0.52 (0.46)	0.68 (0.60)	0.93 (0.87)	1.26 (1.19)	-	2.28	-4.90	-2.62
PT6	0.63 (0.54)	1.20 (1.08)	-	-	-	2.22	-4.89	-2.64
PT1F	0.66 (0.59)	1.12 (1.05)	1.38 (1.33)	-	-	2.56	-4.93	-2.37
PT2F	0.62 (0.57)	0.77 (0.74)	0.96 (0.91)	1.05 (1.01)	1.47 (1.43)	2.36	-4.91	-2.55

^aMeasured using a platinum rod counter electrode, a glassy carbon working electrode and a SCE reference electrode in CH_2Cl_2 containing $n\text{-Bu}_4\text{NPF}_6$ as a supporting electrolyte with scan rate of 0.05 V/s under argon atmosphere, ^bPeak potential, ^cHalf-wave potential, ^dEstimated from the onset

of the absorption spectra ($E_g = 1240/\lambda_{\text{onset}}$), ^cCalculated using the empirical equation from HOMO = $-(4.44 + E_{\text{onset}})$, ^fCalculated from LUMO = HOMO + E_g

2.5 Thermal property

Thermal Analysis is based upon the detection of changes in the heat content (enthalpy) or the specific heat of a sample with temperature. As thermal energy is supplied to the sample its enthalpy increases and its temperature rises by an amount determined, for a given energy input, by the specific heat of the sample. The specific heat of a material changes slowly with temperature in a particular physical state, but alters discontinuously at a change of state. As well as increasing the sample temperature, the supply of thermal energy may induce physical or chemical processes in the sample, e.g. melting or decomposition, accompanied by a change in enthalpy, the latent heat of fusion, heat of reaction etc. Such enthalpy changes may be detected by thermal analysis and related to the processes occurring in the sample. Thermal analysis encompasses a wide variety of techniques such as :

- the measurement of heating curves,
- dynamic adiabatic calorimetry,
- differential thermal analysis, DTA
- differential scanning calorimetry, DSC
- thermogravimetry, TG
- thermal mechanical analysis, TMA
- dynamic mechanical thermal analysis, DMTA

The thermal property of **PT4**, **PT5** and **PT6** were measured by differential scanning calorimetry (DSC) and thermogravimetric analysis (TGA) as solid samples. **PT2**, **PT3**, **PT1F** and **PT2F** were not investigated since the products are oil and semi-solid. The thermograms of oligothiophenes are shown in Figure 2.15 and 2.16 and are summarized in Table 2.3. **PT4** shows T_m transition at 237.60 °C indicating that the solid structure is crystalline phase. Moreover, **PT4** shows high degradation temperature at 271 °C. **PT5** shows glass transition (T_g) at 193.5 °C and quite high T_d at 277 °C. The **PT6** shows T_g transition at 203.9 °C while the TGA show 5% weight lost (T_d) at 227 °C. The results confirm that oligothiophenes is thermal stable.

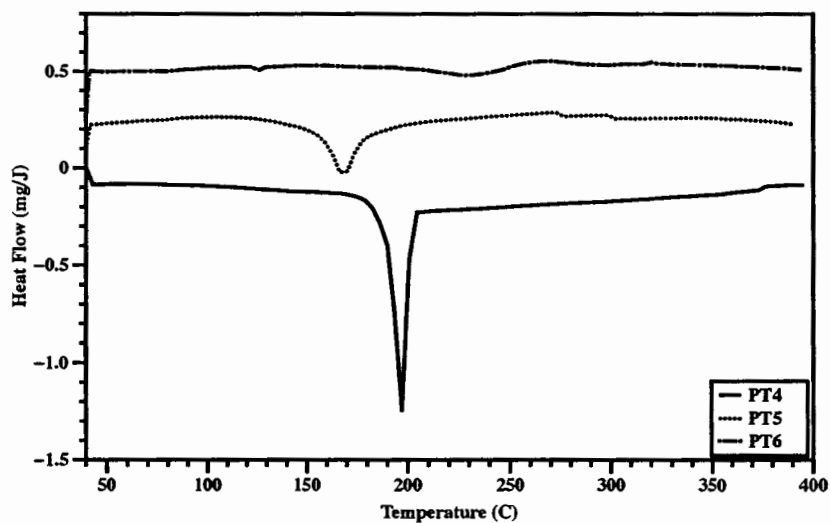


Figure 2.15 The thermograms of DSC plot of PT4, PT5 and PT6

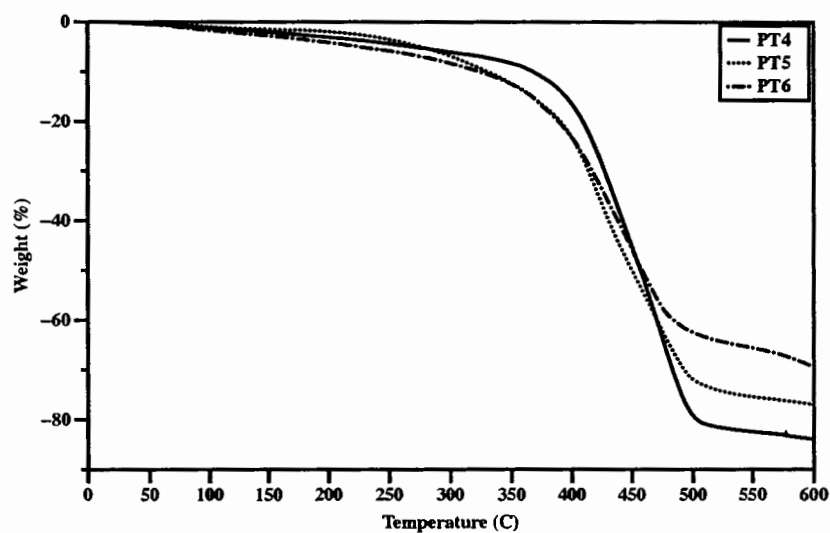


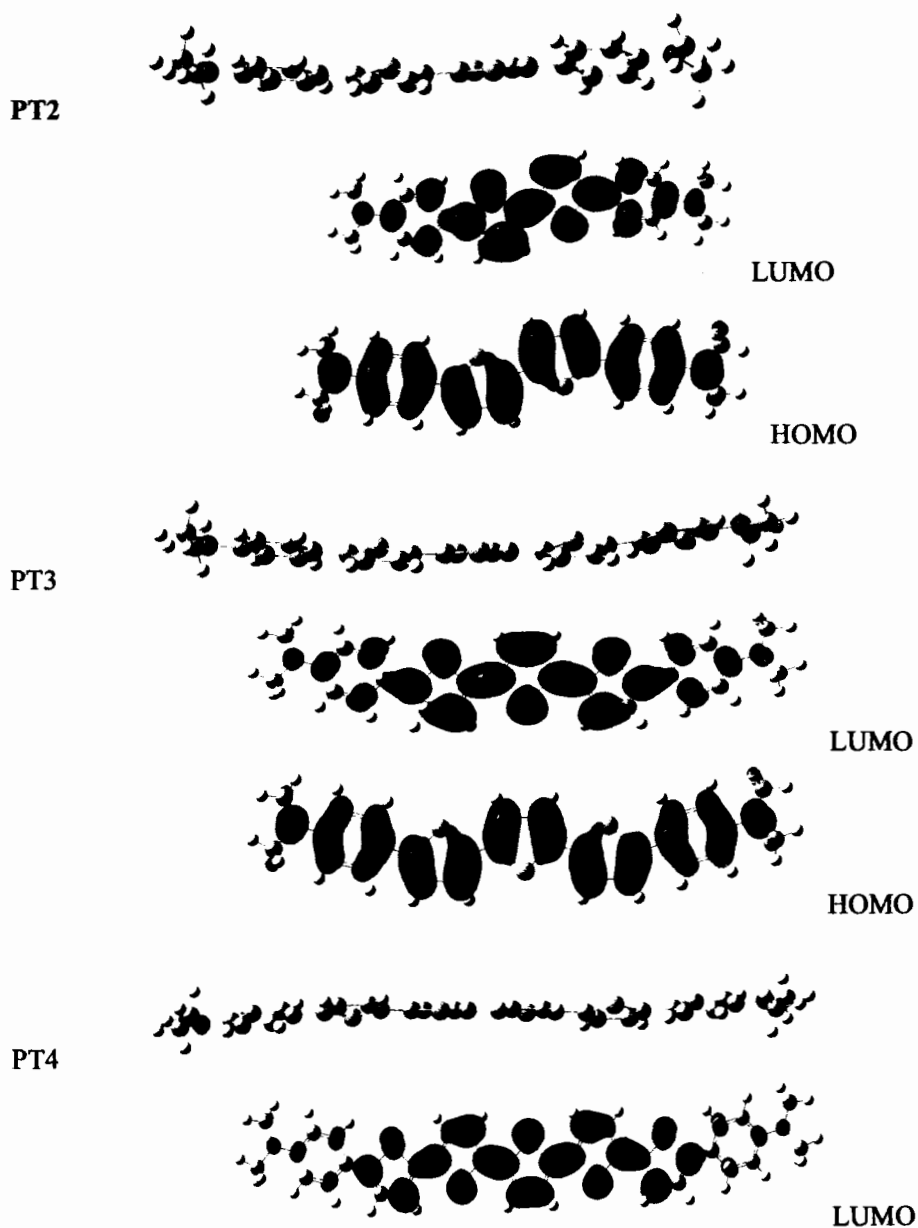
Figure 2.16 TGA plot of PT4, PT5 and PT6

Table 2.3 The DSC and TGA results of PT4, PT5 and PT6

Compound	T_g (°C)	T_m (°C)	T_c (°C)	T_d (°C)
PT4	-	237.60	-	271
PT5	193.50	-	-	277
PT6	203.90	-	-	227

2.6 Computational calculation

The optimized structure and frontier molecular orbital were calculated by DFT/B3LYP/6-31G9(d,p) method. According to the requirement of OFET materials, the molecular structure of the desired molecules should be planar. The optimized structure of oligothiophenes reveals that molecular structure of all target molecules is planar. At HOMO level the electrons distribute at π -conjugation backbone while LUMO level the electrons distribute at anti-bonding atom as shown in Figure 2.18.



HOMO



LUMO



PT16



HOMO



LUMO



PT6



HOMO



LUMO



PT5



HOMO





Figure 2.17 Optimized structure of oligothiophenes derivatives.

2.7 Conclusion

A series of oligothiophenes was successfully synthesised and characterized using combination of alkylation, bromination, Suzuki coupling and Stille coupling reactions. The optical properties in DCM solution reveal that the increasing of thiophene units affect to the absorption and emission wavelength in the trend of longer wavelength. All desired compounds show good reversible electrochemical property. **PT4**, **PT5** and **PT6** show a thermal stable at high temperature. Accordingly, the computational calculation shows the arrangement of molecules in planar.

CHAPTER 3

NOVEL DYE SENSITIZERS BASED ON ANILINE-THIOPHENE FOR DYE-SENSITIZED SOLAR CELLS (DSSCs)

3.1 Introduction

There are two main ways in which the efficiency of a DSSC can be improved: extend the light-harvesting region into the near-infrared (NIR), and lowering the redox potential of the electrolyte to increase V_{oc} . Using a dye that absorbs more wavelengths in the NIR, say to around 940 nm, while still to be able to generate and collect the charge carriers efficiently, could increase the current by over 40%.

Organic dyes have attracted much interest in recent years as they offer several advantages over their ruthenium-based predecessor including structural modification through rich synthetic protocols, lower cost large-scale production, reduced environmental and toxicity issues and high molar extinction coefficients. [100] One of the main goals in this area has been focused upon improving the power-conversion-efficiency of these systems through structural modification.[101] In general, these systems feature donor (D) and acceptor (A) systems separated by a π -conjugated bridge (D- π -A). For example, triphenylamine derivatives have been commonly utilised as the electron donor (D), whilst a cyanoacrylic acid moiety acts as the electron acceptor (A) and anchoring unit in the D- π -A structure. [102] Various π -conjugated bridges, such as benzene, thiophene and benzothiadiazole, have been introduced to broaden their absorption towards the near-infrared region. Interestingly, studies have shown that in addition to optimise the optical properties of the dye, the increase of the number of thiophene π -bridging units tends to result in an increase in power conversion efficiency. [103] Another important goal is to develop systems that may be accessed through short and simple synthetic routes for more widespread implementation in lower cost applications. [104]

Recently Al-Eid et al., presented aniline based metal free dyes were synthesised and characterized. The DSSCs based on dye 6 and 7 reveal that an increase of thiophene units decreases the oxidation and reduction potential and consequently the band gap of the molecule compared to 6. Furthermore, increasing the length of the conjugated spacer also affects on the properties of the DSSCs, with dye 7 providing a higher power conversion efficiency (PCE) compared to 6 ($\eta = 4.49$ versus 3.23%). [105]

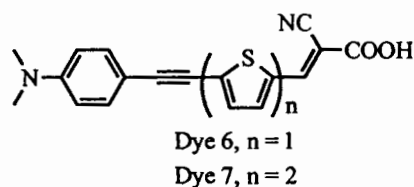
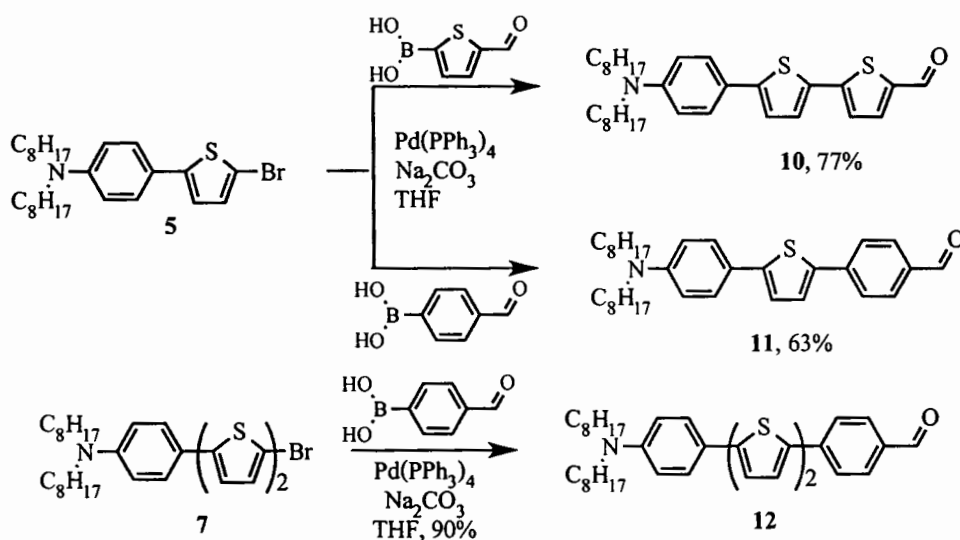


Figure 3.1 Chemical structure of ailine based dyes

In this work a series of dialkylaniline dyes with various π -bridge were synthesised and fully characterized. The optical and electrochemical properties have also been investigated. The devices were fabricated in order to evaluate the power conversion efficiency.

3.2 Synthesis

In order to obtain the desired dyes, their aldehyde derivatives would be synthesised. The aldehyde compounds were successfully synthesised using Suzuki coupling reaction of bromo reagents and appropriated aldehyde boronic acids as shown in Scheme 3.1. The reaction condition was performed as in the literature [106] using $\text{Pd}(\text{PPh}_3)_4$ as catalyst in the presence of Na_2CO_3 as base in THF at reflux for 24h following by column chromatography (silica gel, hexane:DCM) to give 5'-(4-(*N,N*-dioctylamino)phenyl)-[2,2'-bithiophene]-5-carbaldehyde (**10**, 77%), 5-benzaldehyde-4-thiophene-*N,N*-dialkylaniline (**11**, 63%) and 4-(5'-benzaldehyde-[2,2'-bithiophen])-*N,N*-dioctylaniline (**12**, 90%), respectively.

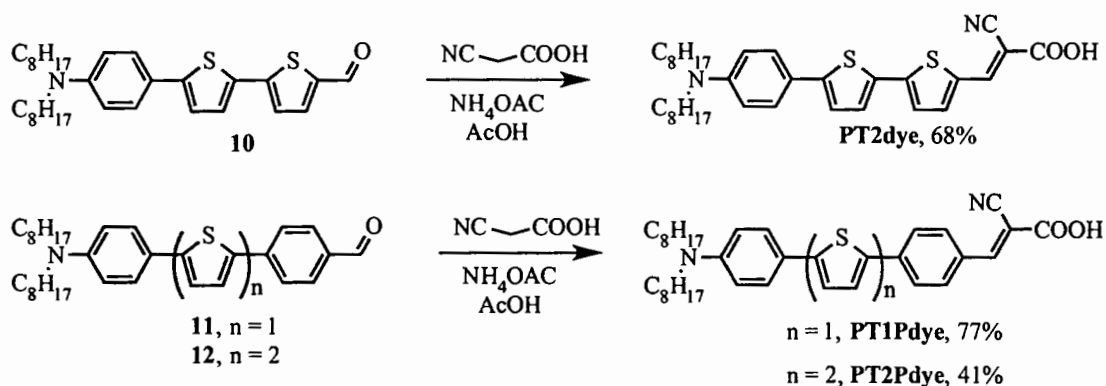


Scheme 3.1 Synthetic routes of the aldehyde intermediates

The chemical structure of aldehyde **10** was confirmed by $^1\text{H-NMR}$ analysis. The $^1\text{H-NMR}$ spectrum shows a triplet peak at a chemical shift of 3.29 ppm (4 protons, $J = 7.8$ Hz)

assigned as the protons of the alkyl chain next to the N-atom and a singlet peak at a chemical shift of 9.83 ppm (1 proton) assigned as the proton of the aldehyde unit. The $^1\text{H-NMR}$ spectrum of **11** shows a triplet peak at 3.30 ppm (4 protons, $J = 7.8$ Hz) assigned as the protons of the alkyl chain next to the N-atom, a doublet peak at a chemical shift of 7.85 ppm (2 protons, $J = 8.1$ Hz) assigned as the protons of the phenyl ring at the C-atom next to the carbonyl group and a singlet peak at a chemical shift of 9.98 ppm (1 proton) assigned as the proton of the aldehyde unit. The chemical structure of **12** was confirmed by $^1\text{H-NMR}$ analysis. The triplet peak at a chemical shift of 3.31 ppm (4 protons, $J = 7.5$ Hz) was assigned as the protons of the alkyl chain at C-atom next which attached to N-atom. The singlet peak at a chemical shift of 10.00 ppm with 1 proton assigned as the aldehyde proton was found.

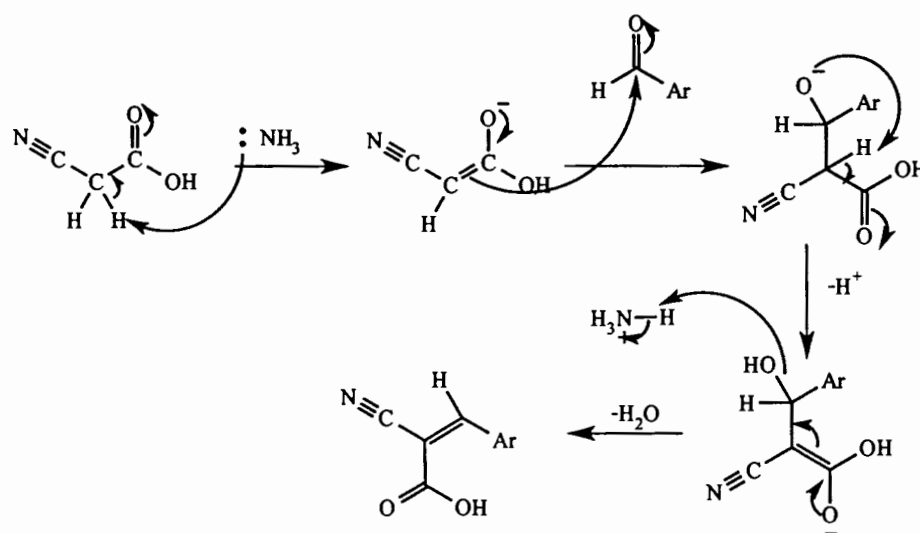
The synthetic pathways of the dye products, the Knoevenagel condensation, are depicted in Scheme 3.2. The aldehyde resultants were reacted with cyano acetic acid in the presence of ammonium acetate in acetic acid. The reaction mechanism are described in Scheme 3.3. The first step is to generate enolate anion by ammonia then the attack at of anion on aldehyde occurred, followed by an E1cB elimination to give an unsaturated carbonyl compound. [107] After purified by column chromatography, the aniline-thiophene dyes were obtained in yield of 68% for **PT2dye**, 77% for **PT1Pdye** and **PT2Pdye** 41%, respectively.



Scheme 3.2 Synthetic routes of **PTdyes**

The chemical structures of the desired dyes were confirmed by IR analysis. The IR spectrum of **PT2dye** shows peak at 2212 cm^{-1} assigned as the $\text{C}\equiv\text{N}$ stretching and O-H stretching was assigned at 3411 cm^{-1} . The MALDI mass spectrometry analysis shows the molecular ion peaks centered at $m/z = 576.173$ corresponding to an expect M^+ mass ion of **PT2dye**. The IR spectrum of **PT1Pdye** shows the transmittance peak at $3,400\text{ cm}^{-1}$ assigned as the O-H stretching and a $\text{C}\equiv\text{N}$ stretching was observed at 2212 cm^{-1} . The MALDI mass spectrometry analysis shows the molecular ion peaks centered at $m/z = 570.6$ corresponding to an expect M^+ mass ion of

PT1Pdye. **PT2Pdye's** structure was confirmed by IR analysis. The IR spectrum shows the O-H stretching peak at 3338 cm^{-1} and $\text{C}\equiv\text{N}$ stretching at 2212 cm^{-1} . The MALDI mass spectrometry analysis shows the molecular ion peaks centered at $m/z = 652.256$ corresponding to an expect M^+ mass ion of **PT2Pdye**. The products were soluble in chlorinated solvents and tetrahydrofuran at room temperature.



Scheme 3.3 Knoevenagel condensation mechanism

3.3 optical properties

The optical properties were measured in dichloromethane solution for **PT2dye** and **PT1Pdye**. **PT2Pdye** was investigated in dimethyl sulfoxide solution since it does not dissolve in dichloromethane. The optical spectra are shown in Figure 3.2, 3.3 and summarized in Table 3.1. The absorption spectra show the intramolecular charge transfer (ICT) absorption locating around 420 nm. [108] The absorption spectrum of **PT2dye** reveals the board absorption wavelength and the maxima absorption peak at 466 nm assigned as the ICT absorption, which is the longest wavelength due to the longest conjugation itself. The board absorption band leads to the effective light harvesting. **PT1Pdye** exhibited, a blue-shift absorption compared with **PT2dye**, a maxima absorption band at 335 and 435 nm indicating that the replacing of thiophene unit by phenyl ring decrease the conjugation length.

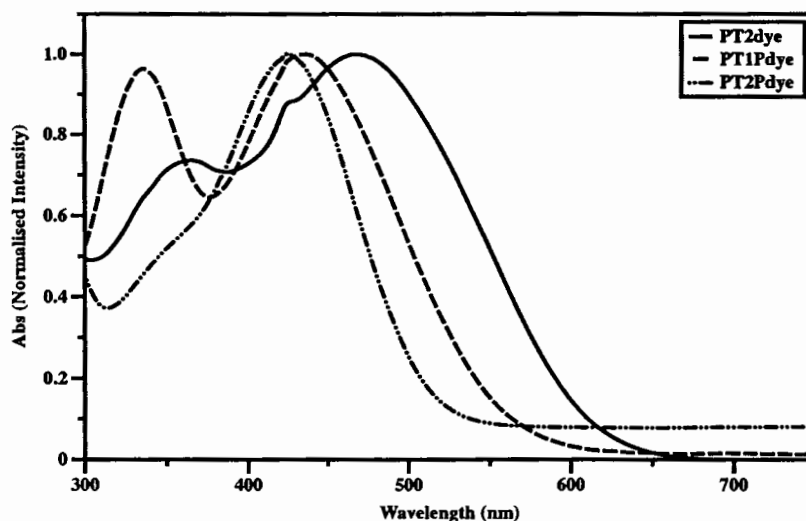
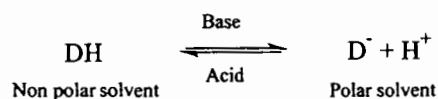


Figure 3.2 The absorption spectra of PT2dye, PT1Pdye and PT2Pdye

PT2Pdye showed the most blue-shift absorption peak at 424 nm. An alternative explanation for the blue shift observed for the dyes in polar aprotic solvents may be explained on the basis of protonation and deprotonation of the dyes. It is possible that the carboxylic acid is partially deprotonated in the ground state. Such a deprotonation would reduce the electron-accepting ability of the acceptor moiety, which in turn may substantially decrease the donor-acceptor interaction in the dye. This will manifest as a blue shift in the absorption spectrum. [109, 110]



(8)

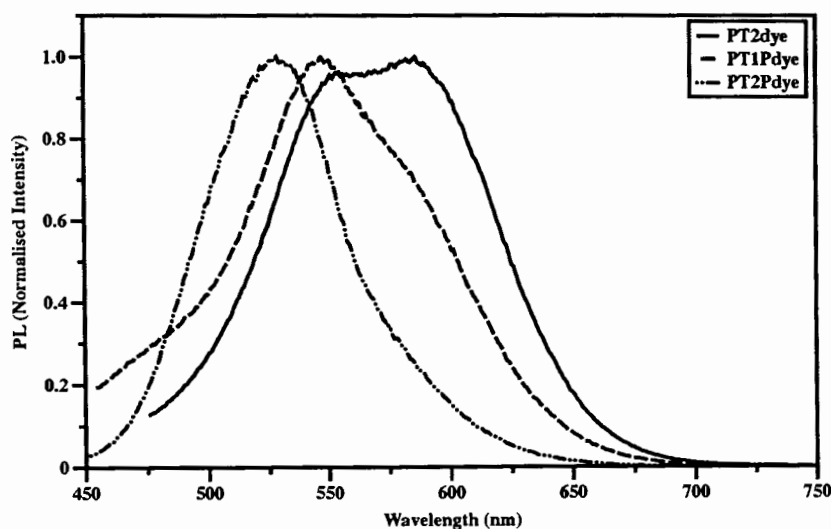


Figure 3.3 Fluorescence spectra of PT2dye, PT1Pdye and PT2Pdye

The photoluminescence spectra reveal the maxima emission peak of PT2dye, PT1Pdye and PT2Pdye 586 nm, 547 nm and 528 nm, respectively which related to the absorption peaks. The emission is completely quenched. This probably indicates the presence of a noticeable dipole in the donor-acceptor compounds due to extensive polarization, which may interact with the solvent dipole and trigger a nonradiative relaxation of the excited state by electron transfer. [109]

Table 3.1 The summary of Absorption and fluorescence data of PT2dye, PT1Pdye and PT2Pdye

Compound	λ_{\max} of absorbance (nm) ^a	λ_{\max} (nm) (log ϵ)	λ_{\max} of emission (nm) ^b
PT2dye	365, 466	367 (3.99), 466 (4.13)	586
PT1Pdye	335, 435	335 (4.26), 435 (4.28)	547
PT2Pdye	424	424 (4.46)	528

^aMeasured in dilute CH₂Cl₂ and DMSO solution, ^bExcited at the absorption maxima

3.4 Electrochemical property

The cyclic voltammogram and different pulse voltammogram of the PT2dye was measured in dry dichloromethane solution (Figure 3.4). The radical cation of aniline was observed at half-wave potential of 0.62 V vs Ag/Ag⁺ while the reversible oxidation peak at half-wave potential of 1.20 V vs Ag/Ag⁺ belongs to radical cation of thiophene moiety. The reduction peaks at half-wave potential of -0.82 and -1.14 V vs Ag/Ag⁺ were found.

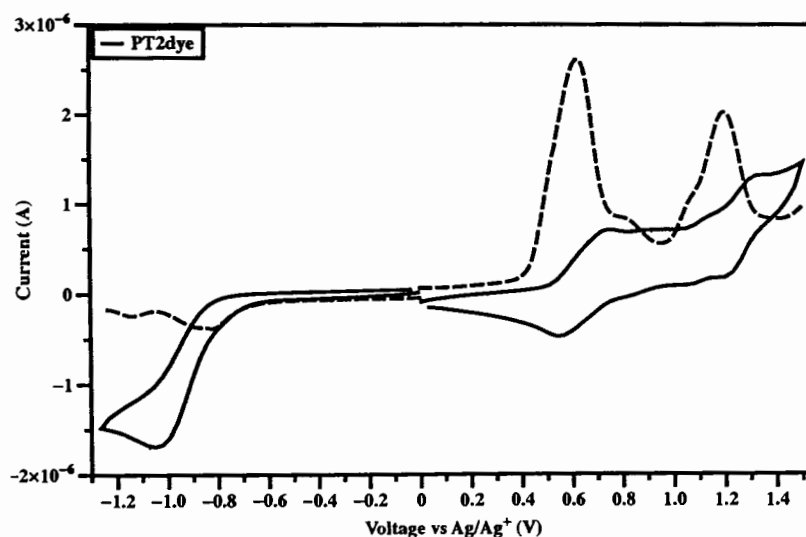


Figure 3.4 Cyclic voltammogram of target molecules PT2dye

The reversible oxidation peak of aniline radical cation was found at half-wave potential 0.61 V vs Ag/Ag^+ , as shown in Figure 3.5. The second reversible oxidation peak at half-wave potential of 1.25 V vs Ag/Ag^+ indicates the thiophene radical cation. The reversible reduction peak of cyanoacetic acid was observed (-0.85 V vs Ag/Ag^+).

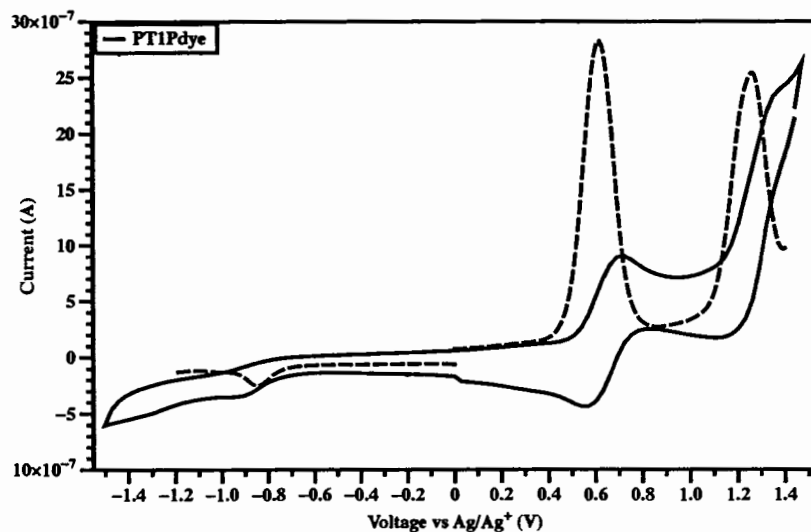


Figure 3.5 Cyclic voltammogram of target molecules PT1Pdye

Due to the poor solubility of PT2Pdye in dichloromethane, the electrochemical property was performed in dimethyl sulfoxide solution. The irreversible oxidation peaks at half-wave potential of 0.57 and 1.05 V vs Ag/Ag^+ were obtained. The reversible reduction peak was found at half-wave potential of -0.75 V vs Ag/Ag^+ .

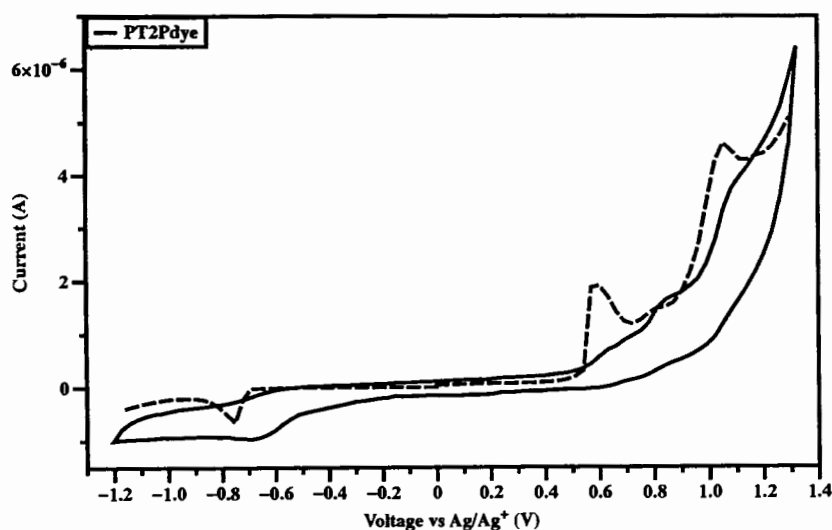


Figure 3.6 Cyclic voltammogram of target molecules PT2Pdye

According to the optical and electrochemical properties, the energy levels can be calculated and shown in Table 3.2. The PT2dye shows the lowest E_{0-0} of 2.44 eV. The HOMO and LUMO level of these target molecules matches well with the conduction band of TiO_2 (-4.2 eV vs SCE) and redox potential (-4.8 eV vs SCE) of electrolyte which means we can use all chemical as dye-sensitisers.

Table 3.2 Cyclic voltammetric results for PT2, PT3, PT4, PT5, PT6, PT1F and PT2F^a

Compound	E_{1o} (V)	E_{2o} (V)	E_{1re} (V)	E_{2re} (V)	E_{0-0} (eV)	HOMO ^e (eV)	LUMO ^f (eV)
PT2dye	0.75 ^b (0.62) ^c	1.32 (1.20)	-0.82 (-0.82)	-1.05 (-1.14)	2.44	-4.88	-2.44
PT1Pdye	0.69 (0.61)	1.38 (1.25)	-0.90 (-0.85)	-	2.49	-4.91	-2.42
PT2Pdye	0.84 (0.57)	1.08 (1.05)	-0.69 (-0.75)	-	2.48	-4.96	-2.48

^aMeasured using a platinum rod counter electrode, a glassy carbon working electrode and a SCE reference electrode in CH_2Cl_2 containing $n\text{-Bu}_4\text{NPF}_6$ as a supporting electrolyte with scan rate of 0.05 V/s under argon atmosphere, ^bPeak potential, ^cHalf-wave potential, ^d E_{0-0} was estimated from the intersection between the absorption and emission spectra, ^eCalculated using the empirical equation from $\text{HOMO} = -(4.44 + E_{\text{onset}})$, ^fCalculated from $\text{LUMO} = \text{HOMO} + E_g$

3.5 Computational calculation

Table 3.3 Computational modeling of PTdyes.

Compound	HOMO	LUMO
PT2dye		
PT1Pdye		
PT2Pdye		

The optimized structure and frontier molecular orbital were calculated by DFT/B3LYP/6-31G9(d,p) method (Table 3.3). At HOMO level the electrons distribute at donor-bridge (bonding orbitals) while LUMO level the electrons distribute at bridge-acceptor (anti-bonding orbitals) indicating that there is electron transferring in dye molecules. This phenomena explains the intramolecular charge transfer absorption peak in absorption spectra.

3.6 Devices performance

Figure 3.7 shows the incident monochromatic photon-to-current conversion efficiencies (IPCEs) obtained with a sandwich-type two electrodes cell. The dye-coated TiO₂ film was used as the working electrode, platinized FTO glass as the counter electrode and 0.5 M LiI, 0.05 M I₂ and 0.4 M PY in gamma-butyrolactone and *N*-methylpyrrolidone (volume ratio, 7: 3) mixture solution as the redox electrolyte.

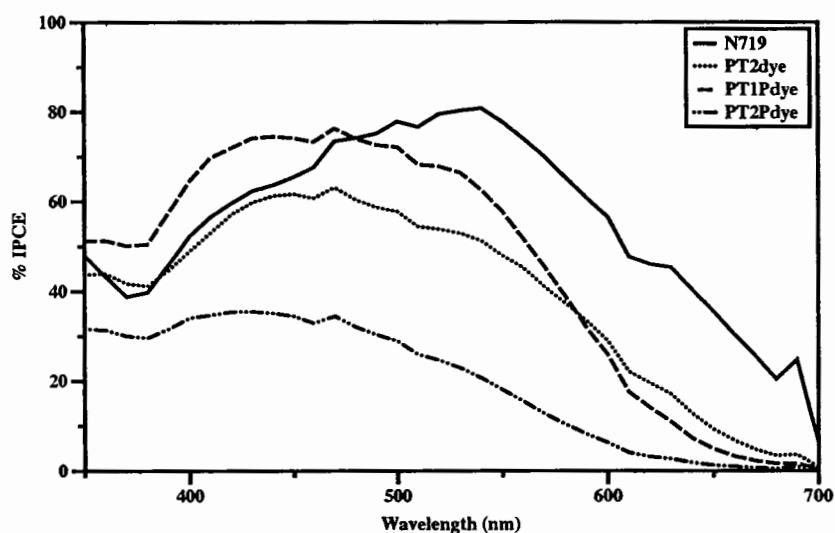


Figure 3.7 Spectra of monochromatic incident photon-to-current conversion efficiencies (IPCEs) for DSSCs based on PT2dye, PT1Pdye and PT2Pdye

The IPCE exceeds 60% in the spectral range 440–490 nm for PT2dye, which reaches its maximum of 63.1% at 470 nm. The IPCE of PT1Pdye reached a maximum (76.3%) at 439 nm. The IPCE of PT2Pdye shows very low value due to the poor solubility of dye itself. All aniline dyes exhibit lower IPCE and narrower absorption than N719. These results will lead to lower performance of aniline based dye-sensitised solar cells.

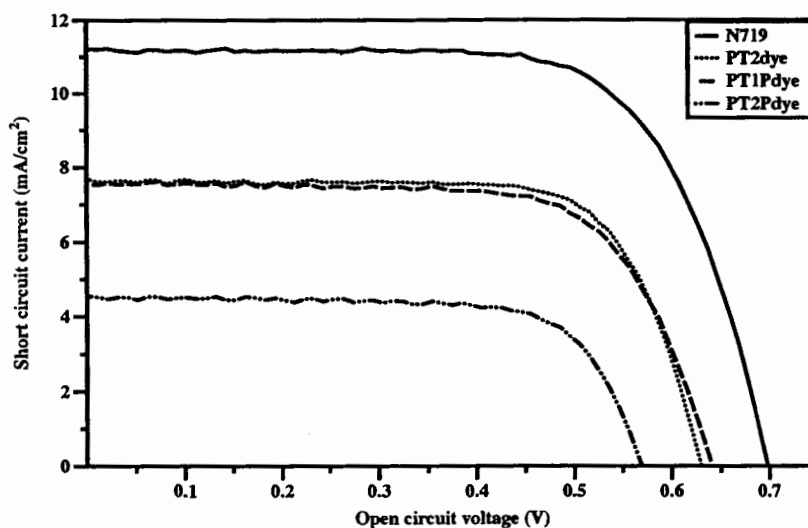


Figure 3.8 *J-V* curves of DSSCs based on PT2dye, PT1Pdye and PT2Pdye

The performance statistics of the devices are also listed in Table 3.4. An overall conversion efficiency (η) of 3.55% was achieved from the DSSC based on the dye **PT2dye** (short-circuit photocurrent density, $J_{sc} = 7.69 \text{ mA cm}^{-2}$; open-circuit photovoltage, $V_{oc} = 0.63 \text{ V}$; fill factor, $ff = 0.73$). This efficiency is higher than the efficiency of 3.38% (short-circuit photocurrent density, $J_{sc} = 7.56 \text{ mA cm}^{-2}$; open-circuit photovoltage, $V_{oc} = 0.64 \text{ V}$; fill factor, $ff = 0.70$) obtained from the DSSC based on the dye **PT1Pdye** because the **PT2dye** has longer conjugation and higher molar extinction coefficient.

Table 3.4 Photovoltaic performance of DSCs based on PT2dye, PT1Pdye and PT2Pdye

Sample	J_{sc} (mA cm^{-2})	V_{oc} (V)	ff	η (%)
N719	11.21	0.70	0.69	5.39
PT2dye	7.69	0.63	0.73	3.55
PT1Pdye	7.56	0.64	0.70	3.38
PT2Pdye	4.54	0.57	0.71	1.85

3.7 Conclusion

A series of dialkylaniline dyes with thiophene phenylene bridge was successfully synthesised and characterized. The desired molecules (**PT2dye** and **PT1Pdye**) can be dissolved in chlorinate solvent at room temperature. The **PT2Pdye** is soluble in dimethyl sulfoxide. The intramolecular charge transfer can be observed by absorption band around 420-460 nm. The

computational calculation confirmed the intramolecular charge transfer occurring in excited state. The DSSC devices base on **PT2dye** show the highest performance with an overall power conversion efficiency at 3.55% (short-circuit photocurrent density, $J_{sc} = 7.69 \text{ mA cm}^{-2}$; open-circuit photovoltage, $V_{oc} = 0.63 \text{ V}$; fill factor, $ff = 0.73$).

CHAPTER 4

NOVEL D- π -A DYE SENSITISERS: SYNTHESIS, CHARACTERIZATION AND DEVICES PERFORMANCE

4.1 Introduction

Phenothiazine-based dye contains electron-rich nitrogen and sulfur heteroatoms in a heterocyclic structure with high electron-donating ability, and its non-planar butterfly conformation can sufficiently inhibit molecular aggregation and the formation of intermolecular excimers. [54, 106] Meanwhile, the 10-substituent on N can further enhance the charge separation at the oxide solution interface. Furthermore, the two phenyl groups are arranged in a small torsion angle related to the N(10) and S(9) atoms, so that π -delocalization can be extended over the entire chromophore. [111-113] The structural features of phenothiazine-based dye make it a promising type of sensitizers for DSSCs. The molecular engineering of sensitizers can enhance the charge separation at the oxide solution interface. As a result, certain structural modifications of this kind of dye give moderate improvement of the PCEs. Hua et al. reported the high efficiency of DSSCs using phenothiazine-based dye with $J_{sc} = 14.75 \text{ mA cm}^{-2}$, $V_{oc} = 0.79 \text{ V}$, $ff = 0.68$ and $\eta = 8.08\%$ from PT-C₆ based devices. [114] They found that the alkyl substituents with different chain length at the N(10) atom of phenothiazine could further optimise the performance through completely shielding the surface of TiO₂ from the I⁻/I₃⁻ electrolyte and subsequently reducing the leakage of dark current.

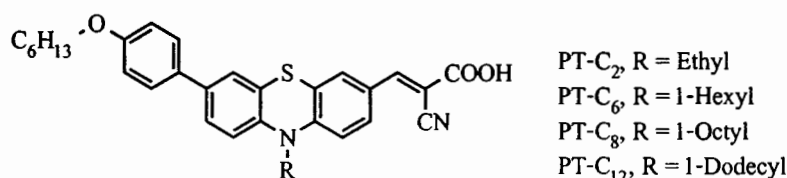


Figure 4.1 Chemical structure of phenothiazine based dyes

Coumarin derivatives have been used successfully as organic dye photosensitizers in DSSC, Hara and co worker reported the DSSC based on coumarin dyes with good performance. [50, 52, 53]

Herein we reported the synthesis and characterization of phenothiazine- and coumarin-base dyes. The optical, electrochemical and thermal properties have also been studied. The DSSC based on desired dyes shows the highest performance at 4.33% under AM 1.5 G.

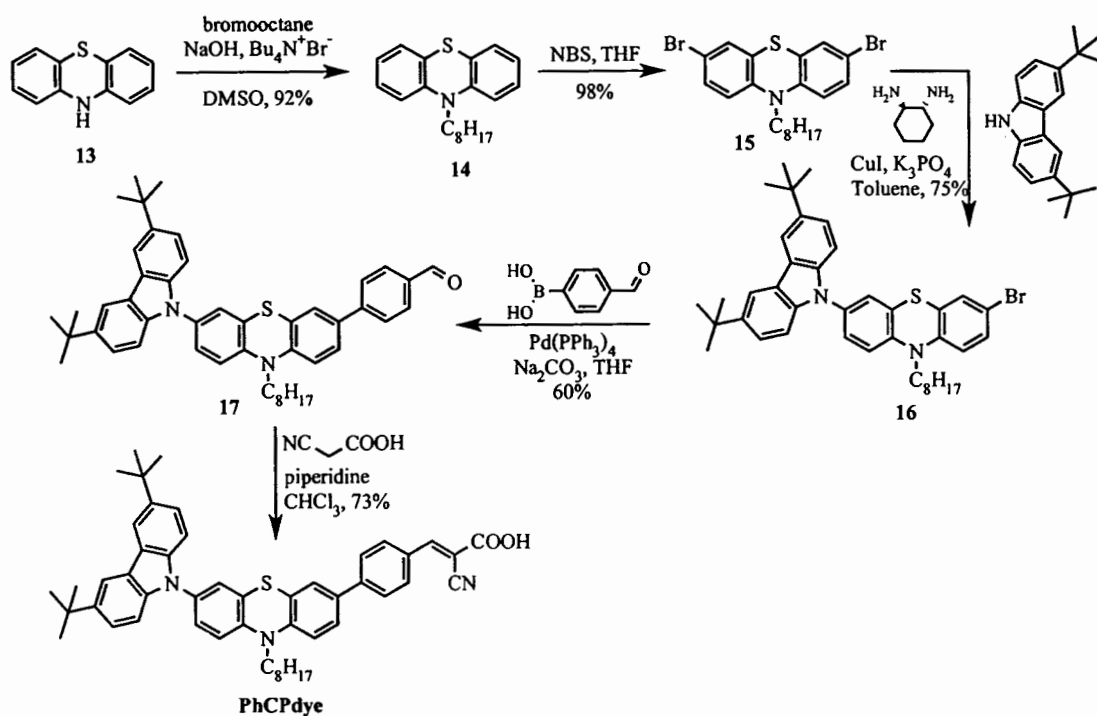
4.2 Synthesis

4.2.1 Synthesis of Phenothiazine derivatives dyes

To obtain (E)-2-cyano-3-(4-(7-(3,6-di-*tert*-butyl-carbazol-9-yl)-10-octyl-phenothiazine-3-yl)phenyl)acrylic acid, the phenothiazine was alkylated with bromooctane using 50% wt/v NaOH solution as base and tetrabutylammonium bromide as phase transfer catalyst in DMSO to give 10-octylphenothiazine (**14**) 92% yield as yellow oil (Scheme 4.1). The chemical structure of **14** was confirmed by $^1\text{H-NMR}$ analysis, which shows the triplet peak at chemical shift of 3.95 ppm (2 protons, $J = 6.7$ Hz) assigned as the protons of alkyl chain next to N-atom. Moreover, a doublet peak at chemical shift of 7.29 ppm (4 protons, $J = 7.6$ Hz) assigned as the protons of aromatic ring was also observed. Then the electrophilic aromatic bromination was used to obtain 3,7-dibromo-10-octylphenothiazine (**15**) 98% yield as brown oil. The $^1\text{H-NMR}$ of the resultant confirmed that there were bromide substituting at C-3 and C-7 position since a doublet peak at chemical shift of 6.64 ppm (2 protons, $J = 8.5$ Hz) assigned as the protons of aromatic ring at C-1 and C-9 position was observed.

The dibrominated compound **15** was further reacted with 3,6-di-*tert*-butyl carbazole under Ullmann coupling reaction. [115] The reaction was carried using CuI as catalyst and (\pm)-*trans*-1,2-diaminocyclohexane as ligand and K_3PO_4 as base in toluene. The reaction mixture was heated at reflux for 48h then the reaction was cooled to room temperature and washed with water. The crude product was purified by column chromatography (silica gel, hexane) to give 3-bromo-7-(3,6-di-*tert*-butyl-carbazol-9-yl)-10-octyl-phenothiazine (**16**) as white solid 75% yield. The chemical structure of **16** was confirmed by $^1\text{H-NMR}$ analysis. The $^1\text{H-NMR}$ spectrum shows a triplet peak at chemical shift of 4.02 ppm (2 protons, $J = 6.6$ Hz) assigned as the protons of alkyl chain next to N-atom and a singlet peak at chemical shift of 8.24 ppm (2 protons) assigned as the protons at C-4 and C-5 position of carbazole indicating that there was the substitution of carbazole to phenothiazine ring. To obtain aldehyde compound **17**, the bromo compound **16** was reacted with 4-formyl-phenylboronic acid using $\text{Pd}(\text{PPh}_3)_4$ as catalyst and Na_2CO_3 as base in THF. The reaction was heated at reflux for 24h, the reaction mixture was cooled to room temperature and washed with water followed by purified using column chromatography (silica gel, hexane:DCM) to give 4-(7-(3,6-di-*tert*-butyl-carbazol-9-yl)-10-octyl-phenothiazin-3-yl)benzaldehyde (**17**) in 30% yield as orange solid. The chemical structure of aldehyde **17** was confirmed using IR and $^1\text{H-NMR}$. The IR spectrum of **17** shows a peak at 1700 cm^{-1} assigned as the C=O stretching of aldehyde. The $^1\text{H-NMR}$ spectrum shows a triplet peak at chemical shift of 3.88 ppm (2 protons, $J = 6.6$ Hz) assigned as the protons of alkyl chain next to N-atom and a singlet peak at chemical shift of 10.06 ppm (1 proton) assigned as the a proton of aldehyde group. The last step is Knoevenagel condensation of aldehyde and cyanoacetic acid in

the presence of piperidine in chloroform [116] afforded (*E*)-2-cyano-3-(4-(7-(3,6-di-*tert*-butyl-carbazol-9-yl)-10-octyl-phenothiazine-3-yl)phenyl) acrylic acid (**PhCPdye**) as red solid in 73% yield. The chemical structure of **PhCPdye** was confirmed using IR and ¹H-NMR analysis. The IR spectrum shows a peak at 2215 cm⁻¹ assigned as the C≡N stretching and a peak at 1617 cm⁻¹ assigned as the C=O stretching. The ¹H-NMR spectrum reveals a singlet peak at chemical shift of 3.92 ppm (2 protons) assigned as the protons of alkyl chain next to N-atom but no peak at 9-10 ppm was found indicating that the aldehyde was completely reacted with cyanoacetic acid. The product was soluble in chlorinated solvents and tetrahydrofuran at room temperature.

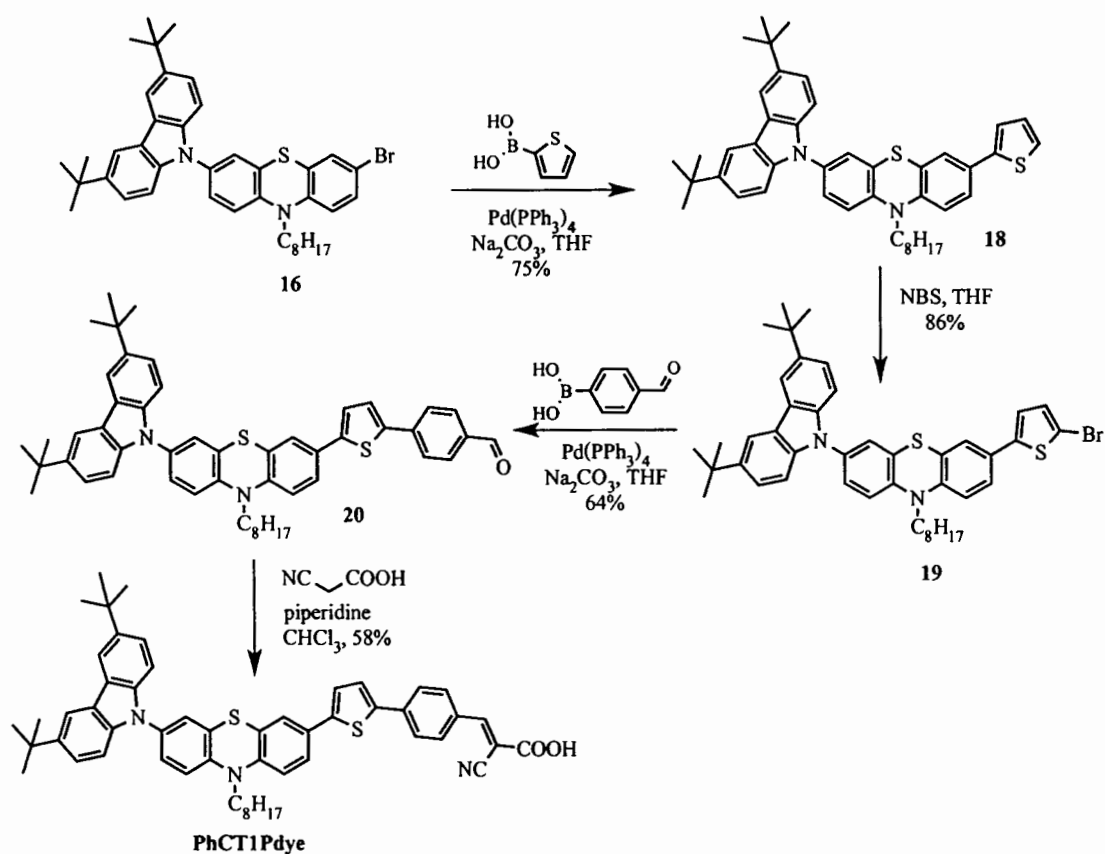


Scheme 4.1 Synthetic route of **PhCPdye**

In order to obtain (*E*)-2-cyano-3-(4-(5-(7-(3,6-di-*tert*-butyl-carbazol-9-yl)-10-octyl-phenothiazin-3-yl)thiophen-2-yl)phenyl)acrylic acid, firstly bromo-phenothiazine **16** was reacted with 2-thiophene boronic acid under Suzuki coupling reaction (Scheme 4.2). In this condition used Pd(PPh₃)₄ as catalyst and Na₂CO₃ as base in THF. The reaction was heated at reflux for 24h. Crude product was purified by column chromatography (silica gel: hexane:DCM) gave 3-(3,6-di-*tert*-butyl-carbazol-9-yl)-10-octyl-7-(thiophen-2-yl)-phenothiazine (**18**) as yellowish solid 75% yield. The chemical structure was confirmed by ¹H-NMR analysis. The ¹H-NMR spectrum shows a triplet peak at chemical shift of 4.08 ppm, (2 protons, *J* = 7.20 Hz) assigned as the protons of alkyl chain next to N-atom and singlet peak at chemical shift of 8.28 ppm (2 protons) assigned as the protons of C-4 and C-5 atom in carbazole ring. The thiophene-

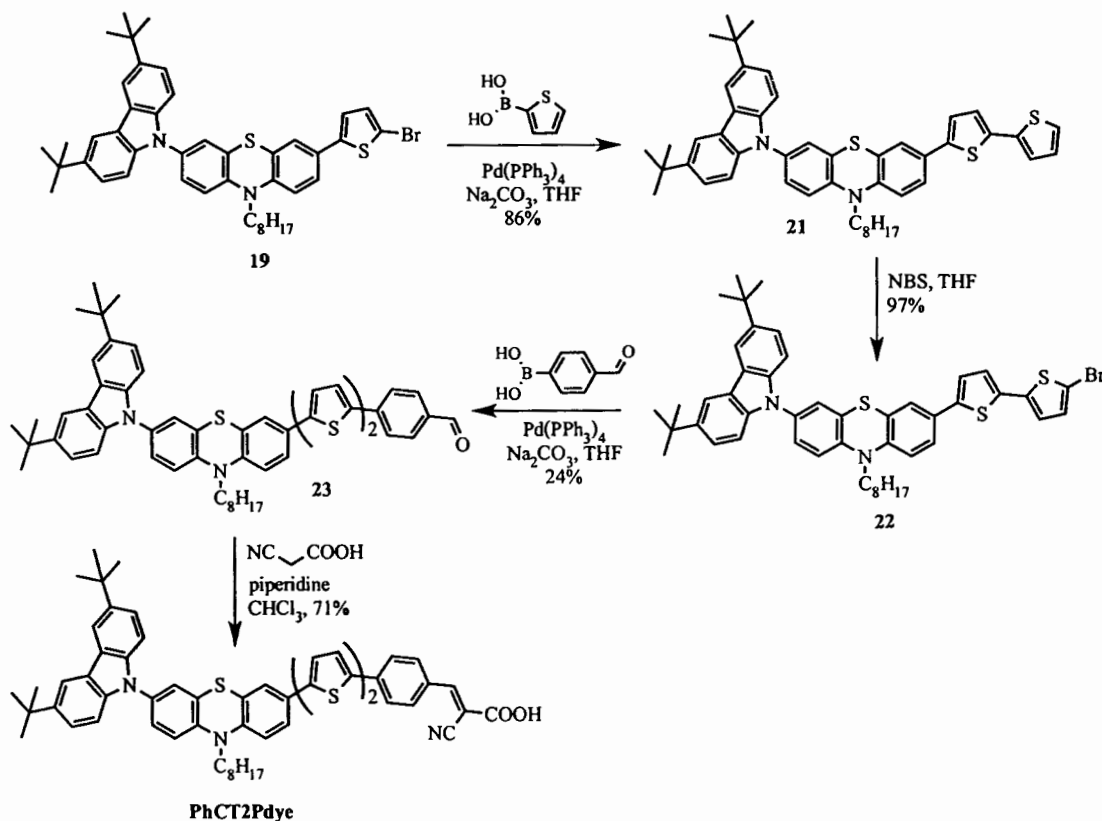
phenothiazine **18** was brominated using NBS in THF in order to get bromo-substituted (**19**) as yellowish solid in 86% yield. This reaction follows electrophilic aromatic substitution mechanism with selected at C-2 position of thiophene ring due to the highest electrophile atom. The chemical structure was confirmed by $^1\text{H-NMR}$ analysis. The $^1\text{H-NMR}$ spectrum shows a doublet peak at chemical shift of 7.18 ppm (1 proton, $J = 3.6$ Hz) assigned as the proton of C-3 atom of thiophene ring.

The aldehyde compound **20** was obtained using Suzuki coupling reaction. According to reaction condition, $\text{Pd}(\text{PPh}_3)_4$ was used as catalyst in the presence of Na_2CO_3 as base in THF. The reaction mixture was heated at reflux for 24h, followed by purification using column chromatography (silica gel, hexane:DCM) to give 4-(5-(7-(3,6-di-*tert*-butyl-carbazol-9-yl)-10-octyl phenothiazin-3-yl)thiophen-2-yl)benzaldehyde **20** as orange solid in 64% yield. The chemical structure was confirmed by IR and $^1\text{H-NMR}$ analysis. The IR spectrum of **20** shows a transmittance peak at 1695 cm^{-1} assigned as the $\text{C}=\text{O}$ stretching of aldehyde unit. The $^1\text{H-NMR}$ spectrum shows a singlet peak at chemical shift of 9.99 ppm (1 proton) assigned as the proton of aldehyde group.



Scheme 4.2 Synthetic route of PhCT1Pdye

The last step is Knoevenagel condensation of aldehyde and cyanoacetic acid in the presence of piperidine in chloroform afforded (*E*)-2-cyano-3-(4-(5'-(7-(3,6-di-*tert*-butyl-carbazol-9-yl)-10-octyl-phenothiazin-3-yl)-[2,2'-bithiophen]-5-yl)phenyl)acrylic acid (**PhCT1Pdye**) as red solid in 73% yield. The chemical structure of **PhCT1Pdye** was confirmed using IR and $^1\text{H-NMR}$ analysis. The IR spectrum shows a peak at 2215 cm^{-1} assigned as the $\text{C}\equiv\text{N}$ stretching and a peak at 1613 assigned as the $\text{C}=\text{O}$ stretching. The $^1\text{H-NMR}$ spectrum reveals a singlet peak at chemical shift of 4.07 ppm (2protons, $J = 6.6\text{ Hz}$) assigned as the protons of alkyl chain next to N-atom but no peak at $9\text{-}10\text{ ppm}$ was found indicating that the aldehyde was completely reacted with cyanoacetic acid. The product was soluble in chlorinated solvents and tetrahydrofuran at room temperature.



Scheme 4.3 Synthetic route of **PhCT2Pdye**

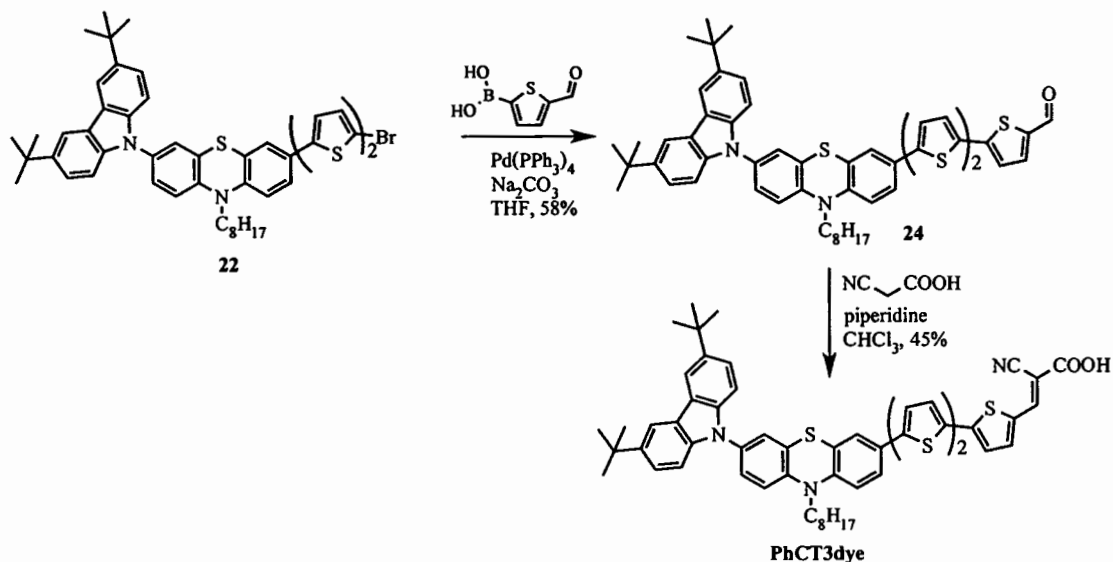
The synthetic route of **PhCT2Pdye** is shown in Scheme 4.3. Firstly, brominated compound **19** was reacted with 2-thiopheneboronic acid using $\text{Pd}(\text{PPh}_3)_4$ as catalyst and Na_2CO_3 as base in THF. The reaction follows Suzuki coupling mechanism as describe in Chapter 2. 3-((2,2'-Bithiophen]-5-yl)-7-(3,6-di-*tert*-butyl-carbazol-9-yl)-10-octyl-phenothiazine (**21**) was obtained after purification as yellowish solid in 86% yield. The resultant was further brominated using NBS in THF to give 3-(5'-bromo-[2,2'-bithiophen]-5-yl)-7-(3,6-di-*tert*-butyl-carbazol-9-yl)-

10-octyl-phenothiazine (**22**) as yellow solid in 82% yield. The chemical structure of **22** was confirmed by $^1\text{H-NMR}$ analysis. The $^1\text{H-NMR}$ spectrum shows a doublet peak at chemical shift of 7.04 ppm (2 proton, $J = 3.6$ Hz) assigned as the proton of C-3 atom of thiophene ring. The aldehyde compound **23** was synthesised using Suzuki coupling reaction between brominated compound **22** and 4-formyl-phenylboronic acid, under this condition $\text{Pd}(\text{PPh}_3)_4$ was used as catalyst and Na_2CO_3 as base in THF. The reaction mixture was heated at reflux for 24h, followed by purified by column chromatography (silica gel, Hexane:DCM) to give 4-(5'-(7-(3,6-di-*tert*-butyl-carbazol-9-yl)-10-octyl-phenothiazin-3-yl)-[2,2'-bithiophen]-5-yl)benzaldehyde (**23**) as orange solid in 24% yield. The chemical structure of **23** was confirmed by IR and $^1\text{H-NMR}$ analysis. The IR spectrum shows a transmittance peak at 1695 cm^{-1} assigned as the C=O stretching of aldehyde unit. The $^1\text{H-NMR}$ spectrum shows a singlet peak at chemical shift of 9.99 ppm (1 proton) assigned as the proton of aldehyde group.

The target molecule **PhCT2Pdye** was successfully synthesised using Knoevenagel condensation of aldehyde **23** and cyanoacetic acid in the presence of piperidine in chloroform. The reaction mixture was heated at reflux for 24h, followed by precipitation in mix solvents (MeOH:DCM) to give 2-(4-(5'-(7-(3,6-di-*tert*-butyl-carbazol-9-yl)-10-octyl-phenothiazin-3-yl)-[2,2'-bithiophen]-5-yl)benzylidene)malonic acid (**PhCT2Pdye**) as red solid 71% yield. The chemical structure of **PhCT2Pdye** was confirmed by IR and $^1\text{H-NMR}$ analysis. The IR spectrum shows a peak at 2215 cm^{-1} assigned as the $\text{C}\equiv\text{N}$ stretching and a peak at 1617 cm^{-1} assigned as the C=O stretching. The $^1\text{H-NMR}$ spectrum reveals a singlet peak at chemical shift of 3.92 ppm (2 protons) assigned as the protons of alkyl chain next to N-atom but no peak at 9-10 ppm was found indicating that the aldehyde was completely reacted with cyanoacetic acid. The product was soluble in chlorinated solvents and tetrahydrofuran at room temperature.

The synthetic pathway of **PhCT3dye** is shown in Scheme 4.4. Bromo-bithiophene **22** was coupled with 5-formyl-2-thiopheneboronic acid under Suzuki coupling reaction. The reaction mixture was heated at reflux for 24h, followed by purification by column chromatography (silica gel, hexane:DCM) to give 5''-(7-(3,6-di-*tert*-butyl-carbazol-9-yl)-10-octyl-phenothiazin-3-yl)-[2,2':5',2''-terthiophene]-5-carbaldehyde (**24**) as orange solid in 45% yield. The resultant was further reacted with cyanoacetic acid under Knoevenagel condensation in the presence of piperidine in chloroform. The crude product was precipitated by mix solvent (MeOH:DCM) to give (*E*)-2-cyano-3-(5''-(7-(3,6-di-*tert*-butyl-carbazol-9-yl)-10-octyl-phenothiazin-3-yl)-[2,2':5',2''-terthiophen]-5-yl)acrylic acid (**PhCT3dye**) as red solid in 45% yield. The chemical structure of **PhCT3dye** was confirmed using IR analysis. The IR spectrum shows a peak at 2213 cm^{-1} assigned as the $\text{C}\equiv\text{N}$ stretching and a peak at 1614 cm^{-1} assigned as the C=O stretching. The MALDI mass spectrometry analysis shows the molecular ion peaks centered at

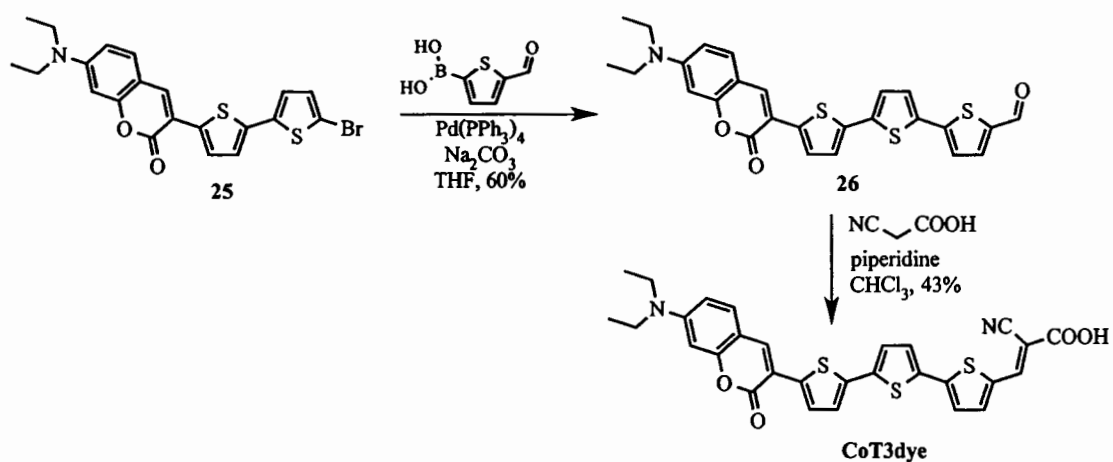
$m/z = 932.1$ corresponding to an expect M^+ mass ion of phenothiazine dye. The product was soluble in chlorinated solvents and tetrahydrofuran at room temperature.



Scheme 4.4 Synthetic route of PhCT3dye

4.2.2 Synthesis of coumarin derivatives dye

To obtain the coumarin base dye, the aldehyde (**26**) was obtained by Suzuki coupling between brominated compound **25** and 5-formyl-2-thiopheneboronic acid at reflux for 24h. The chemical structure of aldehyde resultant was confirmed by IR and $^1\text{H-NMR}$ analysis. The IR spectrum shows a $\text{C}=\text{O}$ stretching at 1698 cm^{-1} which confirms the carbonyl group in the product. The $^1\text{H-NMR}$ spectrum of aldehyde shows a multiplet peak at chemical shift of 3.35-3.40 ppm (4 protons) assigned as the the proton of alkyl chains next to N-atom and a singlet peak at chemical shift of 9.79 ppm (1 proton) assigned as the a proton of aldehyde. The **CoT3dye** was obtained using Knoevenagel condensation of aldehyde and cyanoacetic acid in the present of piperidine in chloroform in 43% yield. The chemical structure of desired product was confirmed by IR analysis and mass spectroscopy. The IR spectrum shows a peak at 2203 cm^{-1} assigned as the $\text{C}\equiv\text{N}$ stretching and a peak at 1615 assigned as the $\text{C}=\text{O}$ stretching. The MALDI mass spectrometry analysis shows the molecular ion peaks centered at $m/z = 558.022$ corresponding to an expect M^+ mass ion of coumarin dye. The product was soluble in chlorinated solvent and common organic solvents.



Scheme 4.5 Synthetic route of CoT3dye

4.3 Optical properties

The optical properties of desired dyes were investigated in dry dichloromethane and dimethyl sulfoxide solution. The results were summarised in Table 4.1. The absorption properties of phenothiazine base dyes were measured using UV-Vis spectroscopy technique. The absorption spectra related to the molar extinction coefficient (ϵ) are shown in Figure 4.2. The maxima absorption peaks of PhCPdye, PhCT1Pdye, PhCT2P and PhCT3dye are 427 nm, 434 nm, 455 nm and 432 nm for, respectively. These absorption peaks can be assigned as the intramolecular charge transfer (ICT) peaks. [54] The PhCT3dye shows the highest molar extinction coefficient (ϵ) at 432 nm because it is the largest chromophore. The molar extinction coefficient (ϵ) increases corresponding to the unit of chromophore.

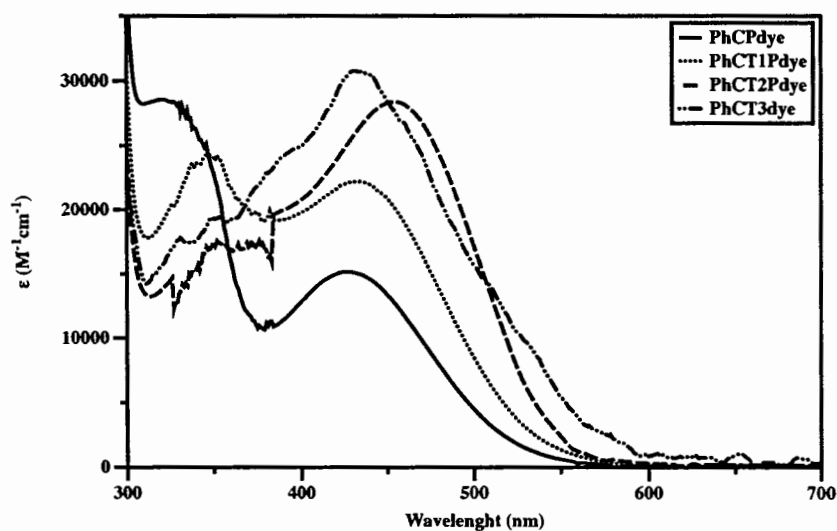


Figure 4.2 The absorption spectra of PhCPdye, PhCT1Pdye, PhCT2Pdye and PhCT3dye

CT3A was used as reference in order to compare the effect of substituent group. [117]

The chemical structure is shown in Figure 4.3.

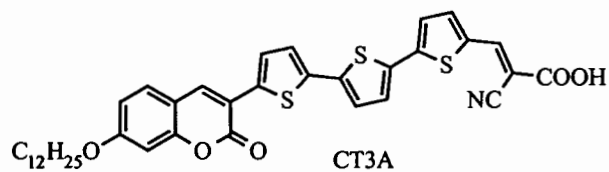


Figure 4.3 The chemical structure of CT3A

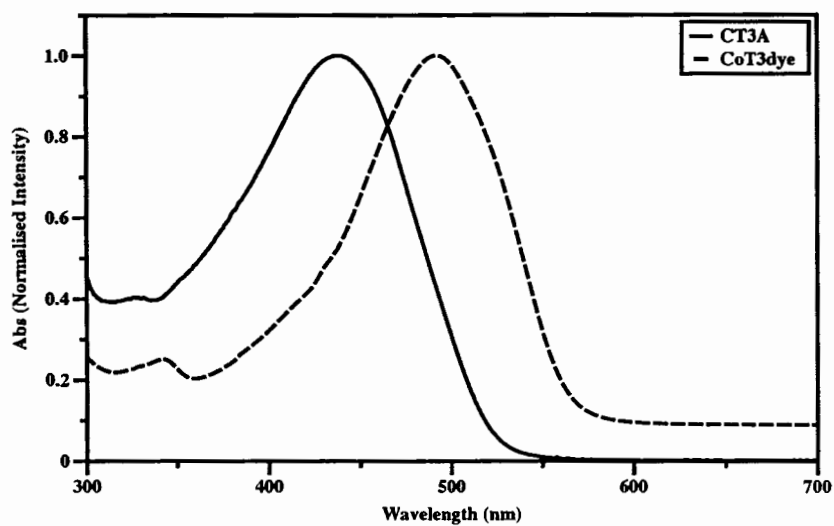


Figure 4.4 The absorption spectra of CoT3dye and CT3A

The absorption spectra of coumarin dyes are shown in Figure 4.4. The CoT3dye exhibits the maximum absorption peak at 492 nm corresponding to the ICT absorption. Accordingly, a large red shift from CT3A (53 nm) was observed indicating that the amino group donates electron density to the coumarin moiety better than alkoxy group.

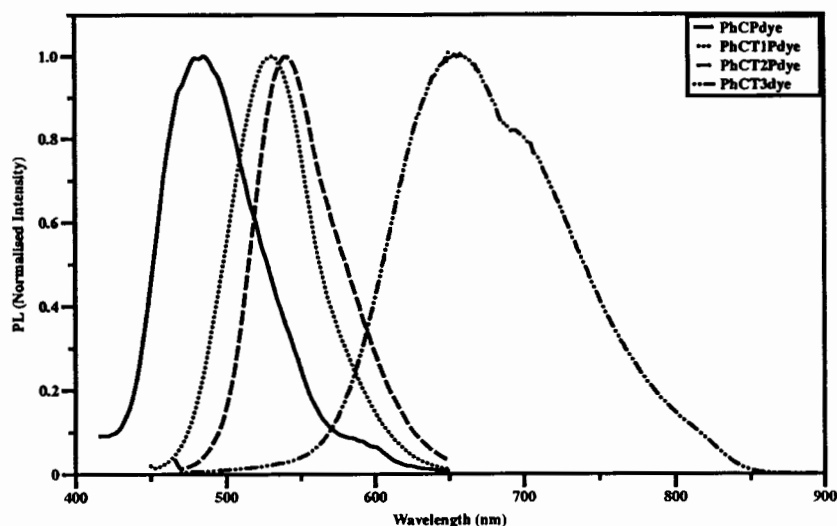


Figure 4.5 The photoluminescence spectra of **PhCPdye**, **PhCT1Pdye**, **PhCT2Pdye** and **PhCT3dye**

The emission spectra of phenothiazine dyes are shown in Figure 4.5 and summarised in Table 4.1. The trend of the emission of the phenothiazine dyes is similar to their absorption. The **PhCPdye** shows the emission peak at 483 nm while the **PhCT1Pdye** exhibits the emission peak at 530 nm. The **PhCT2Pdye** reveals a slightly larger emission peak than **PhCT1Pdye** at 541 nm. The largest emission peak belongs to the **PhCT3dye** at 656 nm due to the largest conjugated of the trithiophene moiety.

The fluorescence spectra of coumarin dyes are shown in Figure 4.6. The **CoT3dye** exhibits the emission peak at 578 nm which is red-shifted from the emission peak of **CT3A** for 44 nm.

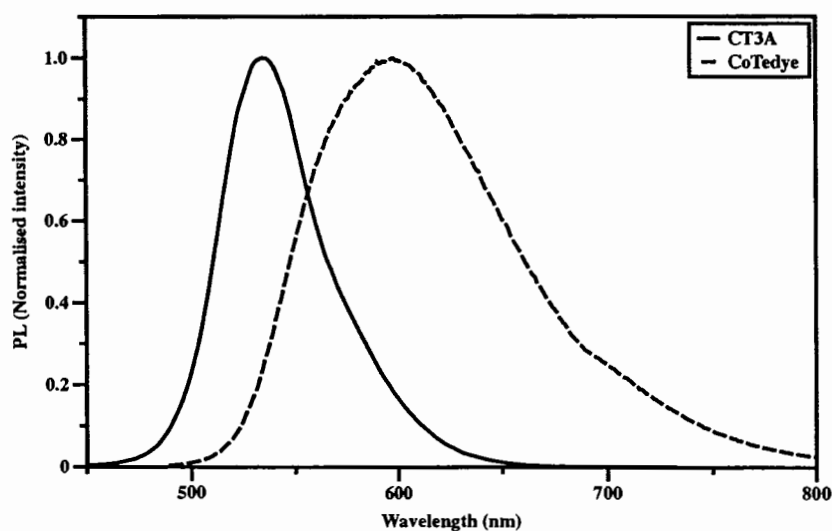


Figure 4.6 The photoluminescence of coumarin base dyes

According to the optical property, the desired molecules can be used as dye-sensitiser in DSSC. The molar extinction coefficient relates to the π -bridge, **PhCT3dye** shows the highest molar extinction coefficient due to the prolonged conjugation. The **CoT3dye** shows the lowest band gap at 2.11 eV.

Table 4.1 The optical properties results of phenothiazine and coumarin base dyes

Compound	λ_{\max} of absorbance (nm) ^a	λ_{\max} (nm) (log ϵ)	λ_{\max} of emission (nm) ^b
PhCPdye	427	427 (4.18)	483
PhCT1Pdye	434	434 (4.35)	530
PhCT2Pdye	455	455 (4.45)	541
PhCT3dye	432	436 (4.48)	656
CoT3dye	492	492 (4.60)	578
CT3A	439	439 (-)	534

^aMeasured in dilute CH_2Cl_2 and DMSO solution, ^bExcited at the absorption maxima

4.4 Electrochemical property

The cyclic voltammograms and different pulse voltammograms of the phenothiazine dyes in dichloromethane solution at scan rate of 0.05V/s are shown in Figure 4.7-10.

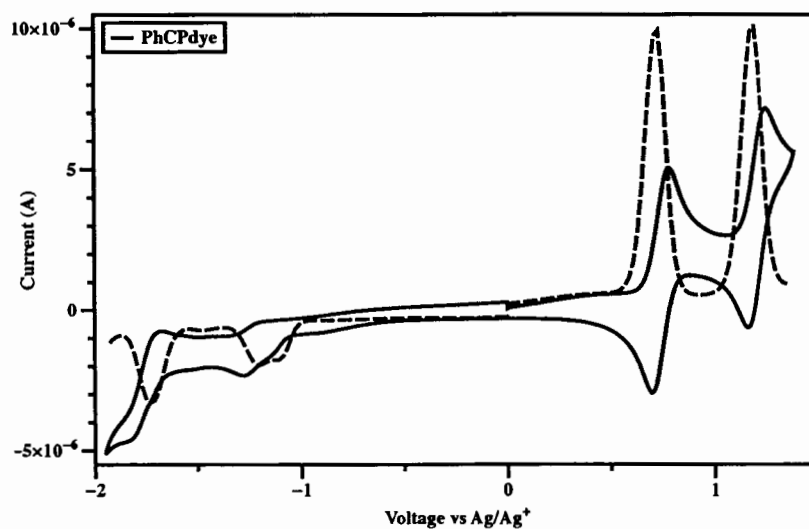


Figure 4.7 The cyclic voltammogram and differential pulse voltammogram of **PhCPdye**

PhCPdye reveals two reversible oxidation peaks with half-wave potential ($E_{1/2}$) at 0.72 and 1.18 V vs Ag/Ag^+ , which are assigned as the formation of phenothiazine radical cation

and carbazole radical cation, respectively. Two reversible reduction waves at -1.21 and -1.73 V Ag/Ag^+ were observed.

PhCT1P dye reveals two reversible oxidation peaks with half-wave potential ($E_{1/2}$) at 0.64 and 1.11 V vs Ag/Ag^+ , which are assigned as the formation of a phenothiazine radical cation and carbazole radical cation, respectively. The one irreversible reduction waves at -1.61 V vs Ag/Ag^+ was observed.

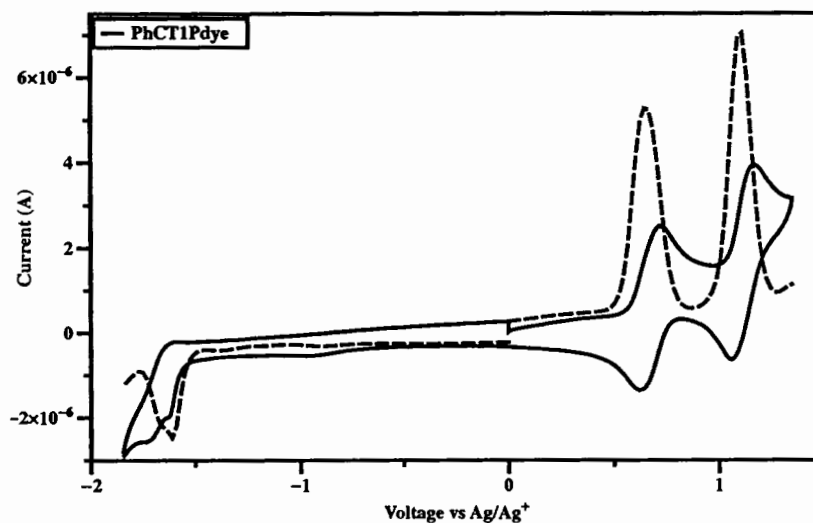


Figure 4.8 The cyclic voltammogram and differential pulse voltammogram of **PhCT1P dye**

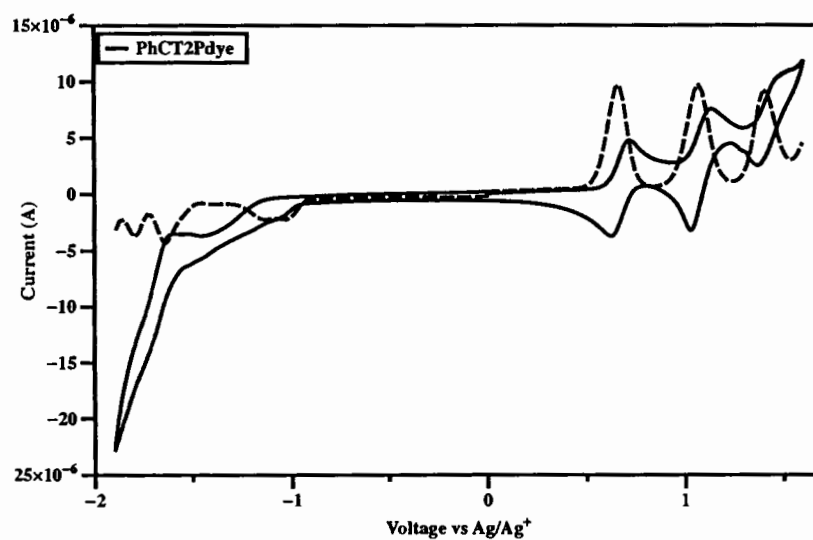


Figure 4.9 The cyclic voltammogram and differential pulse voltammogram of **PhCT2P dye**

PhCT2P dye reveals two reversible oxidation peaks with half-wave potential ($E_{1/2}$) at 0.66 V, 1.06 V and 1.40 V vs Ag/Ag^+ , which are assigned as the formation of phenothiazine

radical cation and carbazole radical cation, respectively. The three irreversible reduction peaks at -1.12, -1.63 V vs Ag/Ag^+ and -1.79 V were observed.

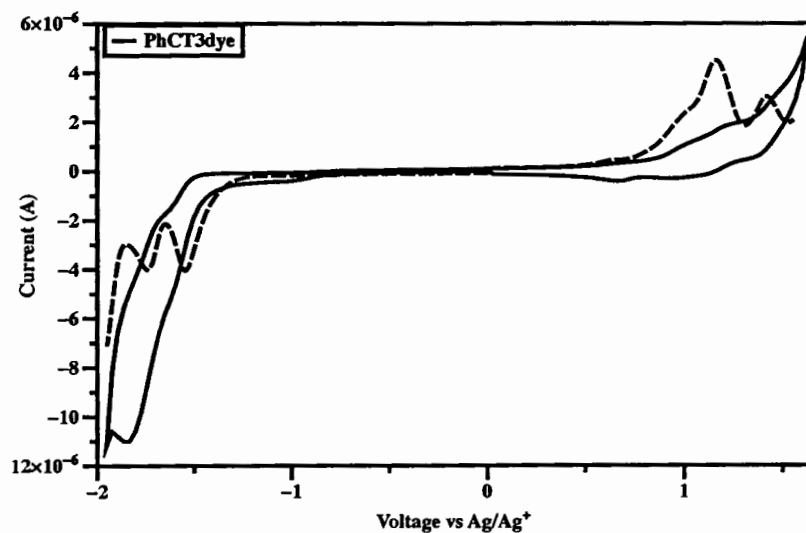


Figure 4.10 The cyclic voltammogram and different pulse voltammogram of PhCT3dye

PhCT3dye shows three reversible oxidation peaks of phenothiazine radical cation, carbazole radical cation and thiophene radical cation at half-wave potential of 0.60, 1.14 and 1.40 V vs Ag/Ag^+ , respectively. Two reversible reduction peaks show at half-wave potential of -1.54 and -1.74 V vs Ag/Ag^+ , respectively. The cyclic voltammogram and diferential pulse voltammogram is shown in Figure 4.10.

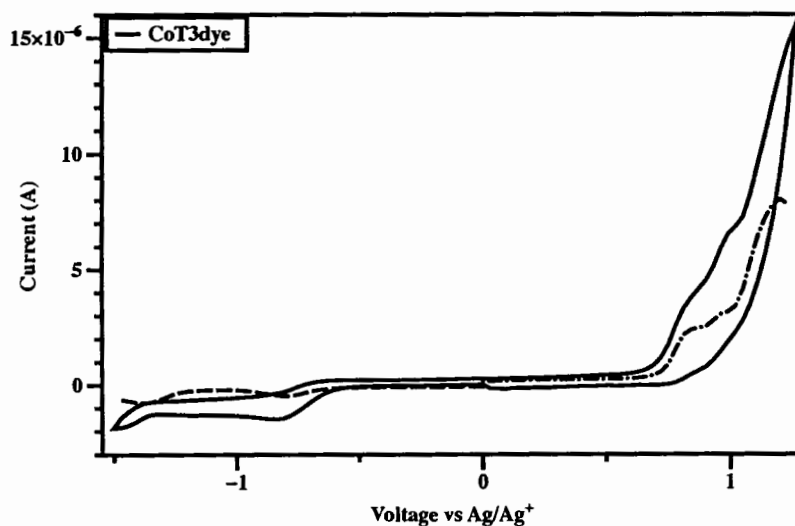


Figure 4.11 The cyclic voltammogram and different pulse voltammogram of CoT3dye

The electrochemical property of **CoT3dye** was obtained in dimethyl sulfoxide solution due to poor solubility in dichloromethane. The three irreversible oxidation peaks at half-wave potential of 0.84, 0.96 and 1.20 V vs Ag/Ag⁺, respectively. Two reversible reduction peaks (-0.81 and -1.38 V vs Ag/Ag⁺) were observed.

The electrochemical results reveal the HOMO value which is above the conduction band of TiO₂. The energy levels of all dyes fit well with the requirements for an efficient flow of electrons. The summary of energy level is shown in Table 4.2.

Table 4.2 Cyclic voltammetry results for phenothiazine and coumarin base dyes

Compound	E _{1^{re}} (V)	E _{2^{re}} (V)	E _{3^{re}} (V)	E _{1^o} (V)	E _{2^o} (V)	E _{3^o} (V)	E _{o-o} ^d (eV)	HOMO ^e (eV)	LUMO ^f (eV)
PhCPdye	1.27 ^b (-1.21) ^c	--1.93 (-1.73)	-	0.78 (0.72)	1.24 (1.18)	-	2.77	-5.06	-2.29
PhCT1Pdye	-1.72 (-1.61)	- -	-	0.72 (0.64)	1.16 (1.11)	-	2.48	-5.0	-2.52
PhCT2Pdye	-1.15 (-1.12)	(-1.63)	(-1.79)	0.71 (0.66)	1.13 (1.06)	1.46 (1.40)	2.43	-5.01	-2.58
PhCT3dye	(-1.54)	-1.93 (-1.74)		0.66 (0.60)	1.23 (1.14)	1.50 (1.40)	2.23	-4.97	-2.74
CoT3dye	-0.78 (-0.81)	-1.41 (-1.38)		0.85 (0.84)	0.99 (0.96)	1.11 (1.20)	2.28	-5.12	-2.84

^aMeasured using a platinum rod counter electrode, a glassy carbon working electrode and a SCE reference electrode in CH₂Cl₂ containing n-Bu₄NPF₆ as a supporting electrolyte with scan rate of 0.05 V/s under argon atmosphere, ^bPeak potential, ^cHalf-wave potential, ^dE_{o-o} was estimated from the intersection between the absorption and emission spectra, ^eCalculated using the empirical equation from HOMO = -(4.44+E_{onset}), ^fCalculated from LUMO = HOMO+E_g

4.5 Thermal property

The thermal property of **PhCPdye**, **PhCT1Pdye** and **PhCT2Pdye** was measured by differential scanning calorimetry (DSC) and thermogravimetric analysis (TGA) as solid samples. The DSC plots of **PhCPdye**, **PhCT1Pdye** and **PhCT2dye** are shown in Figure 4.12. **PhCT1Pdye** shows a glass transition temperature (T_g) at 179.5 °C and **PhCT2dye** shows a T_g at 165 °C.

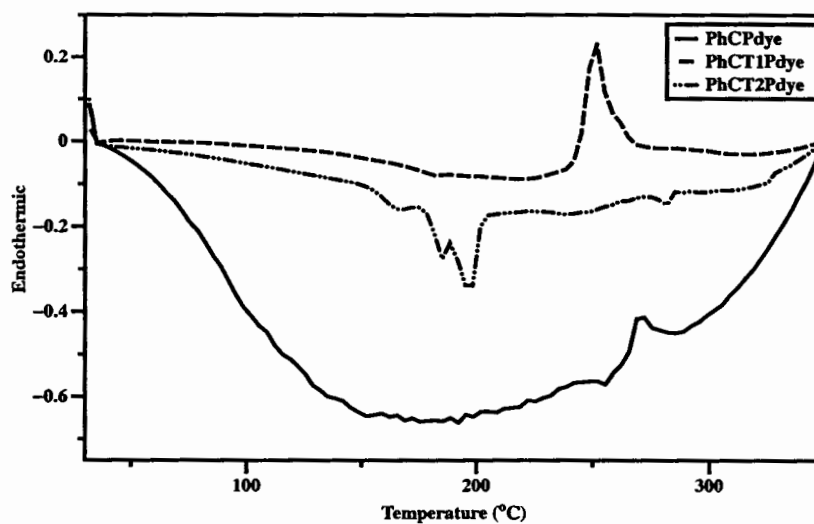


Figure 4.12 The DSC plots of PhCPdye, PhCT1Pdye and PhCT2dye

The desired molecules show high degradation temperature (T_d) at 200, 230 and 230 °C, respectively. These results confirm that the desired product can be used as light harvesting materials with high thermal stability.

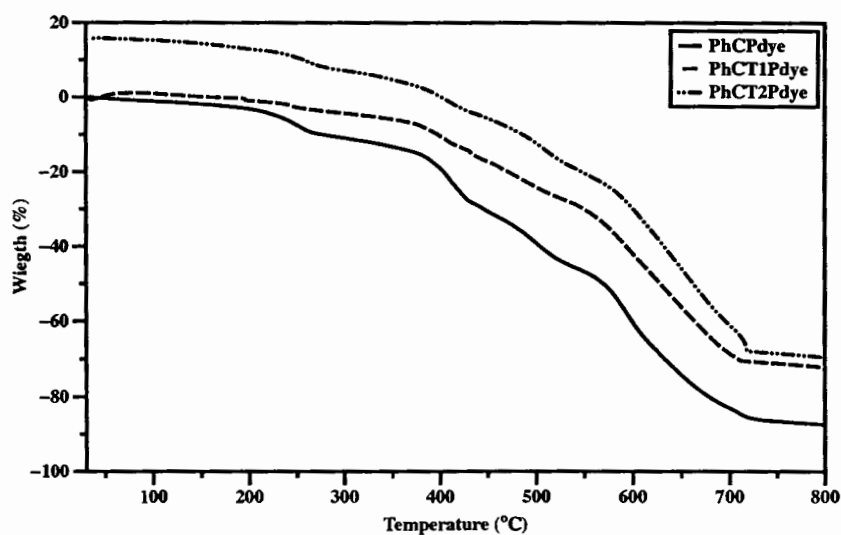


Figure 4.13 The TGA plots of PhCPdye, PhCT1Pdye and PhCT2dye

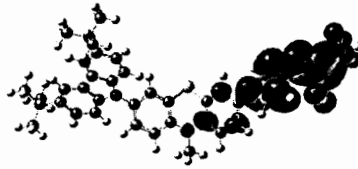
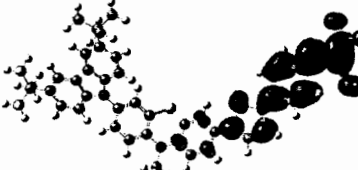
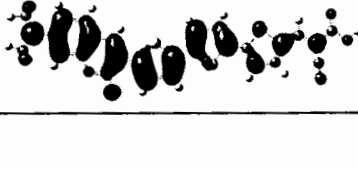
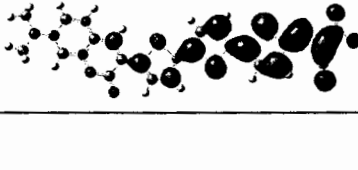
Table 4.3 The thermal property results of PhCPdye, PhCT1Pdye and PhCT2dye

Compound	T_g (°C)	T_m (°C)	T_c (°C)	T_d (°C)
PhCPdye	-	-	-	200
PhCT1Pdye	179.5	-	-	230
PhCT2Pdye	165	-	-	230

4.6 Computational calculation

The optimised structure and frontier molecular orbital were calculated by DFT/B3LYP/6-31G9(d,p) method (Table 4.4). At the HOMO level the electrons distribute at the donor-bridge while at the LUMO level the electrons distribute at the bridge-acceptor indicating that electron transfer occurs in the dye molecules from the donor to the acceptor parts of the molecule when excited.

Table 4.4 The frontier molecular orbital of phenothiazine base dyes and coumarin base dye

Compound	HOMO	LUMO
PhCPdye		
PhCT1Pdye		
PhCT2Pdye		
PhT3dye		
CoT3dye		

4.7 Devices performance

Figure 4.14 shows the incident monochromatic photon-to-current conversion efficiencies (IPCEs) obtained with a sandwich-type two electrodes cell. The dye-coated TiO₂ film was used as the working electrode, platinised FTO glass as the counter electrode and 0.1 M LiI, 0.5 M I₂, 0.4 M TBA and 0.6 M TPAI in acetonitrile and valeronitrile (volume ratio, 85: 15) mixed solution as the redox electrolyte.

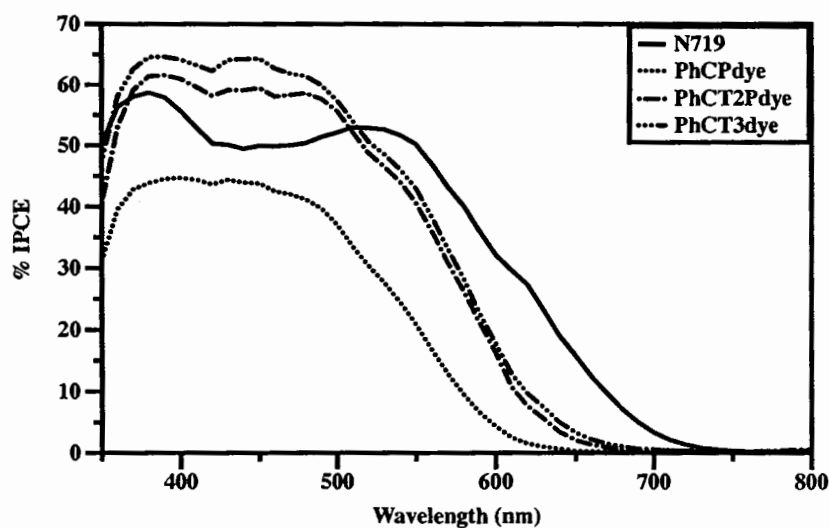


Figure 4.14 Spectra of monochromatic incident photon-to-current conversion efficiencies (IPCEs) for DSSCs based on phenothiazine dyes

The IPCE exceeds 40% in the spectral range of 380-480 nm for **PhCPdye**, which reaches its maximum of 44.6% at 400 nm. The IPCE of **PhCT1Pdye** reached a maximum (59.3%) at 380 nm. The **PhCT2Pdye** shows a maximum IPCE at 61.5% at 390 nm. The IPCE of **PhCT3dye** shows the highest value at 64.6% at 390 nm.

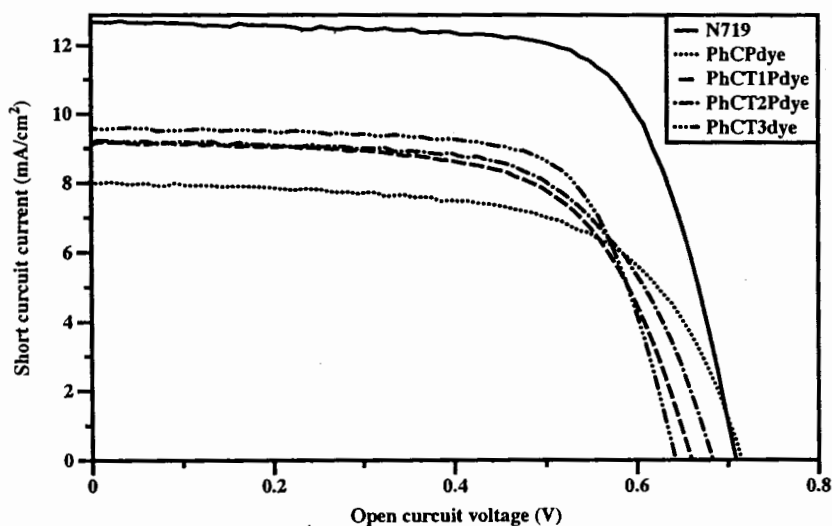


Figure 4.15 *J-V* curves of DSSCs based on phenothiazine dyes

The performance statistics of the devices are also listed in Table 4.5. An overall conversion efficiency (η) of 4.33% was achieved from the DSSC based on **PhCT3dye** (short-circuit photocurrent density, $J_{sc} = 9.58 \text{ mA cm}^{-2}$; open-circuit photovoltage, $V_{oc} = 0.64 \text{ V}$; fill

factor, $ff = 0.70$). This efficiency is higher than the efficiency of 4.02% ($J_{sc} = 9.21 \text{ mA cm}^{-2}$; $V_{oc} = 0.68 \text{ V}$; $ff = 0.64$) obtained from the DSSC based on the dye **PhCT2Pdye** corresponding to the %IPCE and the energy level of **PhCT3dye**. The HOMO level of the **PhCT3dye** is closer to the redox potential of the I^+/I_3^- system than of the other dyes mentioned above, this results in a worse V_{oc} performance compared to the other device performances.

Table 4.5 Photovoltaic performance of DSSCs based on phenothiazine dyes

Sample	J_{sc} (mA cm ⁻²)	V_{oc} (V)	ff	η (%)
N719	12.68	0.71	0.71	6.34
PhCPdye	8.00	0.71	0.63	3.60
PhCT1Pdye	9.12	0.66	0.65	3.90
PhCT2Pdye	9.21	0.68	0.64	4.02
PhCT3dye	9.58	0.64	0.70	4.33

4.8 Conclusion

A series of phenothiazine based dyes was successfully synthesised and fully characterized. A coumarin dye with thiophene-bridge was also synthesised. The optical property of the target molecules was investigated in dry dichloromethane and dimethyl sulfoxide solution. The desired molecules exhibited a maxima absorption band of around 420-490 nm based on ICT. Phenothiazine derivatives show a high thermal stability with T_d at 200, 230 and 230 °C, respectively. The frontier molecular orbitals show the distribution of electron located at the bonding orbital of donor at the HOMO level while at the LUMO level the electron distributes at the anti-bonding orbital of the acceptor group. The devices performances were also studied using phenothiazine base dye, the **PhCT3dye** shows the highest performance with a power conversion efficiency at 4.33% ($J_{sc} = 9.58 \text{ mA cm}^{-2}$, $V_{oc} = 0.64 \text{ V}$ and $ff = 0.70$) at AM 1.5 G.

CHAPTER 5

THE CONJUGATED POLYMER NANOPARTICLES AS ORGANIC SEMICONDUCTOR

5.1 Introduction

In recent years there has been quite a lot of work completed on conjugated polymer nanoparticles (CPNs) with regards to different applications. [118-120] CNPs can offer high brightness, excellent photo-stability, high quantum yields, low cytotoxicity and versatility towards surface modification in biological applications such as bio-imaging, bio-sensing and nanomedicine. CNPs dispersed in water retain low viscosity at high solids content compared to similar solutions of high molar mass conjugated polymer dissolved in organic solvent. In terms of processing for optoelectronic and photonic applications, this means that films for devices can be prepared at room temperature from water based dispersions rather than from hot solutions of chlorinated organic solvents, with their inherent environmental drawbacks. Large area scale processing via ink-jet printing [121, 122] or screen printing [123, 124] whilst possible in organic solvents will be best achieved through deposition from aqueous dispersions.

Most previous work focuses primarily on the post-polymerisation preparation of conjugated polymer nanoparticles via re-precipitation [64, 125, 126], mini-emulsion [127-130] or self-assembly [131] routes. The polymerisation of conjugated polymer nanoparticles has been achieved in a non-aqueous emulsion process using block copolymers as stabilisers. [132] It has also been shown in certain cases that the presence of a surface coating of surfactant on conjugated polymer particles (once excess surfactant has been removed) does not prohibit the transport of charges in the resultant films. [133] Some progress on the direct synthesis of small conjugated polymer nanoparticles (< 30 nm) in water under mini-emulsion conditions via Glaser coupling reactions has been reported. [134] Hyperbranched, conjugated polymer nanoparticles, of about 200 nm particle diameter, have been recently synthesized via Suzuki cross-coupling reactions in a modified emulsion polymerization environment at high temperatures using a non-ionic surfactant from the Tween series. [135] The selection and concentration of non-ionic surfactant used in the emulsion process is critical. The concentrations of non-ionic surfactants in water required to initially stabilise the initial organic phase (monomers and solvent) are often above their cloud points at high temperatures. Trial emulsion polymerisations completed with Triton X-102 surfactant via Suzuki cross-coupling reactions, catalysed by tetrakis (triphenylphosphine) palladium (0), at 60 °C, produced polymers of significant molar mass but generally did not yield

completely stable emulsion systems. [136] A catalyst which could perform Suzuki cross-coupling polymerisation of the monomers at lower temperatures was required. We have recently reported the use of the (N-heterocyclic carbene)PdCl₂ (TEA) complex, (IPr*)PdCl₂(TEA) in Suzuki couplings of aryl chlorides with aryl boronic acids at low temperatures. [137] The 'throw-away' ligand, tetraethylamine (TEA) attached to the Pd centre is deemed to improve activity as a consequence of the ease of its departure and/or the higher tendency of TEA to re-coordinate to the [(NHC)-Pd(0)] and conserve the active species in solution.

There has been much discussion into the relationships between order, disorder, aggregation and charge transport in conjugated polymers. [138-140] The photophysical properties of some conjugated polymers within nanoparticulate systems has been shown to improve in varied situations where there are isolated polymer chains, aggregation of polymer chains and ordered conformations. In the case of polyfluorene, a beta phase (β) conformation, which involves planarization of the main chains, can be adopted (which emits at a lower energy in photoluminescence) rather than a disordered glassy phase under certain conditions. [141] The formation of this ordered phase in dilute PFO solutions can be induced by cooling in poor solvents [142] or produced in films via spin-coating from good solvents. [143] McNeill and Wu have reported that solvent induced swelling of polyfluorene nanoparticles led to increased planarization of the polymer chains in the glassy phase to yield more of the β -phase conformation resulting in increased quantum yields. [144] Significant beta phase content has been recently observed in nanoparticles of polyfluorene modified with pendant triethoxysilyl groups which were prepared in THF via re-precipitation method as part of study which produced hybrid silica/polyfluorene nanoparticles. [145] Each of the emulsions discussed in this report has potentially a concentration in excess of 50 mg/ml of conjugated polymer in the present of xylene in their nanoparticles. It has been reported at high polyfluorene concentrations in solution (> 30 mg/ml) that some polymer chains form aggregate domains within the overlapping polymers. [146]

It has been show that making films from structurally ordered polythiophene nanoparticles can have a positive impact on the performance of organic thin-film transistors. [147] Rod-like features were observed in highly crystalline films obtained from nanoparticle dispersions after annealing. Ellipsoidal polymer colloids have been observed when ordered structures of PFO and PF8BT are created within the nanoparticles (created post-polymerization using mini-emulsion) upon annealing. [148]

We report the direct synthesis of stable emulsions of conjugated polymer nanoparticles via Suzuki cross-coupling emulsion reactions of 9,9-dioctylfluorene-2,7-diboronic acid bis(1,3-propanediol) ester with a number of dibromo monomers in the presence of Triton X-102, using the palladium catalyst, (IPr*)PdCl₂(TEA) and tetraethylammonium hydroxide, at 30°C

after 24-48 hr. The characterization and photophysical properties of the nanoparticulate emulsions are also outlined. Our findings describe for the first time the self-assembly of rod-like nanoparticles resulting from Suzuki cross-coupling emulsion polymerizations of poly(9,9-dioctylfluorene) (PFO) and poly(9,9-dioctylfluorene-*alt*-bithiophene) (PF8T2), in aqueous conditions at low temperatures. The emulsion process can be modified successfully to deliver a range of conjugated polymer concentrations of PFO, PF8T2, PF8BT and PF8TAA in water required for processing devices (up to 11 mg / ml).

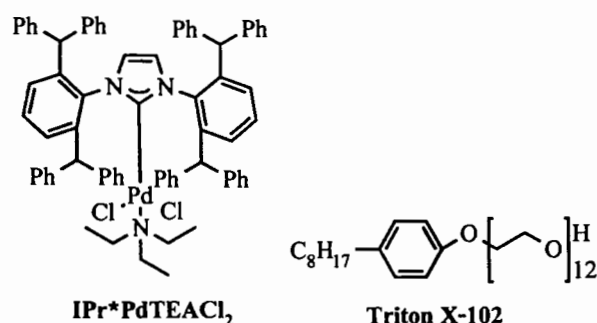
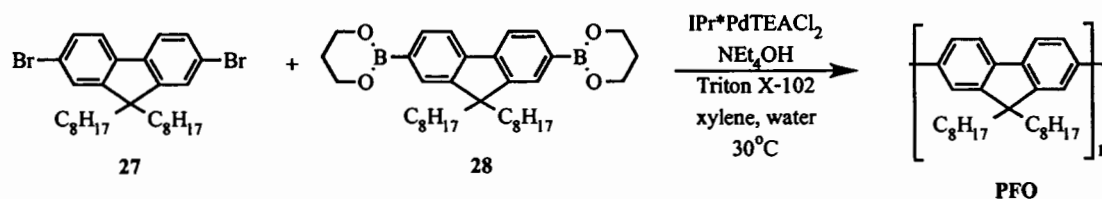


Figure 5.1 Chemical structure of IPr*PdTEACl₂ and Triton X-102

5.2 Synthesis

The poly(9,9-dioctylfluorene) (PFO) was obtained under Suzuki cross-coupling polymerization using IPr*PdTEACl₂ as catalyst (Figure 5.1), NEt₄OH as base and the solution of triton X-102 in deionized water as surfactant in order to stabilise nanoparticles, in xylene as shown in Scheme 5.1. Reaction's colour changed gradually to yellow after stirred for 30 min. The molecular weight was carried out by GPC as THF solution, which is shown in Table 5.1. The four differences polymer concentrations were obtained as 3.0 mg/ml (LM42), 6.0 mg/ml (LM66), 8.6 mg/ml (LM68) and 11.1 mg/ml (LM71), respectively.



Scheme 5.1 Synthetic route of PFO

The GPC results reveal molar mass (Mn) of LM42 = 27,100 g/mol, LM66 = 28,900 g/mol, LM68 = 16,300 g/mol and LM71 = 12,900 g/mol, respectively while the polydispersity (PDI) = 3.22, 3.29, 3.81 and 3.05, respectively. The molar mass decreased when the

concentration of monomer increasing. **LM66** shows the best result with high concentration of polymer and the highest molar mass.

Table 6.1 Sample concentration amount of monomer, percent surfactant, solvent and Molar mass of PFO at various concentration

Sample	Total monomer (mmol)	Triton X-102 (% wt)	Solvent (ml)	Final polymer conc. (mg/ml)	Mn (g/mol)	Mw (g/mol)	PDI
LM42	0.4	5	2	3.0	27,100	87,500	3.22
LM66	0.8	5	2	6.0	28,900	95,400	3.29
LM68	1.2	10	4	8.6	16,300	62,000	3.81
LM71	1.6	15	6	11.1	12,900	39,400	3.05

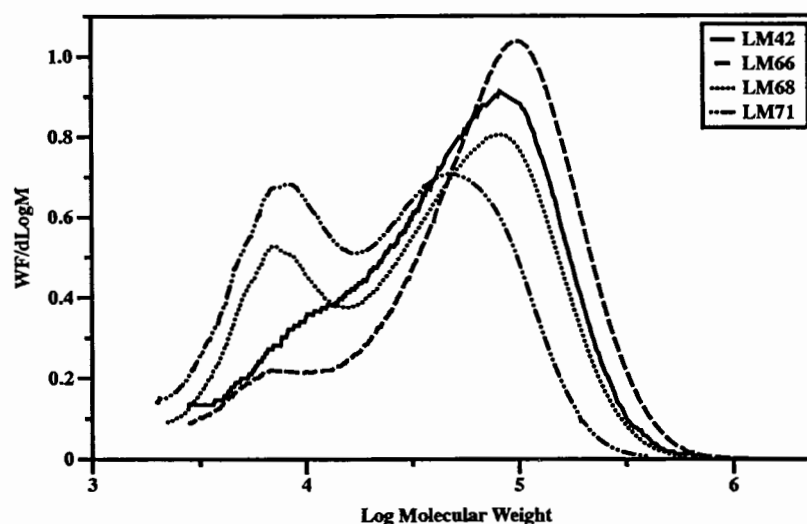
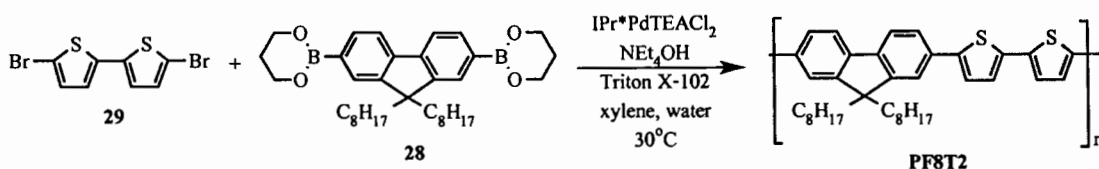


Figure 5.2 Log molecular weight and WF/dLogM plot of PFO

The synthetic route of poly(9,9-dioctylfluorene-2,7-diyl)-*co*-bithiophene (**PF8T2**) was showed in Scheme 5.2. Nanoparticles of **PF8T2** was successfully synthesised under Suzuki cross-coupling polymerisation. The reaction's colour changed gradually from yellow to orange after the monomer mixture was added to surfactant. To obtain molar mass, crude product was washed with methanol and water in order to remove excess surfactant, dried with air and dissolved in THF. The molecular weight of the polymer was obtained as THF solution using GPC analysis. The results were shown in Table 5.2. The optical properties and particles size measurement were measured without further purification. Two differences polymer concentration with 2.13 mg/ml (**LM45**) and 8.22 mg/ml (**LM85**), respectively, were synthesised.



Scheme 5.2 Synthetic route of PF8T2

Table 5.2 Sample concentration amount of monomer, percent surfactant, solvent and Molar mass of PF8T2 at various concentration

Sample	Total monomer (mmol)	Triton X-102 (% wt)	Solvent (ml)	Final polymer conc. (mg/ml)	Mn (g/mol)	Mw (g/mol)	PDI
LM45	0.4	5	2	2.13	12,100	32,700	2.69
LM85	1.6	10	4	8.22	14,900	37,300	2.51

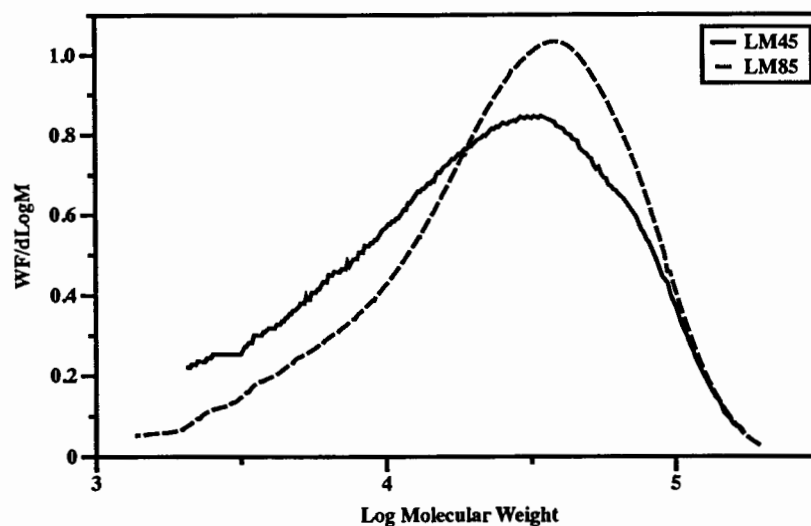
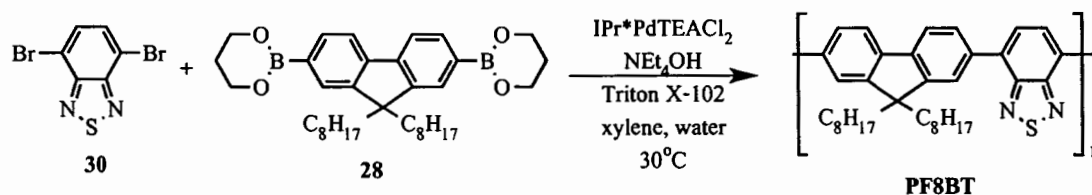


Figure 5.3 Log molecular weight and WF/dLogM plot of PF8T2

The nanoparticles of poly(9,9-di-octylfluorene-2,7-diyl)-*co*-(benzo[2,1,3]thiadiazole) (PF8BT) was successfully carried out using Suzuki cross-coupling polymerisation as shown in Scheme 5.3. The particles size and optical property were measured with out further purification. The molar mass was obtained by GPC analysis as the THF solution. The molar mass of polymer was shown in Figure 5.4 and summarised in Table 5.3. Concerning to IPr*PdTEACl₂ catalyst, 9,9-dioctylfluorene-2,7-bis(boronic acid pinacol ester) was used for trial reaction but no polymer was obtained in this condition indicated that the steric hindrance of pinacol ester affects to catalyst reactivity. Moreover, the reaction conversion hits the limit after 24h, there is no further polymer

observed. Two differences polymer concentration with 2.09 mg/ml (LM47) and 4.18 mg/ml (LM84), respectively, were synthesised.



Scheme 5.3 Synthetic route of PF8BT

Table 5.3 Sample concentration amount of monomer, percent surfactant, solvent and Molar mass of PF8BT at various concentration

Sample	Total monomer (mmol)	Triton X-102 (% wt)	Solvent (ml)	Final polymer conc. (mg/ml)	Mn (g/mol)	Mw (g/mol)	PDI
LM47	0.4	5	2	2.09	24,200	82,700	3.42
LM84	0.8	5	2	4.18	26,000	67,300	2.58

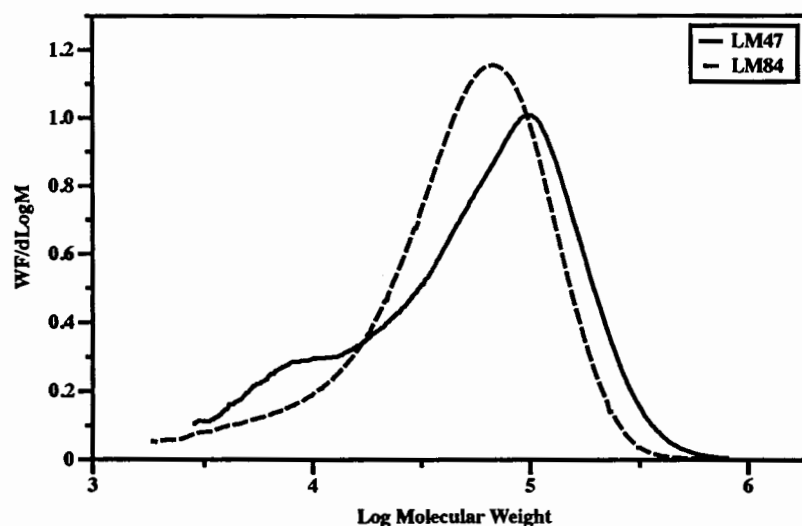
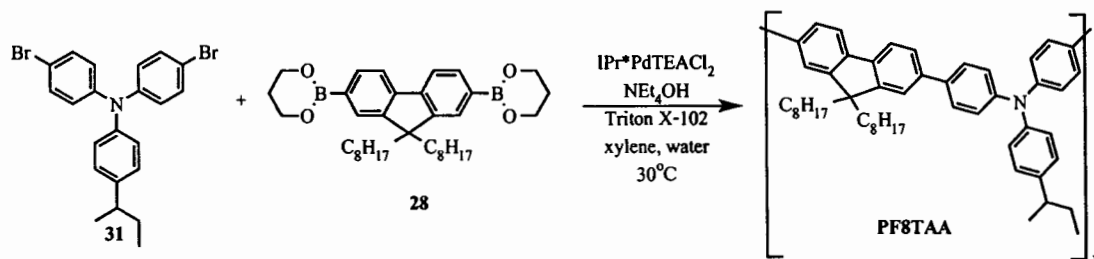


Figure 5.4 Log molecular weight and WF/dLogM plot of PF8BT

Poly(9,9'-dioctylfluorene-2,7-diyl)-*co*-bis-*N,N'*-(4-*sec*-butylphenyl)diphenylamine (PF8TAA) was successfully synthesised using Suzuki cross-coupling polymerisation. IPr*PdTEACl₂ was used as catalyst, Net₄OH as base, Triton X-102 5% wt/v in water as surfactant source in xylene, as shown in Scheme 5.4. The polymer with high concentration shows lower molecular weight. The the large amount of surfactant caused the reaction mixture to become

viscous contents. The GPC results were summarised in Table 5.4 and shown in Figure 5.5. Two differences polymer concentration with 2.65 mg/ml (LM48) and 9.51 mg/ml (LM57), respectively, were synthesised.



Scheme 5.4 Synthetic route of PF8TAA

Table 5.4 Sample concentration amount of monomer, percent surfactant, solvent and Molar mass of PF8TAA at various concentration

Sample	Total monomer (mmol)	Triton X-102 (% wt)	Solvent (ml)	Final polymer conc. (mg/ml)	Mn (g/mol)	Mw (g/mol)	PDI
LM48	0.4	5	2	2.65	18,500	49,800	2.69
LM57	1.6	20	8	9.51	9,200	21,700	2.34

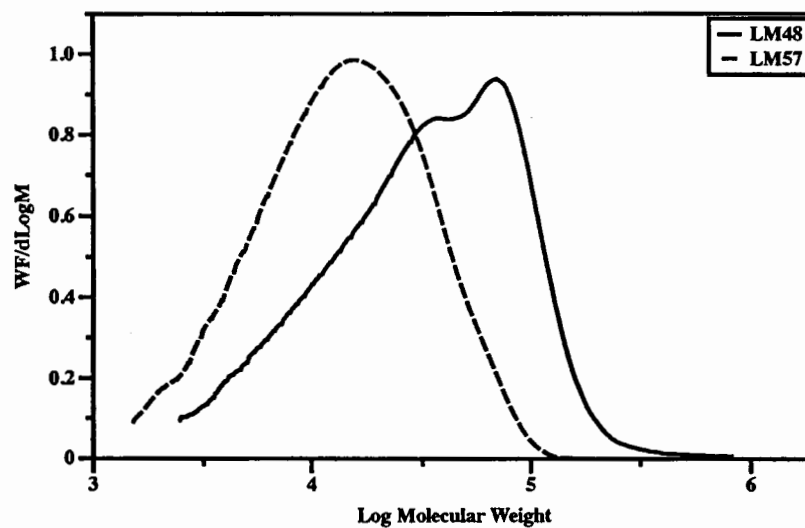


Figure 5.5 Log molecular weight and WF/dLogM plot of PF8TAA

5.3 Particles size analysis

5.3.1 Dynamic Light Scattering (DLS)

Dynamic light scattering (DLS) covers different techniques to measure the particle size due to dynamic changes of scattered light intensity. Photon correlation spectroscopy (PCS) is at present the most widely used name. It relates to the correlation technique that is applied in instruments. Quasi-elastic light scattering (QELS) was used more frequently in the past. This term relates to the type of interaction between particles and light. The term Diffusing Wave Spectroscopy is often used for applications in concentrated dispersions, where multiple scattering leads to a diffusive transport of light.

In the DLS technique, the intensity of the scattered light by an ensemble of particles is measured at a given angle as a function of time. The Brownian motion of the dispersed particles determines the rate of change of the scattered light intensity. The temporal intensity changes are converted to a mean translational diffusion coefficient (or a set of diffusion coefficients). Fast intensity changes are related to a rapid decay of the correlation function and a large diffusion coefficient. The diffusion coefficient is then converted into particle size by means of the Stokes-Einstein equation. For this conversion the particles are assumed to be spherical and without interaction. Note that colloidal particles in a liquid dispersion contain an attached layer of ions and molecules from the dispersion medium that moves with the particle. Therefore, their hydrodynamic particle size is somewhat larger than the size of the particle.

For good operation, a very low particulate concentration is required of at least 500 particles in the measurement zone. Particle-particle interactions and multiple scattering become apparent at increased concentration (above about 0.01% (v/v)) and result in biased sizing results. Such concentrations often show a clearly visible turbidity. Only relative values of apparent size can then be obtained. An apparently larger or smaller particle size may result, depending on the type of interaction (attraction or repulsion between particles). [149] At extremely low concentrations, if less than about 500 particles are in the measurement zone, random changes of the number concentration cause biased sizing results.

5.3.2 Particles size

The particles size was measured by dynamic light scattering (DLS) technique. The neat products were diluted in deionized water with various concentrations from 7.45, 7.47, 7.48 and 7.95 $\mu\text{g/ml}$, respectively. Dynamic light scattering (DLS) of the resultant emulsion indicated nanoparticles with a broad size distribution (polydispersity index, PDI = 0.33) exhibiting a z-average particle diameter size (d_z) of 53 nm. High PDI values (>0.2) were observed for each of the PFO emulsions and indeed, to a lesser extent, for all of the conjugated polymer emulsions studied. In some cases this may reflect the inability of the DLS fitting analysis to resolve

distribution(s) of small conjugated nanoparticles or a potential distribution of surfactant micelles. Micelles of Triton X-102 surfactant exhibit a particle size diameter, d_z of 7.1 nm (PDI = 0.19). DLS analysis also presumes that the particles present are spherical in nature and when nanoparticulate samples deviate significantly from this, the results can be difficult to interpret.

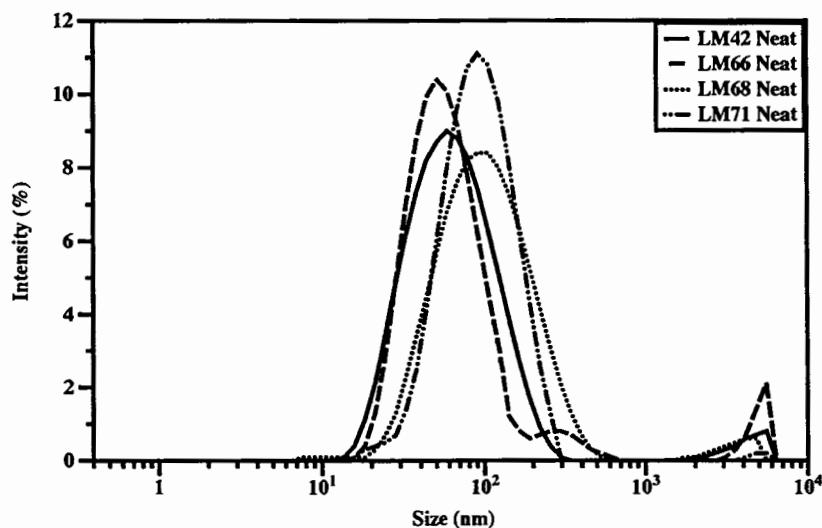
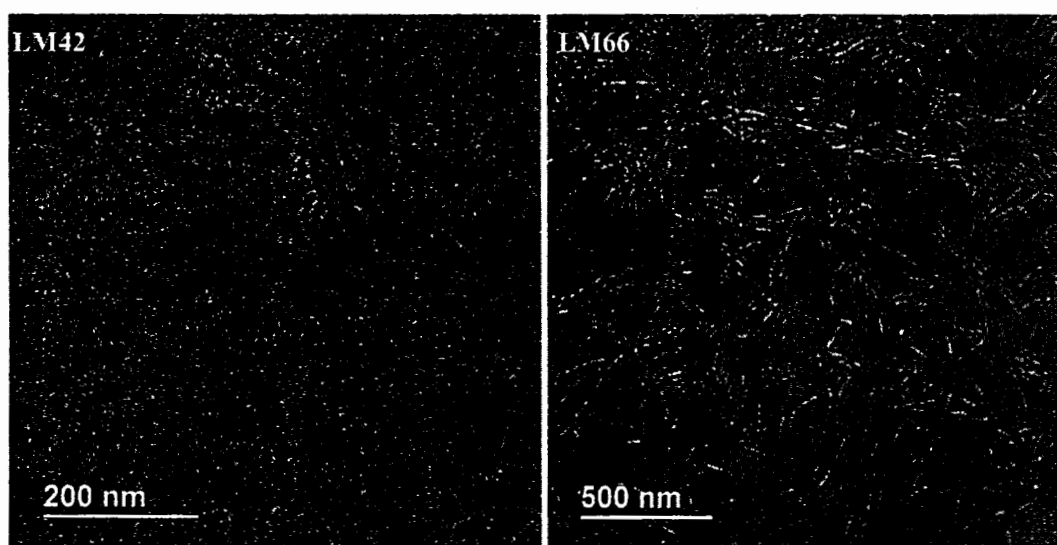


Figure 5.6 Particles size of PFO in water at 25°C

Indeed TEM analysis of the PFO emulsions revealed that they were predominantly composed of rod-like nanoparticles. The general surface features of a nanoparticulate layer of LM66 are clearly evident in the image presented in Figure 5.7: individual rods, with approx. dimensions of 74×16 nm (aspect ratio of almost 5).



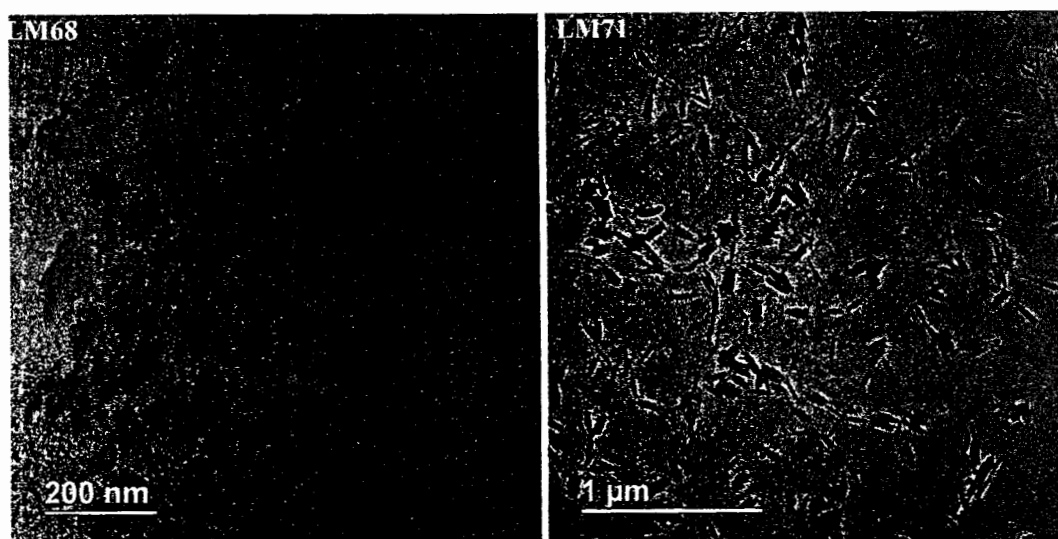


Figure 5.7 TEM images of nanoparticles present in PFO emulsion

Larger rods were observed in TEM analysis of these emulsions, with the largest rods of the PFO emulsion series obtained from reaction LM71, with dimensions measured on average at 106×25 nm, presented in Figure 5.7. The rods appear to order themselves in stacks when found in close proximity to each other (right enlarged image). A small population of spherical particles with number average diameter size of 27 nm was also observed.

Table 5.5 Particles size of PFO in water at 25°C

Compound	Total monomer /mmol	Polymer conc. ^a / mg ml ⁻¹	Particle size / nm		
			DLS ^b		TEM ^c
			d_z [PDI]	d_n	l_n, w_n or d_n
LM42	0.4	3.0	53[0.33]	21	76, 18 <i>r</i>
LM66	0.8	6.0	55[0.41]	26	74, 16 <i>r</i>
LM68	1.2	8.6	81[0.32]	22	99, 23 <i>r</i>
LM71	1.6	11.1	88[0.22]	41	106, 25 <i>r</i>

^aApprox. conjugated polymer concentration of emulsion upon complete conversion. ^bDLS analysis of the z-average and number average particle (d_z and d_n) sizes of emulsion particles at 25 °C; polydispersity index (PDI) of particles presented. ^cTEM analysis of the number average length (l_n) and number average width (w_n) dimensions or the number average particle (d_n) sizes of emulsion nanoparticles (d_n), denoted with *s*: predominantly spherical or *r*: predominantly rod-like in shape. Averages determined from the measurement of at least 100 nanoparticles in each case.

The particles size of PF8T2, LM45 and LM85, nanoparticles were measured as water dispersion with concentration of 8.48 and 5.47 $\mu\text{g/ml}$, respectively. The DLS results were shown and summarized in Figure 5.8 and Table 5.6, respectively. LM85 was filtered by 0.45 μm filter in order to get rid of big particles before measuring. DLS analysis of these emulsions suggested that the higher concentrated PF8T2 is produced the larger nanoparticles ($d_z = 88 \text{ nm}$) with a narrow particle size distribution (PDI = 0.18) are obtained. TEM analysis of both these emulsions actually revealed rod-like structures. In the case of LM85, larger, more uniform, rod-like nanoparticles (205 nm in length, with an aspect ratio of 4) were observed, the TEM images as shown in Figure 5.9. The LM85 equates to producing a PF8T2 emulsion containing 8.2 mg ml^{-1} conjugated polymer in which the nanoparticles themselves contain conjugated polymer in xylene at concentrations approaching 11 %.

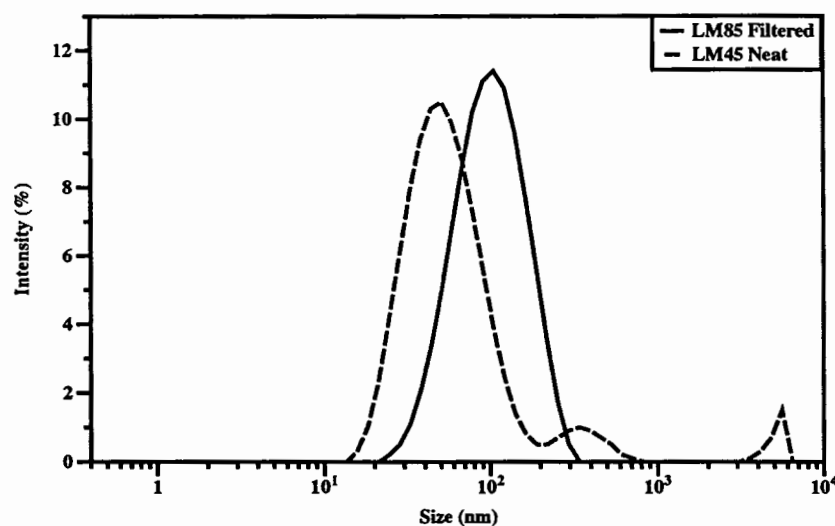


Figure 5.8 Particles size of PF8T2 in water at 25°C

Table 5.6 Particles size of PF8T2 in water at 25°C

Compound	Total monomer /mmol	Polymer conc. ^a / mg ml ⁻¹	Particle size / nm		
			DLS ^b		TEM ^c
			d_z [PDI]	d_n	l_n, w_n or d_n
LM45	0.4	2.1	61[0.34]	23	82, 18 <i>r</i>
LM85	1.6	8.2	88[0.18]	35	205, 52 <i>r</i>

^aApprox. conjugated polymer concentration of emulsion upon complete conversion. ^bDLS analysis of the z-average and number average particle (d_z and d_n) sizes of emulsion particles at 25 °C; polydispersity index (PDI) of particles presented. ^cTEM analysis of the number average length (l_n) and number average width (w_n) dimensions or the number average particle (d_n) sizes of

emulsion nanoparticles (d_n), denoted with *s*: predominantly spherical or *r*: predominantly rod-like in shape. Averages determined from the measurement of at least 100 nanoparticles in each case.

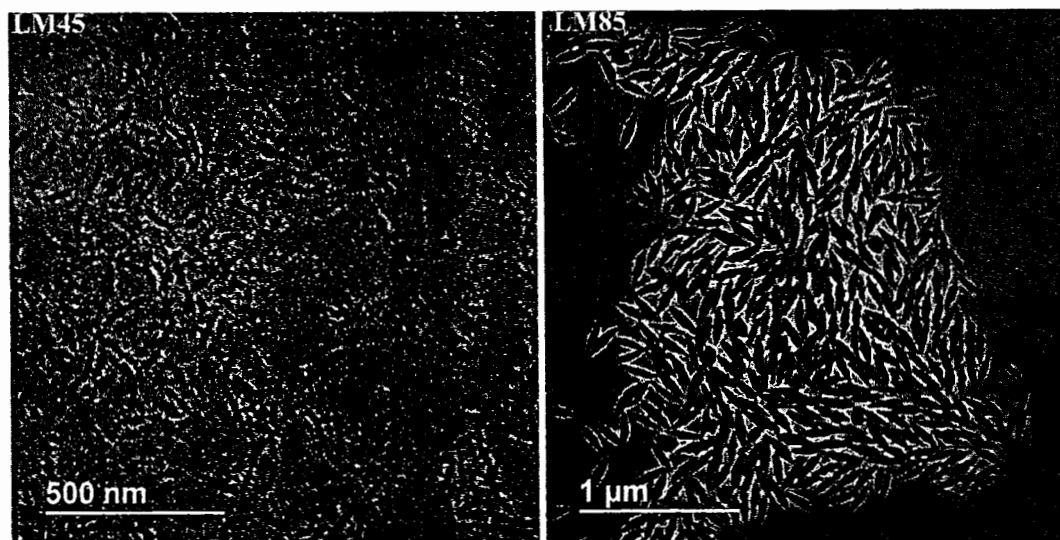


Figure 5.9 TEM images of nanoparticles present in PF8T2 emulsion

The particles size of PF8BT, LM47 and LM84, were measured as water dispersion with concentration of 18.64 $\mu\text{g/ml}$ for LM47 and 13.89 $\mu\text{g/ml}$ for LM84, respectively. The measurement was performed using the crude product, which was dissolved in de-ionised water. PF8BT shows small particles around 34-38 nm with large PDI as shown in Figure 5.10 and Table 5.7. The TEM image obtained of the nanoparticulate material in emulsion LM47 revealed spherical particles exhibiting mean particle diameter of 23 (± 6) nm. The particle size distribution obtained by TEM is not much different to the number average particle distribution observed in DLS analysis (d_n (DLS) = 21 nm), as can be seen in Figure 5.11.

Table 5.7 Particles size of PF8BT in water at 25°C

Compound	Total monomer /mmol	Polymer conc. ^a / mg ml ⁻¹	Particle size / nm		
			DLS ^b d_z [PDI]	d_n	TEM ^c l_n, w_n or d_n
LM47	0.4	2.0	32[0.20]	21	23 <i>s</i>
LM84	0.8	4.0	34[0.16]	23	n/a

^aApprox. conjugated polymer concentration of emulsion upon complete conversion. ^bDLS analysis of the z-average and number average particle (d_z and d_n) sizes of emulsion particles at 25 °C; polydispersity index (PDI) of particles presented. ^cTEM analysis of the number average length (l_n) and number average width (w_n) dimensions or the number average particle (d_n) sizes of emulsion

nanoparticles (d_n), denoted with *s*: predominantly spherical or *r*: predominantly rod-like in shape. Averages determined from the measurement of at least 100 nanoparticles in each case.

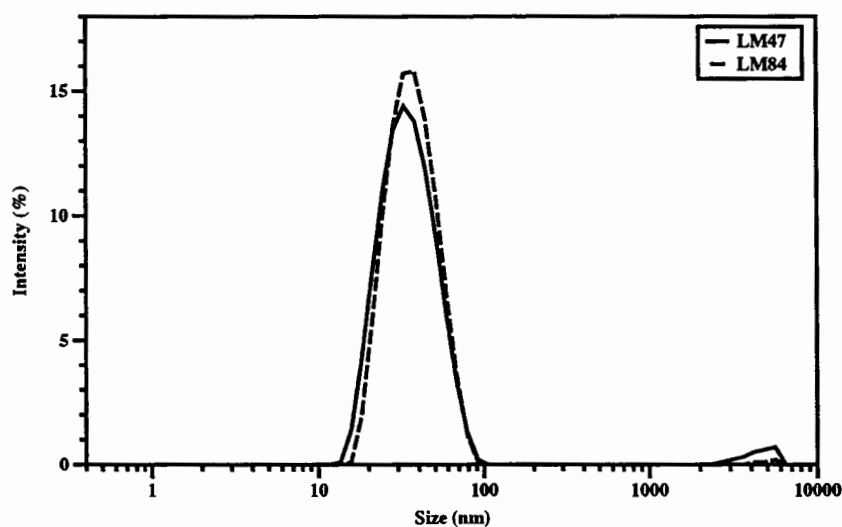


Figure 5.10 Particles size of PF8BT in water at 25°C

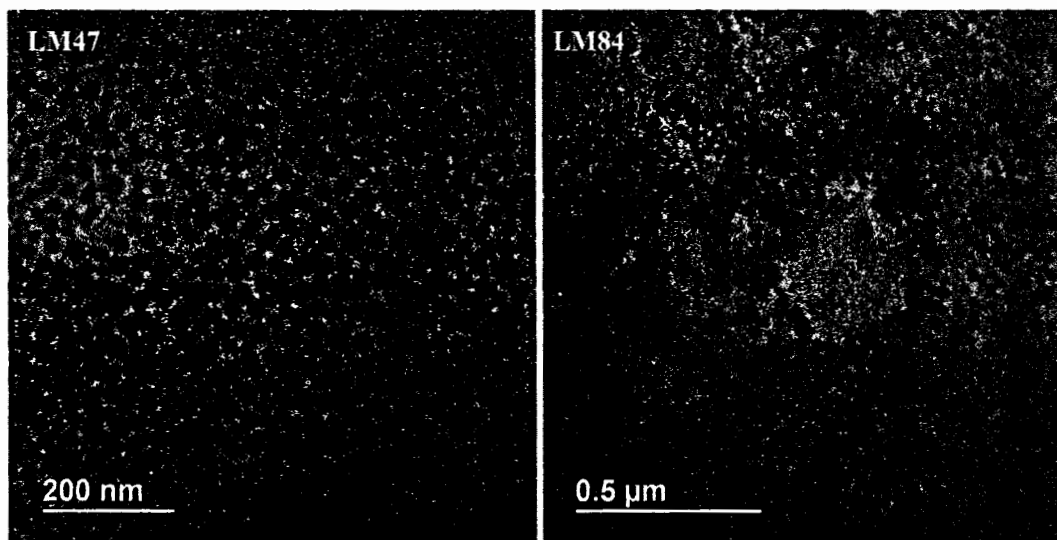


Figure 5.11 TEM images of nanoparticles present in PF8BT emulsion

The particles size of PF8TAA, LM48 and LM57, were measured as water dispersion with concentration of 10.6 $\mu\text{g/ml}$ for LM48 and 13.40 $\mu\text{g/ml}$ for LM57, respectively. The measurement was obtained using the crude product, which was dissolved in de-ionised water. LM48 shows 2 sizes of particles at 28 nm and 324 nm while LM57 shows small particles at 59 nm as shown in Figure 5.12 and Table 5.8. TEM analysis of these PF8TAA emulsions revealed spherical particles, in the case of LM57, exhibiting mean number average particle diameters of 41

(± 6) nm, **LM57** particle size distribution is not much different to that observed for the respective emulsion in DLS analysis (number average particle size distribution displayed, $d_n = 33$ nm), as outlined in Figure 15.13.

Table 5.8 Particles size of **PF8TAA** in water at 25°C

Compound	Total monomer /mmol	Polymer conc. ^a / mg ml ⁻¹	Particle size / nm		
			DLS ^b		TEM ^c
			d_z [PDI]	d_n	l_n, w_n or d_n
LM48	0.4	2.6	41[0.33]	18	19 <i>s</i>
LM57	1.6	9.5	56[0.22]	33	41 <i>s</i>

^aApprox. conjugated polymer concentration of emulsion upon complete conversion. ^bDLS analysis of the z-average and number average particle (d_z and d_n) sizes of emulsion particles at 25 °C; polydispersity index (PDI) of particles presented. ^cTEM analysis of the number average length (l_n) and number average width (w_n) dimensions or the number average particle (d_n) sizes of emulsion nanoparticles (d_n), denoted with *s*: predominantly spherical or *r*: predominantly rod-like in shape. Averages determined from the measurement of at least 100 nanoparticles in each case.

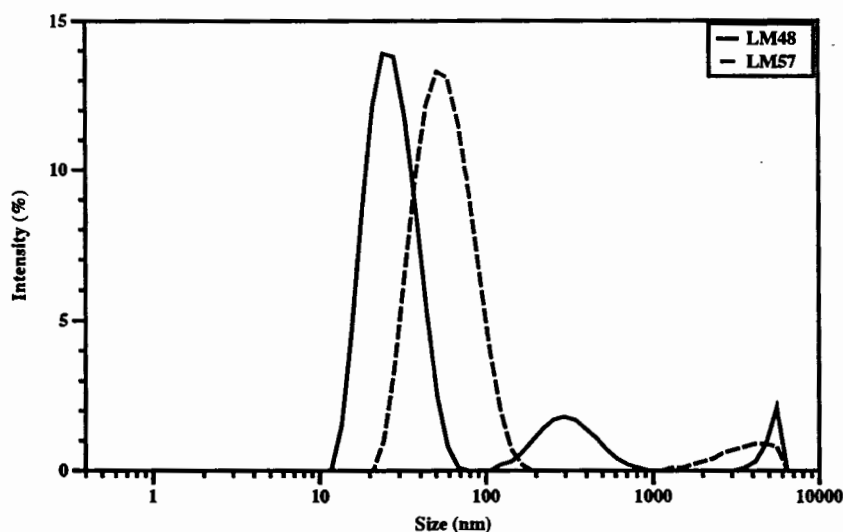


Figure 5.12 Particles size of **PF8TAA** in water at 25°C

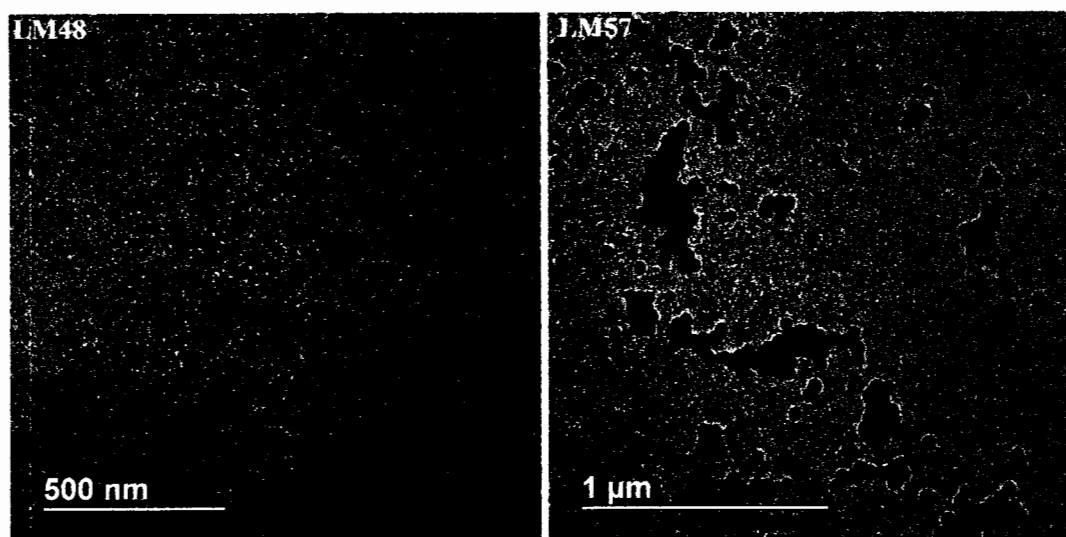


Figure 5.13 TEM images of nanoparticles present in PF8TAA emulsion

5.4 Optical properties

UV/vis absorption spectra of the PFO emulsion series are presented in Figure 5.14. The main band of each emulsion (alpha phase) shows a peak at 408 nm and a shoulder at 390 nm. Each emulsion also exhibits a significant peak at 441 nm corresponding to the beta phase. There are no significant changes in the optical properties of the four PFO emulsions: differences in polymer molar mass or polymer concentration within the particles do not significantly affect the proportion of beta phase present.

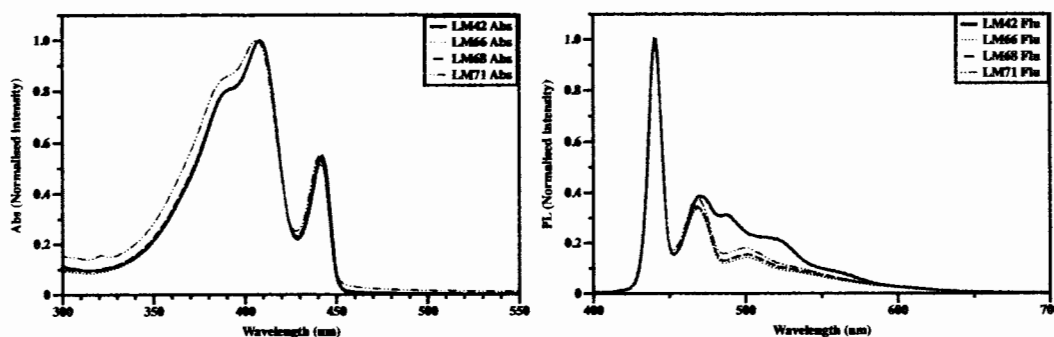


Figure 5.14 Absorption and Emission spectra of PFO in water

The only small difference is that the main alpha phase band obtained for emulsion (LM71) is somewhat blue shifted compared to that observed for the other three emulsions which perhaps reflect on its lower molar mass observed in GPC analysis.

Table 5.9 Summarized optical properties of PFO in water

Sample	Size (nm)	λ_{abs} (nm)	λ_{em} (nm)	QY (%)	E_g^a
LM42	58	408, 442	441	21	2.74
LM66	50	409, 442	440	25	2.74
LM68	91	408, 441	440	22	2.74
LM71	91	407, 441	440	23	2.75

^a E_g was calculated by $E_g = 1240/\lambda_{\text{onset}}$

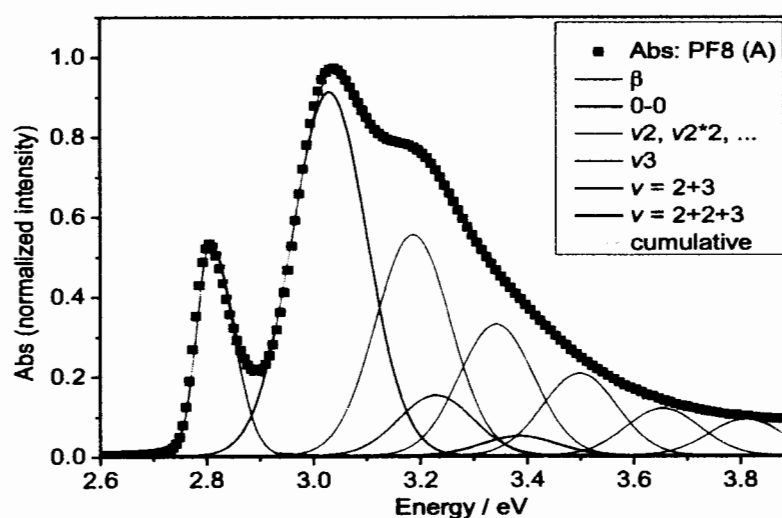


Figure 5.15 Area normalized absorbance of PF8 at ~ 20 °C (LM42) (black symbols) and the overall cumulative fit to the data (cyan solid line). The fits associated with the Gaussian spectral components 0-0 (blue) along with v_2 (magenta) and its replicas, v_3 (green), $v = (2+3)$ (olive) and $v = (2+2+3)$ (navy) and the asymmetric Gaussian fit to the β peak (red). The notation v_n^*m refers to the m th replica of the vibrational mode n .

The percentage of beta phase present in the polymer nanoparticles was calculated at 9 - 10 % from comparing the respective areas of an asymmetric Gaussian peak used to fit the beta phase peak at 441 nm with a constrained multiple-Gaussian peak fitting of the broad main band attributed to the alpha phase, an example for LM42 presented in Figure 5.15. The vibronic replicas applied after selection of the 0-0 peak in the multiple Gaussian fitting correspond to modes with energies of 85 meV (v_1), 156 meV (v_2) and 199 meV (v_3), previously assigned from the β -phase PFO photoluminescence spectrum and in agreement with that observed with Raman spectroscopy of PFO. [150, 151] Molar absorption coefficients at the peak maxima for the four

PFO emulsions were calculated as 38,000, 49,000, 50,000 and 44,000 $M^{-1} cm^{-1}$ respectively. The absorption spectra of the emulsions containing xylene swelled **PFO** nanoparticles closely match those previously observed for **PFO** films produced or swelled in similar solvents. [143] The dominant vibronic peaks in the emission spectra of the **PFO** emulsions (Figure 5.14), at 440, 466 and 500 nm, are solely associated with β phase chromophores which emphasises the efficient energy transfer from glassy regions to the β phase. [152] The photoluminescence quantum yields (PLQY) recorded across the **PFO** emulsion range was between 21 – 25 %. These PLQY values also fit well with those quoted for **PFO** films containing similar high levels of beta phase conformation. [143]

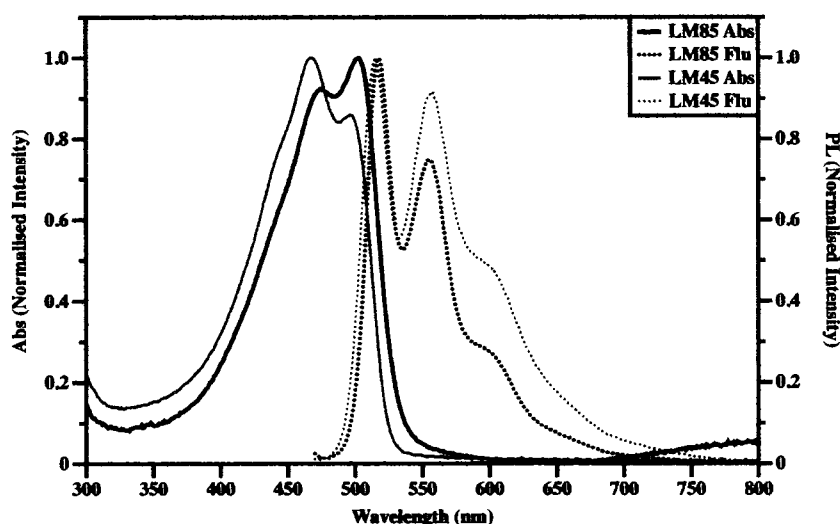


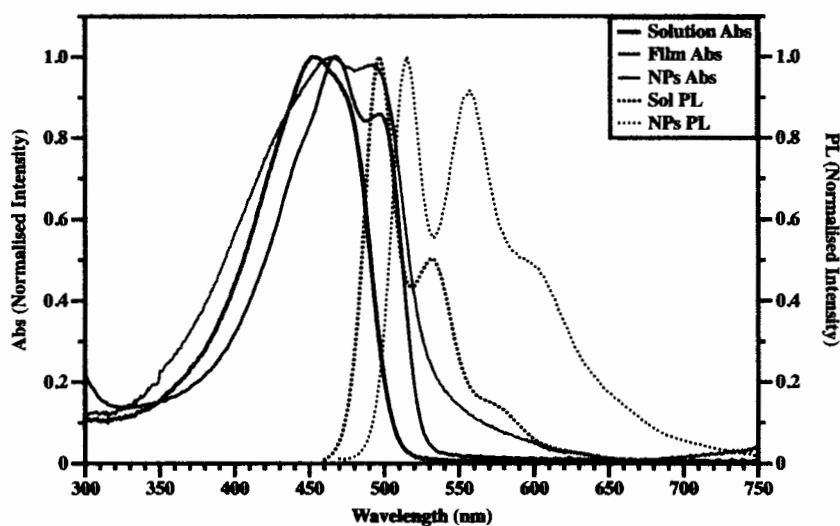
Figure 5.16 Absorption and Emission spectra of **PF8T2** in water

UV/vis absorption spectra of the **PF8T2** emulsions are presented in Figure 5.16. The main band of **LM45** emulsion exhibits a peak maximum at 467 nm whereas the other reaction **LM85** emulsion is somewhat red shifted, exhibiting a peak maximum at 503 nm. The two peak maxima in the emission spectra of the two emulsions more closely converge on average at $\lambda = 517$ & 557 nm. The absorption spectra of the **PF8T2** in nanoparticles more closely reflect that observed for the polymer in the solid state in films [153], as outlined in the comparison of **PF8T2** polymer from **LM45** in nanoparticles (emulsion), dissolved in THF (solution) and as a film in Figure 5.17. PLQY values for the **PF8T2** emulsions of 3 - 5 % were recorded.

Table 5.10 Summarized optical properties of **PF8T2**

Sample	Size (nm)	λ_{abs} (nm)	λ_{em} (nm)	QY (%)	E_g^a
LM45	51	467, 496	515, 557	2.8	2.32
LM45 solution ^b	-	452	497	-	2.41
LM45 film ^c	-	467, 489	-	-	2.23
LM85	109	474, 503	518, 554	5.1	2.28

^a E_g was calculated by $E_g = 1240/\lambda_{onset}$, ^bPF8T2 solution in dry THF, ^cfilm of PF8T2 as chlorobenzene solution 10 mg/ml, annealing at 80°C for 1h

**Figure 5.17** Absorption and Emission spectra of **PF8T2** in water

The absorption spectra were obtained as water dispersion with concentration of 18.64 $\mu\text{g/ml}$ for LM47 and 13.89 $\mu\text{g/ml}$ for LM84, respectively. PF8BT shows two absorption peaks at 329 nm and 468 nm, the latter can be assigned as the charge-transfer absorption peak of PF8BT film. [154] The photoluminescence of polymer shows the maxima emission at 541 nm and 542 nm, respectively. This emission peak can be assigned as the emission of PF8BT film, [155] which confirms aggregation occurring in nanoparticles. Quantum yields of nanoparticles were found as 8.4% for LM47 and 7.9% for LM84, respectively. The optical results were shown in Figure 5.18 and summarised in Table 5.11.

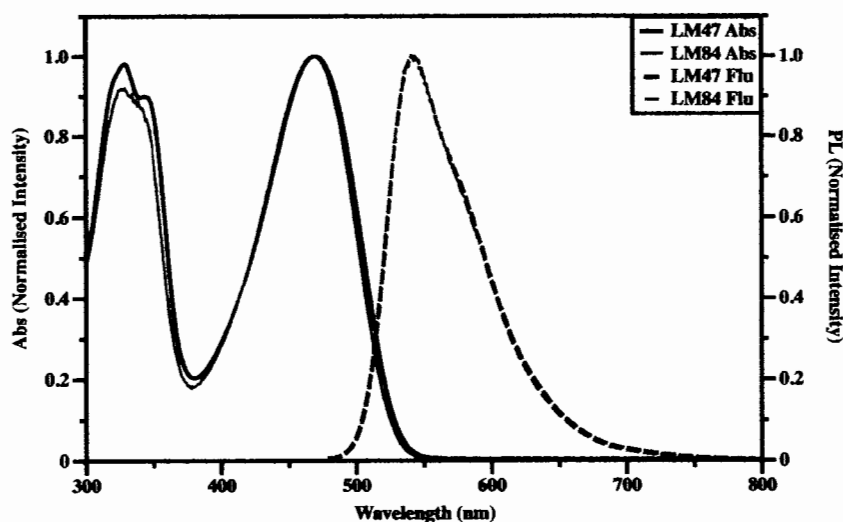


Figure 5.18 Absorption and Emission spectra of PF8BT in water

Table 5.11 Summarized optical properties of PF8BT in water

Sample	Size (nm)	λ_{abs} (nm)	λ_{em} (nm)	QY (%)	E_g^*
LM47	33	469	541	8.7	2.29
LM84	38	468	542	9.1	2.30

* E_g was calculated by $E_g = 1240/\lambda_{onset}$

The optical properties of PF8TAA were investigated as water dispersion sample. The absorption spectra were observed using same concentration as DLS analysis. PF8TAA nanoparticles exhibited absorption peak at 388 nm assigned as the π - π^* transition of polymer film. [156] The emission peaks were observed at a range of 434-460 nm. Both polymers showed the same region of absorption and emission indicated that the particles size and concentration have no effect to optical properties of PF8TAA. The results were shown in Figure 5.19 and summarised in Table 5.12.

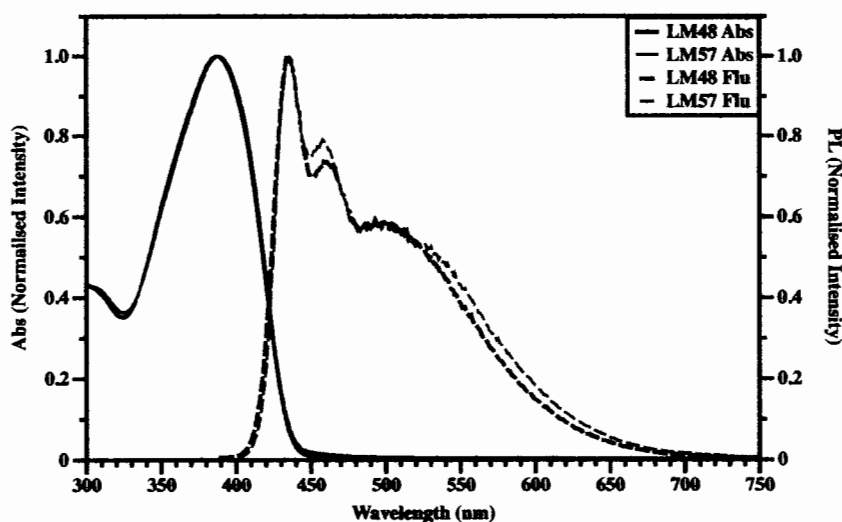


Figure 5.19 Absorption and Emission spectra of PF8TAA in water

Table 5.12 Summarized optical properties of PF8TAA in water

Sample	Size (nm)	λ_{abs} (nm)	λ_{em} (nm)	QY (%)	E_t^*
LM48	28, 324	388	434, 460	3.4	2.78
LM57	59	389	435, 455	5.2	2.78

5.4 Conclusion

This work presents an approach to the direct synthesis of conjugated polymer nanoparticles which facilitates the production of high conjugated polymer concentrations dispersed in water at low temperatures. The polymer chains formed in the nanoparticulate emulsions of PFO and PF8T2 self-assemble in a highly ordered (semicrystalline) manner which translates into the formation of rod-like structures in the resulting emulsions. The less ordered, amorphous polymers, PF8BT and PF8TAA, are present as small, spherical nanoparticles in their respective emulsions. The high ordering in the nanoparticles, particularly in the case of PF8, yielded PLQY (Φ) levels of 21 – 25 %, values which are significant for this particular polymer in solution. The conjugated polymer is present in the nanoparticles at a concentration of 16 % in xylene in the case of PFO in reaction LM66. There is further scope to increase the overall conjugated polymer content in the emulsion preparations above 11,000 ppm.

There is some evidence to suggest that the size of the nanoparticles formed hold some influence on the photophysical properties of the emulsions. The PF8T2 emulsion reactions produced polymer of similar molar mass but rods of distinctly different dimensions. The emulsion

LM85 which produced the larger rods exhibited both an increasingly red shifted absorption spectrum and a higher PLQY value. In the case of the **PFO** emulsions, lower molar mass polymer in larger rods largely matched the optical properties of higher molar mass polymer in smaller rods. Good inter-chain charge transport must be created in the ordered structures within these nanoparticles. The **PF8TAA** emulsion reactions produced polymers of different molar mass in different sized spherical particles. The lower molar mass polymer in larger particles, formed in reaction **LM57**, exhibited a similar absorption spectrum to that observed for higher molar mass in smaller particles, formed in reaction **LM48**, however the PLQY value was higher for the emulsion containing the larger particles.

CHAPTER 6

CONCLUSION

A series of oligothiophenes was successfully synthesised and characterized using combination of alkylation, bromination, Suzuki coupling and Stille coupling reactions. The optical properties in dichloromethane solution reveal that the increasing of thiophene units affect to the absorption and emission wavelength in the trend of longer wavelength. All desired compounds show good reversible electrochemical property. **PT4**, **PT5** and **PT6** show a thermal stable at high temperature. Accordingly, the computational calculation shows the arrangement of molecules in planar. The results indicate that these materials can be used as semiconductors in OFETs.

A series of dialkylaniline dyes with thiophene-phenylene bridge was successfully synthesised and characterized. The desired molecules can be dissolved in chlorinate solvent at room temperature. The intramolecular charge transfer can be observed by absorption band around 420-460 nm. The computational calculation confirmed the intramolecular charge transfer occurring in excited state. The DSSC devices base on **PT2dye** show the highest performance at 3.55% (short-circuit photocurrent density, $J_{sc} = 7.69 \text{ mA cm}^{-2}$; open-circuit photovoltage, $V_{oc} = 0.63 \text{ V}$; fill factor, $ff = 0.73$).

A series of phenothiazine based dyes was successfully synthesised and fully characterized. A coumarin dye with thiophene-bridge was also synthesised. The optical properties of the target molecules were investigated in dry dichloromethane and dimethyl sulfoxide solution. The desired molecules exhibited a maxima absorption band of around 420-490 nm based on ICT. Phenothiazine derivatives show a high thermal stability with T_d at 200, 230 and 230 °C, respectively. The devices performances were also studied using phenothiazine base dye, the **PhCT3dye** shows the highest performance with power conversion efficiency at 4.33% ($J_{sc} = 9.58 \text{ mA cm}^{-2}$, $V_{oc} = 0.64 \text{ V}$ and $ff = 0.70$) at AM 1.5 G.

The conjugated polymer nanoparticles were successfully synthesised using Suzuki coupling polymerization at 30°C. The desired obtain small particles size less than 100 nm. **LM66** shows high quantum yield at 25% in water. **PFO** absorption spectra reveal the β -phase absorption peak at 442 nm with 10% β -phase conformation in particles. The **PF8T2** absorption spectra exhibit shoulder peak at 490-505 nm corresponding to the solid-state structure in nanoparticles. Whilst the concentration do not effect to the maxima wavelength either absorption or emission, the quantum yield depends on the concentration. The particles size of polymer

relates to the concentration of monomer in droplet, the higher concentration, the bigger particles.
The uniform of particles lead a good charge transfer in organic filed-effect transistor.

CHAPTER 7

EXPERIMENTS

7.1 General procedures and instruments

¹H-NMR spectra were recorded on Brüker AVANCE (300 MHz) spectrometer.

¹³C-NMR spectra were recorded on Brüker AVANCE (75 MHz) spectrometer and were fully decoupled. Chemical shifts (δ) are reported relative to the residual solvent peak in part per million (ppm). Coupling constants (J) are given in Hertz (Hz). Multiplicities are quoted as singlet (s), broad (br), doublet (d), triplet (t), quartet (q), AA'BB' quartet system (AA'BB'), AB quartet (ABq) and multiplet (m).

The IR spectra were recorded on a Perkin-Elmer FT-IR spectroscopy as KBr disks or neat liquid between two NaCl plates. The absorption peaks are quoted in wavenumber (cm^{-1}). UV- visible spectra were measured in spectrometric grade dichloromethane on a Perkin-Elmer UV Lambda 25 spectrometer. The absorption peaks are reported as in wavelength (nm) ($\log \epsilon / \text{dm}^3 \text{mol}^{-1} \text{cm}^{-1}$) and sh refers to shoulder. Fluorescence spectra were recorded as a dilute solution in spectroscopic grade dichloromethane on a Perkin-Elmer LS 50B Luminescence Spectrometer. Dichloromethane was distilled from calcium hydride. Tetrahydrofuran (THF) was heated at reflux under nitrogen over sodium wire and benzophenone until the solution became blue and was freshly distilled before use.

Analytical thin-layer chromatography (TLC) was performed with Merck aluminium plates coated with silica gel 60 F₂₅₄. Column chromatography was carried out using gravity feed chromatography with Merck silica gel mesh, 60 Å. where solvent mixtures are used, the portions are given by volume.

The electrochemistry was performed using a AUTOLAB spectrometer. All measurements were made at room temperature on sample dissolved in freshly distilled dichloromethane, 0.1 M tetra-n-butylammoniumhexafluorophosphate as electrolyte. The solutions were degassed by bubbling with argon gas. Dichloromethane was washed with concentrated sulfuric acid and distilled from calcium hydride. A glassy carbon working electrode, platinum wire counter electrode, and a Ag/AgCl/NaCl (Sat.) reference electrode were used. The ferrocenium/ferrocene couple was used as standard, and the ferrocene was purified by recrystallisation from ethanol and then dried under high vacuum and stored over P₂O₅.

The molar mass of the conjugated polymer produced in each reaction was analysed using gel permeation chromatography (GPC). GPC of the conjugated polymers recovered from

the emulsions was completed in tetrahydrofuran (THF) [1-2 mg ml⁻¹] at 35 °C using a Viscotek GPCmax VE2001 solvent/sample module with 2 x PL gel 10 µm mixed-B and a PL gel 500 A column, a Viscotek VE3580 RI detector and a VE3240 UV/Vis multichannel detector.

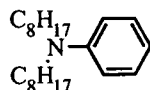
The injection volume was 100 µL and the flow rate was 1 ml min⁻¹. The system was calibrated with low polydispersity polystyrene standards in the range 200 to 6 x 10⁶ g mol⁻¹ from Agilent Technologies, with results analysed using Malvern Omnisec software.

The particle size distributions of diluted samples of the emulsions were measured at 25 °C using a Malvern Zetasizer Nano ZS (DLS). The DLS results quoted are the average of three measurements. TEM analysis was completed using a FEI Tecnai 20 instrument working at 80 kV. Diluted samples containing approx. 100 ppm conjugated polymer concentrations of the emulsions were drop cast onto Formvar coated, 3 mm 400 mesh copper grids (supplied by Agar Scientific). The images were taken in standard diffraction contrast. The particle size analysis of the images was completed using ImageJ software.

UV-Vis absorption spectra were recorded on a Varian Cary 5000UV-Vis-NIR spectrophotometer, either diluted in water (nanoparticles) or dissolved in THF (polymer) at room temperature. Fluorescence spectra were recorded on a Varian Cary Eclipse fluorimeter, either diluted in water (nanoparticles) or dissolved in THF (polymer). All absolute photoluminescence quantum yield (PLQY) measurements were obtained using a Fluoromax-4 spectrofluorometer with integrating sphere attachment (instrument standardised with a Tungsten lamp). Nanoparticle suspensions in water were diluted, to give absorption maxima values between 0.03 to 0.1, for measurements. Background reference measurements were obtained using water (800 µL) in 7 × 40 mm clear glass vials. Nanoparticle suspensions (800 µL) were also measured in 7 × 40 mm clear glass vials. Excitation wavelengths of 380, 460, 470 and 360 nm were used for measurements of PFO, PF8T2, PF8BT and PF8TAA respectively. As an example, to calculate PLQYs of the PFO emulsion samples, four measurements were obtained in each case: (i) background scatter (370 - 390 nm); (ii) background fluorescence (390 - 750 nm); (iii) sample scatter (370 - 390 nm); and (iv) sample fluorescence (390-750 nm). Appropriate optical filters were used to avoid over-saturation of the detector during collection of scatter measurements and these filters were corrected for in the PLQY calculation. For each sample of nanoparticles, PLQY measurements were repeated in triplicate, using a fresh suspension after each set of sample scatter and sample fluorescence measurements. The reported PLQY values are therefore an average of three PLQY measurements. Errors of 10 % were typically associated with the measurements.

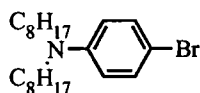
7.2 Synthesis of intermediates

N,N-dioctylaniline (2)

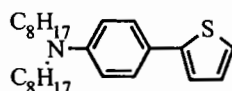


Aniline (10.00 g, 107.3 mmol), bromooctane (51.84 g, 268.44 mmol) and butanol (120 ml) were heated at 100°C in the presence of sodium carbonate (17.60 g, 166.32 mmol) and iodine (0.46 g, 1.82 mmol) for 24 h. The reaction was then cooled to room temperature. The crude product was dissolved in water and then was extracted with ether. The combined extracted was washed with water, dried over sodium sulphate, evaporated to remove solvent and isolated by vacuum distillation. Pure *N,N*-dioctylaniline was isolated as a clear liquid. Yield was 33.83 g, 99%. ; $C_{22}H_{39}N$; IR (NaCl) ν^{-1} 3086-3028, 2949-2855, 1598, 1501-1465, 1360, 742 and 692 cm^{-1} ; UV-Vis; $\lambda_{max,abs}$ (220-600 nm)(dry CH_2Cl_2) (nm) (log $\epsilon/dm^3/mol\ cm$); 266 (4.39); Fluorescence; $\lambda_{max,PL}$ (200-700 nm)(dry CH_2Cl_2) 353 nm; 1H -NMR δ_H (ppm) (300 MHz, $CDCl_3$) 0.99 (6H, d, $J = 6.9$ Hz), 1.39 (20H, d, $J = 4.3$ Hz), 1.67 (4H, s), 3.33 (4H, d, $J = 6.9$ Hz), 6.71 (2H, d, $J = 8.6$ Hz) and 7.28 (1H, t, $J = 7.1$ Hz)

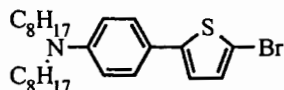
4-Bromo-*N,N*-dioctylaniline (3)



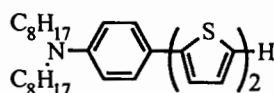
To a mixture of *N,N*-dioctylaniline (5.49 g, 17.29 mmol) and ammonium acetate (0.13 g, 1.79 mmol) in acetonitrile (15 ml). *N*-bromosuccinimide (3.69 g, 20.75 mmol) was added and the mixture was stirred at room temperature. After completion of the reaction as indicated by TLC, the mixture was concentrated in vacuo and extracted with ethyl acetate and water. The organic portion was separated from the extract, dried and concentrated. The residue was subjected to column chromatography (silica gel, hexane) to obtain pure 4-bromo-*N,N*-dioctylaniline. Yield was 6.45 g, 94%. $C_{22}H_{38}NBr$; IR (NaCl) ν^{-1} 2927-2855, 1595, 1501, 1465, 1367, 1299, 1270, 1234, 1187, 114, 1082, 1020, 804 and 724; 1H -NMR δ_H (ppm) (300 MHz, $CDCl_3$) 0.91 (6H, d, $J = 9.3$ Hz), 1.31 (20H, s), 1.55 (4H, d, $J = 6.7$ Hz), 3.19 (4H, t, $J = 7.8$ Hz), 6.48 (2H, d, $J = 6.7$ Hz) and 7.24 (2H, d, $J = 6.9$ Hz)

4-Thiophenyl-*N,N*-dioctylaniline (4)

A mixture of 4-bromo-*N,N*-dioctylaniline (3.34g, 8.41 mmol), 2-thiophene boronic acid (1.02 g, 8.01 mmol), sodium carbonate (16.99 g, 160.20 mmol) and Pd(PPh₃)₄ (0.28 g, 0.24 mmol) in tetrahydrofuran (120 ml) was heated at reflux for 24 h. After cool at room temperature, the mixture was extracted with dichloromethane and washed with water 2 times. The combined extracted was washed with water, dried over sodium sulphate, evaporated to remove solvent and isolated by vacuum distillation. The residue was subjected to column chromatography (silica gel, hexane) to obtain pure 4-thiophenyl-*N,N*-dioctylaniline as yellow oil. Yield was 2.053 g, 61%. C₂₆H₄₁NS; IR (NaCl) ν^{-1} 2927-2847, 1613, 1505 -1465, 1367, 807 and 692 cm⁻¹; UV-Vis; $\lambda_{\text{max, abs}}$ (220-600 nm)(dry CH₂Cl₂) (nm) (log $\epsilon/\text{dm}^3/\text{mol cm}$); 256 (4.49), 331 (4.38); Fluorescence; $\lambda_{\text{max, PL}}$ (200-700 nm)(dry CH₂Cl₂) 393 nm; ¹H-NMR δ_{H} (ppm) (300 MHz, CDCl₃) 0.91 (6H, d, *J* = 9.0 Hz), 1.29 (20H, m), 1.61 (4H, s (broad)), 3.29 (4H, t, *J* = 7.5 Hz), 6.65 (2H, d, *J* = 8.4 Hz), 7.05 (1H, d, *J* = 4.2 Hz) 7.14 (2H, d, *J* = 3.8 Hz) and 7.47 (2H, d, *J* = 7.8 Hz),

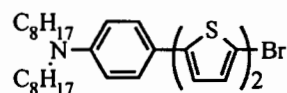
5-Bromo-4-thiophenyl-*N,N*-dialkylaniline (5)

4-thiophene- *N,N*-dioctylaniline (1.44 g, 3.61 mmol) was dissolved in 45 ml THF in a two-necked flask, (0.67 g, 3.77 mmol) NBS was added with stirring monitoring. The water was added, extracted with CH₂Cl₂, dried with anhydrous sodium sulfate evaporated solvent gave light yellow oil of 5-bromo-4-thiophenyl-*N,N*-dialkylaniline. Yield was 1.72 g, 75%. C₂₆H₄₀BrNS; IR (NaCl) ν^{-1} 2927-2869, 1609, 1501 -1461, 1371, 814 and 786 cm⁻¹; ¹H-NMR δ_{H} (ppm) (300 MHz, CDCl₃) 0.89 (6H, t, *J* = 6.8 Hz), 1.30 (20H, t, *J* = 3.7 Hz), 1.58 (4H, s (broad)), 3.27 (4H, t, *J* = 7.6 Hz), 6.62 (2H, d, *J* = 8.6 Hz), 7.33 (2H, d, *J* = 8.4 Hz), 6.85 (1H, d, *J* = 3.6 Hz), and 6.94 (1H, d, *J* = 3.7 Hz)

4-(2,2'-Bithiophen)-*N,N*-dioctylaniline (6)

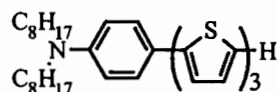
A mixture of 5-bromo-4-thiophenyl-*N,N*-dialkylaniline (3.35 g, 7.00 mmol), 2-thiophene boronic acid (0.85 g, 6.67 mmol), sodium carbonate (14.14 g, 133.40 mmol) and Pd(PPh₃)₄ (0.38 g, 0.33 mmol) in tetrahydrofuran (100 ml) was heated at reflux for 24 h. After cool at room temperature, the mixture was extracted with dichloromethane and washed with water 2 times. The combined extracted was washed with water, dried over sodium sulphate, evaporated to remove solvent and isolated by vacuum distillation. The residue was subjected to column chromatography (silica gel, hexane) to obtain pure 4-(2,2'-bithiophen)-*N,N*-dioctylaniline as yellow oil. Yield was 2.86 g, 89%. C₃₀H₄₃NS₂; IR (NaCl) ν^{-1} 3072, 2920-2855, 1609, 1505-1465, 1371, 796 and 684 cm⁻¹; UV-Vis; $\lambda_{\text{max, abs}}$ (220-600 nm)(dry CH₂Cl₂) (nm) (log $\epsilon/\text{dm}^3/\text{mol cm}$); 222 (4.24), 380 (4.59); Fluorescence; $\lambda_{\text{max, PL}}$ (200-700 nm)(dry CH₂Cl₂) 470 nm; ¹H-NMR δ_{H} (ppm) (300 MHz, CDCl₃) 0.93 (6H, s), 1.34 (20H, m), 1.62 (4H, s), 3.30 (4H, t, *J* = 6.7 Hz), 6.64 (2H, d, *J* = 6.7 Hz), 7.02 (2H, t, *J* = 4.0 Hz), 7.12 (1H, d, *J* = 3.5 Hz) 7.18 (2H, d, *J* = 4.8 Hz) and 7.49 (2H, d, *J* = 7.8 Hz); ¹³C-NMR δ_{C} (ppm) (75 MHz, CDCl₃) 14.11, 22.67, 27.14, 29.32, 29.46, 29.73, 31.62, 31.84, 51.15, 111.74, 121.16, 123.04, 123.76, 124.59, 126.84, 127.77 and 137.92; *M*⁺/*Z* cal. = 481.8010, found = 482.4

4-(5'-Bromo-[2,2'-bithiophen])-*N,N*-dioctylaniline (7)



5-thiophene-4,4'-bithiophenyl-*N,N*-dioctylaniline (5.22 g, 10.83mmol) was dissolved in 80 ml THF in a two-necked flask, (2.12 g, 11.91 mmol) NBS was added with stirring monitoring. The water was added, extracted with CH₂Cl₂, dried with anhydrous sodium sulfate evaporated solvent gave yellow-green oil of 4-(5'-bromo-[2,2'-bithiophen])-*N,N*-dioctylaniline. Yield was 3.09 g, 51%. C₃₀H₄₂BrNS₂; IR (NaCl) ν^{-1} 2921-2850, 1637-1615, 1502-1426, 1363, 790 and 620 cm⁻¹; ¹H-NMR δ_{H} (ppm) (300 MHz, CDCl₃) 0.97 (6H, t, *J* = 6.9 Hz), 1.38 (20H, m), 1.66 (4H, s), 3.33 (4H, s), 6.70 (2H, s), 6.92 (1H, d, *J* = 3.9 Hz), 6.99 (2H, d, *J* = 3.9 Hz), 7.01 (1H, s) and 7.49 (2H, d, *J* = 8.7 Hz)

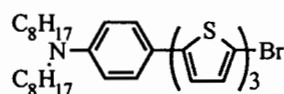
4-(2,2':5',2''-terthiophen)-*N,N*-dioctylaniline (8)



A mixture of 4-(5'-bromo-[2,2'-bithiophen])-*N,N*-dioctylaniline (1.95 g, 3.48 mmol), 2-thiophene boronic acid (0.34 g, 2.68 mmol), sodium carbonate (5.67 g, 53.54 mmol) and

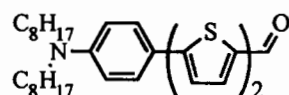
$\text{Pd}(\text{PPh}_3)_4$ (0.06 g, 0.05 mmol) in tetrahydrofuran (40 ml) was heated at reflux for 24 h. After cool at room temperature, the mixture was extracted with dichloromethane and washed with water 2 times. The combined extracted was washed with water, dried over sodium sulphate, evaporated to remove solvent and isolated by vacuum distillation. The residue was subjected to column chromatography (silica gel, hexane) to obtain pure 4-(2,2':5',2''-terthiophen)-*N,N*-dioctylaniline as yellow solid. Yield was 1.07 g, 60%. $\text{C}_{34}\text{H}_{45}\text{NS}_3$; IR (KBr) ν^1 2950-2849, 1604, 1514, 1495, 1459, 1446, 1360, 1207, 1178, 1139, 1051, 866, 857, 843, 791, 722 and 677 cm^{-1} ; UV-Vis; $\lambda_{\text{max,abs}}$ (200-800 nm)(dry CH_2Cl_2) (nm) (log $\epsilon/\text{dm}^3/\text{mol cm}$); 420 (4.55); Fluorescence; $\lambda_{\text{max,PL}}$ (430-800 nm)(dry CH_2Cl_2) 523 nm; $^1\text{H-NMR}$ δ_{H} (ppm) (300 MHz, CDCl_3) 0.89 (6H, t, $J = 6.9$ Hz), 1.30 (20H, t, $J = 4.2$ Hz), 1.58 (4H, s), 3.28 (4H, t, $J = 7.8$ Hz), 6.61 (2H, d, $J = 8.7$ Hz), 7.05 (5H, m), 7.16 (1H, d, $J = 3.6$ Hz), 7.20 (1H, d, $J = 5.1$ Hz) and 7.43 (2H, d, $J = 8.7$ Hz); $^{13}\text{C-NMR}$ δ_{C} (ppm) (75 MHz, CDCl_3) 14.10, 22.65, 27.18, 27.30, 29.33, 29.50, 31.84, 51.08, 121.67, 121.04, 123.42, 123.47, 124.24, 124.34, 124.56, 126.83, 127.85, 133.69, 135.37, 136.92, 137.36, 144.76 and 147.80; M^+/Z cal. = 563.9210, found = 564.5.

4-(5''-bromo-[2,2':5',2''-terthiophen])-*N,N*-dioctylaniline (9)



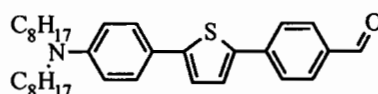
4-(2,2':5',2''-Terthiophen)-*N,N*-dioctylaniline (1.05 g, 1.86 mmol) was dissolved in 30 ml THF in a two-necked flask, (0.35 g, 1.95 mmol) NBS was added with stirring monitoring. The water was added, extracted with CH_2Cl_2 , dried with anhydrous sodium sulfate evaporated solvent gave yellow-green oil of 4-(5''-bromo-[2,2':5',2''-terthiophen])-*N,N*-dioctylaniline. Yield was 0.55 g, 46%. UV-Vis; $\lambda_{\text{max,abs}}$ (200-800 nm)(dry CH_2Cl_2) (nm) (log $\epsilon/\text{dm}^3/\text{mol cm}$); 415 (4.74); Fluorescence; $\lambda_{\text{max,PL}}$ (430-800 nm)(dry CH_2Cl_2) 514 nm; $^1\text{H-NMR}$ δ_{H} (ppm) (300 MHz, CDCl_3) 0.87 (6H, d, $J = 6.9$ Hz), 1.29 (20H, s), 1.78 (4H, s), 3.28 (4H, t, $J = 7.5$ Hz), 6.61 (2H, d, $J = 8.7$ Hz), 7.01-7.10 (4H, m), 7.16 (1H, d, $J = 2.7$ Hz), 7.20 (1H, d, $J = 5.1$ Hz) and 7.43 (2H, d, $J = 8.7$ Hz); $^{13}\text{C-NMR}$ δ_{C} (ppm) (75 MHz, CDCl_3) 14.11, 22.67, 27.18, 27.29, 29.34, 29.51, 31.84, 51.08, 111.65, 121.04, 123.42, 123.47, 124.24, 124.34, 124.57, 126.83, 127.85, 133.69, 135.37, 136.91, 137.36, 144.75 and 147.78

5'-(4-(*N,N*-dioctylamino)phenyl)-[2,2'-bithiophene]-5-carbaldehyde (10)



5-Bromo-4-thiophenyl-*N,N*-dialkylaniline (1.00 g, 2.10mmol) 5-Formyl-2-thienylboronic acid (0.21 g, 1.40mmol), sodium carbonate (2.97 g, 28 mmol) and Pd(PPh₃)₄ (0.08 g, 0.07mmol) in tetrahydrofuran (20 ml) was heated at reflux for 24h. After cool at room temperature, the mixture was extracted with dichloromethane and washed with water 2 times. The combined extracted was washed with water, dried over sodium sulphate, evaporated to remove solvent and isolated by vacuum distillation. The residue was subjected to column chromatography (silica gel, hexane:DCM, 2:1) to obtain pure 5'-(4-(*N,N*-dioctylamino)phenyl)-[2,2'-bithiophene]-5-carbaldehyde as orange solid. Yield was 0.55 g, 77%. C₃₁H₄₃NOS₂: ¹H-NMR δ_H(ppm) (300 MHz, CDCl₃) 0.9 (6H, s), 1.26 (20H, m), 1.59 (4H, d, *J* = 17.1 Hz), 3.29 (4H, t, *J* = 7.8 Hz), 6.14 (2H, d, *J* = 8.7 Hz), 7.07 (1H, d, *J* = 3.6 Hz), 7.19 (1H, d, *J* = 3.9 Hz), 7.28 (1H, d, *J* = 3.6 Hz), 7.44 (2H, d, *J* = 8.7 Hz), 7.64 (1H, d, *J* = 3.9 Hz) and 9.83 (1H, s); ¹³C-NMR δ_C (ppm) (75 MHz, CDCl₃) 14.08, 22.65, 27.16, 27.29, 29.32, 29.42, 29.70, 31.83, 51.07, 111.55, 111.65, 120.41, 120.56, 123.19, 127.03, 127.32, 127.69, 132.31, 133.99, 137.53, 149.72, 140.72, 147.90, 148.10 and 148.23

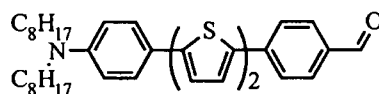
5-Benzaldehyde-4-thiophene-*N,N*-dialkylaniline (11)



5-Bromo-4-thiophenyl-*N,N*-dialkylaniline (1.14 g, 2.39 mmol) 4-Formyl phenylboronic acid (0.33 g, 2.17 mmol) sodium carbonate (4.60 g, 43.40mmol) and Pd(PPh₃)₄ (0.07 g, 0.06mmol) in tetrahydrofuran (34ml) was heated at reflux for 24h. After cool at room temperature, the mixture was extracted with dichloromethane and washed with water 2 times. The combined extracted was washed with water, dried over sodium sulphate, evaporated to remove solvent and isolated by vacuum distillation. The residue was subjected to column chromatography (silica gel, hexane) to obtain pure 5-Benzaldehyde-4-thiophene-*N,N*-dialkylaniline as orange solid. Yield was 0.69 g, 63%. C₃₃H₄₅N₂OS: IR (NaCl) ν⁻¹ 3072, 2955, 2919, 2850, 1692, 1595, 1560, 1540, 1520, 1496, 1448, 1425, 1406, 1370, 1307, 1281, 1217, 1191, 1167, 1109, 1066, 828, 790, 719 and 688 cm⁻¹; UV-Vis; λ_{max,abs} (220-600 nm)(dry CH₂Cl₂) (nm) (log ε/dm³/mol cm); 316 (4.22), 431 (4.56); Fluorescence; λ_{max,PL} (440-800 nm)(dry CH₂Cl₂) 590 nm; ¹H-NMR δ_H(ppm) (300 MHz, CDCl₃) 0.90 (6H, t, *J* = 6.9 Hz), 1.31 (20H, t, *J* = 3.9 Hz), 1.60 (4H, s), 3.30 (4H, t, *J* = 7.8 Hz), 6.63(2H, d, *J* = 8.7 Hz), 7.14(1H, d, *J* = 3.6 Hz), 7.39(1H, d, *J* = 3.6 Hz) 7.48(2H, d, *J* = 8.7 Hz), 7.72 (2H, d, *J* = 8.4 Hz), 7.85 (2H, d, *J* = 8.1 Hz) and 9.98(1H, s); ¹³C-NMR δ_C (ppm) (75 MHz, CDCl₃) 14.10, 22.66, 27.17, 27.30, 29.33, 29.50, 29.71,

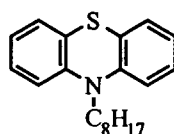
31.84, 51.08, 111.64, 120.82, 121.67, 125.23, 126.16, 126.97, 130.47, 134.49, 138.83, 140.54, 147.54, 148.08 and 191.39

4-(5'-Benzaldehyde-[2,2'-bithiophen])-N,N-dioctylaniline (12)



4-(5'-Bromo-[2,2'-bithiophen])-N,N-dioctylaniline (0.59 g, 1.04 mmol) 4-Formyl phenyl boronic acid (0.13 g, 0.81 mmol) sodium carbonate (1.84 g, 17.40 mmol) and Pd(PPh₃)₄ (0.03 g, 0.02 mmol) in tetrahydrofuran (14ml) was heated at reflux for 24h. After cool at room temperature, the mixture was extracted with dichloromethane and washed with water 2 times. The combined extracted was washed with water, dried over sodium sulphate, evaporated to remove solvent and isolated by vacuum distillation. The residue was subjected to column chromatography (silica gel, hexane) to obtain pure 4-(5'-Benzaldehyde-[2,2'-bithiophen])-N,N-dioctylaniline as orange solid. Yield was 0.46 g, 90%. C₃₇H₄₇NOS: IR (KBr) ν^{-1} 2955, 2920, 2852, 1694, 1597, 1556, 1529, 1514, 1494, 1455, 1399, 1366, 1308, 1276, 1236, 1215, 1188, 1167, 1111, 1058, 868, 821, 790, 721, and 694 cm⁻¹; UV-Vis; $\lambda_{\text{max, abs}}$ (200-800 nm)(dry CH₂Cl₂) (nm) (log $\epsilon/\text{dm}^3/\text{mol cm}$); 455 (4.60); Fluorescence; $\lambda_{\text{max, PL}}$ (450-800 nm)(dry CH₂Cl₂) 633 nm; ¹H-NMR δ_{H} (ppm) (300 MHz, CDCl₃) 0.91 (6H, t, *J* = 6.9 Hz), 1.32 (20H, t, *J* = 4.20 Hz), 1.62 (4H, d, *J* = 10.2 Hz), 3.31 (4H, t, *J* = 7.5 Hz), 6.64 (2H, d, *J* = 8.7 Hz), 7.06 (1H, d, *J* = 3.3 Hz) 7.17(2H, d, *J* = 3.6 Hz), 7.39(1H, d, *J* = 3.6 Hz), 7.46 (2H, d, *J* = 8.7 Hz), 7.74 (2H, d, *J* = 8.1 Hz) 7.88(2H, d, *J* = 8.1 Hz) and 10.0 (1H, s); ¹³C-NMR δ_{C} (ppm) (75 MHz, CDCl₃) 14.10, 22.66, 27.17, 27.30, 29.33, 29.50, 31.84, 51.08, 111.66, 120.88, 121.13, 123.98, 125.18, 125.49, 125.91, 126.88, 130.50, 133.37, 134.87, 139.76, 139.93, 140.17, 145.51, 147.91 and 191.35; *M*⁺/*Z* cal. = 585.9052, found = 585.6.

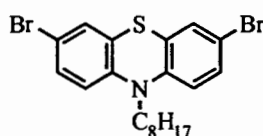
10-Octylphenothiazine (14)



Phenothiazine (10.0 g, 50.18mmol) was dissolved in *N,N*-dimethylsulphoxide (86 ml), then 50% NaOH (8 ml) and tetrabutylammonium bromide was added with stirring. The solution became deep red, bromooctane (10.17 ml, 52.63 mmol) was added and the solution became black. Stirring at room temperature overnight, water (100 ml) was added and extracted with CH₂Cl₂

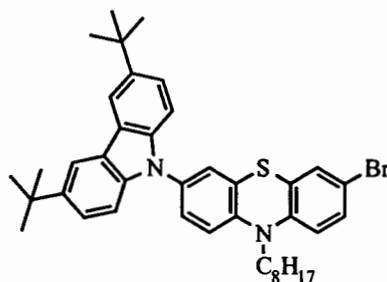
twice. The combined organic layer was washed with dilute HCl (100 ml), dried over anhydrous sodium sulfate, filtered and purified by column chromatography (silica gel, hexane) to give the yellow oil. Yield was 9.1 g (92%). $C_{20}H_{25}NS$; 1H -NMR δ_H (ppm) (300 MHz, acetone- D_6) 1.09 (3H, t, $J = 6.9$ Hz), 1.58 (10H, m), 1.95 (2H, m), 3.95 (2H, t, $J = 6.7$ Hz), 7.02 (4H, m) and 7.29 (4H, d, $J = 7.3$ Hz); ^{13}C -NMR δ_C (ppm) (125 MHz, acetone- D_6) 13.46, 22.38, 26.51, 26.65, 31.56, 46.83, 115.77, 122.34, 124.70, 127.10, 127.37 and 145.43; M^+/Z cal. = 311.487, found = 311.2649.

3,7-Dibromo-10-octylphenothiazine (15)



10-Octylphenothiazine (3.00 g, 9.63 mmol) was dissolved in 20 ml THF in a two-necked flask, (3.59 g, 20.23 mmol) NBS was added with stirring and monitoring. The water was added, extracted with CH_2Cl_2 , dried with anhydrous sodium sulfate evaporated solvent gave 3,7-dibromo-10-octylphenothiazine as brown oil. Yield was 4.90 g (98%). $C_{20}H_{23}Br_2NS$; 1H -NMR δ_H (ppm) (300 MHz, acetone- D_6) 0.89 (3H, t, $J = 6.9$ Hz), 1.29 (10H, m), 1.73 (2H, m), 3.73 (2H, t, $J = 7.4$ Hz), 6.64 (2H, d, $J = 8.5$ Hz) and 7.20 (4H, m); ^{13}C -NMR δ_C (ppm) (125 MHz, acetone- D_6) 13.45, 22.36, 26.36, 47.08, 114.26, 117.51, 126.34, 129.24, 130.36 and 144.43; M^+/Z cal. = 469.279, found = 469.038.

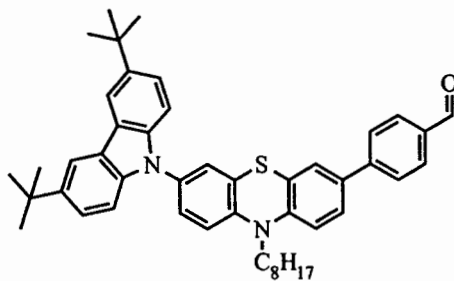
3-Bromo-7-(3,6-di-*tert*-butyl-carbazol-9-yl)-10-octyl-phenothiazine (16)



To a mixture of CuI (0.88 g, 4.62 mmol), K_3PO_4 (4.91 g, 23.12 mmol), and 3,6-di-*tert*-butylcarbazole (2.30 g, 8.25 mmol) in toluene (80 mL) were added 3,7-Dibromo-10-octylphenothiazine (13.02 g, 27.74 mmol) and (+/-)-*trans*-1,2-diaminocyclohexane (0.57 g, 4.99 mmol). The reaction mixture was stirred at 110 °C under nitrogen. After 48 h, water (100 ml) was added until the two phases mixed. The solution was extracted with CH_2Cl_2 (100 ml x 3), washed with water (100 ml), brine solution (100 ml) and dried with Na_2SO_4 , filtered, and the

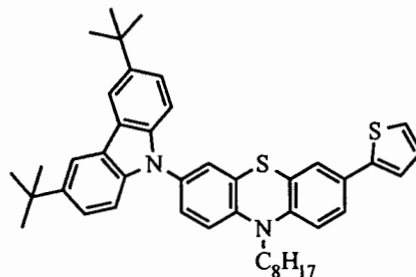
solvents removed to dryness. After the solvent was evaporated. The crude product was purified by column chromatography on silica gel with hexane as eluent to yield 3-bromo-7-(3,6-di-*tert*-butyl-carbazol-9-yl)-10-octyl-phenothiazine (4.16 g, 75%) as white solid. $C_{40}H_{47}BrN_2S$; 1H -NMR δ_H (ppm) (300 MHz, acetone- D_6) 0.84 (3H, d, $J = 4.8$ Hz), 1.42 (28H, m), 1.86 (2H, t, $J = 6.9$ Hz), 4.02 (2H, t, $J = 6.6$ Hz), 7.01 (1H, d, $J = 8.7$ Hz), 7.29-7.49 (9H, m) and 8.24 (1H, s); ^{13}C -NMR δ_C (ppm) (125 MHz, acetone- D_6) 13.53, 22.40, 26.51, 26.88, 31.48, 34.40, 47.26, 54.96, 69.56, 91.17, 92.75, 96.67, 98.98, 107.03, 107.32, 108.51, 109.10, 110.78, 113.23, 115.36, 116.16, 116.36, 116.78, 117.47, 118.87, 119.45, 123.61, 124.83, 125.34, 126.11, 127.54, 129.31, 130.30 and 142.64; M^+/Z cal. = 666.794, found = 666.3814.

4-(7-(3,6-Di-*tert*-butyl-carbazol-9-yl)-10-octyl-phenothiazine)benzaldehyde (17)



A mixture of 3-bromo-7-(3,6-di-*tert*-butyl-carbazol-9-yl)-10-octyl-phenothiazine (0.5 g, 0.75mmol) 4-formyl-phenylboronic acid (0.11 g, 0.75mmol), sodium carbonate (1.06 g, 10.0mmol) and $Pd(PPh_3)_4$ (0.02 g, 0.02mmol) in tetrahydrofuran (8 ml) was heated at reflux for 24h. After cool at room temperature, the mixture was extracted with dichloromethane and washed with water 2 times. The combined extracted was washed with water, dried over sodium sulphate, evaporated to remove solvent and isolated by vacuum distillation. The residue was subjected to column chromatography (silica gel, hexane:DCM, 2:1) to obtain pure 4-(7-(3,6-di-*tert*-butyl-carbazol-9-yl)-10-octyl-phenothiazin-3-yl)benzaldehyde as orange solid. Yield was 0.31 g, 60%. $C_{47}H_{52}NOS$; IR (KBr) ν^{-1} 3554, 3473, 3406, 2956, 2928, 2851, 1700, 1602, 1264, 1168, 809 cm^{-1} ; 1H -NMR δ_H (ppm) (300 MHz, acetone- D_6) 0.80 (3H, d, $J = 6.6$ Hz), 1.25 (18H, t, $J = 10.8$ Hz), 1.41(10H, s), 3.88(2H, t, $J = 6.9$ Hz), 6.92(1H, d, $J = 8.4$ Hz), 7.19 (5H, m), 7.43 (4H, m), 7.27 (2H, d, $J = 8.1$ Hz), 7.88 (2H, d, $J = 8.1$ Hz), 8.28 (2H, s) and 10.06(1H, s); ^{13}C -NMR δ_C (ppm) (75 MHz, $CDCl_3$) 14.10, 22.64, 26.93, 26.99, 29.24, 31.76, 32.03, 34.73, 47.85, 109.16, 115.77, 116.05, 116.22, 123.26, 123.57, 125.06, 125.76, 125.86, 126.14, 126.47, 126.84, 130.35, 132.95, 134.99, 139.44, 142.80, 143.70, 145.80 and 191.72; M^+/Z cal. = 693.006, found = 693.5336.

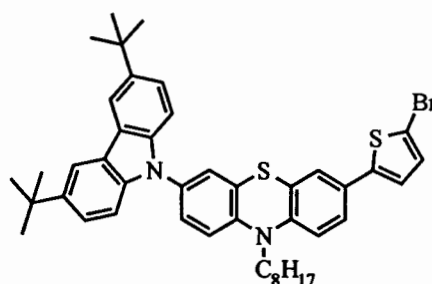
3-(3,6-Di-*tert*-butyl-carbazol-9-yl)-10-octyl-7-(thiophen-2-yl)-phenothiazine (18)



A mixture of 3-bromo-7-(3,6-di-*tert*-butyl-carbazol-9-yl)-10-octyl-phenothiazine (4.00 g, 5.99 mmol), 2-thiopheneboronic acid (0.77 g, 5.99mmol), sodium carbonate (7.63 g, 74.82mmol) and Pd(PPh₃)₄ (0.10 g, 0.09 mmol) in tetrahydrofuran (36 ml) was heated at reflux for 24 h. After cool at room temperature, the mixture was extracted with dichloromethane and washed with water 2 times. The combined extracted was washed with water, dried over sodium sulphate, evaporated to remove solvent and isolated by vacuum distillation. The residue was subjected to column chromatography (silica gel, hexane) to obtain pure 3-(3,6-di-*tert*-butyl-carbazol-9-yl)-10-octyl-7-(thiophen-2-yl)-phenothiazine as yellow solid. Yield was 3.03 g, 75%. C₄₄H₅₀N₂S₂; IR (KBr) ν ¹3412, 2956, 2917, 2857, 2357, 1604, 1476, 1327, 1294, 1262, 1198, 875, 812 and 694 cm⁻¹; ¹H-NMR δ _H(ppm) (500 MHz, acetone-D₆) 0.87 (3H, t, *J* = 6.5 Hz), 1.29 (12H, s), 1.44 (10H, s), 1.75 (2H, m), 4.07 (2H, s), 7.12 (2H, m), 7.29 (3H, t, *J* = 8.5 Hz), 7.38 (4H, m), 7.50 (4H, m) and 8.26 (2H, s); ¹³C-NMR δ _C (ppm) (75 MHz, CDCl₃) 14.13, 22.67, 27.01, 29.26, 31.79, 32.07, 34.75, 109.23, 115.95, 116.20, 123.25, 123.57, 124.32, 1255.82, 127.97, 139.49 and 142.77; M⁺/Z cal. = 671.018, found = 670.521.

3-(5-Bromothiophen-2-yl)-7-(3,6-di-*tert*-butyl-carbazol)-10-octyl-phenothiazine

(19)

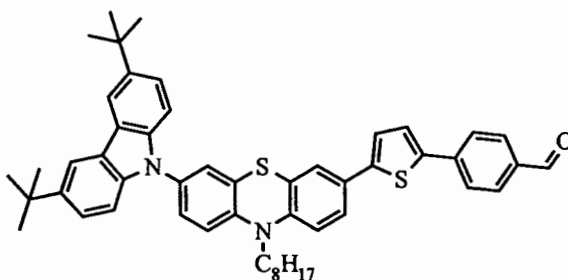


A mixture of 3-(3,6-di-*tert*-butyl-carbazol-9-yl)-10-octyl-7-(thiophen-2-yl)-phenothiazine (2.37 g, 3.53mmol) was dissolved in 30 ml THF in a two-necked flask, (0.66 g, 3.71mmol) NBS was added with stirring monitoring. The water was added, extracted with

CH_2Cl_2 , dried with anhydrous sodium sulfate evaporated solvent gave 3-(5-bromothiophen-2-yl)-7-(3,6-di-*tert*-butyl-carbazol)-10-octyl-phenothiazine as yellow solid. Yield was 2.28 g, 86%. IR (KBr) ν^{-1} 3401, 2956, 2923, 2857, 2357, 1476, 1294, 1292, 877, 812, 784 and 614 cm^{-1} ; $^1\text{H-NMR}$ δ_{H} (ppm) (500 MHz, acetone- D_6) 0.86 (3H, t, $J = 7.0$ Hz), 1.35 (8H, m), 1.44 (14H, m), 1.55 (2H, t, $J = 8.0$ Hz), 4.05 (2H, t, $J = 7.0$ Hz), 7.08 (1H, d, $J = 8.5$ Hz), 7.12 (1H, d, $J = 4.0$ Hz), 7.20 (1H, d, $J = 4.0$ Hz), 7.28 (3H, t, $J = 8.5$ Hz), 7.34 (1H, d, $J = 2.0$ Hz), 7.42 (3H, m), 7.47 (2H, dd, $J = 8.7$ Hz) and 8.26 (2H, s); $^{13}\text{C-NMR}$ δ_{C} (ppm) (125 MHz, acetone- D_6) 13.54, 22.42, 26.55, 26.61, 31.49, 31.60, 34.42, 47.26, 109.12, 116.27, 116.36, 116.65, 123.14, 123.29, 123.62, 123.92, 124.93, 125.29, 125.42, 125.99, 128.22, 131.41, 132.71, 139.40, 142.63, 143.92 and 144.77; M^+/Z cal. = 749.914, found = 748.455.

4-(5-(7-(3,6-Di-*tert*-butyl-carbazol)-10-octylphenothiazine)thiophene)

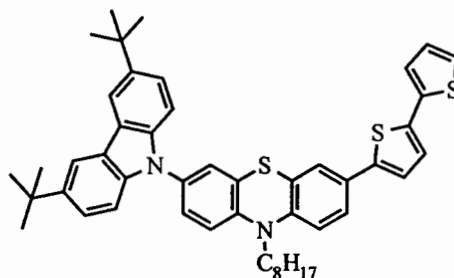
benzaldehyde (20)



A mixture of 3-(5-bromothiophen-2-yl)-7-(3,6-di-*tert*-butyl-carbazol)-10-octyl-phenothiazine (0.5 g, 0.67mmol) 4-formyl-phenylboronic acid (0.09 g, 0.67mmol), sodium carbonate (1.69 g, 16.0 mmol) and $\text{Pd}(\text{PPh}_3)_4$ (0.01 g, 0.01mmol) in tetrahydrofuran (10 ml) was heated at reflux for 24 h. After cool at room temperature, the mixture was extracted with dichloromethane and washed with water 2 times. The combined extracted was washed with water, dried over sodium sulphate, evaporated to remove solvent and isolated by vacuum distillation. The residue was subjected to column chromatography (silica gel, hexane:DCM, 2:1) to obtain pure 4-(5-(7-(3,6-Di-*tert*-butyl-carbazol)-10-octylphenothiazine)thiophene)benzaldehyde as orange solid. Yield was 0.31 g, 60%. $\text{C}_{51}\text{H}_{54}\text{NOS}_2$; IR (KBr) ν^{-1} 3549, 3462, 3412, 2950, 2923, 2857, 1695, 1559, 1476, 1443, 1256, 872 and 795 cm^{-1} ; $^1\text{H-NMR}$ δ_{H} (ppm) (300 MHz, CDCl_3) 0.94 (3H, t, $J = 6.9$ Hz), 1.37 (12H, s), 1.57 (16H, m), 1.93 (2H, d, $J = 6.3$ Hz), 3.90 (2H, d, $J = 6.9$ Hz), 6.85 (1H, d, $J = 8.7$ Hz), 7.02 (1H, d, $J = 9.0$ Hz), 7.19 (1H, d, $J = 3.9$ Hz), 7.47 (7H, m), 7.53 (2H, dd, $J = 6.9$ Hz), 7.72 (2H, d, $J = 8.1$ Hz), 7.86 (2H, d, $J = 8.4$), 8.26 (2H, s) and 9.99 (1H, s); $^{13}\text{C-NMR}$ δ_{C} (ppm) (75 MHz, CDCl_3) 14.23, 22.74, 26.95, 27.04, 29.33, 31.86, 32.14, 34.81, 47.82, 109.31, 115.69, 116.31, 123.36, 123.68, 124.58, 124.97, 125.03, 125.51, 125.58, 125.67,

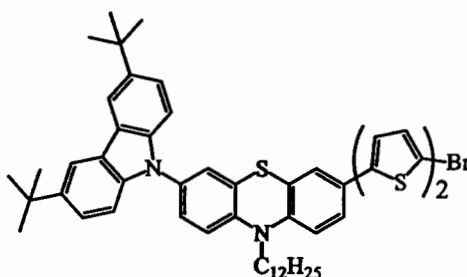
125.80, 126.14, 128.61, 130.48, 132.89, 134.97, 139.47, 139.96, 140.98, 142.87, 143.68, 144.67, 144.92, and 191.24; M^+/Z cal. = 775.1266, found = 774.5890.

3-(2,2'-Bithiophene)-7-(3,6-di-*tert*-butyl-carbazol)-10-octylphenothiazine (21)



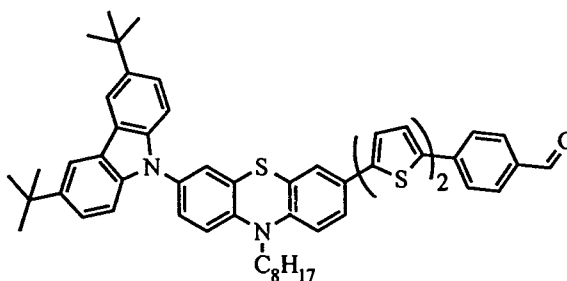
A mixture of 3-(5-bromothiophen-2-yl)-7-(3,6-di-*tert*-butyl-carbazol)-10-octylphenothiazine (2.46 g, 3.28mmol), 2-thiopheneboronic acid (0.42 g, 3.28mmol), sodium carbonate (6.36 g, 60.00mmol) and $\text{Pd}(\text{PPh}_3)_4$ (0.07 g, 0.07 mmol) in tetrahydrofuran (40 ml) was heated at reflux for 24 h. After cool at room temperature, the mixture was extracted with dichloromethane and washed with water 2 times. The combined extracted was washed with water, dried over sodium sulphate, evaporated to remove solvent and isolated by vacuum distillation. The residue was subjected to column chromatography (silica gel, hexane) to obtain 3-(2,2'-bithiophene)-7-(3,6-di-*tert*-butyl-carbazol)-10-octylphenothiazine as orange solid. Yield was 2.21 g, 87%. $\text{C}_{48}\text{H}_{52}\text{N}_2\text{S}_3$: IR (KBr) ν^1 3549, 3412, 2956, 2846, 2362, 1635, 1618, 1467, 1481, 1448, 1360, 1294, 1259, 809, 688 and 614 cm^{-1} ; $^1\text{H-NMR}$ δ_{H} (ppm) (500 MHz, acetone- D_6) 0.87 (3H, t, J = 6.5 Hz), 1.30 (7H, s), 1.45 (18H, s), 1.57 (2H, d, J = 7.0 Hz), 4.10 (2H, t, J = 7.0 Hz), 7.11 (1H, t, J = 3.6 Hz), 7.15 (1H, d, J = 8.5 Hz), 7.26 (1H, d, J = 3.5 Hz), 7.31 (3H, d, J = 8.5 Hz), 7.38 (2H, d, J = 4.5 Hz), 7.43 (2H, d, J = 5.5 Hz), 7.52 (3H, m) and 8.30 (2H, s); $^{13}\text{C-NMR}$ δ_{C} (ppm) (125 MHz, acetone- D) 13.49, 22.40, 26.53, 26.62, 31.43, 31.59, 34.39, 47.23, 109.12, 116.31, 116.40, 116.67, 123.31, 123.56, 123.64, 123.69, 123.84, 124.76, 124.82, 124.87, 125.31, 125.45, 126.02, 128.10, 128.73, 132.68, 139.43, 142.64, and 144.01; M^+/Z cal. = 753.138, found = 753.4824.

3-(5'-Bromo-[2,2'-bithiophen])-7-(3,6-di-*tert*-butyl-carbazol)-10-dodecylphenothiazine (22)



A mixture of 3-([2,2'-bithiophen])-7-(3,6-di-*tert*-butyl-carbazol)-10-dodecyl-phenothiazine (0.24 g, 0.31 mmol) was dissolved in 20 ml THF in a two-necked flask, (0.06 g, 0.32 mmol) NBS was added with stirring monitoring. The water was added, extracted with CH_2Cl_2 , dried with anhydrous sodium sulfate evaporated solvent gave yellow solid of 3-(5'-bromo-[2,2'-bithiophen])-7-(3,6-di-*tert*-butyl-carbazol)-10-dodecyl-phenothiazine as yellow solid. Yield was 0.26 g, 98%. $\text{C}_{49}\text{H}_{53}\text{BrN}_2\text{S}_3$: IR (KBr) ν^1 3549, 3483, 3412, 2956, 2923, 2851, 2362, 1637, 1613, 1478, 1454, 1259, 787 and 609 cm^{-1} ; $^1\text{H-NMR}$ δ_{H} (ppm) (500 MHz, acetone- D_6) 0.87 (3H, t, $J = 6.5$ Hz), 1.29 (12H, s), 1.41 (16H, s), 1.55 (2H, t, $J = 7.0$ Hz), 4.06 (2H, t, $J = 7.0$ Hz), 7.11 (2H, d, $J = 4.0$ Hz), 7.15 (1H, d, $J = 3.5$ Hz), 7.24 (1H, d, $J = 4.0$ Hz), 7.28 (3H, t, $J = 7.0$ Hz), 7.36 (2H, s), 7.40 (1H, d, $J = 8.5$ Hz), 7.51 (4H, t, $J = 7.6$ Hz) and 8.30 (2H, s); $^{13}\text{C-NMR}$ δ_{C} (ppm) (125 MHz, acetone- D_6) 13.49, 22.40, 26.53, 26.61, 31.44, 31.59, 34.39, 47.23, 109.12, 116.28, 116.40, 116.66, 123.31, 123.63, 124.06, 124.86, 124.95, 125.29, 125.42, 125.99, 128.46, 131.39, 132.70, 132.70, 134.42, 139.40, 142.56, 142.64, 143.92 and 144.66; M^+/Z cal. = 830.0340, found = 830.3154.

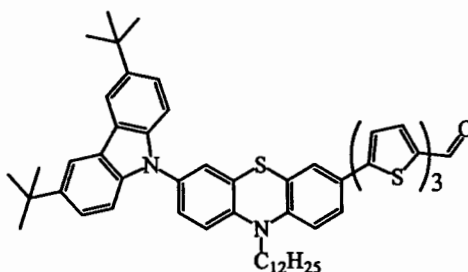
4-(5'-(7-(3,6-Di-*tert*-butylcarbazole)-10-octylphenothiazine)-[2,2'-bithiophen]) benzaldehyde (23)



A mixture of 3-(5'-bromo-[2,2'-bithiophen])-7-(3,6-di-*tert*-butyl-carbazol)-10-dodecyl-phenothiazine (0.2 g, 0.23mmol) 4-formyl-phenylboronic acid (0.03 g, 0.23mmol), sodium carbonate (0.53 g, 5.0 mmol) and $\text{Pd}(\text{PPh}_3)_4$ (0.01 g, 0.01mmol) in tetrahydrofuran (10 ml) was heated at reflux for 24 h. After cool at room temperature, the mixture was extracted with dichloromethane and washed with water 2 times. The combined extracted was washed with water, dried over sodium sulphate, evaporated to remove solvent and isolated by vacuum distillation. The residue was subjected to column chromatography (silica gel, hexane:DCM, 2:1) to obtain pure 4-(5'-(7-(3,6-di-*tert*-butylcarbazole)-10-octylphenothiazine)-[2,2'-bithiophen]) benzaldehyde as orange solid. Yield was 0.05 g, 24%. $\text{C}_{55}\text{H}_{56}\text{N}_2\text{OS}_3$: IR (KBr) ν^1 3549, 3412, 2956, 2857, 1695, 1599, 1481, 1262, 872 and 792 cm^{-1} ; $^1\text{H-NMR}$ δ_{H} (ppm) (500 MHz, acetone- D_6) 0.94 (3H, t, $J = 6.5$ Hz), 1.36 (12H, s), 1.52 (16H, s), 1.60 (2H, t, $J = 7.5$ Hz), 4.10 (2H, t, $J = 7.0$

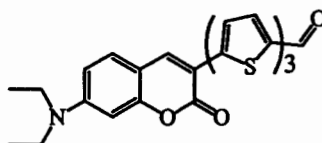
Hz), 7.13 (1H, d, $J = 8.5$ Hz), 7.30 (1H, d, $J = 8.5$ Hz), 7.36-7.47 (7H, m), 7.56 (4H, m), 7.68 (1H, d, $J = 4.0$ Hz), 7.93 (2H, d, $J = 8.5$ Hz), 8.00 (2H, d, $J = 8.5$ Hz), 8.34 (2H, s) and 10.09 (1H, s); $^{13}\text{C-NMR}$ δ_c (ppm) (125 MHz, acetone- D_6) 13.57, 22.43, 26.58, 26.63, 31.51, 31.62, 34.42, 47.29, 109.15, 116.20, 116.36, 116.59, 123.30, 123.62, 123.67, 123.93, 124.93, 124.96, 125.47, 125.52, 125.92, 126.53, 128.51, 130.30, 132.68, 135.52, 139.38, 142.62 and 191.07; M^+/Z cal. = 857.2460, found = 856.7830.

[2,2':5',2''-Terthiophene]-5-carbaldehyde-7-(3,6-di-*tert*-butyl-carbazol)-10-dodecyl-phenothiazine (24)



A mixture of 3-(5'-bromo-[2,2'-bithiophen])-7-(3,6-di-*tert*-butyl-carbazol)-10-dodecyl-phenothiazine (0.29 g, 0.33 mmol) 5-formyl-2-thienylboronic acid (0.05 g, 0.34 mmol), sodium carbonate (0.69 g, 6.58 mmol) and $\text{Pd}(\text{PPh}_3)_4$ (0.01 g, 0.009 mmol) in tetrahydrofuran (5 ml) was heated at reflux for 24 h. After cool at room temperature, the mixture was extracted with dichloromethane and washed with water 2 times. The combined extracted was washed with water, dried over sodium sulphate, evaporated to remove solvent and isolated by vacuum distillation. The residue was subjected to column chromatography (silica gel, hexane:DCM, 2:1) to obtain pure [2,2':5',2''-terthiophene]-5-carbaldehyde-7-(3,6-di-*tert*-butyl-carbazol)-10-dodecyl-phenothiazine as orange solid. Yield was 0.16 g, 55%.

3-[2,2':5',2''-Terthiophene]-5-carbaldehyde-7-(diethylamino)-coumarin (26)

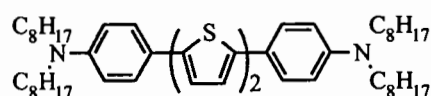


A mixture of 3-(5'-bromo-[2,2'-bithiophen])-7-(diethylamino)-coumarin (0.22g, 0.48 mmol), 5-formyl-2-thienylboronic acid (0.08 g, 0.51 mmol), sodium carbonate (1.01 g, 9.60 mmol) and $\text{Pd}(\text{PPh}_3)_4$ (0.03 g, 0.02 mmol) in tetrahydrofuran (10 ml) was heated at reflux for 24 h. After cool at room temperature, the mixture was extracted with dichloromethane and washed with water 2 times. The combined extracted was washed with water, dried over sodium sulphate,

evaporated to remove solvent and isolated by vacuum distillation. The residue was subjected to column chromatography (silica gel, hexane:DCM, 2:1) to obtain pure 3-[2,2':5',2''-terthiophene]-5-carbaldehyde-7-(diethylamino)-coumarins orange solid. Yield was 0.23 g, 60%. $C_{26}H_{21}NO_3S_3$; IR (KBr) ν^{-1} 2950-2849, 1698, 1651, 1615, 1589, 1515, 1444, 1378, 1350, 1257, 1233, 1133, 861 and 790 cm^{-1} ; UV-Vis; $\lambda_{max, abs}$ (200-800 nm)(dry CH_2Cl_2) (nm) (log $\epsilon/dm^3/mol\ cm$); 486 (4.52); Fluorescence; $\lambda_{max, PL}$ (430-800 nm)(dry CH_2Cl_2) 598 nm; 1H -NMR δ_H (ppm) (500 MHz, $CDCl_3$) 1.15 (6H, s), 3.35-3.40 (4H, m), 6.48 (1H, s), 6.55 (1H, dd, $J = 5.5$ Hz), 7.11 (1H, d, $J = 3.9$ Hz), 7.14 (1H, d, $J = 5.0$ Hz), 7.16 (1H, d, $J = 5.0$ Hz), 7.23 (1H, d, $J = 5.1$ Hz), 7.26 (1H, d, $J = 7.9$ Hz), 7.49 (1H, d, $J = 6.9$ Hz), 7.60 (1H, d, $J = 6.9$ Hz), 7.84 (1H, s) and 9.79 (1H, s); M^+Z cal. = 491.636, found = 491.2.

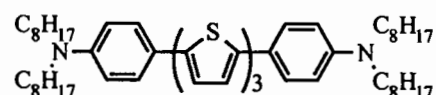
7.3 Synthesis of target molecules

4,4'-2,2'-Bithiophene-5,5'-bis(*N,N*-dioctylaniline) (PT2)



A total of 5-bromo-4-thiophenyl-*N,N*-dialkylaniline (0.71 g, 1.48 mmol), $[Me_3Sn]_2$ (0.19 g, 0.59 mmol) and $Pd(PPh_3)_4$ (0.01 g, 0.01 mmol) were refluxed in anhydrous toluene over night under N_2 . The resulting mixture was collected via vacuum filtration and filtered through a silica gel column to remove tin by product afforded 4,4'-2,2'-bithiophene-5,5'-bis(*N,N*-dioctylaniline) as orange viscos oil. Yield was 0.22 g, 48%. $C_{52}H_{80}N_2S_2$; IR (KBr) ν^{-1} 3072-2855, 1743, 1609, 1537, 1508, 1458, 1432, 1367, 1277, 1201, 118, 1010, 843, 804 and 684; UV-Vis; λ_{abs} (200-800 nm)(dry CH_2Cl_2) (nm) (log $\epsilon/dm^3/mol\ cm$); 421 (4.65); Fluorescence; λ_{PL} (400-800 nm)(dry CH_2Cl_2) 495 nm; 1H -NMR δ_H (ppm) (300 MHz, $CDCl_3$) 0.90 (12H, t, $J = 6.8$ Hz), 1.30 (40H, t, $J = 8.1$ Hz), 1.60 (8H, d, $J = 8.0$ Hz), 3.28 (8H, t, $J = 7.8$ Hz), 6.61 (4H, dd, $J = 6.1$ Hz), 7.12 (2H, d, $J = 3.5$ Hz), 7.23 (2H, d, $J = 3.2$ Hz) and 7.45 (4H, d, $J = 8.7$ Hz); ^{13}C -NMR δ_C (ppm) (75 MHz, $CDCl_3$) 14.10, 22.66, 24.88, 27.16, 29.14, 29.47, 29.72, 29.78, 31.61, 31.83, 31.94, 51.15, 111.74, 120.60, 122.41, 127.12 and 127.79.

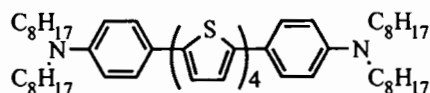
4,4'-[2,2':5',2''-Terthiophene]-5,5''-bis(*N,N*-dioctylaniline) (PT3)



A mixture of 5-bromo-4-thiophenyl-*N,N*-dialkylaniline (0.55 g, 1.15 mmol), 2,5-thiophene-diboronic acid (0.078 g, 0.46 mmol), sodium carbonate (0.97 g, 9.20 mmol) and

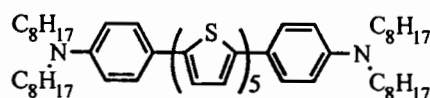
$\text{Pd}(\text{PPh}_3)_4$ (0.03 g, 0.02 mmol) in tetrahydrofuran (20 ml) was heated at reflux for 24 h. After cool at room temperature, the mixture was extracted with dichloromethane and washed with water 2 times. The combined extracted was washed with water, dried over sodium sulphate, evaporated to remove solvent and isolated by vacuum distillation. The residue was subjected to column chromatography (silica gel, hexane) to obtain pure 4,4'-[2,2':5',2''-terthiophene]-5,5''-bis(*N,N*-dioctylaniline) as orange viscos oil. Yield was 0.25 g, 62%. $\text{C}_{36}\text{H}_{82}\text{N}_2\text{S}_3$; IR (NaCl) ν^{-1} 2855-3072, 1869, 1743, 1609, 1537, 1508, 1458, 1432, 1367, 1277, 1201, 1118, 1010, 843, 804 and 684 cm^{-1} ; UV-Vis; $\lambda_{\text{max, abs}}$ (220-600 nm)(dry CH_2Cl_2) (nm) (log $\epsilon/\text{dm}^3/\text{mol cm}$); 438 (3.95); Fluorescence; $\lambda_{\text{max, PL}}$ (400-700 nm)(dry CH_2Cl_2) 528 nm; $^1\text{H-NMR}$ δ_{H} (ppm) (500 MHz, CDCl_3) 0.81 (12H, m), 1.18 (40H, m), 1.47 (8H, s), 3.21 (8H, t, $J = 10.0$ Hz), 6.55 (4H, d, $J = 5.0$ Hz), 6.69 (6H, t, $J = 5.0$ Hz) and 7.36 (4H, d, $J = 10.0$ Hz); M^+/Z cal. = 879.450, found = 879.

4,4'-[2,2':5',2'':5'',2''':5''',2''''-Quaterthiophene]-5,5''''-bis(*N,N*-dioctylaniline) (PT4)



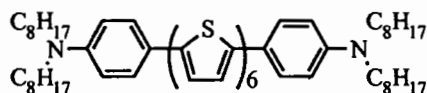
A total of 4-(5'-bromo-[2,2'-bithiophen])-*N,N*-dioctylaniline (0.42 g, 0.75 mmol), $[\text{Me}_3\text{Sn}]_2$ (0.12 g, 0.37 mmol), and $\text{Pd}(\text{PPh}_3)_4$ (0.004 g, 0.0037 mmol) were refluxed in anhydrous toluene under N_2 for 48 h. After cool at room temperature, the mixture was extracted with dichloromethane and washed with water 2 times. The combined extracted was washed with water, dried over sodium sulphate, evaporated to remove solvent and isolated by vacuum distillation. The residue was subjected to column chromatography (silica gel, DCM:hexane) to obtain 4,4'-[2,2':5',2'':5'',2''':5''',2''''-quaterthiophene]-5,5''''-bis(*N,N*-dioctylaniline). Yield was 0.1822 g, 51%. $\text{C}_{60}\text{H}_{84}\text{N}_2\text{S}_4$; IR (KBr) ν^{-1} 2934-2862, 1606, 1497 -1454, 1367, 796 and 616 cm^{-1} ; UV-Vis; $\lambda_{\text{max, abs}}$ (220-600 nm)(dry CH_2Cl_2) (nm) (log $\epsilon/\text{dm}^3/\text{mol cm}$); 260 (4.60), 336 (4.47), 457 (4.95); Fluorescence; $\lambda_{\text{max, PL}}$ (200-700 nm)(dry CH_2Cl_2) 543 nm; $^1\text{H-NMR}$ δ_{H} (ppm) (300 MHz, CDCl_3) 0.90 (12H, t, $J = 6.6$ Hz), 1.32 (40H, d, $J = 8.4$ Hz), 3.30 (8H, s), 6.65 (4H, s (broad)), 7.09 (8H, d, $J = 8.4$ Hz), 7.46 (4H, s); $^{13}\text{C-NMR}$ δ_{C} (ppm) (75 MHz, CDCl_3) 14.08, 22.63, 27.10, 29.28, 29.42, 31.80, 51.08, 76.58, 77.01, 77.21, 77.43, 111.73, 121.12, 123.69, 124.15, 124.61 and 126.85. M^+/Z cal. = 961.58, found = 961.

4,4'-[2,2':5',2'':5'',2''':5''',2''''-quinquethiophene]-5,5''''-bis(*N,N*-dioctylaniline) (PT5)



A mixture of 4-(5'-bromo-[2,2'-bithiophen])-*N,N*-dioctylaniline (1.76 g, 3.15 mmol), 2,5-thiophene-diboronic acid (0.208 g, 1.21 mmol), sodium carbonate (2.64 g, 25.02 mmol) and Pd(PPh₃)₄ (0.07 g, 0.06 mmol) in tetrahydrofuran (20 ml) was heated at reflux for 24 h. After cool at room temperature, the mixture was extracted with dichloromethane and washed with water 2 times. The combined extracted was washed with water, dried over sodium sulphate, evaporated to remove solvent and isolated by vacuum distillation. The residue was subjected to column chromatography (silica gel, hexane) to obtain pure 4,4'-[2,2':5',2'':5'',2''':5''',2''':5''',2''''-quinquethiophene]-5,5''''-bis(*N,N*-dioctylaniline) as yellow oil. Yield was 0.57 g, 33%. C₆₄H₈₆N₂S₅; IR (KBr) ν^1 3095-2851, 1605, 1518, 1494, 1455, 1366, 1143, 1070, 849, 787, 720 and 623; UV-Vis; $\lambda_{\max, \text{abs}}$ (220-600 nm)(dry CH₂Cl₂) (nm) (log $\epsilon/\text{dm}^3/\text{mol cm}$); 464 (4.70); Fluorescence; $\lambda_{\max, \text{PL}}$ (400-700 nm)(dry CH₂Cl₂) 549 nm; ¹H-NMR δ_{H} (ppm) (300 MHz, CDCl₃) 0.89 (12H, t, *J* = 12.6 Hz), 1.32 (40H, m), 1.61 (8H, s), 3.30 (8H, t, *J* = 6.90 Hz), 6.63 (4H, d, *J* = 8.7 Hz), 7.08 (10H, m) and 7.45 (4H, d, *J* = 8.7 Hz) ; ¹³C-NMR δ_{C} (ppm) (75 MHz, CDCl₃) 14.09, 22.65, 27.18, 27.30, 29.32, 29.50, 29.70, 31.83, 51.08, 111.68, 121.07, 123.52, 124.11, 124.30, 124.65, 126.84, 133.63, 135.05, 135.99, 137.06, 144.88 and 147.82. *M*⁺/*Z* cal. = 1043.76, found = 1044.

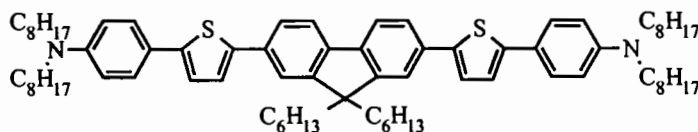
4,4'-[2,2':5',2'':5'',2''':5''',2''':5''',2''''-Sexithiophene]-5,5''''-bis(*N,N*-dioctylaniline) (PT6)



A total of 4-(5'-bromo-[2,2'-bithiophen])-*N,N*-dioctylaniline (0.54 g, 0.85 mmol), [Me₃Sn]₂ (0.13 g, 0.41 mmol) and Pd(PPh₃)₄ (0.009 g, 0.008 mmol) were refluxed in anhydrous toluene (15 ml) under N₂ for 48 h. After cool at room temperature, the mixture was extracted with dichloromethane and washed with water 2 times. The combined extracted was washed with water, dried over sodium sulphate, evaporated to remove solvent and isolated by vacuum distillation. The residue was subjected to column chromatography (silica gel, DCM:hexane) to obtain 4,4'-[2,2':5',2'':5'',2''':5''',2''':5''',2''''-sexithiophene]-5,5''''-bis(*N,N*-dioctylaniline) as red solid. Yield was 0.14 g, 31%. C₆₈H₈₈N₂S₆; IR (KBr) ν^1 3095-2850, 1605, 1514, 1493, 1455, 1399, 1366, 1270, 1142, 1069, 847, 788, 720, 689 and 623; UV-Vis; $\lambda_{\max, \text{abs}}$ (220-600 nm)(dry CH₂Cl₂) (nm) (log $\epsilon/\text{dm}^3/\text{mol cm}$); 433 (4.63); Fluorescence; $\lambda_{\max, \text{PL}}$ (400-700 nm)(dry CH₂Cl₂) 549 nm; ¹H-NMR δ_{H} (ppm) (300 MHz, CDCl₃) 0.87 (12H, t, *J* = 6.6 Hz), 1.29 (40H, t, *J* = 10.2 Hz), 1.58 (8H, s), 3.17 (8H, s), 6.61 (4H, d, *J* = 8.4 Hz), 7.06 (8H, m), 7.16 (4H, dd, *J* = 3.3 Hz) and 7.43 (4H, d, *J* = 8.70 Hz) ; ¹³C-NMR δ_{C} (ppm) (75 MHz, CDCl₃) 14.10, 22.65, 27.10, 27.18, 27.29, 29.23, 29.33, 29.50, 29.71, 31.83, 43.87, 51.08, 109.81, 111.11, 111.68, 121.04, 122.06, 123.48,

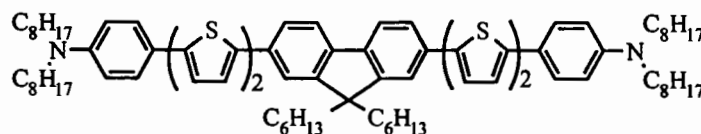
123.61, 123.78, 124.25, 124.36, 124.51, 126.05, 126.83, 127.85, 129.54, 134.77, 137.22, 144.68 and 147.79. M^+/Z cal. = 1124.5271, found = 1124.

4,4'-((9,9-dihexylfluorene-2,7-diyl)-bis(thiophene))-bis(*N,N*-dioctylaniline) (PT1F)



A mixture of 5-bromo-4-thiophenyl-*N,N*-dialkylaniline (0.70 g, 1.46 mmol), 9,9-dihexylfluorene-2,7-diboronic acid (0.29 g, 0.69 mmol), sodium carbonate (1.46 g, 13.8 mmol) and Pd(PPh₃)₄ (0.024 g, 0.02 mmol) in tetrahydrofuran (15 ml) was heated at reflux for 24 h. After cool at room temperature, the mixture was extracted with dichloromethane and washed with water 2 times. The combined extracted was washed with water, dried over sodium sulphate, evaporated to remove solvent and isolated by vacuum distillation. The residue was subjected to column chromatography (silica gel, hexane) to obtain pure 4,4'-((5,5'-(9,9-dihexyl-fluorene-2,7)-bis(thiophene-5,2-))bis(*N,N*-dioctylaniline) as yellowish viscos oil. Yield was 0.33 g, 42%. C₇₇H₁₁₂N₂S₂; IR (KBr) ν^1 2952-2851, 1606, 1541, 1515, 1472, 1397, 1367, 1271, 1233, 1190, 1110, 1064, 946, 879, 813, 790, 721 and 652; UV-Vis; $\lambda_{\max, \text{abs}}$ (220-600 nm)(dry CH₂Cl₂) (nm) (log $\epsilon/\text{dm}^3/\text{mol cm}$); 423 (4.11); Fluorescence; $\lambda_{\max, \text{PL}}$ (200-700 nm)(dry CH₂Cl₂) 491 nm; ¹H-NMR δ_{H} (ppm) (300 MHz, CDCl₃) 0.73 (6H, m), 0.90 (12H, d, $J = 6.9$ Hz), 1.11 (12H, m), 1.30 (40H, m), 1.59 (12H, s), 2.02 (4H, t, $J = 7.8$ Hz), 3.29 (8H, s), 6.64 (4H, d, $J = 7.8$ Hz), 7.13 (2H, s), 7.31 (2H, d, $J = 3.6$ Hz) and 7.58 (10H, m); ¹³C-NMR δ_{C} (ppm) (75 MHz, CDCl₃) 14.00, 14.11, 22.59, 22.67, 23.75, 27.20, 27.32, 29.34, 29.52, 29.71, 31.47, 31.85, 40.52, 51.11, 55.21, 111.70, 119.50, 119.92, 121.38, 121.56, 123.66, 124.34, 126.82, 133.48, 139.87, 141.73, 141.73, 144.68, 147.69 and 151.62. M^+/Z cal. = 1128.83, found = 1129.

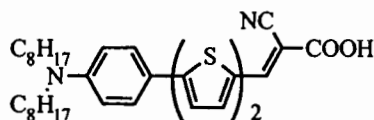
4,4'-((9,9-dihexylfluorene-2,7-diyl)-bis(2,2'-bithiophene))-bis(*N,N*-dioctylaniline) (PT2F)



A mixture of 4-(5'-bromo-[2,2'-bithiophen])-*N,N*-dioctylaniline (0.73 g, 1.31 mmol), 9,9-dihexylfluorene-2,7-diboronic acid (0.26 g, 0.62 mmol), sodium carbonate (1.32 g, 12.48 mmol) and Pd(PPh₃)₄ (0.022 g, 0.018 mmol) in tetrahydrofuran (15 ml) was heated at reflux for 24h. After cool at room temperature, the mixture was extracted with dichloromethane and washed

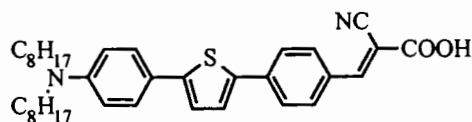
with water 2 times. The combined extracted was washed with water, dried over sodium sulphate, evaporated to remove solvent and isolated by vacuum distillation. The residue was subjected to column chromatography (silica gel, hexane) to obtain pure 4,4'-(5',5''-(9,9-dihexyl-fluorene-2,7-)bis([2,2'-bithiophene]-5',5'-))bis(*N,N*-dioctylaniline) as orange solid. Yield was 0.29 g, 27%. $C_{85}H_{116}N_2S_4$; IR (KBr) ν^1 2953-2851, 1604, 1553, 1508, 1497, 1400, 1367, 1324, 1271, 1235, 1190, 1111, 1054, 872, 810, 795, 721, 667 and; UV-Vis; $\lambda_{max,abs}$ (220-600 nm)(dry CH_2Cl_2) (nm) (log $\epsilon/dm^3/mol\ cm$); 443 (5.02); Fluorescence; $\lambda_{max,PL}$ (200-700 nm)(dry CH_2Cl_2) 530 nm; 1H -NMR δ_H (ppm) (300 MHz, $CDCl_3$) 0.77 (6H, t, $J = 6.9$ Hz), 0.88 (12H, d, $J = 6.6$ Hz), 1.08 (12H, s), 1.30 (44H, d, $J = 8.7$ Hz), 1.58 (12H, s), 2.05 (4H, s), 3.29 (8H, t, $J = 7.2$ Hz), 6.63 (4H, d, $J = 8.4$ Hz), 7.06 (3H, s), 7.16 (3H, s), 7.29 (2H, d, $J = 3.6$ Hz), 7.45 (4, d, $J = 8.1$ Hz), 7.58 (4H, m) and 7.66 (2H, d, $J = 8.1$ Hz); ^{13}C -NMR δ_C (ppm) (75 MHz, $CDCl_3$) 13.99, 14.09, 22.57, 22.66, 23.77, 27.11, 27.20, 27.33, 29.24, 29.34, 29.51, 29.69, 31.46, 31.85, 40.45, 43.89, 51.10, 55.31, 109.84, 111.13, 111.72, 119.72, 119.94, 120.10, 121.09, 121.19, 121.43, 122.10, 123.56, 123.80, 124.08, 124.15, 124.44, 124.58, 126.05, 126.18, 126.83, 129.55, 129.75, 132.95, 133.08, 134.16, 136.80, 137.14, 140.20, 140.36, 140.56, 143.08, 144.61, 147.81, 151.77 and 151.89. M^+/Z cal. = 1294.10, found = 1294.

(*E*)-2-Cyano-3-(5'-(4-(dioctylamino)phenyl)-[2,2'-bithiophen])acrylic acid (PT2dye)



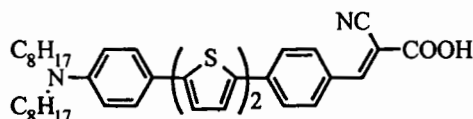
The appropriate 5'-(4-(*N,N*-dioctylamino)phenyl)-[2,2'-bithiophene]-5-carbaldehyde (0.30 g, 0.59 mmol) was added to solution of cyano acetic acid (0.13 g, 1.47 mmol) in ammonium acetate (0.23 g, 2.95 mmol) and acetic acid (15 ml). The solution mixture was heated at 80°C for 24h. The mixture was cooled and poured into ice-cold water and the solid obtained was filtered, washed and recrystallized from methanol to obtain (*E*)-2-cyano-3-(4-(5'-(4-(dioctylamino)phenyl)-[2,2'-bithiophen])phenyl)acrylic acid as red solid. Yield was 0.23 g, 68%. $C_{34}H_{44}N_2O_2S_2$; IR (KBr) ν^1 3411, 2924, 285, 2358, 2212, 1605, 1490, 1448, 1390, 1367, 1186, 1051 and 788 cm^{-1} ; UV-Vis; $\lambda_{max,abs}$ (220-600 nm)(dry CH_2Cl_2) (nm) (log $\epsilon/dm^3/mol\ cm$); 365 (3.99) and 466 (4.13); Fluorescence; $\lambda_{max,PL}$ (200-700 nm)(dry CH_2Cl_2) 586 nm; M^+/Z cal. = 576.8580, found = 576.173.

**(E)-2-Cyano-3-(4-(5-(4-(dioctylamino)phenyl)thiophen)phenyl)acrylic acid
(PT1Pdye)**



The appropriate 4-Benzaldehyde-4-thiophene-*N,N*-dialkylaniline (0.10 g, 0.20 mmol) was added to solution of cyano acetic acid (0.017 g, 2.0 mmol) in ammonium acetate (0.08 g, 1.01 mmol) and acetic acid (5 ml). The solution mixture was heated at 80°C for 24h. The mixture was cooled and poured into ice-cold water and the solid obtained was filtered, washed and recrystallized from methanol to obtain ((*E*)-2-cyano-3-(4-(5-(4-(dioctylamino)phenyl)thiophen)phenyl)acrylic acid as red solid. Yield was 0.08 g, 77%. $C_{36}H_{46}N_2O_2S$: IR (KBr) ν^{-1} 3400, 2918, 2845, 2364, 2212, 1597, 1496, 1451, 1367, 1281, 1186, 937, 827 and 788 cm^{-1} ; UV-Vis; $\lambda_{max, abs}$ (220-600 nm)(dry CH_2Cl_2) (nm) (log $\epsilon/dm^3/mol\ cm$); 335 (4.26), and 435 (4.28); Fluorescence; $\lambda_{max, PL}$ (200-700 nm)(dry CH_2Cl_2) 547 nm; ^1H-NMR δ_H (ppm) (300 MHz, $DMSO-D_6$) 0.76 (6H, d, $J = 6.6$ Hz), 1.18 (20H, t, $J = 10.0$ Hz), 1.48 (4H, s), 3.26 (4H, s), 6.46 (2H, d, $J = 8.1$ Hz), 6.91 (1H, s), 7.13 (1H, s), 7.27 (2H, d, $J = 7.8$ Hz), 7.39 (2H, d, $J = 5.1$ Hz), 7.74 (2H, d, $J = 5.1$ Hz) and 8.13 (1H, s); $^{13}C-NMR$ δ_C (ppm) (75 MHz, $CDCl_3$) 14.10, 22.56, 27.05, 27.24, 29.23, 29.42, 31.73, 50.92, 107.65, 111.57, 112.7, 118.52, 120.73, 121.90, 124.93, 125.61, 126.74, 130.88, 131.11, 137.45, 139.00, 146.40, 147.86, 151.00 and 168.4; M^+/Z cal. = 570.8276, found = 570.6

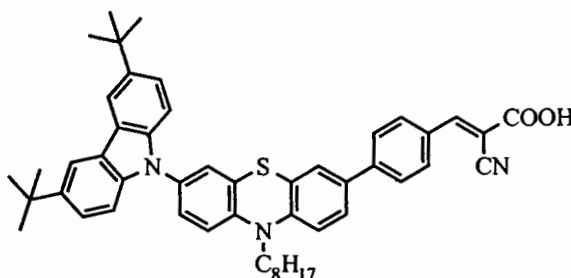
(E)-2-Cyano-3-(4-(5'-(4-(dioctylamino)phenyl)-[2,2'-bithiophen])phenyl)acrylic acid (PT2Pdye)



The appropriate 5-Benzaldehyde-4-thiophene-*N,N*-dialkylaniline (0.2 g, 0.34 mmol) was added to solution of cyano acetic acid (0.06 g, 0.68 mmol) in ammonium acetate (0.13 g, 1.7 mmol) and acetic acid (10 ml). The solution mixture was heated at 80°C for 24h. The mixture was cooled and poured into ice-cold water and the solid obtained was filtered, washed and recrystallized from methanol to obtain (*E*)-2-cyano-3-(4-(5'-(4-(dioctylamino)phenyl)-[2,2'-bithiophen])phenyl)acrylic acid as red solid. Yield was 0.09 g, 41%. $C_{40}H_{48}N_2O_2S_2$; IR (KBr) ν^{-1} 3338, 2918, 2851, 2212, 1622, 1597, 1530, 1496, 1454, 1367, 1186, 956, 867, 827 and 791 cm^{-1} ; UV-Vis; $\lambda_{max, abs}$ (220-600 nm)(dry DMSO) (nm) (log $\epsilon/dm^3/mol\ cm$); 424 (4.46); Fluorescence; $\lambda_{max, PL}$ (200-700 nm)(dry DMSO) 528 nm; ^1H-NMR δ_H (ppm) (300 MHz, $DMSO-D_6$) 0.87 (3H, d,

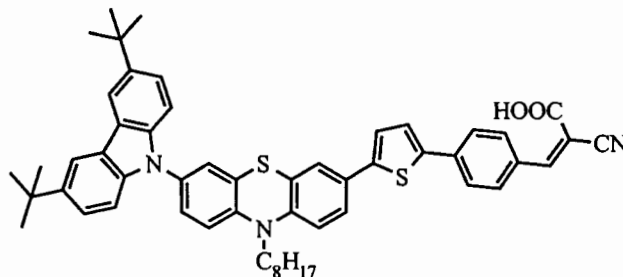
$J = 6.90$ Hz), 1.24 (12H, s), 2.06 (13H, s), 3.36 (4H, s) 6.62 (1H, m), 7.20 (1H, d, $J = 4.50$ Hz), 7.29 (2H, t, $J = 3.60$ Hz), 7.38 (2H, m), 7.62 (2H, t, $J = 3.60$ Hz), 7.72 (2H, t, $J = 8.10$ Hz) and 7.89 (3H, d, $J = 5.70$ Hz); $^{13}\text{C-NMR}$ δ_c (ppm) (75 MHz, CDCl_3) 14.39, 22.53, 26.88, 27.13, 27.31, 29.16, 29.32, 31.13, 31.68, 43.11, 50.58, 112.13, 112.53, 119.86, 121.85, 125.05, 125.73, 125.84, 126.57, 126.82, 130.62, 132.88, 135.67, 146.63 and 206.99; M^+/Z cal. = 652.956, found = 652.256.

(E)-2-Cyano-3-(4-(7-(3,6-di-*tert*-butyl-cabazol-9-yl)-10-octyl-phenothiazine-3-yl)phenyl)acrylic acid (PhCPdye)



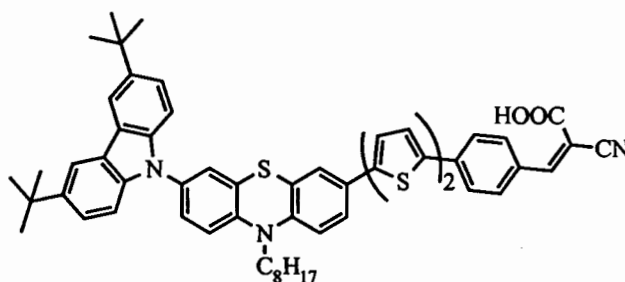
The appropriate 4-(7-(3,6-di-*tert*-butyl-cabazol-9-yl)-10-octyl-phenothiazin-3-yl)benzaldehyde (0.30 g, 0.43 mmol) was added to solution of cyanoacetic acid (0.18 g, 2.16 mmol) in piperidine (0.17 g, 2.02 mmol) and chloroform (20 ml). The solution mixture was heated at 80°C for 24h. The mixture was cooled and poured into ice-cold water and the solid obtained was filtered, washed and recrystallized from methanol to obtain (E)-2-cyano-3-(4-(7-(3,6-di-*tert*-butyl-cabazol-9-yl)-10-octyl-phenothiazine-3-yl)phenyl)acrylic acid as red solid. Yield was 0.24 g, 73%. $\text{C}_{50}\text{H}_{53}\text{N}_3\text{O}_2\text{S}$; IR (KBr) (ν^1) 3547, 3474, 3418, 2956, 2926, 2857, 2215, 1617, 1593, 1477, 1363, 1260, 1187 and 809 cm^{-1} ; UV-Vis; $\lambda_{\text{max, abs}}$ 220-800 nm)(dry CH_2Cl_2 ()nm) ($\log \epsilon/\text{dm}^3/\text{mol cm}$ (; 320 (4.46) and 427 (4.18); Fluorescence; $\lambda_{\text{max, PL}}$ 200-700 nm)(dry CH_2Cl_2 (483 nm; $^1\text{H-NMR}$ δ_{H})ppm) (300 MHz, acetone- D_6 (0.90)3H, s(, 1.29)18H, d, $J = 30.0$ Hz(,1.48 (10H, s), 1.90 (2H, s), 3.92 (2H, s), 6.99 (2H, d, $J = 9.9$ Hz), 7.29 (5H, d, $J = 8.1$ Hz), 7.45 (4H, d, $J = 8.4$ Hz), 7.68 (2H, s) and 8.15 (4H, s); $^{13}\text{C-NMR}$ δ_c) ppm) (75 MHz, acetone- D_6 (14.09, 22.62, 26.85, 26.96, 29.21, 29.36, 29.70, 30.04, 30.38, 31.74, 32.01, 34.70, 38.75, 47.83, 68.19, 109.14, 115.74, 115.98, 116.18, 123.21, 123.55, 124.89, 125.51, 125.66, 125.78, 126.38, 126.81, 128.81, 130.88, 132.03, 132.88, 133.50, 139.36, 142.75, 143.49, 144.73 and 145.35; M^+/Z cal. = 760.053, found = 759.5574.

(E)-2-Cyano-3-(4-(5-(7-(3,6-di-*tert*-butylcarbazole)-10-octylphenothiazine)thiophene)phenyl)acrylic acid (PhCT1Pdye)



The appropriate pure 4-(5-(7-(3,6-Di-*tert*-butyl-carbazol)-10-octylphenothiazine)thiophene)benzaldehyde (0.23 g, 0.30mmol) was added to solution of cyanoacetic acid (0.13 g, 1.51mmol) in piperidine (0.17 g, 2.02 mmol) and chloroform (20 ml). The solution mixture was heated at 80°C for 24h. The mixture was cooled and poured into ice-cold water and the solid obtained was filtered, washed and recrystallized from methanol to obtain (*E*)-2-cyano-3-(4-(5-(7-(3,6-di-*tert*-butylcarbazole)-10-octylphenothiazine)thiophene)phenyl)acrylic acid as red solid. Yield was 0.15 g, 58%. $C_{54}H_{55}N_3O_2S_2$; IR (KBr) $\nu^{13551, 3474, 3409, 2952, 2918, 2862, 2215, 1638, 1613, 1477, 1336, 1260, 798$ and 611 cm^{-1} ; UV-Vis; $\lambda_{\text{max, abs}}$ (220-800 nm)(dry CH_2Cl_2) (nm) (log $\epsilon/\text{dm}^3/\text{mol cm}$); 347 (4.39) and 434 (4.35); Fluorescence; $\lambda_{\text{max, PL}}$ (200-700 nm)(dry CH_2Cl_2) 530 nm; $^{13}C\text{-NMR}^c$ (ppm) (75 MHz, acetone- D_6)14.04, 22.51, 26.81, 28.94, 29.11, 29.70, 31.63, 31.94, 32.02, 34.57, 38.76, 47.53, 68.18, 109.16, 115.66, 116.19, 123.15, 123.45, 123.55, 124.89, 125.34, 125.77, 128.55, 128.81, 130.87, 132.45, 139.21, 139.45, 142.56 and 143.86

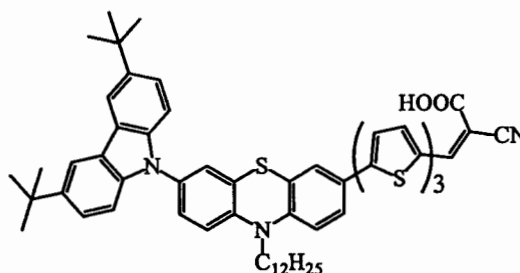
(E)-2-Cyano-3-(4-(5'-(7-(3,6-di-*tert*-butylcarbazole)-10-octylphenothiazine)-[2,2'-bithiophen])phenyl)acrylic acid (PhCT2Pdye)



The appropriate 4-(5'-(7-(3,6-di-*tert*-butylcarbazole)-10-octylphenothiazine)-[2,2'-bithiophen])benzaldehyde (0.13 g, 0.15mmol) was added to solution of cyanoacetic acid (0.06 g, 0.75 mmol) in piperidine (0.03g, 0.40 mmol) and chloroform (7 ml). The solution mixture was heated at 80°C for 24h. The mixture was cooled and poured into ice-cold water and the solid obtained was filtered, washed and recrystallized from methanol to obtain (*E*)-2-cyano-3-(4-(5'-(7-(3,6-di-*tert*-butylcarbazole)-10-octylphenothiazine)-[2,2'-bithiophen])phenyl)acrylic acid as red solid.

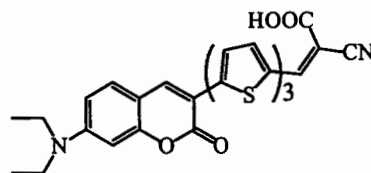
(3,6-di-*tert*-butylcarbazole)-10-octylphenothiazine)-[2,2'-bithiophen])phenyl)acrylic acid as red solid. Yield was 0.09 g, 71%. $C_{58}H_{57}N_3O_2S_3$: IR (KBr) ν^1 3556, 3478, 3405, 2956, 2926, 2215, 1617, 1593, 1477, 1363, 1260, 1187 and 809 cm^{-1} ; UV-Vis; $\lambda_{max, abs}$ (220-800 nm)(dry CH_2Cl_2) (nm) (log $\epsilon/dm^3/mol\ cm$); 350 (4.24) and 455 (4.45); Fluorescence; $\lambda_{max, PL}$ (200-700 nm)(dry CH_2Cl_2) 541 nm; 1H -NMR δ_H (ppm) (300 MHz, acetone- D_6) 0.82 (3H, m), 1.28 (12H, s), 1.43 (16H, s), 1.51 (2H, m), 4.10 (2H, t, $J = 6.6$ Hz), 7.15 (1H, d, $J = 8.4$ Hz), 7.29 (3H, m), 7.37-7.44 (4H, m), 7.48 (3H, d, $J = 8.7$ Hz), 7.55 (1H, d, $J = 8.4$ Hz), 7.69 (1H, d, $J = 3.9$ Hz), 7.91 (2H, d, $J = 8.1$ Hz), 8.15 (2H, d, $J = 8.4$ Hz), 8.27 (2H, s) and 8.32 (1H, s); ^{13}C -NMR c (ppm) (75 MHz, acetone- D_6) 14.07, 22.61, 26.94, 29.20, 29.69, 32.00, 34.69, 47.80, 68.18, 109.14, 116.18, 123.20, 123.54, 128.80, 130.85, 132.75, 139.40 and 142.73; M^+/Z cal. = 924.2930, found = 923.6046.

(*E*)-2-Cyano-3-(5''-(7-(3,6-di-*tert*-butyl-carbazol)-10-octyl-phenothiazin-3-yl)-[2,2':5',2''-terthiophen]-5-yl)acrylic acid (PhCT3dye)



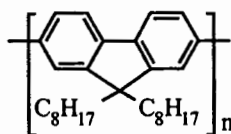
The appropriate 3-(5'-bromo-[2,2'-bithiophen])-7-(3,6-di-*tert*-butyl-carbazol)-10-dodecyl-phenothiazine (0.10 g, 0.11 mmol) was added to solution of cyanoacetic acid (0.014 g, 0.16 mmol) in piperidine (0.03 g, 0.32 mmol) and chloroform (20 ml). The solution mixture was heated at 80°C for 24h. The mixture was cooled and poured into ice-cold water and the solid obtained was filtered, washed and recrystallized from methanol to obtain (*E*)-2-cyano-3-(5''-(7-(3,6-di-*tert*-butyl-carbazol)-10-octyl-phenothiazin-3-yl)-[2,2':5',2''-terthiophen]-5-yl)acrylic acid as red solid. Yield was 0.04 g, 43%. $C_{56}H_{55}N_3O_2S_4$: IR (KBr) ν^1 2954, 2924, 2854, 2215, 1614, 1528, 1477, 1454, 1375, 1363, 1295, 1261, 1049, 877, 790 and 741 cm^{-1} ; $\lambda_{max, abs}$ (220-800 nm)(dry CH_2Cl_2) (nm) (log $\epsilon/dm^3/mol\ cm$); 436 (4.48); Fluorescence; $\lambda_{max, PL}$ (200-700 nm)(dry CH_2Cl_2) 656 nm; M^+/Z cal. = 930.3148, found = 932.1.

(E)-2-cyano-3-(5''-(7-(diethylaminocoumarin)-[2,2':5',2''-terthiophen]-5-yl)acrylic acid (CoT3dye)



The appropriate 3-[2,2':5',2''-terthiophene]-5-carbaldehyde-7-(diethylamino)-coumarin (0.12 g, 0.24 mmol) was added to solution of cyano acetic acid (0.03 g, 0.36 mmol) in piperidine (0.06 g, 0.73 mmol) and chloroform (25 ml). The solution mixture was heated at 80°C for 24h. The mixture was cooled and poured into ice-cold water and the solid obtained was filtered, washed and recrystallized from methanol to obtain (E)-2-cyano-3-(4-(5'-(4-(diethylamino)phenyl)-[2,2'-bithiophen])phenyl)acrylic acid as red solid. Yield was 0.05 g, 43%. $C_{29}H_{22}N_2O_4S_3$: IR (KBr) ν^1 3401, 2924, 2853, 2207, 1706, 1616, 1588, 1513, 1441, 1377, 1359, 1272, 1133, 1018 and 791 cm^{-1} ; UV-Vis; $\lambda_{max, abs}$ (220-800 nm)(dry CH_2Cl_2) (nm) (log $\epsilon/dm^3/mol\ cm$); 491 (4.61); Fluorescence; $\lambda_{max, PL}$ (200-700 nm)(dry CH_2Cl_2) 578 nm; ^1H-NMR δ_H (ppm) (300 MHz, DMSO- D_6) 1.10 (6H, t, $J = 6.9$ Hz), 3.40 (4H, m), 6.60 (1H, s), 6.76 (1H, dd, $J = 6.9$ Hz), 7.33 (1H, d, $J = 3.9$ Hz), 7.43 (2H, m), 7.50 (1H, d, $J = 9.0$ Hz), 7.62 (1H, d, $J = 3.9$ Hz), 7.66 (1H, d, $J = 3.9$ Hz), 8.00 (1H,s) and 8.46 (1H, s); M^+/Z cal. = 558.691, found = 558.022.

Synthesis of Poly(9,9-dioctylfluorene) (PFO)



Concentration 2.99 mg/ml

Tetraethylammonium hydroxide solution (40% in water) (0.16 g, 0.4 mmol) was added to an aqueous solution (50 ml) of non-ionic surfactant, Triton x-102 (2.5 g, 5 wt% in de-ionised water) in a 100 ml three necked round bottom flask. Then contents were then through degassed for 30 min by bubbling nitrogen gas through the stirred solution. Then a separate 10 ml two necked round bottom flask was used to mix together the monomers in the organic solvent prior to addition to the reaction flask 9,9-Dioctylfluorene-2,7-di-boronic acid-bis(1,3-propanediol)ester (0.1151g, 0.2 mmol), 2,7-dibromo-9,9-dioctylfluorene (0.1096 g, 0.2 mmol) were dissolved in xylene (2 ml). The monomer solution was degassed and then the catalyst $IPr^*PdTEACl_2$ (0.0095 g, 0.008 mmol) was added, followed by further degassing of the resultant solution. A syringe was used to transfer the monomer/catalyst into the stirred surfactant/base

solution in the main reaction flask now maintained at 30°C with stirring and maintaining under nitrogen gas for 24h. $M_n = 24,200$ g/mol, $M_w = 75,000$ g/mol and PDI = 3.08

Concentration 5.99 mg/ml

Tetraethylammonium hydroxide solution (40% in water) (0.3134 g, 0.8 mmol) was added to an aqueous solution (50 ml) of non-ionic surfactant, Triton x-102 (2.5 g, 5 wt% in de-ionised water) in a 100 ml three necked round bottom flask. Then contents were then through degassed for 30 min by bubbling nitrogen gas through the stirred solution. Then a separate 10 ml two necked round bottom flask was used to mix together the monomers in the organic solvent prior to addition to the reaction flask 9,9-Dioctylfluorene-2,7-di-boronic acid-bis(1,3-propanediol)ester (0.2306 g, 0.4 mmol), 2,7-dibromo-9,9-dioctylfluorene (0.2192 g, 0.4 mmol) were dissolved in xylene (2 ml). The monomer solution was degassed and then the catalyst $IPr^*PdTEACl_2$ (0.019 g, 0.016 mmol) was added, followed by further degassing of the resultant solution. A syringe was used to transfer the monomer/catalyst into the stirred surfactant/base solution in the main reaction flask now maintained at 30°C with stirring and maintaining under nitrogen gas for 24h. $M_n = 28,900$ g/mol, $M_w = 95,400$ g/mol and PDI = 3.29

Concentration 8.65 mg/ml

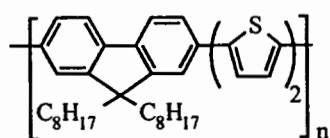
Tetraethylammonium hydroxide solution (40% in water) (0.4701 g, 1.2 mmol) was added to an aqueous solution (50 ml) of non-ionic surfactant, Triton x-102 (5 g, 10 wt% in de-ionised water) in a 100 ml three necked round bottom flask. Then contents were then through degassed for 30 min by bubbling nitrogen gas through the stirred solution. Then a separate 10 ml two necked round bottom flask was used to mix together the monomers in the organic solvent prior to addition to the reaction flask 9,9-Dioctylfluorene-2,7-di-boronic acid-bis(1,3-propanediol)ester (0.3454 g, 0.6 mmol), 2,7-dibromo-9,9-dioctylfluorene (0.3276 g, 0.6 mmol) were dissolved in xylene (4 ml). The monomer solution was degassed and then the catalyst $IPr^*PdTEACl_2$ (0.0285 g, 0.024 mmol) was added, followed by further degassing of the resultant solution. A syringe was used to transfer the monomer/catalyst into the stirred surfactant/base solution in the main reaction flask now maintained at 30°C with stirring and maintaining under nitrogen gas for 24h. $M_n = 48,120$, 6,100 g/mol, $M_w = 83,500$, 7,300 g/mol and PDI = 1.73, 1.20

Concentration 11.13 mg/ml

Tetraethylammonium hydroxide solution (40% in water) (0.6268 g, 1.6 mmol) was added to an aqueous solution (50 ml) of non-ionic surfactant, Triton x-102 (7.5 g, 15 wt% in de-ionised water) in a 100 ml three necked round bottom flask. Then contents were then through degassed for 30 min by bubbling nitrogen gas through the stirred solution. Then a separate 10 ml two necked round bottom flask was used to mix together the monomers in the organic solvent

prior to addition to the reaction flask 9,9-Dioctylfluorene-2,7-di-boronic acid-bis(1,3-propanediol)ester (0.4605 g, 0.8 mmol), 2,7-dibromo-9,9-dioctylfluorene (0.4431 g, 0.8 mmol) were dissolved in xylene (6 ml). The monomer solution was degassed and then the catalyst $\text{IPr}^*\text{PdTEACl}_2$ (0.0382 g, 0.032 mmol) was added, followed by further degassing of the resultant solution. A syringe was used to transfer the monomer/catalyst into the stirred surfactant/base solution in the main reaction flask now maintained at 30°C with stirring and maintaining under nitrogen gas for 24h. $M_n = 12,900$ g/mol, $M_w = 39,400$ g/mol and PDI = 3.05

Synthesis of Poly(9,9-dioctylfluorene-2,7-diyl)-*co*-bithiophene (PF8T2)



Concentration 2.13 mg/ml

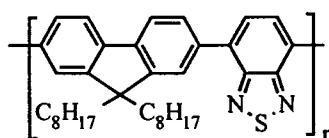
Tetraethylammonium hydroxide solution (40% in water) (0.16 g, 0.4 mmol) was added to an aqueous solution (50 ml) of non-ionic surfactant, Triton x-102 (2.5 g, 5 wt% in de-ionised water) in a 100 ml three necked round bottom flask. Then contents were then through degassed for 30 min by bubbling nitrogen gas through the stirred solution. Then a separate 10 ml two necked round bottom flask was used to mix together the monomers in the organic solvent prior to addition to the reaction flask 9,9-Dioctylfluorene-2,7-di-boronic acid-bis(1,3-propanediol)ester (0.1151g, 0.2 mmol), 2,7-dibromo-9,9-dioctylfluorene (0.0648 g, 0.2 mmol) were dissolved in xylene (2 ml). The monomer solution was degassed and then the catalyst $\text{IPr}^*\text{PdTEACl}_2$ (0.0095 g, 0.008 mmol) was added, followed by further degassing of the resultant solution. A syringe was used to transfer the monomer/catalyst into the stirred surfactant/base solution in the main reaction flask now maintained at 30°C with stirring and maintaining under nitrogen gas for 24h. $M_n = 12,100$ g/mol, $M_w = 32,700$ g/mol and PDI = 2.69

Concentration 8.72 mg/ml

Tetraethylammonium hydroxide solution (40% in water) (0.6268 g, 1.6 mmol) was added to an aqueous solution (50 ml) of non-ionic surfactant, Triton x-102 (5 g, 10 wt% in de-ionised water) in a 100 ml three necked round bottom flask. Then contents were then through degassed for 30 min by bubbling nitrogen gas through the stirred solution. Then a separate 10 ml two necked round bottom flask was used to mix together the monomers in the organic solvent prior to addition to the reaction flask 9,9-Dioctylfluorene-2,7-di-boronic acid-bis(1,3-propanediol)ester (0.4605 g, 0.8 mmol), 2,7-dibromo-9,9-dioctylfluorene (0.2618 g, 0.8 mmol) were dissolved in xylene (6 ml). The monomer solution was degassed and then the catalyst

$\text{IPr}^*\text{PdTEACl}_2$ (0.0382 g, 0.032 mmol) was added, followed by further degassing of the resultant solution. A syringe was used to transfer the monomer/catalyst into the stirred surfactant/base solution in the main reaction flask now maintained at 30°C with stirring and maintaining under nitrogen gas for 24h. $M_n = 14,900$ g/mol, $M_w = 37,300$ g/mol and $\text{PDI} = 2.50$

Synthesis of Poly(9,9-di-octylfluorene-2,7-diyl)-co-(benzo[2,1,3]thiadiazole) (PF8BT)



Concentration 2.02 mg/ml

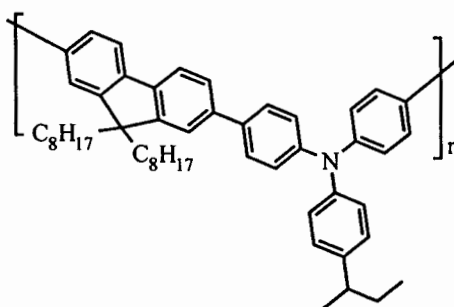
Tetraethylammonium hydroxide solution (40% in water) (0.16 g, 0.4 mmol) was added to an aqueous solution (50 ml) of non-ionic surfactant, Triton x-102 (2.5 g, 5 wt% in de-ionised water) in a 100 ml three necked round bottom flask. Then contents were then through degassed for 30 min by bubbling nitrogen gas through the stirred solution. Then a separate 10 ml two necked round bottom flask was used to mix together the monomers in the organic solvent prior to addition to the reaction flask 9,9-Dioctylfluorene-2,7-di-boronic acid-bis(1,3-propanediol)ester (0.1151g, 0.2 mmol), 2,7-dibromo-9,9-dioctylfluorene (0.058 g, 0.2 mmol) were dissolved in xylene (2 ml). The monomer solution was degassed and then the catalyst $\text{IPr}^*\text{PdTEACl}_2$ (0.0095 g, 0.008 mmol) was added, followed by further degassing of the resultant solution. A syringe was used to transfer the monomer/catalyst into the stirred surfactant/base solution in the main reaction flask now maintained at 30°C with stirring and maintaining under nitrogen gas for 48h. $M_n = 28,500$ g/mol, $M_w = 93,000$ g/mol and $\text{PDI} = 3.25$

Concentration 4.10 mg/ml

Tetraethylammonium hydroxide solution (40% in water) (0.3134 g, 0.8 mmol) was added to an aqueous solution (50 ml) of non-ionic surfactant, Triton x-102 (2.5 g, 5 wt% in de-ionised water) in a 100 ml three necked round bottom flask. Then contents were then through degassed for 30 min by bubbling nitrogen gas through the stirred solution. Then a separate 10 ml two necked round bottom flask was used to mix together the monomers in the organic solvent prior to addition to the reaction flask 9,9-Dioctylfluorene-2,7-di-boronic acid-bis(1,3-propanediol)ester (0.2306 g, 0.4 mmol), 2,7-dibromo-9,9-dioctylfluorene (0.1175 g, 0.4 mmol) were dissolved in xylene (2 ml). The monomer solution was degassed and then the catalyst $\text{IPr}^*\text{PdTEACl}_2$ (0.019 g, 0.016 mmol) was added, followed by further degassing of the resultant solution. A syringe was used to transfer the monomer/catalyst into the stirred surfactant/base

solution in the main reaction flask now maintained at 30°C with stirring and maintaining under nitrogen gas for 24h. $M_n = 26,000$ g/mol, $M_w = 67,324$ g/mol and PDI = 2.58

Synthesis of Poly(9,9'-dioctylfluorene-2,7-diyl)-co-bis-*N,N'*-(4-sec-butylphenyl) diphenylamine) (PF8TAA)



Concentration 2.5 mg/ml

Tetraethylammonium hydroxide solution (40% in water) (0.16 g, 0.4 mmol) was added to an aqueous solution (50 ml) of non-ionic surfactant, Triton x-102 (2.5 g, 5 wt% in de-ionised water) in a 100 ml three necked round bottom flask. Then contents were then through degassed for 30 min by bubbling nitrogen gas through the stirred solution. Then a separate 10 ml two necked round bottom flask was used to mix together the monomers in the organic solvent prior to addition to the reaction flask 9,9-Dioctylfluorene-2,7-di-boronic acid-bis(1,3-propanediol)ester (0.1151 g, 0.2 mmol), 4-bromo-(4-bromophenyl)-(4-(*sec*-butyl)phenyl)aniline (0.0918 g, 0.2 mmol) were dissolved in xylene (2 ml). The monomer solution was degassed and then the catalyst IPr*PdTEACl₂ (0.0095 g, 0.008 mmol) was added, followed by further degassing of the resultant solution. A syringe was used to transfer the monomer/catalyst into the stirred surfactant/base solution in the main reaction flask now maintained at 30°C with stirring and maintaining under nitrogen gas for 48h. $M_n = 18,500$ g/mol, $M_w = 49,800$ and PDI = 2.69

Concentration 10 mg/ml

Tetraethylammonium hydroxide solution (40% in water) (0.6268 g, 1.6 mmol) was added to an aqueous solution (50 ml) of non-ionic surfactant, Triton x-102 (10 g, 20 wt% in de-ionised water) in a 100 ml three necked round bottom flask. Then contents were then through degassed for 30 min by bubbling nitrogen gas through the stirred solution. Then a separate 10 ml two necked round bottom flask was used to mix together the monomers in the organic solvent prior to addition to the reaction flask 9,9-Dioctylfluorene-2,7-di-boronic acid-bis(1,3-propanediol)ester (0.4605 g, 0.8 mmol), 4-bromo-(4-bromophenyl)-(4-(*sec*-butyl)phenyl)aniline (0.3674 g, 0.8 mmol) were dissolved in xylene (2 ml). The monomer solution was degassed and then the catalyst IPr*PdTEACl₂ (0.038 g, 0.008 mmol) was added, followed by further degassing

of the resultant solution. A syringe was used to transfer the monomer/catalyst into the stirred surfactant/base solution in the main reaction flask now maintained at 30°C with stirring and maintaining under nitrogen gas for 48h. $M_n = 9,200$ g/mol, $M_w = 21,700$ g/mol and PDI = 2.30

REFERENCES

REFERENCES

- [1] Chiang, C. K., et al. (1977). "Electrical Conductivity in Doped Polyacetylene", Physical Review Letters. 39(17): 1098-1101.
- [2] Tang, C. W. (1986). "Two-layer organic photovoltaic cell", Applied Physics Letters. 48(2): 183-185.
- [3] Koezuka, H., Tsumura, A., and Ando, T. (1987). "Field-effect transistor with polythiophene thin film", Synthetic Metals. 18(1-3): 699-704.
- [4] Burroughes, J. H., Jones, C. A., and Friend, R. H. (1988). "New semiconductor device physics in polymer diodes and transistors", Nature. 335(6186): 137-141.
- [5] Horowitz, G., et al. (1989). "A field-effect transistor based on conjugated alpha-sexithienyl", Solid State Communications. 72(4): 381-384.
- [6] Tang, C. W. and VanSlyke, S. A. (1987). "Organic electroluminescent diodes", Applied Physics Letters. 51(12): 913-915.
- [7] Burroughes, J. H., et al. (1990). "Light-emitting diodes based on conjugated polymers", Nature. 347(6293): 539-541.
- [8] Brown, A. R., et al. (1995). "Logic Gates Made from Polymer Transistors and Their Use in Ring Oscillators", Science. 270(5238): 972-974.
- [9] Drury, C. J., et al. (1998). "Low-cost all-polymer integrated circuits", Applied Physics Letters. 73(1): 108-110.
- [10] Crone, B., et al. (2000). "Large-scale complementary integrated circuits based on organic transistors", Nature. 403(6769): 521-523.
- [11] Horowitz, G., et al. (1993). "All-organic field-effect transistors made of π -conjugated oligomers and polymeric insulators", Synthetic Metals. 54(1-3): 435-445.
- [12] Fix, W., et al. (2002). "Fast polymer integrated circuits", Applied Physics Letters. 81(9): 1735-1737.
- [13] Garnier, F., et al. (1994). "All-Polymer Field-Effect Transistor Realized by Printing Techniques", Science. 265(5179): 1684-1686.
- [14] Kane, M. G., et al. (2000). "Analog and digital circuits using organic thin-film transistors on polyester substrates", Electron Device Letters. 21(11): 534-536.
- [15] Granlund, T., et al. (2000). "Patterning of Polymer Light-Emitting Diodes with Soft Lithography", Advanced Materials. 12(4): 269-273.
- [16] Rogers, J. A., et al. (2000). "Printing, molding, and near-field photolithographic methods for patterning organic lasers, smart pixels and simple circuits", Synthetic Metals. 115(1-3): 5-11.

REFERENCES (CONTINUED)

- [17] Sirringhaus, H., Tessler, N., and Friend, R.H. (1998). "Integrated Optoelectronic Devices Based on Conjugated Polymers", Science. 280(5370): 1741-1744.
- [18] Dodabalapur, A., et al. (1998). "Organic smart pixels", Applied Physics Letters. 73(2): 142-144.
- [19] Huitema, H. E. A., et al. (2002). "Active-Matrix Displays Driven by Solution-Processed Polymeric Transistors", Advanced Materials. 14(17): 1201-1204.
- [20] Sheraw, C. D., et al. (2002). "Organic thin-film transistor-driven polymer-dispersed liquid crystal displays on flexible polymeric substrates", Applied Physics Letters. 80(6): 1088-1090.
- [21] Brown, A. R., et al. (1997). "Field-effect transistors made from solution-processed organic semiconductors", Synthetic Metals. 88(1): 37-55.
- [22] Horowitz, G. (1998). "Organic Field-Effect Transistors", Advanced Materials. 10(5): 365-377.
- [23] Wu, W., Liu, Y., and Zhu, D. (2010). " π -Conjugated molecules with fused rings for organic field-effect transistors: design, synthesis and applications", Chemical Society Reviews. 39(5): 1489-1502.
- [24] Aleshin, A. N., et al. (2004). "Mobility studies of field-effect transistor structures based on anthracene single crystals", Applied Physics Letters. 84(26): 5383-5385.
- [25] Jurchescu, O. D., et al. (2007). "Interface-Controlled, High-Mobility Organic Transistors", Advanced Materials. 19(5): 688-692.
- [26] Takeyama, Y., Ono, S., and Matsumoto, Y. (2012). "Organic single crystal transistor characteristics of single-crystal phase pentacene grown by ionic liquid-assisted vacuum deposition", Applied Physics Letters. 101(8): 083303 1-4.
- [27] Usta, H., Facchetti, A., and Marks, T. J. (2011). "n-Channel Semiconductor Materials Design for Organic Complementary Circuits", Accounts of Chemical Research. 44(7): 501-510.
- [28] Jones, B. A., et al. (2004). "High-Mobility Air-Stable n-Type Semiconductors with Processing Versatility: Dicyanoperylene-3,4:9,10-bis(dicarboximides)", Angewandte Chemie International Edition. 43(46): 6363-6366.
- [29] Amin, A. Y., et al. (2012). "Low-Voltage Organic Field Effect Transistors with a 2-Tridecyl[1]benzothieno[3,2-b][1]benzothiophene Semiconductor Layer", Journal of the American Chemical Society. 134(40): 16548-16550.

REFERENCES (CONTINUED)

- [30] Reese, C., et al. (2009). "Tuning Crystalline Solid-State Order and Charge Transport via Building-Block Modification of Oligothiophenes", Advanced Materials. 21(36): 3678-3681.
- [31] Yuan, Q., et al. (2008). "Microstructure of Oligofluorene Asymmetric Derivatives in Organic Thin Film Transistors", Chemistry of Materials. 20(8): 2763-2772.
- [32] Bao, Z., Rogers, J. A., and Katz, H. E. (1999). "Printable organic and polymeric semiconducting materials and devices", Journal of Materials Chemistry. 9(9): 1895-1904.
- [33] O'Regan, B. and Grätzel, M. (1991). "A low-cost, high-efficiency solar cell based on dye-sensitized colloidal TiO₂ films", Nature. 353(6346): 737-740.
- [34] Kim, J.-J., et al. (2008). "A polymer gel electrolyte to achieve [greater-than-or-equal]6% power conversion efficiency with a novel organic dye incorporating a low-band-gap chromophore", Journal of Materials Chemistry. 18(43): 5223-5229.
- [35] Mikroyannidis, J. A., et al. (2010). "Triphenylamine- and benzothiadiazole-based dyes with multiple acceptors for application in dye-sensitized solar cells", Journal of Power Sources. 195(9): 3002-3010.
- [36] Tang, Z.-M., et al. (2010). "Benzothiadiazole Containing D- π -A Conjugated Compounds for Dye-Sensitized Solar Cells: Synthesis, Properties, and Photovoltaic Performances", Chemistry-An Asian Journal. 5(8): 1911-1917.
- [37] Velusamy, M., et al. (2005). "Organic Dyes Incorporating Low-Band-Gap Chromophores for Dye-Sensitized Solar Cells", Organic Letters. 7(10): 1899-1902.
- [38] Zhu, W., et al. (2011). "Organic D-A- π -A Solar Cell Sensitizers with Improved Stability and Spectral Response", Advanced Functional Materials. 21(4): 756-763.
- [39] Nelson, J. (2003). "The Physics of Solar Cells", London, Imperial College Press.
- [40] Keith Emery. "Reference Solar Spectral Irradiance: Air Mass 1.5",
<http://rredc.nrel.gov/solar/spectra/am1.5/>. May 23, 2010
- [41] Hagfeldt, A., et al. (2010). "Dye-Sensitized Solar Cells" Chemical Reviews. 110(11): 6595-6663.
- [42] Grätzel, M. (2003). "Dye-sensitized solar cells", Journal of Photochemistry and Photobiology C: Photochemistry Reviews. 4(2): 145-153.
- [43] Liang, M. and Chen, J. (2013). "Arylamine organic dyes for dye-sensitized solar cells", Chemical Society Reviews. 42(8): 3453-3488.

REFERENCES (CONTINUED)

- [44] Hardin, B. E., Snaith, H. J., and McGehee, M. D. (2012). "The renaissance of dye-sensitized solar cells", Nat Photon. 6(3): 162-169.
- [45] Hara, K., et al. (2005). "Novel Conjugated Organic Dyes for Efficient Dye-Sensitized Solar Cells", Advanced Functional Materials. 15(2): 246-252.
- [46] Hara, K., et al. (2003). "Novel polyene dyes for highly efficient dye-sensitized solar cells", Chemical Communications. (2): 252-253.
- [47] Kitamura, T., et al. (2004). "Phenyl-Conjugated Oligoene Sensitizers for TiO₂ Solar Cells", Chemistry of Materials. 16(9): 1806-1812.
- [48] Li, S.-L., et al. (2006). "Novel organic dyes for efficient dye-sensitized solar cells", Chemical Communications. (26): 2792-2794.
- [49] Hara, K., et al. (2003). "Design of new coumarin dyes having thiophene moieties for highly efficient organic-dye-sensitized solar cells", New Journal of Chemistry. 27(5): 783-785.
- [50] Hara, K., et al. (2005). "Electron Transport in Coumarin-Dye-Sensitized Nanocrystalline TiO₂ Electrodes", The Journal of Physical Chemistry B. 109(50): 23776-23778.
- [51] Hara, K., et al. (2002). "Molecular Design of Coumarin Dyes for Efficient Dye-Sensitized Solar Cells", The Journal of Physical Chemistry B. 107(2): 597-606.
- [52] Hara, K., et al. (2001). "A coumarin-derivative dye sensitized nanocrystalline TiO₂ solar cell having a high solar-energy conversion efficiency up to 5.6%", Chemical Communications. (6): 569-570.
- [53] Hara, K., et al. (2005). "Oligothiophene-Containing Coumarin Dyes for Efficient Dye-Sensitized Solar Cells", The Journal of Physical Chemistry B. 109(32): 15476-15482.
- [54] Tian, H., et al. (2007). "Phenothiazine derivatives for efficient organic dye-sensitized solar cells", Chemical Communications. (36): 3741-3743.
- [55] Tian, H., et al. (2010). "Effect of different electron donating groups on the performance of dye-sensitized solar cells", Dyes and Pigments. 84(1): 62-68.
- [56] Kim, S.H., et al. (2011). "Effect of Five-Membered Heteroaromatic Linkers to the Performance of Phenothiazine-Based Dye-Sensitized Solar Cells", Organic Letters. 13(21): 5784-5787.
- [57] Medintz, I. L., et al. (2005). "Quantum dot bioconjugates for imaging, labelling and sensing", Nature Materials. 4(6): 435-446.
- [58] Jaiswal, J.K., et al. (2003). "Long-term multiple color imaging of live cells using quantum dot bioconjugates", Nature Biotechnology. 21(1): 47-51.

REFERENCES (CONTINUED)

- [59] Alivisatos, A.P., Gu, W., and Larabell, C. (2005). "Quantum Dots as Cellular Probes", Annual Review of Biomedical Engineering. 7(1): 55-76.
- [60] Michalet, X., et al. (2005). "Quantum Dots for Live Cells, in Vivo Imaging, and Diagnostics", Science. 307(5709): 538-544.
- [61] Bruchez, M., et al. (1998). "Semiconductor Nanocrystals as Fluorescent Biological Labels", Science. 281(5385): 2013-2016.
- [62] Kolodny, L. A. et al. (2001). "Spatially Correlated Fluorescence/AFM of Individual Nanosized Particles and Biomolecules", Analytical Chemistry. 73(9): 1959-1966.
- [63] Santra, S., et al. (2001). "Conjugation of Biomolecules with Luminophore-Doped Silica Nanoparticles for Photostable Biomarkers", Analytical Chemistry. 73(20): 4988-4993.
- [64] Wu, C., C. Szymanski, and McNeill, J. (2006). "Preparation and Encapsulation of Highly Fluorescent Conjugated Polymer Nanoparticles", Langmuir. 22(7): 2956-2960.
- [65] Wu, C., et al. (2008). "Multicolor Conjugated Polymer Dots for Biological Fluorescence Imaging", ACS Nano. 2(11): 2415-2423.
- [66] Szymanski, C., et al. (2005). "Single Molecule Nanoparticles of the Conjugated Polymer MEH-PPV, Preparation and Characterization by Near-Field Scanning Optical Microscopy", The Journal of Physical Chemistry B. 109(18): 8543-8546.
- [67] Yu, J., et al. (2009). "Nanoscale 3D Tracking with Conjugated Polymer Nanoparticles", Journal of the American Chemical Society. 131(51): 18410-18414.
- [68] Gesquiere, A. J., Park, S.-J., and Barbara, P. F. (2004). "Photochemistry and kinetics of single organic nanoparticles in the presence of charge carriers", European Polymer Journal. 40(5): 1013-1018.
- [69] Palacios, R.E., et al. (2007). "Charging and discharging of single conjugated-polymer nanoparticles", Nature Materials. 6(9): 680-685.
- [70] Landfester, K., et al. (2002). "Semiconducting Polymer Nanospheres in Aqueous Dispersion Prepared by a Miniemulsion Process", Advanced Materials. 14(9): 651-655.
- [71] Kietzke, T., et al. (2003). "Novel approaches to polymer blends based on polymer nanoparticles", Nature Materials. 2(6): 408-412.
- [72] Landfester, K. (2009). "Miniemulsion Polymerization and the Structure of Polymer and Hybrid Nanoparticles", Angewandte Chemie International Edition. 48(25): 4488-4507.

REFERENCES (CONTINUED)

- [73] Baier, M.C., J. (2009). "Huber, and S. Mecking, Fluorescent Conjugated Polymer Nanoparticles by Polymerization in Miniemulsion", Journal of the American Chemical Society. 131(40): 14267-14273.
- [74] Müller, K., Klapper, M., and Müllen, K. (2006). "Synthesis of Conjugated Polymer Nanoparticles in Non-Aqueous Emulsions", Macromolecular Rapid Communications. 27(8): 586-593.
- [75] Yang, Z., et al. (2005). "Shape-memory nanoparticles from inherently non-spherical polymer colloids", Nature Materials. 4(6): 486-490.
- [76] Jenekhe, S.A., et al. (2007). "Single-Molecule Nanomaterials from π -Stacked Side-Chain Conjugated Polymers", Advanced Materials. 19(4): 536-542.
- [77] Taranekar, P., et al. (2006). "Conjugated Polymer Nanoparticles via Intramolecular Crosslinking of Dendrimeric Precursors", Advanced Materials. 18(18): 2461-2465.
- [78] Chern, C. S. (2006). "Emulsion polymerization mechanisms and kinetics", Progress in Polymer Science. 31(5): 443-486.
- [79] Priest, W. J. (1952). "Partice Growth in the Aqueous Polymerization of Vinyl Acetate", The Journal of Physical Chemistry. 56(9): 1077-1082.
- [80] Roe, C. P. (1968). "Surface Chemistry Aspects of Emulsion Polymerization", Industrial & Engineering Chemistry. 60(9): 20-33.
- [81] Fitch, R. M. (1973). "The homogeneous nucleation of polymer colloids", British Polymer Journal. 5(6): 467-483.
- [82] Landfester, K. (2001). "Polyreactions in Miniemulsions", Macromolecular Rapid Communications. 22(12): 896-936.
- [83] Landfester, K. (2001). "The Generation of Nanoparticles in Miniemulsions", Advanced Materials. 13(10): 765-768.
- [84] Sarrazin, P., et al. (2009). "Surfactant (TTAB) Role in the Preparation of 2,7-Poly(9,9-dialkylfluorene-co-fluorenone) Nanoparticles by Miniemulsion", Langmuir. 25(12): 6745-6752.
- [85] Laquindanum, J. G., Katz, H. E., and Lovinger, A. J. (1998). "Synthesis, Morphology, and Field-Effect Mobility of Anthradithiophenes", Journal of the American Chemical Society. 120(4): 664-672.
- [86] Perepichka, I.F., et al. (2005). "Light-Emitting Polythiophenes", Advanced Materials. 17(19): 2281-2305.

REFERENCES (CONTINUED)

- [87] Mishra, A., Ma, C.-Q., and Bäuerle, P. (2009). "Functional Oligothiophenes: Molecular Design for Multidimensional Nanoarchitectures and Their Applications", Chemical Reviews. 109(3): 1141-1276.
- [88] Yum, J.-H., et al. (2009). "A Light-Resistant Organic Sensitizer for Solar-Cell Applications", Angewandte Chemie. 121(9): 1604-1608.
- [89] Noda, T., et al. (1997). "A novel family of amorphous molecular materials containing an oligothiophene moiety as color-tunable emitting materials for organic electroluminescent devices", Advanced Materials. 9(9): 720-722.
- [90] Shirota, Y. and Kageyama, H. (2007). "Charge Carrier Transporting Molecular Materials and Their Applications in Devices", Chemical Reviews. 107(4): 953-1010.
- [91] Jung, M.-H., et al. (2010). "Nonvolatile memory organic field effect transistor induced by the steric hindrance effects of organic molecules", Journal of Materials Chemistry. 20(37): 8016-8020.
- [92] Liu, Y., et al. (2009). "Synthesis, Characterization, and Field-Effect Transistor Performance of Thieno[3,2-b]thieno[2',3':4,5]thieno[2,3-d]thiophene Derivatives", Advanced Functional Materials. 19(5): 772-778.
- [93] Hong, X. M., et al. (2001). "Thiophene-Phenylene and Thiophene-Thiazole Oligomeric Semiconductors with High Field-Effect Transistor On/Off Ratios", Chemistry of Materials. 13(12): 4686-4691.
- [94] Mushrush, M., et al. (2003). "Easily Processable Phenylene-Thiophene-Based Organic Field-Effect Transistors and Solution-Fabricated Nonvolatile Transistor Memory Elements", Journal of the American Chemical Society. 125(31): 9414-9423.
- [95] Chen, H., et al. (1996). "Aggregation of Surfactant Squaraine Dyes in Aqueous Solution and Microheterogeneous Media: Correlation of Aggregation Behavior with Molecular Structure", Journal of the American Chemical Society. 118(11): 2584-2594.
- [96] Das, B., et al. (2007). "A facile nuclear bromination of phenols and anilines using NBS in the presence of ammonium acetate as a catalyst", Journal of Molecular Catalysis A: Chemical. 267(1-2): 30-33.
- [97] Tanemura, K., et al. (2004). "A mild and efficient procedure for [small alpha]-bromination of ketones using N-bromosuccinimide catalysed by ammonium acetate", Chemical Communications. (4): 470-471.
- [98] Espinet, P. and Echavarren, A. M. (2004). "The Mechanisms of the Stille Reaction", Angewandte Chemie International Edition. 43(36): 4704-4734.

REFERENCES (CONTINUED)

- [99] Grova, I.R., et al. (2013). "Correlations between the number of thiophene units and the photovoltaic behavior of fluorene-oligothiophene copolymers", European Polymer Journal. 49(11): 3539-3547.
- [100] Mishra, A., Fischer, M. K. R., and Bäuerle, P. (2009). "Metal-Free Organic Dyes for Dye-Sensitized Solar Cells: From Structure: Property Relationships to Design Rules", Angewandte Chemie International Edition. 48(14): 2474-2499.
- [101] Yella, A., et al. (2011). "Porphyrin-Sensitized Solar Cells with Cobalt (II/III)-Based Redox Electrolyte Exceed 12 Percent Efficiency", Science. 334(6056): 629-634.
- [102] Olivier, C., et al. (2011). "Fine-Tuning of Triarylamine-Based Photosensitizers for Dye-Sensitized Solar Cells", ChemSusChem. 4(6): 731-736.
- [103] Kim, S., et al. (2006). "Molecular Engineering of Organic Sensitizers for Solar Cell Applications", Journal of the American Chemical Society. 128(51): 16701-16707.
- [104] Jung, H.S. and Lee, J.-K. (2013). "Dye Sensitized Solar Cells for Economically Viable Photovoltaic Systems", The Journal of Physical Chemistry Letters. 4(10): 1682-1693.
- [105] Al-Eid, M., et al. (2014). "Facile synthesis of metal-free organic dyes featuring a thienylethynyl spacer for dye sensitized solar cells", Dyes and Pigments. 104(0): 197-203.
- [106] Wu, W., et al. (2010). "Efficient and stable dye-sensitized solar cells based on phenothiazine sensitizers with thiophene units", Journal of Materials Chemistry. 20(9): 1772-1779.
- [107] Clayden, J., Greeves, N., and Warren, S. (2012). "Organic Chemistry" 2nd ed., Oxford, Oxford University Press: 1264.
- [108] Tian, H., et al. (2008). "Effect of Different Dye Baths and Dye-Structures on the Performance of Dye-Sensitized Solar Cells Based on Triphenylamine Dyes", The Journal of Physical Chemistry C. 112(29): 11023-11033.
- [109] Baheti, A., et al. (2009). "Simple Triarylamine-Based Dyes Containing Fluorene and Biphenyl Linkers for Efficient Dye-Sensitized Solar Cells", The Journal of Physical Chemistry C. 113(20): 8541-8547.
- [110] Singh, P., et al. (2012). "Fluorene-based organic dyes containing acetylene linkage for dye-sensitized solar cells", Dyes and Pigments. 95(3): 523-533.
- [111] Xie, Z., et al. (2010). "Highly efficient dye-sensitized solar cells using phenothiazine derivative organic dyes", Progress in Photovoltaics: Research and Applications. 18(8): 573-581.

REFERENCES (CONTINUED)

- [112] Chang, Y.J., et al. (2012). "Organic dyes containing oligo-phenothiazine for dye-sensitized solar cells", Journal of Materials Chemistry. 22(40): 21704-21712.
- [113] Meyer, T., et al. (2012). "Phenothiazinyl Rhodanylidene Merocyanines for Dye-Sensitized Solar Cells", The Journal of Organic Chemistry. 77(8): 3704-3715.
- [114] Hua, Y., et al. (2013). "Significant Improvement of Dye-Sensitized Solar Cell Performance Using Simple Phenothiazine-Based Dyes", Chemistry of Materials. 25(10): 2146-2153.
- [115] Beletskaya, I. P. and Cheprakov, A. V. (2004). "Copper in cross-coupling reactions: The post-Ullmann chemistry", Coordination Chemistry Reviews. 248(21-24): 2337-2364.
- [116] Li, R., et al. (2009). "Dye-Sensitized Solar Cells Based on Organic Sensitizers with Different Conjugated Linkers: Furan, Bifuran, Thiophene, Bithiophene, Selenophene, and Biselenophene", The Journal of Physical Chemistry C. 113(17): 7469-7479.
- [117] Potjanasopa, S. (2011). "Synthesis and characterization of organic materials for optoelectronic devices", Department of Chemistry. Ubon Ratchathani University: Ubon Ratchathani, Thailand.
- [118] Tuncel, D. and Demir, H. V. (2010). "Conjugated polymer nanoparticles", Nanoscale. 2(4): 484-494.
- [119] Feng, L., et al. (2013). "Conjugated polymer nanoparticles: preparation, properties, functionalization and biological applications", Chemical Society Reviews. 42(16): 6620-6633.
- [120] Pecher, J. and Mecking, S. (2010). "Nanoparticles of Conjugated Polymers", Chemical Reviews. 110(10): 6260-6279.
- [121] Hebner, T. R., et al. (1998). "Ink-jet printing of doped polymers for organic light emitting devices", Applied Physics Letters. 72(5): 519-521.
- [122] Yang, Y., et al. (2000). "Organic/polymeric electroluminescent devices processed by hybrid ink-jet printing", Journal of Materials Science Materials in Electronics. 11(2): 89-96.
- [123] Mori, K., et al. (2000). "Organic light-emitting devices patterned by screen-printing", Japanese Journal of Applied Physics; Part 2. 39(9A/B): L942-L944.
- [124] Bao, Z., et al. (1997). "High Performance Plastic Transistors Fabricated by Printing Techniques", Chemistry of Materials. 9(6): 1299-1301.

REFERENCES (CONTINUED)

- [125] Szymanski, C., et al. (2005). "Single molecule nanoparticles of the conjugated polymer MEH-PPV, preparation and characterization by near-field scanning optical microscopy", Journal of Physical Chemistry B. 109(18): 8543-8546.
- [126] Fischer, C. S., M. C. Baier, and Mecking, S. (2013). "Enhanced Brightness Emission-Tuned Nanoparticles from Heterodifunctional Polyfluorene Building Blocks", Journal of the American Chemical Society. 135(3): 1148-1154.
- [127] Landfester, K., et al. (2002). "Semiconducting polymer nanospheres in aqueous dispersion prepared by a miniemulsion process", Advanced Materials. 14(9): 651-655.
- [128] Kietzke, T., et al. (2003). "Novel approaches to polymer blends based on polymer nanoparticles", Nature Materials. 2(6): 408-412.
- [129] Kietzke, T., et al. (2005). "Probing the local optical properties of layers prepared from polymer nanoparticles", Synthetic Metals. 152(1-3): 101-104.
- [130] Landfester, K. (2009). "Miniemulsion Polymerization and the Structure of Polymer and Hybrid Nanoparticles", Angewandte Chemie International Edition. 48(25): 4488-4507.
- [131] Jenekhe, S.A., et al. (2007). "Single-molecule nanomaterials from π -stacked side-chain conjugated polymers", Advanced Materials. 19(4): 536-542.
- [132] Müller, K., Klapper, M., and Müllen, K. (2006). "Synthesis of conjugated polymer nanoparticles in non-aqueous emulsions", Macromolecular Rapid Communications. 27(8): 586-593.
- [133] Bag, M., et al. (2013). "Efficient Charge Transport in Assemblies of Surfactant-Stabilized Semiconducting Nanoparticles", Advanced Materials. 25(44): 6411-6415.
- [134] Baier, M.C., Huber, J., and Mecking, S. (2009). "Fluorescent Conjugated Polymer Nanoparticles by Polymerization in Miniemulsion", Journal of the American Chemical Society. 131(40): 14267-14273.
- [135] Wang, R., et al. (2010). "Preparation, morphology, and biolabeling of fluorescent nanoparticles based on conjugated polymers by emulsion polymerization", Journal of Polymer Science Part A Polymer Chemistry. 48(21): 4867-4874.
- [136] Foster, A.B. (2011). unpublished results.
- [137] Chen, M.-T., et al. (2011). "(N-Heterocyclic Carbene)PdCl₂(TEA) Complexes: Studies on the Effect of the "Throw-Away" Ligand in Catalytic Activity", Organometallics. 30(18): 5052-5056.

REFERENCES (CONTINUED)

- [138] Nguyen, T.-Q., et al. (2000). "Controlling Interchain Interactions in Conjugated Polymers: The Effects of Chain Morphology on Exciton-Exciton Annihilation and Aggregation in MEH-PPV Films", Journal of Physical Chemistry B. 104(2): 237-255.
- [139] Noriega, R., et al. (2013). "A general relationship between disorder, aggregation and charge transport in conjugated polymers", Nature Materials. 12(11): 1038-1044.
- [140] Schwartz, B. J. (2003). "Conjugated polymers as molecular materials: How chain conformation and film morphology influence energy transfer and interchain interactions", Annual Review of Physical Chemistry. 54: 141-172.
- [141] Knaapila, M. and Monkman, A. P. (2013). "Methods for Controlling Structure and Photophysical Properties in Polyfluorene Solutions and Gels", Advanced Materials. 25(8): 1090-1108.
- [142] Bright, D. W., et al. (2009). "The influence of alkyl-chain length on beta-phase formation in polyfluorenes", Advanced Functional Materials. 19(1): 67-73.
- [143] Bansal, A.K., et al. (2010). "Fluorescence Quenchers in Mixed Phase Polyfluorene Films", Journal of Physical Chemistry C. 114(41): 17864-17867.
- [144] Wu, C. and McNeill, J. (2008). "Swelling-Controlled Polymer Phase and Fluorescence Properties of Polyfluorene Nanoparticles", Langmuir. 24(11): 5855-5861.
- [145] Behrendt, J. M., et al. (2013). "Hybrid inorganic-organic composite nanoparticles from crosslinkable polyfluorenes", Journal of Materials Chemistry C. 1(20): 3297-3304.
- [146] Rahman, M. H., et al. (2007). "Segmental alignment in the aggregate domains of poly(9,9-dioctylfluorene) in semidilute solution", Macromolecules. 40(18): 6572-6578.
- [147] Ong, B. S., et al. (2005). "Structurally ordered polythiophene nanoparticles for high-performance organic thin-film transistors", Advanced Materials. 17(9): 1141-1144.
- [148] Yang, Z., et al. (2005). "Shape-memory nanoparticles from inherently non-spherical polymer colloids", Nature Materials. 4(6): 486-490.
- [149] Finsy, R. (1994). "Particle sizing by quasi-elastic light scattering", Advances in Colloid and Interface Science. 52(0): 79-143.
- [150] Ariu, M., Lidzey, D. G., and Bradley, D. D. C. (2000). "Influence of film morphology on the vibrational spectra of dioctyl substituted polyfluorene (PFO) ", Synthetic Metals. 111-112: 607-610.
- [151] Knaapila, M., et al. (2011). "Network structure of polyfluorene sheets as a function of alkyl side chain length", Physical review E, Statistical, nonlinear, and soft matter physics. 83(5-1): 051803/1-051803/11.

REFERENCES (CONTINUED)

- [152] Khan, A. L. T., et al. (2004). "Morphology-dependent energy transfer within polyfluorene thin films", Physical Review B: Condensed Matter and Materials Physics. 69(8): 085201/1-085201/8.
- [153] Lim, E., Jung, B.-J., and Shim, H.-K. (2003). "Synthesis and Characterization of a New Light-Emitting Fluorene-Thieno[3,2-b]thiophene-Based Conjugated Copolymer", Macromolecules. 36(12): 4288-4293.
- [154] Bolis, S., Pasini, M., and Virgili, T. (2013). "A core copolymer approach to improve the gain properties of a red-emitting molecule", Chemical Communications. 49(100): 11761-11763.
- [155] He, Y., et al. (1999). "High performance organic polymer light-emitting heterostructure devices", Applied Physics Letters. 74(16): 2265-2267.
- [156] Su, W.-F., Chen, R.-T. and Chen, Y. (2011). "Thermally crosslinkable hole-transporting poly(fluorene-co-triphenylamine) for multilayer polymer light-emitting diodes", Journal of Polymer Science Part A: Polymer Chemistry. 49(2): 352-360.

APPENDIX

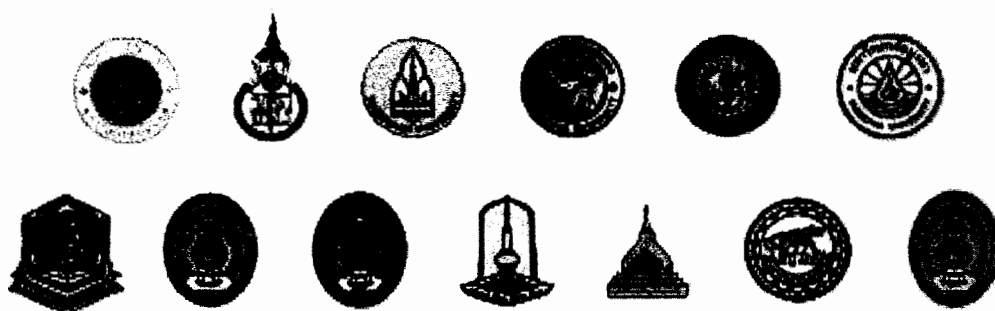
APPENDIX

PERCH-CIC Congress VII

การประชุมวิชาการ
ศูนย์ความเป็นเลิศด้านนวัตกรรมทางเคมี ครั้งที่ 7

4-7 พฤษภาคม 2554

โรงแรมจอมเทียน ปาล์มบีช แอนด์ รีสอร์ท เมืองพัทยา จังหวัดชลบุรี



The International Congress for Innovation in Chemistry

4-7 May 2011, Jomtien Palm Beach Hotel & Resort Pattaya, Chonburi

Center of Excellence for Innovation in Chemistry (PERCH-CIC)

Office of the Higher Education Commission (OHEC), Ministry of Education

S2A-O2

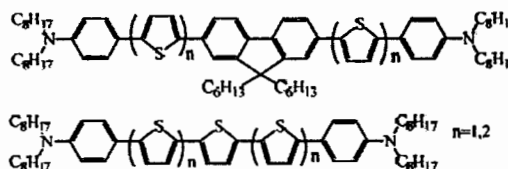
Synthesis and Characterization of Novel Oligothiophenes Bearing Dialkylaniline End-capped for OFETs

Duangratchaneekorn Muenmart, Taweesak Sudyoadsuk, Tinnagon Keawin, Sayant Saengsuwan, Siriporn Jungsuttiwong and Vinich Promarak

Center for Organic Electronic and Alternative Energy, Department of Chemistry and Center of Excellence for Innovation in Chemistry, Faculty of Science, Ubon Ratchathani University, Ubon Ratchathani, 34190 Thailand.

Introduction and Objective

Oligothiophenes are mostly investigated as organic semiconductors for organic field-effect transistors (OFETs) with high on-off current ratio and charge transport properties. The molecular structure of desired molecules can be modified using various organic synthetic methodologies. In this work, we reported on the synthesis, characterization and electronic properties of novel oligothiophenes with dialkylaniline end-capped for using as organic semiconductor in OFETs.



Methods

Suzuki coupling was carried out with $\text{Pd}(\text{PPh}_3)_4$ as catalyst and Na_2CO_3 as base in $\text{THF}/\text{H}_2\text{O}$. Bromination was done by NBS in THF. The chemical structures were confirmed by NMR and IR analysis. UV-Vis and Fluorescence spectra were recorded in CH_2Cl_2 . CV was measured with glassy C, Pt and SCE electrodes in the present of $n\text{-Bu}_4\text{NPF}_6$ as supporting electrolyte in CH_2Cl_2 .

Results

A series of oligothiophenes was synthesized using a combination of alkylation, iodination, bromination and Suzuki coupling reactions in moderate yields. The desired molecules were soluble in common organic solvents at room temperature. The number of thiophene units increased within the molecules result in red shift in absorption and fluorescence spectra due to the extended π -conjugation length of oligothiophenes. CV traces exhibit the oxidation of dialkylaniline donor.

Conclusion

Oligothiophenes with dialkylaniline end-capped were successfully synthesized. According to their electronic properties, it expected that these oligothiophenes can be used as organic semiconductor in OFETs.

Keywords: oligothiophenes, OFETs, organic semiconductor

Selected References:

1. Yamao T.; Ota S.; Miki T.; Hotta S.; Azumi R. *Thin Solid Films*, 2008, 516, 2527–2531.
2. Iosip M. D.; Destri S.; Pasini M.; Porzio W.; Pernstich K. P. *Synthetic Metals*, 2004, 146, 251–257.



Duangratchaneekorn Muenmart (ดวงรัตน์ มั่นมณเฑาะว์) Ph.D. Student
b 1983 in Srisaket, Thailand
Ubon Ratchathani University, Thailand, Chemistry, B.Sc. 2006
Ubon Ratchathani University, Thailand, Chemistry M.Sc. 2008
Research field: organic synthesis and organic materials

เครือข่ายที่ 1, 2 (Grant group(s))
**Synthesis and Characterization of Oligothiophenes Bearing
 Dialkylaniline End-Capped for Organic Field-Effect Transistor**

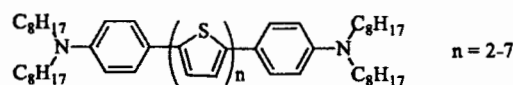
Duangratchaneekom Muenmart*, Taweesak Sudyoadsuk, Tinnagon Keawin,
 Sayant Saengsuwan, Siriporn Jungstittiwong and Vinich Promarak
*Center for Organic Electronics and Polymers, Department of Chemistry and
 Center of Excellence for Innovation in Chemistry, Faculty of Science, Ubon
 Ratchathani University, Ubon Ratchathani, Thailand 34190*

Introduction

Oligothiophenes are mostly studied as organic semiconductors for organic field-effect transistors (OFETs) with high on-off current ratio and charge transport properties. Moreover, the molecular structure of target molecules can be easily modified using various organic synthetic methodologies. In this work, we reported synthesis and characterization of novel oligothiophenes with dialkylaniline end-capped used as organic semiconductor in OFETs.

Objectives

To synthesize and characterize novel oligothiophenes bearing dialkylaniline end-capped for OFETs. To investigate optical, electrochemical and thermal properties of target molecules.



Results

The target molecules were synthesized using combination of alkylation, iodination, bromination followed by palladium catalyzed Suzuki coupling and Stille coupling reaction with $\text{Pd}(\text{PPh}_3)_4$ as catalyst. Crude products were purified by column chromatography with hexane and dichloromethane as eluent. The optical properties were analyzed in dry CH_2Cl_2 solution. Electrochemical property was investigated in dry CH_2Cl_2 with 0.1 M $n\text{-Bu}_4\text{NPF}_6$ as electrolyte.

Discussion and Conclusion

A series of oligothiophenes derivatives was successfully synthesized and characterized. The desired molecules were soluble in common organic solvents at room temperature. The number of thiophene units increased within the molecules result in red shift in absorption and fluorescence spectra due to the extended π -conjugation length of oligothiophenes. Electrochemical property was investigated by cyclic voltammetry. CV curves of the desired molecules exhibit oxidation process indicating electron donor property. According to their electronic and electrochemical properties, it expected that the novel oligothiophenes with dialkylaniline end-capped can be used as organic semiconductor in OFETs.

Keywords: Oligothiophenes, OFETs, Organic semiconductor

*corresponding/first author e-mail: d.muenmart@gmail.com



Synthesis and Characterization of Oligothiophenes Bearing Dialkylaniline End-Capped for Organic Field-Effect Transistors

Duangratchaneekorn Muenmart*, T. Sudyoasuk, T. Keawin, S. Saengsuwan, S. Jungstittiwong and V. Promarak



Center for Organic Electronics and Polymers, Department of Chemistry and Center of Excellence for Innovation in Chemistry, Faculty of Science, Ubon Ratchathani University, Ubon Ratchathani, Thailand 34190
E-mail: d.muenmart@gmail.com



Introduction

Organic semiconducting materials have been the subject of intense study in recent year because they have shown potential as alternatives to inorganic semiconductors for low cost optoelectronics devices, such as organic field-effect transistors and photovoltaic cells. Oligothiophenes are mostly studied as organic semiconductors for organic field-effect transistors (OFETs) with high on-off current ratio and charge transport properties. Moreover, the molecular structure of target molecules can be easily modified using various organic synthetic methodologies. In this work, we reported synthesis and characterization of novel oligothiophenes with dialkylaniline end-capped used as organic semiconductor in OFETs.

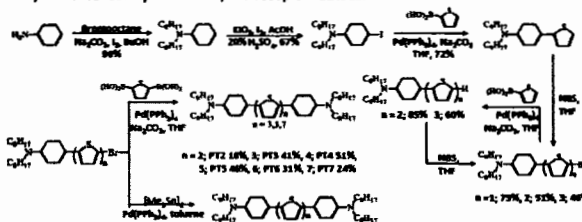


Aims

- To synthesize and characterize novel oligothiophenes bearing dialkylaniline end-capped for OFETs.
- To investigate optical, electrochemical and thermal properties of target molecules.

Results and Discussion

Synthesis and Characterization : A series of novel oligothiophenes with dialkylaniline end-capped was synthesized using combination of alkylation, iodination, bromination followed by palladium catalyzed Suzuki coupling and Stille coupling reaction. They were soluble in common organic solvent at room temperature. The desired molecules were fully characterized by standard spectroscopic methods.



Scheme 1. Synthetic route of target molecules

Conclusion

A series of oligothiophenes derivatives was successfully synthesized and characterized by using NMR, UV-vis and CV techniques. The desired molecules were soluble in common organic solvents at room temperature. According to their electronic and electrochemical properties, it expected that PT4 and PT5 can be used as organic semiconductor in OFETs. The devices performance will be investigated.

Acknowledgements

I would like to thank the Office of the Higher Education Commission, Thailand for supporting by grant fund under the program strategic scholarships for Frontier Research Network for the Joint Ph.D Program Thai Doctoral degree for this research. This work was supported by the Commission on Higher Education (CHE-RES-RGSO), Center of Excellence for Innovation in Chemistry (PERCH-CIC) and the Thailand Research Fund (TRF)

Optical properties : The optical properties were analyzed in dry CH_2Cl_2 solution. The number of thiophene units increased within the molecules result in red shift in absorption and fluorescence spectra due to the extended π -conjugation length of oligothiophenes.

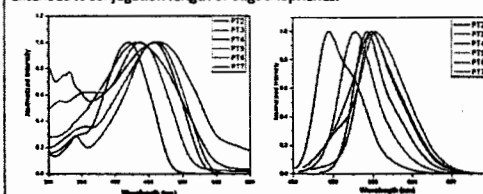


Figure 1. Absorption spectra of oligothiophenes in dry CH_2Cl_2

Figure 2. Fluorescence spectra of oligothiophenes in dry CH_2Cl_2 excited at λ_{max} absorption

Thermal property : The desired molecules, PT4, PT5, PT6 and PT7 show good thermal property with high T_g and T_d .

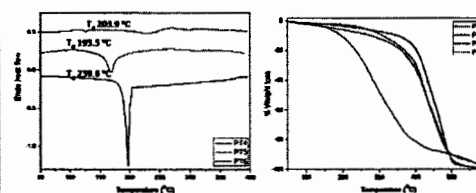


Figure 3. DSC (1st scan) and TGA thermograms measured with heating rate of 10 °C/min under N_2

Electrochemical property : CV using glassy carbon working electrode; Pt counter electrode; Ag/Ag^+ reference electrode in CH_2Cl_2 ; $n\text{-Bu}_4\text{NPF}_6$ as electrolyte. PT6 and PT7 don't show oxidation peak because of their solubility.

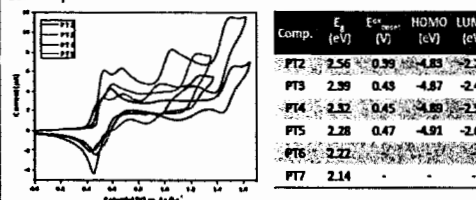
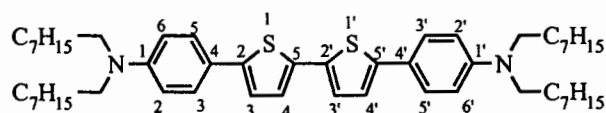


Figure 4. Cyclic voltammograms of the desired molecules

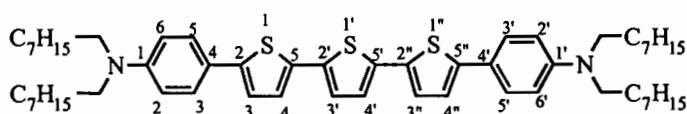
References

1. Takeshi Yamao et al. *Thin Solid Films*, 2008, 516, 2527–2531
2. M.D. Islop et al. *Synthetic Metals*, 2004, 146, 251–257
3. A.-L. Deman et al. *Synthetic Metals*, 2004, 146, 365–371

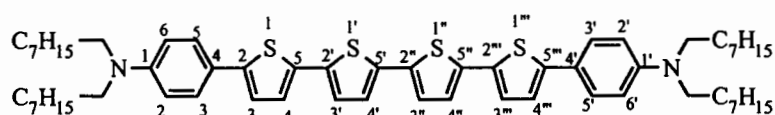
Chemical structures



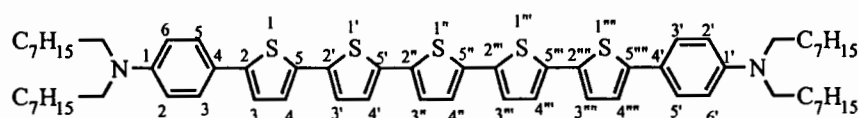
PT2



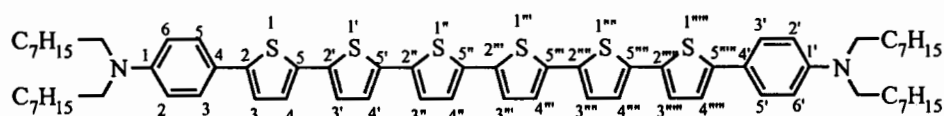
PT3



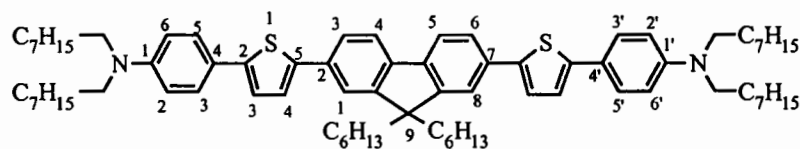
PT4



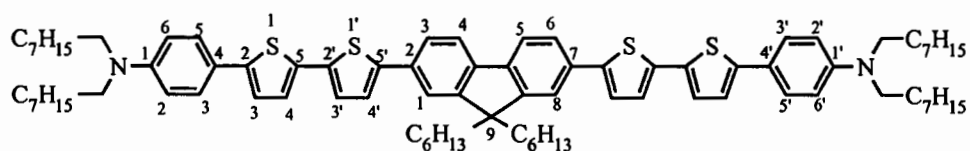
PT5



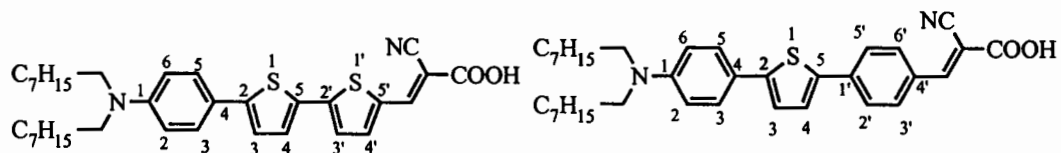
PT6



PT1F

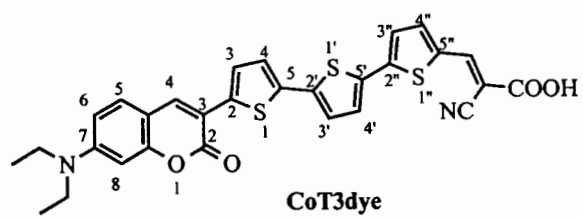


PT2F



PT2dye

PT1Pdye



VITAE

NAME Miss Duangratchaneekorn Muenmart

BORN 29 March 1983, Sri-Sa-Ket, Thailand

EDUCATION Bachelor of Science, 2002-2005
Master of Science, 2006-2007

SCHOLARSHIPS Scholarship from Thailand Graduate Institute of Science and Technology (TGIST), 2006-2007
Research Prize from Center for Innovation in Chemistry: Postgraduate Education and Research Program in Chemistry (PERCH-CIC), 2007
Research Prize from Ubon Ratchathani University, 2007
Scholarship from the Office of the Higher Education Commission, Thailand under the program Strategic Scholarships for Frontier Research Network for the Joint Ph.D. Program Thai Doctoral degree, 2008-2012

PUBLICATIONS Muenmart, D.; Tarsang, R.; Jungsuttiwong, S.; Keawin, T.; Sudyoadsuk, T.; Promarak, V., Synthesis and Properties of Fluorene-oligothiophenes Perylenediimide Triads and Their Electropolymerizations. **Journal of Materials Chemistry**, 2012, **22**, 14579-14586
Meunmart, D., Prachumrak, N.; Keawin, T.; Jungsuttiwong, S.; Sudyoadsuk, T.; Promarak, V., Bis(4-diphenylaminophenyl)carbazole end-Capped Fluorene as Solution-processed Deep-blue Light-emitting and Hole-transporting Materials for Electroluminescent Devices, **Tetrahedron Letters**, 2012, **53**, 3615-3618

